



Delft University of Technology

MSc Thesis Relative Density Differences of a Sand Fill

ing. W.C.N. Vessies

Dredging and Marine Contractors

03 August 2012

Relative Density Differences of a Sand Fill

ing. W.C.N. Vessies

Delft University of Technology

Faculty of Civil Engineering and Geosciences

Section of Hydraulic Engineering

In association with

Van Oord Dredging and Marine Contractors

Department of Estimate & Engineering

A thesis submitted for the degree of
Master of Science in Civil Engineering

August 16th, 2012

Version 13, August 16th, 2012

Relative Density Differences of a Sand Fill

Zand is spotgoedkoop. Als je het op de juiste manier gebruikt is het een veelzijdig, sterk en duurzaam materiaal; bij verkeerd gebruik is het niet meer dan een hoop korrels. Ieder kind weet dat instinctief en proefondervindelijk; ingenieurs plegen het soms te vergeten.

- G.F. Sowers [1981] -

Author:

Ing. W.C.N. Vessies, 1524585

Thesis Committee:

Delft University of Technology

Prof. dr. ir. C. van Rhee

Ir. G.L.M. van der Schrieck

Dr. ir. P.H.A.J.M. van Gelder

Van Oord

Ir. M.J.M. van den Heuvel

Ir. H. Oostinga

Ir. J.P. van der Meer

Under the Authority of:

Van Oord Dredging and Marine Contractors

Acknowledgements

Writing a MSc-thesis is the last part of the curriculum of the Master in Science in Civil Engineering at Delft University of Technology.

During the last two years of my Masters, I was working on the construction of the Maasvlakte II Project for Van Oord, during the weekends. This project is an expansion of the Port of Rotterdam. I requested Van Oord for a topic for my MSc-thesis. The most interesting topic was about the differences in the density of the hydraulically placed sand in an above water sand fill and in an under water sand fill. An above water sand fill can also be constructed by rainbowing the sand. An underwater sand fill, can also be constructed either by dumping or by rainbowing the sand. Sometimes, a spraying pontoon is used to place the sand. By using the spraying pontoon, the density of the sand was higher then expected. The aim of this MSc-thesis is to explain possible causes for differences in the relative density.

I would like to express my gratitude to ir. M.J.M. van den Heuvel from the Estimate and Engineering department of Van Oord for his assistance, support and time that he has put in my graduation work. Also, I would like to thank ir. H. Oostinga from PUMA for his time and advice. Furthermore, I would like to thank prof. dr. ir. C. van Rhee and ir. G.L.M. van der Schrieck of the Delft University of Technology for their advice and assistance.

Rotterdam, August 3th, 2012

W.C.N. Vessies

Abstract

The Maasvlakte II project is a joint venture between Boskalis and Van Oord. During the construction, they have measured the relative density for different kind of work methods, by making cone penetration tests. The result of those measurement is, that the measured relative density for the Maasvlakte II project is higher then the values that can be found in literature for the different kind of work methods. Thus the objective of this MSc-thesis is to understand the influencing and determining processes for the relative density of dumped or sprayed sand underwater.

This MSc-thesis can be divided in four parts. The first part describes the characteristics of sand and the relation between the density and the relative density. Laboratory testing is executed to determine the relevant parameters of the sand, such as the minimum and maximum density and the particle size distribution. The second part describes the used work methods, such as dumping, rainbowing, back filling through the suction pipe and spraying with a spray pontoon, that are used by the construction of the Maasvlakte II project. The third part describes the analysis of the CPT data. The CPT data is linked to the work methods and the relative density based on the correlations of Baldi and Lunne and Christoffersen. Also, a statistical analysis is made. The statistical analysis is based upon different kinds of statistical tests, such as Kruskal-Wallis and Wilcoxon Rank Sum Test. The last part consist of physical hypotheses that explain the potential influencing and determining processes for the relative density of dumped and sprayed sand underwater.

The work methods used for the hydraulic placement, the discharge conditions, the layer thickness, the water depth and the soil properties of the borrow area are all important in the achieved relative densities. From statistical testing, with the Kruskal-Wallis and Wilcoxon Rank Sum Test, the used work method has an influence on the achieved relative density.

Contents

Contents	vii
Nomenclature	xviii
List of Figures	xx
List of Tables	xxvi
1 Introduction	1
2 Physical Characteristics of Sand	3
2.1 Pore Volume or Porosity	3
2.2 Water Content	5
2.3 Degree of Saturation	5
2.4 Particle Size Distribution	6
2.5 Grain Shape	8
2.6 Geology at the Maasvlakte II	8
2.6.1 Holocene Sand	8
2.6.2 Pleistocene Sand	9
3 Density	11
3.1 Density	11
3.1.1 Determination of Maximum Dry Density	11
3.1.2 Determination of Minimum Dry Density	13
3.2 Relative Density	13
3.3 Cone Penetration Test	17
3.4 Comparison between CPT and mini-CPT	20
4 Work Methods	23
4.1 Dumping	23
4.2 Rainbowing	24
4.3 Spraying	25
4.3.1 Back filling through Suction Pipe with a TSHD	25
4.3.2 Spraying with Suction Dredger “Sliedrecht 27”	26
4.3.3 Spraying with Multicat “Coastal Discovery”	27

CONTENTS

5	Data Analysis	29
5.1	CPT Data	29
5.1.1	Work Methods and Survey Data	30
5.1.2	CPT Analysis	31
5.2	Statistical Analysis of Relative Density Data	36
5.2.1	Determination of the Probability Distributions and Statistical Parameters per Work Method	36
5.2.2	Statistical Testing of the Statistical Hypotheses	38
5.3	Hydrodynamics	42
5.3.1	Wave Environments	42
5.3.2	Hydrodynamic Data of Maasvlakte II Project	43
6	Physical Hypotheses	47
6.1	Under Water Slope built-up	49
6.1.1	Slope Development	50
6.1.2	Sedimentation Length	52
6.2	Shear Stress	55
6.2.1	Shear Stress as a Result of a Density Current	57
6.2.1.1	Shear Stress as a Result of a Density Current for the Initial Condition	57
6.2.1.2	Shear Stress as a Result of a Density Current for the Stationary Condition	58
6.2.2	The influence of Hydrodynamic Conditions on the Relative Density	59
6.2.3	Relation between Shear Stress and Porosity	62
6.3	The influence of the Sedimentation Velocity on the Relative Density	63
7	Physical Processes and Parameter Calculations of a Sand Fill	67
7.1	Input Parameters for the Computations	67
7.2	Fall Processes of a Sand-Water Mixture	69
7.3	Sand-Water Mixture Flow on a Sand Fill	72
7.4	Computation Results for the Sedimentation Length and Slope Type	75
7.5	Computation Results for the Density Current	79
7.6	Computation Results for the Hydrodynamics	86
8	Conclusions and Recommendations	89
8.1	Conclusions	89
8.2	Recommendations	90
	References	93
	Appendices	
	Appendix A: General Overview of Maasvlakte II Project	103

CONTENTS

Appendix B: Results Grains Shape Analyse	109
Appendix C: Comparison between Standard CPT's and Mini-CPT's	117
Appendix D: CPT Analysis	121
Appendix E: Cross Sections	173
Appendix F: Statistical Analysis of Relative Density Data Histograms	181
Appendix G: Hydrodynamics	201
Appendix H: Progress of The Maasvlakte II Project	207
Appendix I: Bathymetry and Profiles	225
Appendix J: Initiation of Motion and Suspension as an Indicator of the Shear Stress Level	237
Appendix K: Computation Results for the Density Current	247
Appendix L: Computations Results for Hydrodynamics	253

CONTENTS

Nomenclature

Roman Capital Symbols

\hat{A}_δ	orbital excursion amplitude	[m]
A	surface of discharge area	[m ²]
C	Chézy coefficient	[$\sqrt{\text{m}}/\text{s}$]
C_0	soil constant	[-]
C_1	soil constant	[-]
C_2	soil constant	[-]
C_c	coefficient of curvature	[-]
C_D	drag coefficient	[-]
C_u	coefficient of uniformity	[-]
D^*	particle parameter	[-]
D_{comp}	degree of compaction	[-]
E	erosion flux	[kg/m ² s]
H	wave height	[m]
H^*	ratio between occurring slope height and critical slope height	[-]
H_{m0}	significant wave height	[m]
H_{wd}	required water depth under discharge point	[m]
I_d	density index	[-]
K_0	lateral stress ratio	[-]
L	wave length	[m]

NOMENCLATURE

L^*	dimensionless hydraulic sedimentation length	[-]
L_{sed}	sedimentation length	[m]
Mz	sand median	[μm]
N^*	ratio between occurring porosity and critical porosity	[-]
P	production	[m^3/s]
P_s	sand production of a TSHD	[kg/s]
Q	flow rate	[m^3/s]
R	angularity parameter	[-]
R_e	relative density based on void ratio	[-]
R_f	friction ratio (q_c/f_s)	[-]
R_n	relative density based on porosity	[-]
RC	degree of compaction	[-]
Re_*	particle Reynolds number	[-]
Re_p	particle Reynolds number	[-]
S	sedimentation flux	[kg/ m^2s]
S_r	degree of saturation	[%]
SRV_{10}	flow direction (Stroomrichtingsvector 10 min)	[$^\circ$]
SSV_{10}	flow velocity (Stroomsnelheidsvector 10 min)	[m/s]
T	wave period	[s]
T_{m-10}	mean wave energy period	[s]
\hat{U}_δ	orbital velocity	[m/s]
V	bulk volume of sand	[m^3]
V_a	volume of air in pores	[m^3]
V_p	volume of pores	[m^3]
V_s	volume of solid particles	[m^3]
V_w	volume of pore water	[m^3]

NOMENCLATURE

V_{load}	volume of sand (incl. pores) in TSHD	[m ³]
Var	variance	[-]
W	width of the sand fill	[m]
Roman Symbols		
b_0	width of discharge opening	[m]
c_b	near-bed volumetric concentration	[-]
c_v	volume concentration	[-]
d_0	diameter of velocity meter	[mm]
d_{10}	grain size, corresponding 10 % by weight of finer particles	[μ m]
d_{50}	medium grain size	[μ m]
d_{60}	grain size, corresponding 60 % by weight of finer particles	[μ m]
d_{impact}	diameter of impact area	[m]
d_{nozzle}	diameter of rainbow nozzle	[mm]
e	void ratio	[-]
e_{max}	maximum void ratio	[-]
e_{min}	minimum void ratio	[-]
f_0	Darcy-Weisbach friction = 0.15	[-]
f_s	sleeve friction (CPT)	[kPa]
f_w	friction factor	[-]
g	acceleration of gravity $\approx 9,81$ m/s ²	[m/s ²]
h	occurring slope height	[m]
h_{cr}	critical slope height	[m]
h_{dc}	layer thickness of the density current	[m]
i	slope	[-]
k	wave number defined by $\frac{2\pi}{L}$	[m ⁻¹]
k_s	Nikuradse roughness	[m]

NOMENCLATURE

k_s^+	non-dimensional roughness height	[-]
l	slope length	[m]
m_d	mass of dry bulk material	[kg]
m_w	mass of water in pores of bulk material	[kg]
mpd	maximum proctor density	[kg/m ³]
n	porosity	[-]
n_{cr}	critical porosity	[-]
n_{max}	maximum void ratio	[-]
n_{min}	minimum void ratio	[-]
n_{situ}	occurring porosity	[-]
p	probability	[-]
q_c	cone resistance	[kPa]
q_m	specific mixture flow	[m ² /s]
s	specific sand production	[kg/ms]
sod	stand off distance	[m]
$t_{discharge}$	discharge time of a TSHD	[s]
\bar{u}_c	depth averaged current velocity	[m/s]
u	measured pore pressure	[kPa]
u_*	shear velocity	[m/s]
u_0	flow velocity on velocity meter	[m/s]
$u'_b(t)$	instantaneous deviation from u_b , where $u'_b(t) = u_b(t) - u_b$	[m/s]
u_b	time averaged velocity at a particle	[m/s]
u_f	flow velocity	[m/s]
$u_{dc;ic}$	density current velocity for initial conditions	[m/s]
$u_{dc;sc}$	density current velocity for stationary conditions	[m/s]
$u_{impact;w}$	flow velocity at impact on water surface	[m/s]

NOMENCLATURE

u_{nozzle}	flow velocity at tip rainbow nozzle	[m/s]
u_{out}	flow velocity at discharge point	[m/s]
$u_{rms,b}$	$\sqrt{u'^2}$ = standard deviation of $u'_b(t)$	[m/s]
v_{sed}	sedimentation velocity	[m/s]
v_{sp}	sailing speed	[m/s]
w	moisture content or water content	[%]
w_0	particle fall velocity	[m/s]
w_s	particle fall velocity in suspension	[m/s]
x	x-coordinate in RD coordinate system (Easting)	[m]
y	y-coordinate in RD coordinate system (Northing)	[m]
z	water depth	[m]
z	z-coordinate (surface elevation)	[m to NAP]

Greek Symbols

α	factor, multiple of u'_{rms}	[-]
β	slope angle	[°]
Δ	specific density	[-]
ϵ	ratio of the sand production that settles below MSL	[-]
η	median	[-]
γ	specific weight	[kN/m ³]
γ_s	specific weight of sand	[kN/m ³]
γ_w	specific weight of water	[kN/m ³]
μ	mean	[-]
μ_d	dynamic viscosity	[Pa · s]
ν	kinematic viscosity	[m ² /s]
ϕ'	angle of grain contact	[°]
ϕ	internal angle of friction	[°]

NOMENCLATURE

ϕ_p	pick-up flux	[-]
ϕ_{pn}	net pick-up flux	[-]
Ψ	shape factor	[-]
ρ	density	[kg/m ³]
ρ_d	dry density	[kg/m ³]
ρ_m	mixture density	[kg/m ³]
ρ_s	density of solids	[kg/m ³]
ρ_w	density of water	[kg/m ³]
ρ_{bulk}	bulk density	[kg/m ³]
$\rho_{d;max}$	maximum dry density	[kg/m ³]
$\rho_{d;min}$	minimum dry density	[kg/m ³]
$\rho_{d;situ}$	in situ dry density	[kg/m ³]
$\rho_{m;0}$	discharge mixture density	[kg/m ³]
$\rho_{m;impact}$	mixture density on point of impact	[kg/m ³]
σ	standard deviation	[-]
σ_g	ground pressure	[kPa]
σ_v	vertical effective stress	[kPa]
σ_w	pore pressure	[kPa]
τ	shear stress	[N/m ²]
$\tau_{b,cr}$	critical bed shear stress	[N/m ²]
$\tau_{b,cw}$	current and wave related bed shear stress	[N/m ²]
$\tau_{b,c}$	current related bed shear stress	[N/m ²]
$\tau_{b,w}$	wave related bed shear stress	[N/m ²]
$\tau_{dc;ic}$	density current related shear stress for the initial condition	[N/m ²]
$\tau_{dc;sc}$	density current related shear stress for the stationary condition	[N/m ²]
θ	Shields parameter	[-]

NOMENCLATURE

$\theta_{b,cr}$	critical Shields parameter for initiation of motion	[-]
θ_{cr}	critical Shields parameter	[-]
$\theta_{s,cr}$	critical Shields parameter for initiation of suspension	[-]

Abbreviations

A-D Test	Anderson-Darling Test
ANOVA	Analysis of variance
PDF	Probability density distribution
BA	Baldi
BF	Back filling through suction pipe
CLK	Chek Lap Kok
CPT	Cone Penetration Test
DU	Dumping
GWS	Groundwater level
MSL	Mean sea level
K-S Test	Kolmogorov-Smirnov Test
LAT	Lowest astronomical tide
LU	Lunne
MC Test	Multiple Comparison Test
NAP	Dutch ordnance datum
NH	Northern hemisphere
PS	Port side
PSD	Particle Size Distribution
PU	Pumping
RB	Rainbowing
RD	Dutch coordinate system (Rijksdriehoeksmeting)
SB	Starboard

NOMENCLATURE

SBT	Soil Behaviour Type
SD	Suction Dredger
SP	Spraying with SD “Sliedrecht 27”
TSHD	Trailing Suction Hopper Dredger
WM	Work Method

NOMENCLATURE

List of Figures

2.1	Relation between different sand parameters.	5
2.2	Particle size distribution of the soil sample of the Maasvlakte II Project.	7
2.3	Grain shape according to Powers.	8
3.1	Dry density moisture relationship.	12
3.2	Minimum and maximum void ratio and porosity in relation to the gradation and the angularity [VBKO, 1998], modified from Youd [1973].	14
3.3	Density/porosity relations.	15
3.4	Comparison between degree of compaction and relative density for Dutch sands [CROW, 2004].	17
3.5	Cone penetration test truck. (<i>Courtesy PUMA</i>)	17
3.6	“Blockbuster” placing concrete blocks in the hard sea defence. (<i>Courtesy PUMA</i>)	19
3.7	Correlations of Baldi, Lunne and Christoffersen between cone resistance and relative density as function of the vertical effective stress for quartz sands.	21
4.1	TSHD discharge method: dumping.	23
4.2	TSHD discharge method: rainbowing.	24
4.3	TSHD “HAM 318” rainbowing with two nozzles at Palm Deira, Dubai (<i>Courtesy Van Oord</i>)	25
4.4	Spraying by using the back fill method of a TSHD.	26
4.5	TSHD “HAM 316” connected to the SD “Sliedrecht 27” to spray the under water sand bodies.	26
4.6	Dustpan of the SD “Sliedrecht 27”.	27
4.7	Multicat “Coastal Discovery” equipped with spray pipe.	28
5.1	Scheme for TSHD trip, survey database and work method.	31
5.2	CPT and discharge locations Maasvlakte II project.	32
5.3	CPT Soil Behaviour Type (SBT) chart [Robertson <i>et al.</i> , 1986] for CPT-001.	33
5.4	Histograms of the measured d_{50} on-board of the TSHD.	35
5.5	Comparison between porosity and the different kind of relative densities.	37
5.6	Test results of the Kruskal-Wallis Test.	41
5.7	World wide distribution of wave environments. From Masselink <i>et al.</i> [2011] modified from Davies [1980].	43

LIST OF FIGURES

5.8	Wave statistics “Stroommeetpaal Maasmond”	44
6.1	Different packings for particles.	48
6.2	Spraying of thin layers.	49
6.3	Slides and flow slides, modified from Schiereck [2004].	50
6.4	Development of sand slopes, modified from CUR 152 [1991].	51
6.5	Definition sketch for the sedimentation length according to Mastbergen & Bezuijen [1988].	53
6.6	Definition sketch for the density current with initial conditions.	58
6.7	Definition sketch for the density current with stationary conditions.	59
6.8	Definition sketch for the orbital motion of the water particles under a harmonic wave. Modified from Holthuijsen [2010].	61
6.9	Bed concentration versus velocity for all sands, from van Rhee [2002a].	62
6.10	Sheltering and interlocking of particles into the bed.	63
6.11	Relation between the sedimentation velocity and the near-bed volumetric concentration.	64
7.1	Types of fall processes, modified from CUR 152 [1991].	69
7.2	Physical processes of the work method rainbowing.	70
7.3	Relation between the mixture density and the diameter of the impact area.	71
7.4	Relation between the mixture density and the flow velocity on impact of the rainbow jet.	71
7.5	Physical processes of the work method pumping.	72
7.6	Sedimentation length and concentration development for the different work methods.	76
7.7	Example of increases of the pore pressure and decrease of the porosity during a flow slide [CUR 152, 1991], from Mastbergen <i>et al.</i> [1988].	76
7.8	Relation between the relative density and the dimensionless hydraulic sedimentation length.	78
7.9	Computation results for the initial condition.	82
7.10	Computation results for the stationary condition.	83
7.11	Relation between the relative density based on Lunne and Christofferson and the Shields parameter.	84
7.12	Relation between the relative density based on Baldi and the Shields parameter.	85
7.13	Relation between current velocity and the Shields parameter.	87
7.14	Relation between Shields parameter and waves.	88
C.1	Comparison between standard CPT’s and mini-CPT’s (offshore).	119
C.2	Comparison between standard CPT’s and mini-CPT’s (onshore).	120
E.1	Cross section - area D1 & D2 (CPT001 untill CPT140).	175
E.2	Cross section - area HZ (offset 100 m).	176
E.3	Cross section - area HZ (offset 130 m).	177

LIST OF FIGURES

E.4	Cross section - area HZ (offset 160 m).	178
E.5	Cross section - area HZ (offset 185 m).	179
E.6	Cross section - area ZI (CPT264 untill CPT267).	180
F.1	Histogram for dumping, with the correlation of Baldi for all the data. . .	188
F.2	Histogram for dumping, with the correlation of Baldi for area D1 & D2. .	188
F.3	Histogram for dumping, with the correlation of Baldi for area HZw, HZm & HZo.	189
F.4	Histogram for dumping, with the correlation of Baldi for area ZI.	189
F.5	Histogram for dumping, with the correlation of Lunne for all the data. . .	190
F.6	Histogram for dumping, with the correlation of Lunne for area D1 & D2. .	190
F.7	Histogram for dumping, with the correlation of Lunne for area HZw, HZm & HZo.	191
F.8	Histogram for dumping, with the correlation of Lunne for area ZI.	191
F.9	Histogram for rainbowing, with the correlation of Baldi for all the data. .	192
F.10	Histogram for rainbowing, with the correlation of Baldi for area D1 & D2. .	192
F.11	Histogram for rainbowing, with the correlation of Baldi for area HZw, HZm & HZo.	193
F.12	Histogram for rainbowing, with the correlation of Baldi for area ZI.	193
F.13	Histogram for rainbowing, with the correlation of Lunne for all the data. .	194
F.14	Histogram for rainbowing, with the correlation of Lunne for area D1 & D2. .	194
F.15	Histogram for rainbowing, with the correlation of Lunne for area HZw, HZm & HZo.	195
F.16	Histogram for rainbowing, with the correlation of Lunne for area ZI.	195
F.17	Histogram for pumping, with the correlation of Baldi for all the data. . .	196
F.18	Histogram for pumping, with the correlation of Baldi for area D1 & D2. .	196
F.19	Histogram for pumping, with the correlation of Baldi for area ZI.	197
F.20	Histogram for pumping, with the correlation of Lunne for all the data. . .	197
F.21	Histogram for pumping, with the correlation of Lunne for area D1 & D2. .	198
F.22	Histogram for pumping, with the correlation of Lunne for area ZI.	198
F.23	Histogram for back filling through the suction pipe, with the correlation of Baldi for area HZ.	199
F.24	Histogram for back filling through the suction pipe, with the correlation of Lunne for area HZ.	199
F.25	Histogram for spraying with SD “Slidrecht 17”, with the correlation of Baldi for area HZ.	200
F.26	Histogram for spraying with SD “Slidrecht 17”, with the correlation of Lunne for area HZ.	200
G.1	Measured significant wave height and mean wave energy period.	203
G.2	Measured current velocity and direction.	204
G.3	Measured and astronomic water level, Hoek van Holland.	205
H.1	Overview of the Maasvlakte II project. Survey data of April 1 st , 2009. . .	209

LIST OF FIGURES

H.2	Overview of the Maasvlakte II project. Survey data of April 29 th , 2009. . .	210
H.3	Overview of the Maasvlakte II project. Survey data of June 2 nd , 2009. . .	211
H.4	Overview of the Maasvlakte II project. Survey data of July 2 nd , 2009. . .	212
H.5	Overview of the Maasvlakte II project. Survey data of August 4 th , 2009. . .	213
H.6	Overview of the Maasvlakte II project. Survey data of August 30 th , 2009. . .	214
H.7	Overview of the Maasvlakte II project. Survey data of October 2 nd , 2009. . .	215
H.8	Overview of the Maasvlakte II project. Survey data of November 1 st , 2009. . .	216
H.9	Overview of the Maasvlakte II project. Survey data of November 30 th , 2009.	217
H.10	Overview of the Maasvlakte II project. Survey data of December 30 th , 2009.	218
H.11	Overview of the Maasvlakte II project. Survey data of February 2 nd , 2010. . .	219
H.12	Overview of the Maasvlakte II project. Survey data of March 2 th , 2010. . .	220
H.13	Overview of the Maasvlakte II project. Survey data of April 2 nd , 2010. . .	221
H.14	Overview of the Maasvlakte II project. Survey data of May 1 st , 2010. . .	222
H.15	Overview of the Maasvlakte II project. Survey data of May 31 th , 2010. . .	223
I.1	Bathymetry of CPT no. 89 for work method: Dumping.	227
I.2	Profiles of CPT no. 89 for work method: Dumping.	228
I.3	Bathymetry of CPT no. 4 for work method: Rainbowing.	229
I.4	Profiles of CPT no. 4 for work method: Rainbowing.	230
I.5	Bathymetry of CPT no. 120 for work method: Pumping.	231
I.6	Profiles of CPT no. 120 for work method: Pumping.	232
I.7	Bathymetry of CPT no. 214 for work method: Back filling through suction pipe.	233
I.8	Profiles of CPT no. 214 for work method: Back filling through suction pipe.	234
I.9	Bathymetry of CPT no. 238 for work method: Spraying with “Sliedrecht 27”.	235
I.10	Profiles of CPT no. 238 for work method: Spraying with “Sliedrecht 27”.	236
J.1	Schematic representation of sediment transport modes showing particle paths. Note that bed load includes both saltation and traction. (From Masselink <i>et al.</i> [2011], modified from Allen [1994].)	239
J.2	Original Shields diagram [Shields, 1936].	240
J.3	Initiation of motion according to Shields by van Rijn [1984b].	241
J.4	Initiation of motion by Zanke [2003].	243
J.5	Initiation of motion and suspension by van Rijn [1984c].	244
J.6	Computation results for the critical Shields parameter.	245
K.1	Relation between the Shields parameter and flow velocity of a density current (initial conditions).	249
K.2	Relation between the Shields parameter and flow velocity, with equal particle diameter (initial conditions).	249

LIST OF FIGURES

K.3	Relation between the Shields parameter and mixture density of a density current (initial conditions).	250
K.4	Relation between the Shields parameter and mixture density, with equal particle diameter (initial conditions).	250
K.5	Relation between the Shields parameter and flow velocity of a density current (stationary conditions).	251
K.6	Relation between the Shields parameter and flow velocity, with equal particle diameter (stationary conditions).	251
K.7	Relation between the Shields parameter and mixture density of a density current (stationary conditions).	252
K.8	Relation between the Shields parameter and mixture density, with equal particle diameter (stationary conditions).	252
L.1	Relation between Shields parameter and significant wave height.	255
L.2	Relation between Shields parameter and mean wave energy period.	255
L.3	Relation between Shields parameter and significant wave height, with equal water depth per work method.	256
L.4	Relation between Shields parameter and mean wave energy period, with equal water depth per work method.	256
L.5	Relation between Shields parameter and significant wave height, equal particle diameter depth per work method.	257
L.6	Relation between Shields parameter and mean wave energy period, with equal particle diameter per work method.	257
L.7	Relation between Shields parameter and significant wave height, with equal water depth and particle diameter per work method.	258
L.8	Relation between Shields parameter and mean wave energy period, with equal water depth and particle diameter per work method.	258
L.9	Relation between Shields parameter and current velocity.	259
L.10	Relation between Shields parameter and current velocity, with equal water depth per work method.	259
L.11	Relation between Shields parameter and current velocity, with equal particle diameter per work method.	260
L.12	Relation between Shields parameter and current velocity, with equal water depth and particle diameter per work method.	260

LIST OF FIGURES

List of Tables

2.1	Particle size fractions [NEN-EN-ISO 14688-1, 2002].	4
2.2	Results of the sieving.	6
2.3	Main results of the sieve analysis.	7
3.1	Moisture content of tested soil sample.	12
3.2	Dry density moisture relationship.	12
3.3	Test results for the minimum dry density.	13
3.4	Relative densities for different kind of activities.	18
5.1	CPT's analysed per area.	30
5.2	Relative densities for different kind of activities from literature, projects and Maasvlakte II.	39
5.3	Test results of the Kruskal-Wallis Test.	40
5.4	Test results of the Wilcoxon Rank Sum Test.	42
5.5	Construction time per area.	44
5.6	Maximum hydrodynamic values per area.	44
7.1	The input parameters for the different kind of computations.	68
7.2	The output parameters at sea bottom from JET computations.	72
7.3	The output parameters at sea bottom for the work method: pumping.	75
7.4	Computation results for sedimentation length, critical slope height and slope type, with lowest measured value of d_{50}	77
7.5	Computation results for sedimentation length, critical slope height and slope type, with average value of d_{50}	77
7.6	Computation results for sedimentation length, critical slope height and slope type, with highest measured value of d_{50}	77
7.7	Guilford & Fruchter [1973] suggested interpretation for correlation coef- ficient values.	79
7.8	Computation results for the density current.	80
7.9	Hydrodynamic data used for computations	86
F.1	The different distributions per work method and area.	185
F.2	Results of the mean (μ), standard deviate (σ), median (η) and variance (Var).	186

LIST OF TABLES

J.1	Computation results for the critical shear stress and Shields parameter. .	245
-----	--	-----

LIST OF TABLES

Chapter 1

Introduction

The Maasvlakte II Project (a joint venture between Boskalis and Van Oord) is constructed with different kinds of techniques for placing sand at the correct location. The following techniques have been used:

- Dumping (DU) by a Trailing Suction Hopper Dredger (TSHD);
- Rainbowing (RB) by a TSHD;
- Pumping (PU) through steel pipelines (hydraulic reclamation);
- Back filling through the suction pipe (BF);
- Spraying by using a spray pontoon (SP).

Sand can be dumped through the bottom doors of the TSHD when enough water depth is available compared to the draught of the TSHD. When the dumping area becomes too shallow for dumping, rainbowing is usually applied to place sand in the fill. Pumping through steel pipelines is applied for reclamation above water in areas that are out of reach for rainbowing. Spraying is used, when slope design requires precise placing of the sand within predefined tolerances.

Before the construction of the hard sea defence, the lower parts of the slopes underwater are constructed by backfilling through the suction pipe of a TSHD. The sand volumes that are placed at the higher parts of the slope are sprayed with a spraying pontoon. The slope of the hard sea defence is constructed with these methods since the construction processes are well controllable and have a high precision and accuracy in comparison to the other mentioned methods.

A high relative density of the sand is required for geotechnical reasons. Methods used to place sand above the waterline usually provide a higher relative density. Methods used for the underwater placing of sand usually result in a lower relative density. Therefore underwater dumping requires additional measures to acquire the required relative density. Each underwater construction method was expected to deliver comparable relative densities. At the Maasvlakte II project, however, the relative density of the sand which was sprayed underwater appeared to be higher than the underwater dumped or underwater rainbowed sand. If higher relative densities are being reached when underwater spraying is applied, additional measures for increasing the compaction of the sand is not required. Client requirements for properties of the fill are met, without extra costs.

1. INTRODUCTION

The aim of this research is to verify which processes influence the relative density of placed sand underwater by various techniques. The following question is central to the research:

What are the influencing and determining processes for achieving the relative density of dumped or sprayed sand underwater?

The following sub-questions can be derived from this central question. To what extent is the relative density of sand depending on:

- work method;
- water depth;
- particle size distribution;
- hydrodynamic processes.

The purpose of this thesis is, after careful consideration of the different aspects, to produce a report about the processes that determine the relative density of dumped and sprayed sand underwater.

The following subjects are studied from literature to gain insight into:

- a. Relative density and porosity of sand (chapter 2 and 3);
- b. Measuring the relative density of sand (chapter 3);
- c. Relation between Cone Penetration Test (CPT) and relative density (chapter 3);
- d. Relation between work method and the relative density of sand; thin layer spraying versus thick layer lump dumping (chapter 4, 6 and 7);
- e. Physical processes of a sand fill (settling, density currents) (chapter 6 and 7).

Chapter 5 of the thesis discusses an analysis of the data which have been collected during the construction of the Maasvlakte II project. The data is also processed in a statistical way. The aim is to find relations between the work methods and the obtained relative density of the sand, and which parameters determine the relative density of the sand. Chapter 6 discusses the physical hypothesis that explains why the relative density of the Maasvlakte II is higher than found in literature. Chapter 7 discusses the computations and their results belong to the physical hypothesis of chapter 6. Chapter 8 describes the conclusions and recommendations.

Chapter 2

Physical Characteristics of Sand

In this chapter, the relevant soil parameters for density and relative density, such as volume, porosity, water content and degree of saturation are described.

Sand is a cohesionless aggregate of rounded sub-angular or angular fragments of more or less unaltered rocks or minerals with a diameter from 63 μm to 2 mm according to the Dutch norm [NEN-EN-ISO 14688-1, 2002], see table [2.1]. The composition of sand is highly variable, depending on the local rock sources and conditions, but the most common constituent of sand in inland continental settings and non-tropical settings is silica (silicon dioxide, or SiO_2), usually in the form of quartz particles. The mineralogistic composition of sand can vary significantly with the geographical and geological origin. The colour of sand is mainly determined by addition of minerals other than quartz.

Sand can be characterized by the medium grain size (d_{50}) and the grain size distribution (gradation uniformity coefficient = $d_{60}/d_{10} = C_u$).

2.1 Pore Volume or Porosity

The bulk volume of sand is defined as combined volume of solid particles and voids (pores) between the particles. The pore volume can be divided in two parts namely the volume of air in the pores and the volume of pore water.

$$V = V_s + V_p = V_s + V_w + V_a \quad [2.1]$$

Where:

- V = bulk volume of sand [m^3];
- V_s = volume of solid particles [m^3];
- V_p = volume of pores [m^3];
- V_a = volume of air in pores [m^3];
- V_w = volume of pore water [m^3].

In figure [2.1a] the relation is given between the different volumes. The void ratio is the ratio between the volume of pores and the volume of solid particles [BS 1377, 1990]. This

2. PHYSICAL CHARACTERISTICS OF SAND

Table 2.1: Particle size fractions [NEN-EN-ISO 14688-1, 2002].

Soil Fractions	Sub-fractions	Symbols	Particle sizes [mm]		
Very coarse soil	Large Boulder	LBO	< 630		
	Boulder	Bo	< 200	to 630	
	Cobble	Co	< 63	to 200	
Coarse soil	Gravel	Gr	< 2	to 63	
		Coarse Gravel	CGr	< 20	to 63
		Medium Gravel	MGr	< 6.3	to 20
	Sand	Fine Gravel	FGr	< 2	to 6.3
		Sa		< 0.063	to 2
		Coarse Sand	CSa	< 0.63	to 2
		Medium Sand	MSa	< 0.2	to 0.63
		Fine Sand	FSa	< 0.063	to 0.2
Fine soil	Silt	Si	< 0.002	to 0.063	
		Coarse Silt	CSi	< 0.02	to 0.063
	Medium Silt	MSi	< 0.0063	to 0.02	
		Fine Silt	FSi	< 0.002	to 0.0063
	Clay	CL	≤ 0.002		

relation is given in equation [2.2].

$$e = \frac{V_p}{V_s} = \frac{\rho_s}{\rho_d} - 1 = \frac{n}{1 - n} \quad [2.2]$$

Where:

- e = void ratio [-];
- ρ_s = density of solids (quartz = 2650 kg/m³) [kg/m³];
- ρ_d = dry density [kg/m³];
- n = porosity [-].

The void ratio is commonly used in Anglo-Saxon engineering practice and the porosity in Dutch engineering practice. The porosity is the ratio between the volume of pores and the bulk volume [BS 1377, 1990]. This relation is given in equation [2.3]. In figure [2.1b] the relation is given between void ratio and porosity.

$$n = \frac{V_p}{V} = \frac{e}{1 + e} \quad [2.3]$$

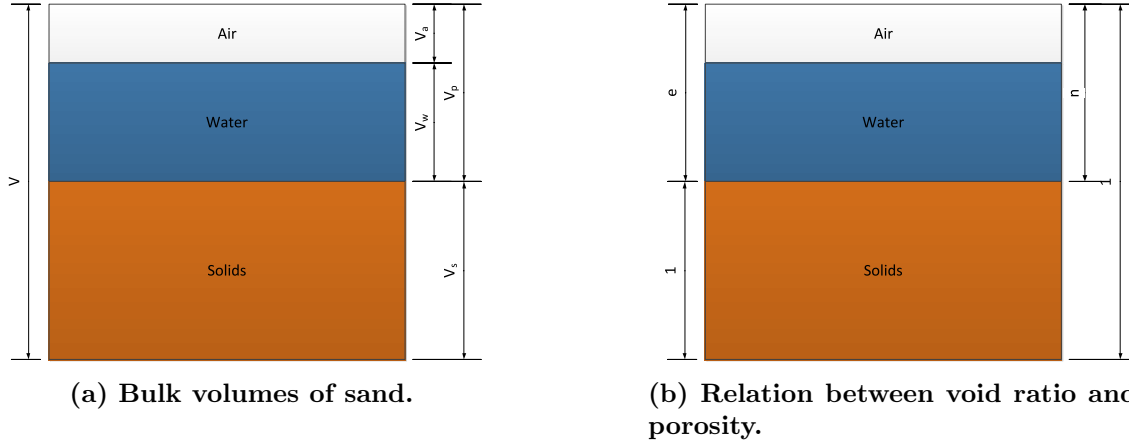


Figure 2.1: Relation between different sand parameters.

2.2 Water Content

The water content, also called the moisture content, is the mass of water which can be removed from the sand by heating at 105 °C [BS 1377, 1990], expressed as a percentage of the dry mass [BS 1377, 1990]. This relation is given in equation [2.4].

$$w = \frac{m_w}{m_d} \cdot 100\% = \frac{V_w \cdot \rho_w}{V_s \cdot \rho_s} \cdot 100\% \quad [2.4]$$

Where:

- w = moisture content or water content [%];
- m_w = mass of water in pores of bulk material [kg];
- m_d = mass of dry bulk material [kg];
- ρ_w = density of water [kg/m³].

2.3 Degree of Saturation

The degree of saturation is the volume of water contained in the pores expressed as a percentage of the total volume [BS 1377, 1990]. This relation is given in equation [2.5].

$$S_r = \frac{V_w}{V_p} \cdot 100\% = \frac{w \cdot \rho_s}{e \cdot \rho_w} \quad [2.5]$$

Where:

- S_r = degree of saturation [%].

2. PHYSICAL CHARACTERISTICS OF SAND

2.4 Particle Size Distribution

Five sand samples have been taken at the Maasvlakte II project (for the location of the samples see Appendix A). These samples were taken at different locations in the project area. These samples have been tested in the soil laboratory of Van Oord in Moerdijk. The laboratory tests are carried out according to the Dutch regulations, which are given in the Standaard RAW 2010, chapter 2 [CROW, 2011]. The mentioned sample in this chapter is a mixture of five samples taken of the Maasvlakte II project.

A dry sieve test has been carried out to determine the PSD of a soil sample. The following sieves have been used 63, 90, 125, 180, 250, 355, 500, 710 μm and 1, 1.4, 2 mm. The sieve analysis has been carried out according to the relevant standards, such as Proef 11 in the Dutch Standaard RAW 2011 [CROW, 2011] and BS 1377 part 2 [BS 1377, 1990]. The results of the sieving are given in table [2.2] and the PSD is given in figure [2.2]. In table [2.3] the specifications are given of the tested soil sample. The tested soil sample is representative for Pleistocene Sand. In figure [5.4] are the values of the d_{50} illustrated in histograms per work method. These values are used in the computations of chapter 7.

Table 2.2: Results of the sieving.

sieve [mm]	container [gr]	cont. +sample [gr]	sample [gr]			
2.000	46.4	49.2	2.8	1.53%	98.47%	
1.400	46.6	48.8	2.2	1.20%	97.26%	
1.000	48.3	52.5	4.2	2.30%	94.97%	
0.710	44.5	53.0	8.5	4.65%	90.32%	
0.500	46.9	70.4	23.5	12.86%	77.46%	
0.355	34.8	77.9	43.1	23.58%	53.88%	
0.250	47.6	98.1	50.5	27.63%	26.26%	
0.180	33.5	65.3	31.8	17.40%	8.86%	
0.125	47.8	60.3	12.5	6.84%	2.02%	
0.090	46.9	49.6	2.7	1.48%	0.55%	
0.063	38.7	39.5	0.8	0.44%	0.11%	
0.000	49.3	49.5	0.2	0.11%	0.00%	
total			182.8	100.00%		

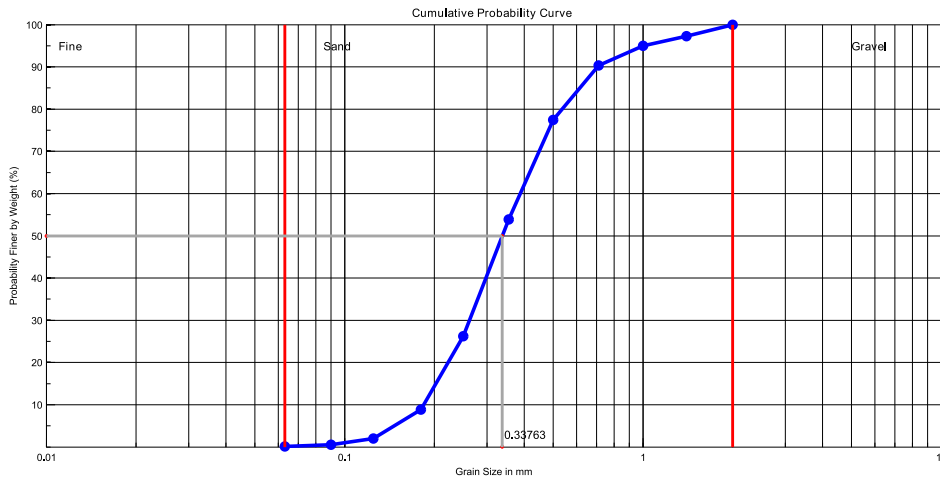


Figure 2.2: Particle size distribution of the soil sample of the Maasvlakte II Project.

Table 2.3: Main results of the sieve analysis.

d_5	= 0.156 mm
d_{10}	= 0.186 mm
d_{16}	= 0.213 mm
d_{30}	= 0.264 mm
d_{50}	= 0.338 mm
d_{60}	= 0.384 mm
d_{75}	= 0.478 mm
d_{84}	= 0.576 mm
d_{95}	= 1.003 mm
Mean grain size	= 0.346 mm
Standard deviation	= 1.7492
Skewness	= 0.9193
Kurtosis	= 0.45296
Coefficient of curvature (C_c)	= 0.97567
Coefficient of uniformity (C_u)	= 2.0628
Skewness classification	= Fine skewed
Kurtosis classification	= Leptokurtic (peaked)
ASTM classification	= Fine sand
NEN-ISO 14688 classification	= Medium Sand
% of gravel	= 1.53
% of sand	= 98.36
% of fines	= 0.11
Wentworth classification	= Medium sand
USCS classification	= SP

2. PHYSICAL CHARACTERISTICS OF SAND

2.5 Grain Shape

The shape of sand can vary from round to angular shapes. The angularity or roundness of the grains influences important properties of the sand such as minimum and maximum density and the angle of friction. The more angular the sand, the higher the angle of friction and the lower minimum and maximum densities. [VOUW, 2010a].

Powers [1953] has set up a system that uses a visual assessment to recognize the angularity and roundness of sand grains, see figure [2.3].

For the samples taken at the Maasvlakte II project the grain shape according to Powers is defined. The Maasvlakte II sand has a roundness class of sub angular / sub rounded shape with a angularity parameter (R) of 0.30 - 0.40. In Appendix B the results are given.













Roundness classes	Very Angular	Angular	Sub-angular	Sub-rounded	Rounded	Well Rounded
High Sphericity						
Low Sphericity						
Roundness indices	0.12 to 0.17	0.17 to 0.25	0.25 to 0.35	0.35 to 0.49	0.49 to 0.70	0.70 to 1.00

Figure 2.3: Grain shape according to Powers.

2.6 Geology at the Maasvlakte II

In this sub-paragraph the geology of the sand, that is used for the construction of the Maasvlakte II project, is described. Also the soil parameters are mentioned.

2.6.1 Holocene Sand

The Holocene sand is the so called Bligh Bank Formation, it is a fine (150 - 160 μm) sand. In this formation are some clay laminae layers and some gravel bands. The Bligh Bank Formation is a open marine deposit. The following in-situ soil parameter information is achieved from the Maasvlakte II project [Booster *et al.*, 2008]:

percentage of gravel = 3 %;

percentage of sand = 83 %;

percentage of fines	= 8 %;
sand median (Mz)	= 158 μm ;
d_{50}	= 172 μm ;
C_u	= 2.2;
$\rho_{d;min}$	= 1360 kg/m^3 ;
$\rho_{d;max}$	= 1646 kg/m^3 ;
n_{max}	= 0.4868;
n_{min}	= 0.3789;
e_{max}	= 0.9485;
e_{min}	= 0.6100;
ϕ	= 30° or $\frac{\pi}{6}$ rad.

2.6.2 Pleistocene Sand

The Pleistocene sand is the so called Kreftenheye Formation, it is a medium to coarse (180 - 800 μm) sand with gravel, shells and wood residues. The formation contains Eemian Mollusca. It is a fluvial deposit of the Rhine and Meuse. The shape of the grains is sub-angular [EMSAGG, 2010]. The following in-situ soil parameter information is achieved from the Maasvlakte II project [Booster *et al.*, 2008]:

percentage of gravel	= 2 %;
percentage of sand	= 91 %;
percentage of fines	= 5 %;
sand median (Mz)	= 300 μm ;
d_{50}	= 303 μm ;
C_u	= 2.5;
$\rho_{d;min}$	= 1423 kg/m^3 ;
$\rho_{d;max}$	= 1697 kg/m^3 ;
n_{max}	= 0.4630;
n_{min}	= 0.3596;
e_{max}	= 0.8623;
e_{min}	= 0.5616;
ϕ	= 30° or $\frac{\pi}{6}$ rad.

2. PHYSICAL CHARACTERISTICS OF SAND

Chapter 3

Density

3.1 Density

Density or mass density of sand is defined as the mass per unit volume. In some cases density is also defined as weight per unit of volume although, this quantity is more properly called specific weight. The relation between density and specific weight is given in equation [3.1].

$$\gamma = \rho \cdot g \quad [3.1]$$

Where:

- γ = specific weight [kN/m³];
- ρ = density [kg/m³];
- g = acceleration of gravity $\approx 9,81$ m/s².

Sand samples have been taken at the Maasvlakte II project (for the location of the samples see Appendix A). These samples are taken on different locations in the project area and have been tested in the soil laboratory of Van Oord in Moerdijk. From the soil samples, the maximum and minimum dry density is determined. The laboratory tests are carried out according to the Dutch regulations, which are given in the Standaard RAW 2010, chapter 2 [CROW, 2011]. The mentioned sample in this chapter is a mixture of five samples taken at the Maasvlakte II project.

3.1.1 Determination of Maximum Dry Density

The maximum dry density of a soil sample can be determined by the proctor test. The equipment used is a rammer of 2.5 kg and a mould with a volume of approximately 1 litre. The proctor test has been carried out according to the relevant standards, such as Proef 5.1 in the Dutch Standaard RAW 2011 [CROW, 2011] and BS 1377 part 4 [BS 1377, 1990]. The proctor test is carried out with different moisture contents as presented in table [3.1]. The proctor test results are presented in table [3.2]. In figure [3.1] the maximum dry density is presented in relation to the moisture content.

3. DENSITY

Table 3.1: Moisture content of tested soil sample.

Test number		1	2	3	4	5
Mass of wet soil + container	g	128.6	111.7	130.4	120.1	137.2
Mass of dry soil + container	g	126.9	109.8	128.4	118	132.4
Mass of container	g	104.1	87	109.6	101.9	101.2
Mass of moisture (m_w)	g	1.7	1.9	2	2.1	4.8
Mass of dry soil (m_d)	g	22.8	22.8	18.8	16.1	31.2
Moisture content (w)	%	7.46	8.33	10.64	13.04	15.38

Table 3.2: Dry density moisture relationship.

Initial sample mass	g	Particle density (ρ_s)		2650	kg/m ³	
Retained on 20 mm/ 37.5 mm sieve	g	0	%			
Test number		1	2	3	4	5
Mass of mould + compacted specimen	g	5916.7	5958.2	6038.4	6066.5	6083.7
Mass of mould	g	4227.0	4227.0	4227.0	4227.0	4227.0
Mass of compacted specimen	g	1689.7	1731.2	1811.4	1839.5	1856.7
Bulk density (ρ_{bulk})	kg/m ³	1793	1837	1922	1951	1970
Moisture content (w)	%	7.46	8.33	10.64	13.04	15.38
maximum dry density ($\rho_{d,max}$)	kg/m ³	1668	1695	1737	1726	1707
		Maximum dry density		1737	kg/m ³	
		Optimum moisture content		10.64	%	

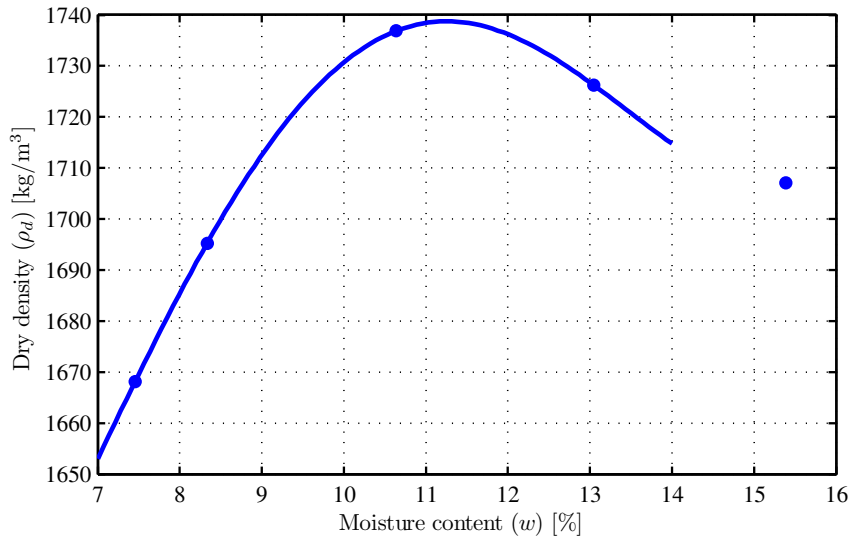


Figure 3.1: Dry density moisture relationship.

The n_{min} and e_{min} are computed with equations [3.2] and equation [2.2].

$$n_{min} = 1 - \frac{\rho_{d;max}}{\rho_s} \quad [3.2]$$

The results of the Proctor test are:

$$\begin{aligned} \rho_{d;max} &= 1737 \text{ kg/m}^3; \\ w &= 10.64\%; \\ n_{min} &= 0.3446; \\ e_{min} &= 0.5258. \end{aligned}$$

3.1.2 Determination of Minimum Dry Density

The minimum dry density of a soil sample can be determined by a minimum dry density test. The minimum dry density test has been carried out according the relevant standards, such as BS 1377 part 4 [BS 1377, 1990]. In table [3.3] the test result are presented.

Table 3.3: Test results for the minimum dry density.

Test		1	2	3	4	5
Mass of container	g	102.9	102.9	102.9	102.9	102.9
Mass of container + sample	g	148.3	148.2	148.1	148	147.9
Mass of sample (m_d)	g	45.4	45.3	45.2	45.1	45.0
Volume (V)	ml	30	30	29	29	29
Minimum dry density ($\rho_{d;min}$)	kg/m ³	1513	1510	1559	1555	1552

The n_{max} and e_{max} are computed with equations [3.3]) and equation [2.2].

$$n_{max} = 1 - \frac{\rho_{d;min}}{\rho_s} \quad [3.3]$$

The results of the minimum dry density test are:

$$\begin{aligned} \rho_{d;min} &= 1510 \text{ kg/m}^3; \\ n_{max} &= 0.4302; \\ e_{max} &= 0.7550. \end{aligned}$$

3.2 Relative Density

The relative density is the dry density in situ, expressed in relation to two boundaries, the minimum and maximum density, which are defined in a laboratory. These densities are defined by standard tests which are described in BS 1377 [1990] for the United Kingdom, Standaard RAW Bepalingen 2010 [CROW, 2011] for the Netherlands and ASTM D4253 [2006] and ASTM D4254 [2006] or ASTM D698 [2007] for the United States.

The relative density can also be related to the void ratio or the porosity. To determine

3. DENSITY

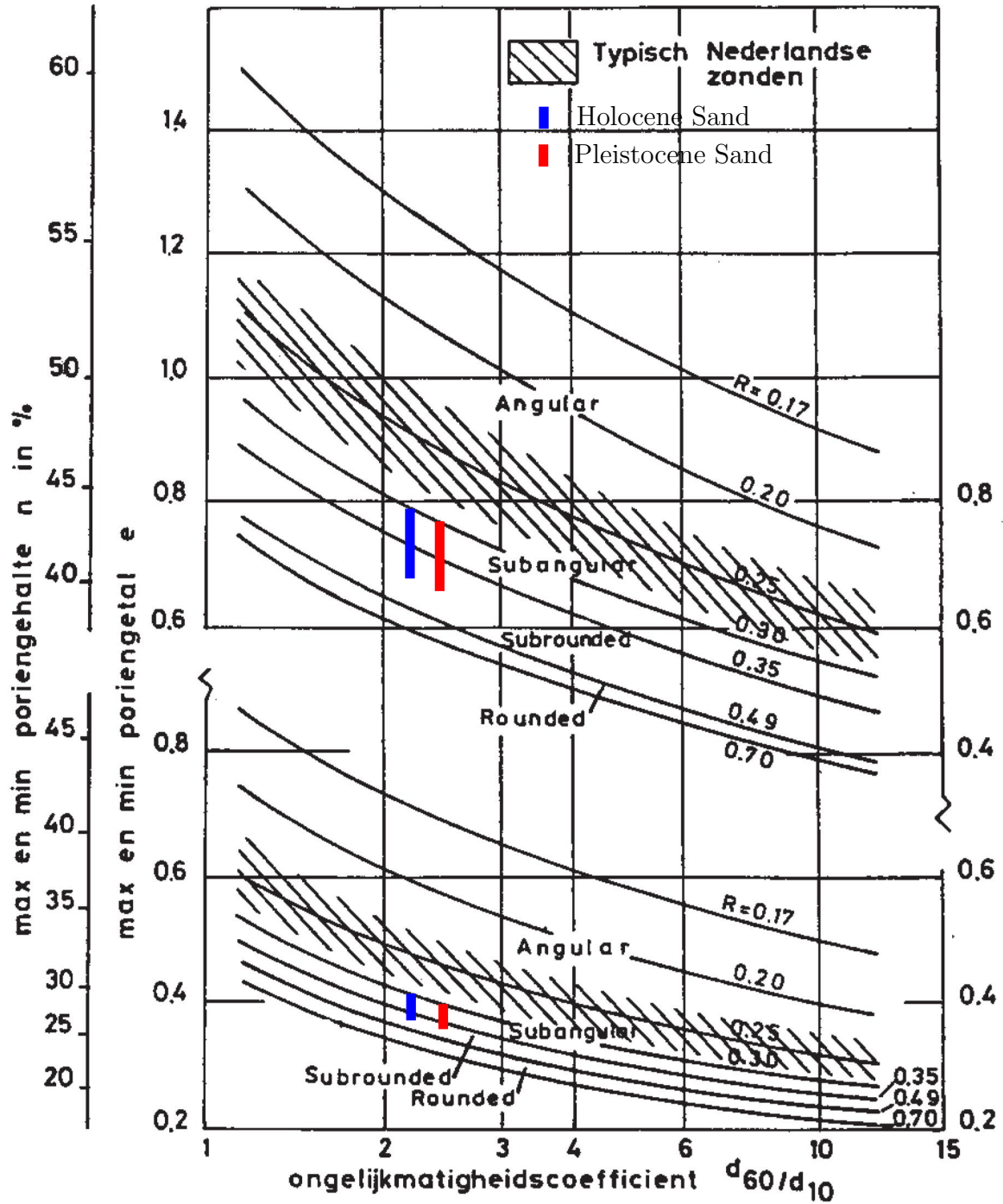


Figure 3.2: Minimum and maximum void ratio and porosity in relation to the gradation and the angularity [VBKO, 1998], modified from Youd [1973].

the minimum and maximum void ratio and porosity, laboratory tests are needed. It is also possible to use the graph of Youd [1973] (figure [3.2]). The relative density related to the void ratio (R_e) is generally used in Anglo-Saxon engineering practice and is given in equation [3.4]. This definition of relative density is also mentioned as 'density index' (I_D) [BS 1377, 1990].

$$R_e = I_D = \frac{e_{max} - e}{e_{max} - e_{min}} = \frac{\rho_{d;max}}{\rho_d} \cdot \frac{\rho_d - \rho_{d;min}}{\rho_{d;max} - \rho_{d;min}} \quad [3.4]$$

Where:

- R_e = relative density based on void ratio [-];
- I_d = density index [-];
- e_{max} = maximum void ratio [-];
- e_{min} = minimum void ratio [-];
- $\rho_{d;min}$ = minimum dry density [kg/m^3];
- $\rho_{d;max}$ = maximum dry density [kg/m^3].

The relative density based on the porosity (R_n) is generally used in Dutch engineering practice and is given in equation [3.5].

$$R_n = \frac{n_{max} - n}{n_{max} - n_{min}} = \frac{\rho_d - \rho_{d;min}}{\rho_{d;max} - \rho_{d;min}} \quad [3.5]$$

Where:

- R_n = relative density based on porosity [-];
- n_{max} = maximum porosity [-];
- n_{min} = minimum porosity [-].

In figure [3.3] the relation between density, porosity and relative density is given.

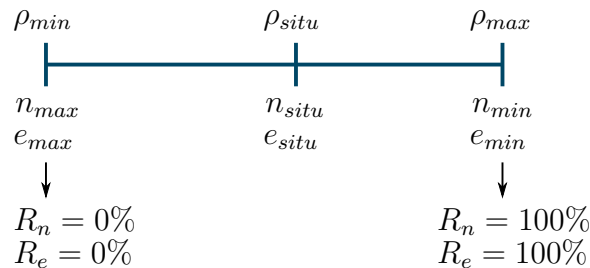


Figure 3.3: Density/porosity relations.

The relative density (R_e) based on void ratio and the relative density (R_n) based on porosity are related together as given in equation [3.6] and equation [3.7].

$$R_e = \frac{\rho_{d;max}}{\rho_d} \cdot R_n = \frac{1 + e}{1 + e_{min}} \cdot R_n = \frac{1 - n_{min}}{1 - n} \cdot R_n \quad [3.6]$$

3. DENSITY

$$R_n = \frac{\rho_d}{\rho_{d;max}} \cdot R_e = \frac{1 + e_{min}}{1 + e} \cdot R_e = \frac{1 - n}{1 - n_{min}} \cdot R_e \quad [3.7]$$

To compute the relative density of the cohesionless soil (sand). Therefore, first a Proctor Test [ASTM D698, 2007; BS 1377, 1990; CROW, 2011], Modified Proctor Test [ASTM D1557, 2009; BS 1377, 1990; CROW, 2011] or a test with a vibrating table [ASTM D4253, 2006] must be carried out to determine the maximum density of the cohesion less soil. Following relation exists between the proctor density and modified proctor density:

100% Proctor density \approx 95% Modified Proctor density [Veldhuis, 1992]

The in situ density of the cohesion less soil can be determined with a Troxler (Nucliar method) [ASTM D6938, 2010; BS 1377, 1990; CROW, 2011], core cutter method [BS 1377, 1990; CROW, 2011], rubber-balloon method [ASTM D2167, 2008] or sand replacement test [BS 1377, 1990]. The maximum and in situ density is used in equation [3.8], to compute the degree of compaction.

$$RC = D_{comp} = \frac{\rho_d}{\rho_{d;max}} = \frac{\rho_{d;situ}}{mpd} \quad [3.8]$$

Where:

- RC = degree of compaction [-];
- D_{comp} = degree of compaction [-];
- mpd = maximum proctor density [kg/m³].

Confusion often arises concerning the difference between relative density and degree of compaction. Both definitions are found in contract specifications. A requirement of 90% relative density is, however, something completely different compared to a degree of compaction of 90%. The difference between the two definitions can best be illustrated by figure [3.4]. This figure is based on test collections for Dutch sands and is intended to be indicative; no direct link exists between degree of compaction and relative density that could be used for conversion of one into the other [VOUW, 2010a]. In the upper part of figure [3.4] the difference is given between the relative density based on void ratio and porosity and the lower part gives the comparison between degree of compaction based on the Modified Proctor Test or on the Standard Proctor Test. The minimum value for the degree of compaction is for Dutch sands 80%, by a relative density of 0%.

A list of relative densities, that have been achieved at certain activities, is presented in table [3.4]. The table [3.4] is based on dredging related research in the 1980s and experience of the dredging companies (i.a. Blommaart & Viergever [1995]; CROW [2004]; de Groot *et al.* [1988]; Heezen & van der Stap [1985, 1988]; Hoogeveen *et al.* [1987]; Lee [2001]; Lee *et al.* [1999]; Mastbergen & Bezuijen [1988]). Normally the following rule of thumb is used: The relative density above water is more than 50% and under water less

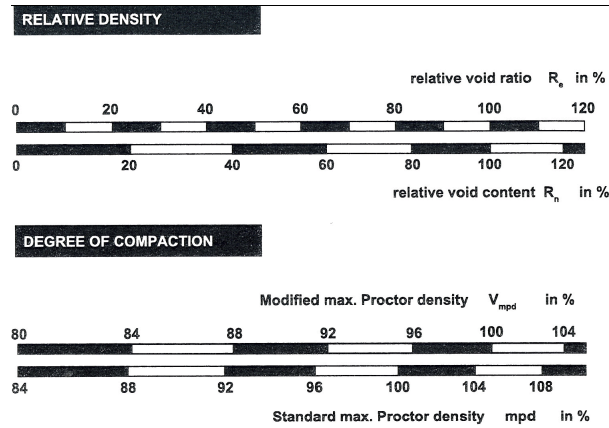


Figure 3.4: Comparison between degree of compaction and relative density for Dutch sands [CROW, 2004].

than 50%. VBKO [1998] suggest to use the high values of R_n from table [3.4], for sand coarser than $150 \mu m$. This suggests that there is a relation between the particle size and the relative density.

3.3 Cone Penetration Test

The cone penetration test is an in situ testing method used to determine the soil properties and delineating soil stratigraphy. It was initially developed in the 1950s at the Dutch Laboratory for Soil Mechanics, nowadays Deltares, to investigate soft soils. The CPT is one of the most used and accepted in situ test methods for soil investigation worldwide. The test method consists of pushing an instrumented cone, with the tip facing down, into the ground at a controlled rate. The resolution of the CPT in delineating stratigraphic layers is related to the size of the cone tip.



Figure 3.5: Cone penetration test truck. (Courtesy PUMA)

Table 3.4: Relative densities for different kind of activities.

Activity	Relative Density		
	[CROW, 2004] [VBKO, 1998] R_n	West Kowloon, Hong Kong, [Lee <i>et al.</i> , 1999] R_e	Chek Lap Kok (CLK) Hong Kong, [Lee, 2001] R_e
Dumping under water (< 10 m)	0.30-0.50	0.43	0.37-0.45
Dumping under water (> 10 m)	0.40-0.60	0.62	0.50-0.60
Spraying under water	0.20-0.40	-	-
Rainbowing (below lowest astronomical tide (LAT))	0.20-0.40	0.50	0.37-0.45
Rainbowing (above LAT)	0.60-0.70	-	-
Hydraulic reclamation (below LAT)	0.20-0.40	-	0.37-0.45
Hydraulic reclamation (above LAT)	0.60-0.70	0.80	0.70-1.00
Compaction by bulldozers & trucks	+0.10	-	-
Compaction by vibro compaction	to 1.00	-	-

The cone penetration tests is used at the Maasvlakte II project for two reasons. Reason one is to determine the relative density of the sand fills and the other reason is for the geotechnical analysis of the road construction for the “Blockbuster” (figure [3.6]).



Figure 3.6: “Blockbuster” placing concrete blocks in the hard sea defence. (Courtesy PUMA)

Cone penetration tests (CPT) can also be used to compute the relative density. The most familiar correlations of cone resistance and relative density are from Baldi [Baldi *et al.*, 1982; Lunne, 2006; Lunne *et al.*, 1997], Lunne and Christoffersen [Lunne & Christoffersen, 1983; Lunne *et al.*, 1997]. Those relations are based on Calibration Chamber Tests. Baldi has presented the correlation between cone resistance, in situ vertical effective stress and relative density. Baldi’s correlations are based mainly on the Italian Ticino sand and the Norwegian Hokksund sand. Thus the correlations are strictly valid for freshly deposited sands of moderate compressibility, with 30-50% quartz particles, with uniform grading and fine to medium sized particles, with no fines content.

For freshly deposited sands which can be assumed to have lateral stress ratio (K_0) of 0.4 to 0.5, equation [3.9] and figure [3.7] are valid.

$$R_e = \frac{1}{C_2} \cdot \ln \left(\frac{q_c}{C_0 \cdot \sigma_v^{C_1}} \right) = \frac{1}{2.41} \cdot \ln \left(\frac{q_c}{157 \cdot \sigma_v^{0.55}} \right) \quad [3.9]$$

Where:

- q_c = cone resistance [kPa];
- C_0 = soil constant [-];
- C_1 = soil constant [-];
- C_2 = soil constant [-];
- σ_v = vertical effective stress [kPa].

The correlation of Baldi is generally considered as one of the better correlations between cone resistance and relative density as a function of the vertical effective stress for quartz sands with normal compressibility.

3. DENSITY

Based on the results of numerous laboratory experiments by various researchers, Lunne and Christoffersen [CROW, 2004; Lunne *et al.*, 1997] came to a slightly modified graph compared to the graph of Schmertmann [CROW, 2004; Lunne *et al.*, 1997]. This graph of Lunne and Christoffersen is very widely used and is considered quite reliable. The graph of Lunne and Christoffersen as well as the graph of Schmertmann are valid for normally consolidated, saturated, young, uncemented sand. The relation of Lunne and Christoffersen is given in equation [3.10] and figure [3.7].

$$R_e = \frac{1}{2.91} \cdot \ln \left(\frac{q_c}{61 \cdot \sigma_v^{0.71}} \right) \quad [3.10]$$

For the top layer (1.5 m – mv) or a vertical effective stress $\sigma_v < 20$ kPa often the correlation of Teferra (equation [3.11]) is used.

$$R_e = -26 + 34 \cdot \log \frac{q_c}{\sigma_v} \quad [3.11]$$

The sand at the Maasvlakte II Project is normally consolidated, saturated and young. The sand fill is not over-consolidated or cemented, because it is recently placed. The sand fill is saturated as can be seen from the hydrostatic pore pressure in CPT-001, see for CPT-001 Appendix D.1. The sand is dominated by quartz and volcanic minerals [EMSAGG, 2010]. Therefore the sand of the Maasvlakte II Project satisfies the conditions to use the graphs (figure [3.7]) and correlations (equations [3.9] and equation [3.10]) of Baldi, Lunne and Christoffersen.

3.4 Comparison between CPT and mini-CPT

Two types of CPT's are executed at the Maasvlakte II Project. On land the standard cone is used, with a cone surface of 10 cm² and nearshore a mini-CPT, from Marine Sampling Holland, is used with a cone surface of 2 cm². The results of the mini-cone have been compared with the standard cone to define a correlation between the two cones.

Marine Sampling Holland has done research on the correlation of the mini-cone with the standard cone. The observed differences were too small to be significant, and well within the limits that are allowed in international standards for CPT testing [Marine Sampling Holland, 2009].

Tufenkjian *et al.* [2010] has done research on the comparison between the standard cone and the mini-cone. His conclusion is that the tip in loose sand, produces a lower penetration resistance (30% - 40%) for the mini-cone compared to the standard cone. In medium dense sand, the tip resistance profiles were practically similar. In dense sand, the mini cone produced a higher penetration resistance (20% - 30%) than the standard cone. Their observations show a dependency on the density state which they could not explain by boundary or grain size effects and which are believed to be a possible scale effect between the different cone sizes.

Yoon & Tumay [2010] have also made a comparison between mini- and standard cone.

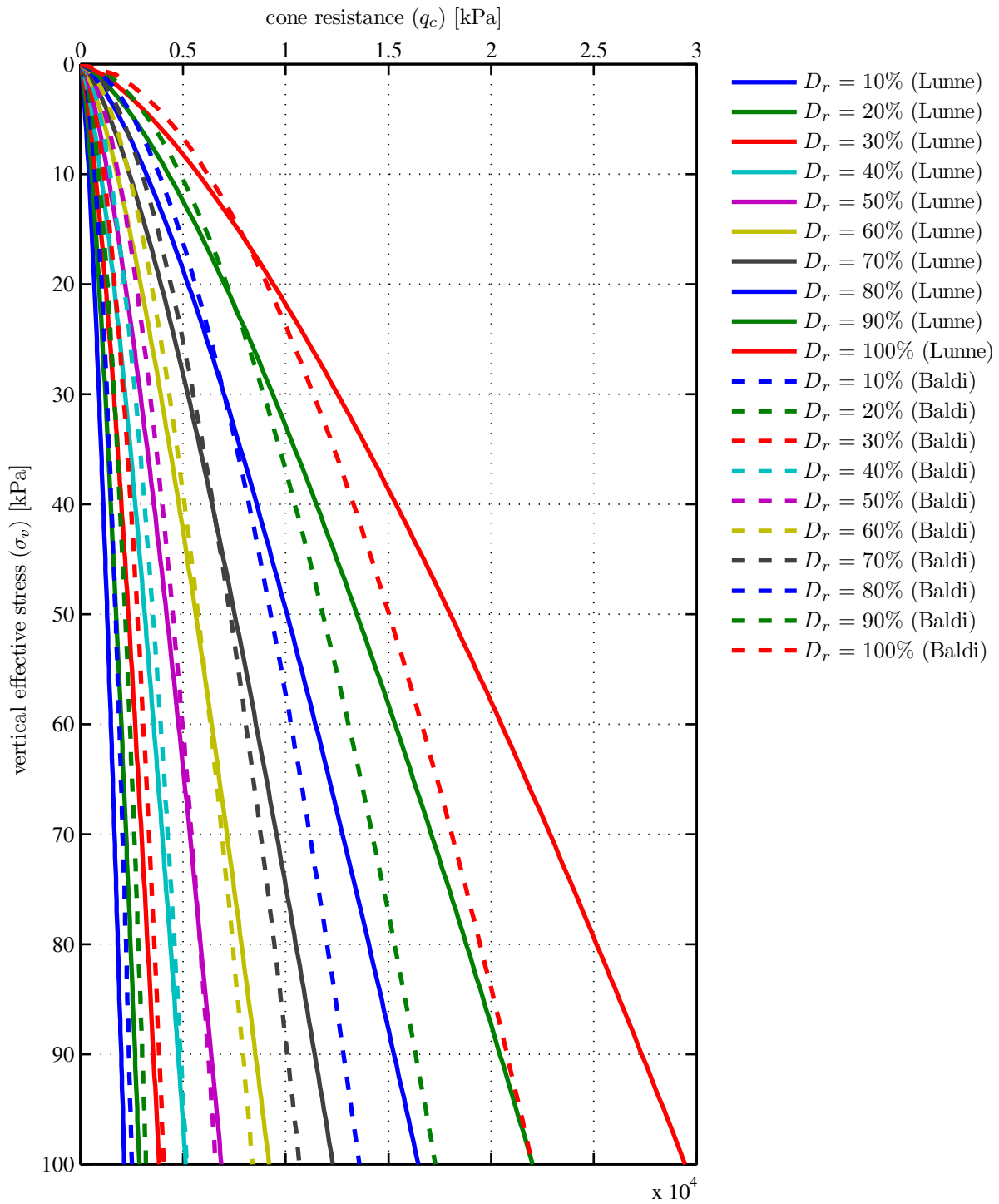


Figure 3.7: Correlations of Baldi, Lunne and Christoffersen between cone resistance and relative density as function of the vertical effective stress for quartz sands.

3. DENSITY

Their comparison is based on field tests at a well-characterized construction site near Seoul in South Korea. The conclusion of Yoon and Tumay is that both methods give similar results.

At the location of a standard CPT, a mini-CPT has been made. The results of these standard CPT's and mini-CPT's are given in Appendix C. In Appendix A the locations of all CPT's at the Maasvlakte II Project are shown.

The land CPT's correlate very well with each other. The marine CPT's show some variation in the correlation. One of the reasons can be the inaccuracy of the position of the CPT's. The positioning of the offshore CPT's is less accurate than the positioning of the onshore CPT's.

Because of its greater influence depth (length scale), the standard cone is expected to respond better to deeper softer / stiffer layers than the mini-CPT. The mini-cone should response more sharply to stratigraphic changes and it should be able to resolve thinner layers. This effect is shown in the CPT results a higher resolution for the mini cone.

Based on above findings the results of the mini-CPT have been used for the correlations with the relative density, which are given in paragraph 3.2.

Chapter 4

Work Methods

This chapter, describes the work methods that have been used at the Maasvlakte II Project.

4.1 Dumping

A trailing suction hopper dredger (TSHD) has different methods to discharge the load. One of them is dumping (figure [4.1]) by opening the bottom doors of the TSHD. When the bottom doors are open the sand is liquefied with jets. The sand-water mixture flows through the bottom doors vertical down to the seabed. The dumping process is physically described by curtain-like dumping. The other dumping process, lump-like dumping is not used by the construction of the Maasvlakte II project and so not mentioned further (see also figure [7.1]). The maximum dumping depth, for the Maasvlakte II project is about 10 m.

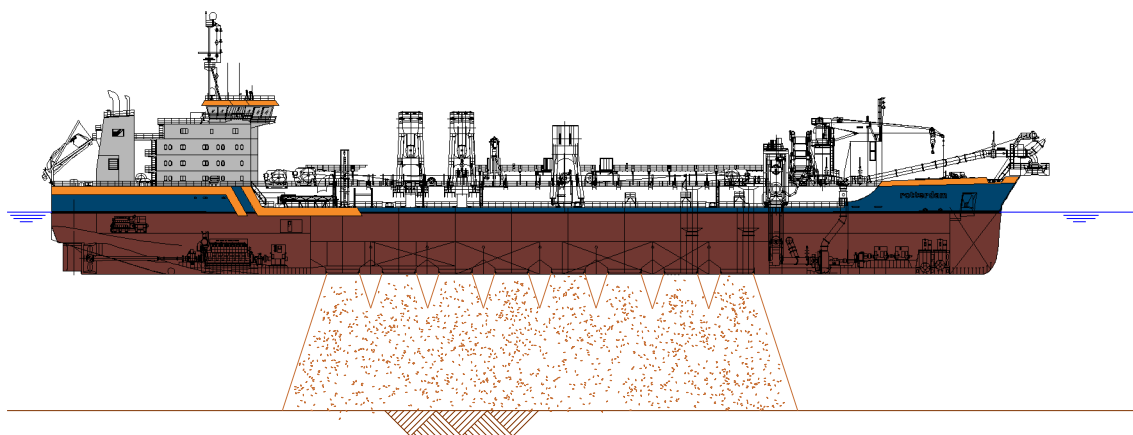


Figure 4.1: TSHD discharge method: dumping.

4. WORK METHODS

4.2 Rainbowing

Another method for a TSHD to discharge her load is rainbowing (figure [4.2]).



Figure 4.2: TSHD discharge method: rainbowing.

Rainbowing is the method of choice to discharge huge quantities of sand in shallow locations or ashore. This technique does not require a floating pipeline, and a land line, with all the associated extra costs. During rainbowing, following parameters are important for production output of the dredger [van de Velde, 2008]:

- Vertical angle of the rainbow nozzle;
- Nozzle design;
- Nozzle opening diameter;
- Loaded draught of the dredger (and especially: forward draught).

In the 1990s most TSHD were equipped with a rainbow nozzle in a 45° angle to the vertical. This was indeed the best angle to reach long distance, from a ballistic point of view. Since then, it was observed that a 45° nozzle creates large craters on the sand fill area, and that a large part of the sand flows back towards the TSHD. A 30° nozzle is now commonly used [VOUW, 2010b]. The sand is projected in a more flat trajectory, and end up further on the sand fill. Back flow is less then by using a 45° rainbow nozzle. The final distance reached is comparable to a 45° rainbow nozzle [Burgmans, 2003]. Another factor to be kept in mind is the height of the rainbow nozzle (and the height of the discharge area) above the waterline.

The most important parameter of all is the nozzle diameter. A small diameter nozzle means less flow, hence less hourly production, but the sand will be projected over a longer distance, because of the higher exit velocity. Rainbow distances in excess of 150 m are possible, with the power available on most jumbo TSHD's today, but at the cost of some 30% extra discharge time [van de Velde, 2008]. More flexibility in the choice of rainbow distance versus production, for large jumbo TSHD's, such as the TSHD "HAM 318" (figure [4.3]), are equipped with two nozzles of different diameter; which can be used together if maximum output is required.



Figure 4.3: TSHD “HAM 318” rainbowing with two nozzles at Palm Deira, Dubai
(*Courtesy Van Oord*)

The only prerequisite for rainbowing is close access of the loaded TSHD to the discharge location. This may often require to manoeuvre the TSHD against the beach slope. Draught can be a limitation, as the ship may not be able to reach the sand fill. However, in most cases, the dredger can change forward draught fast during the first minutes of rainbowing, spraying massive amounts of sand, then pushing forward on the beach. Beaching the TSHD (pushing the bow through the sand) wears down the steel plates in contact with the sand slope. Some TSHD are limited by design and dare not touch the underwater sand slope. Design limitations are mostly: position of cooling water intake and strengthening of the bow.

The maximum reclamation height for rainbowing, for the Maasvlakte II project, is around mean sea level (MSL).

4.3 Spraying

4.3.1 Back filling through Suction Pipe with a TSHD

One of the methods of spraying is by using one of the suction pipes of the TSHD (figure [4.4]). Normally the suction pipe is used for loading, but some of the TSHD’s can use it for back filling. This results in a process that can be described as spraying. On the Maasvlakte II project this method is among others used by the TSHD “Geopotes 14”. The sand is pumped from the hopper through the starboard (SB) pump to the port side (PS) where it normally goes through the PS pump to the front of the vessel, to discharge the load by rainbowing or pumping through a pipeline. In this case it goes directly to the PS suction pipe. The suction pipe has a stand off distance (*sod*) of 3.5 m from the seabed. The discharge mixture density must be high ($\approx 1600 \text{ kg/m}^3$) and the discharge

4. WORK METHODS

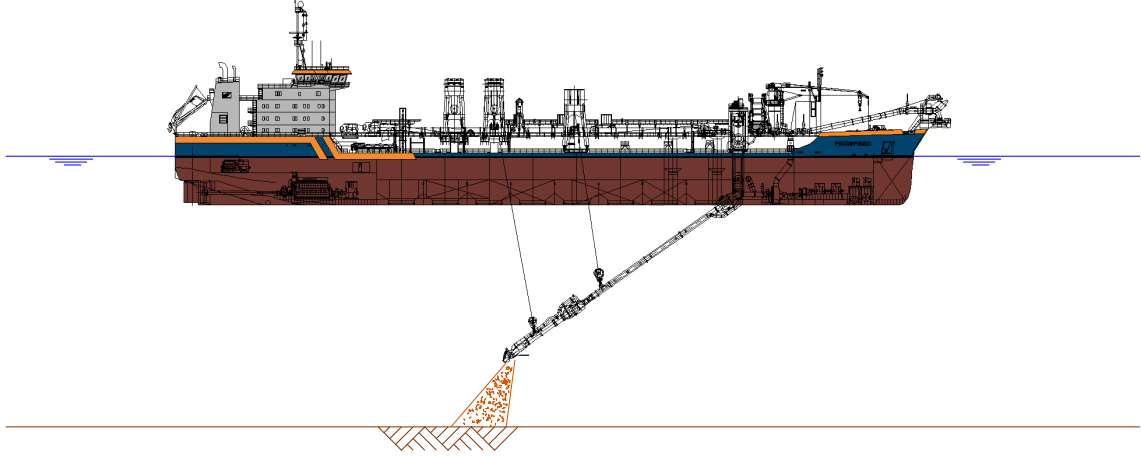


Figure 4.4: Spraying by using the back fill method of a TSHD.

velocity low (≈ 4 m/s). These figures are achieved from field test on the Maasvlaket II project. The field test are carried out to achieve under which discharge properties, the most accurate slope is constructed.

The main goal of this method is to create under water sand bodies with great accuracy. Relative densities of about 70% have been achieved. This is checked by using the correlation of Baldi and Lunne and Christoffersen. This method is limited to a certain water depth because the draghead needs to be lower than the maximum draught of the vessel and has a stand off distance of 3.5 m from the sand body. The sailing speed (v_{sp}) during backfilling through the suction pipe is about 0.31 m/s until 0.62 m/s.

4.3.2 Spraying with Suction Dredger “Slidrecht 27”

The suction dredger (SD) “Slidrecht 27” (figure [4.5]) is equipped with a dustpan (figure [4.6]). Normally it sucks up the sand with this dustpan but on the Maasvlakte II Project this dustpan is used as the spray nozzle. So the flow direction is now opposite to the normal situation.



Figure 4.5: TSHD “HAM 316” connected to the SD “Slidrecht 27” to spray the under water sand bodies.

A floating pipeline is connected at the back of the SD “Slidrecht 27”, where a TSHD can be connected to discharge her load. The draught of the SD “Slidrecht 27” is less than that of a TSHD and the dustpan sticks out in the front of the vessel, so it is possible to

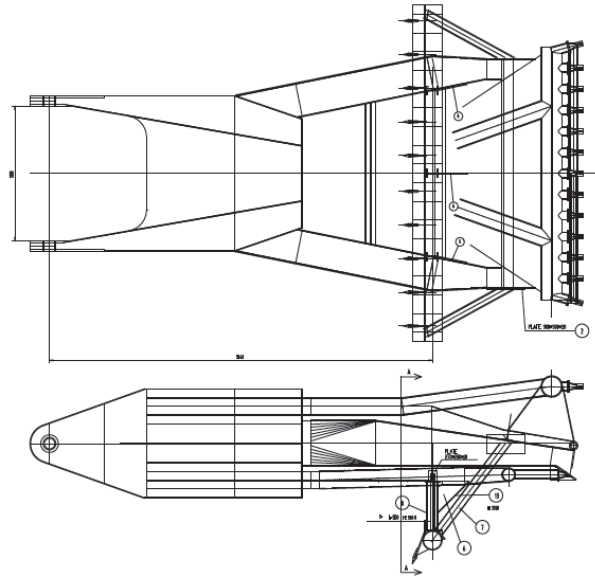


Figure 4.6: Dustpan of the SD “Sliedrecht 27”.

construct higher sand bodies under water compared to spraying with a TSHD. A stand off distance of 3 m is used for the dustpan. One of the short comings of using the dustpan is causing the insufficiency to the spreading of the mixture is insufficient. Another limitation of this method is that the SD “Sliedrecht 27” is less flexible in its movement due to anchor handling. Therefore it is more difficult to spray thin layers on the slope accurately. Another important restriction is the incidental use of the SD “Sliedrecht 27”, at Maasvlakte II, so chancing crews has to adjust to this type of work. Another important factor is the co-operation between the TSHD and the SD “Sliedrecht 27”.

4.3.3 Spraying with Multicat “Coastal Discovery”

This method is an improvement of the method of spraying with SD “Sliedrecht 27”, because the multicat “Coastal Discovery” (figure [4.7]) has its own propulsion and is equipped with a dynamic position system. So the multicat “Coastal Discovery” is more flexible then the SD “Sliedrecht 27”.

The spray installation is mounted on the SB side of the multicat. A stand off distance of 3.0 m is used during spraying. This results in a footprint width of approximately 40 m. A stand off distance of 3.5 m is used for a thinner layer and larger footprint. A higher stand off distance than 3.5 m is not used. The spreading of the sand is then to large. With a lower stand off distance than 3.0 m the mixture flow blows holes into the bed.

The sailing speed controls the layer thickness. In most cases the sailing speed is between 0.10 and 0.15 m/s which results in a layer thickness of 0.5 m. The sailing speed is also depending on the mixture density. A high sailing speed is required when a high mixture density is used and a low sailing speed is required for a low mixture density.

4. WORK METHODS

The coupled TSHD must be capable of giving a discharge velocity of 5 m/s and an averaged mixture density of 1600 kg/m³. Another important factor is the co-operation between the TSHD and the multicat “Coastal Discovery”.



Figure 4.7: Multicat “Coastal Discovery” equipped with spray pipe.

Chapter 5

Data Analysis

In this chapter the data analysis of the Maasvlakte II project is described. In paragraph 5.1 the analysis of the CPT's, that have been executed on the Maasvlakte II project, is described. This paragraph can be divided into three parts. The first part describes which CPT's are eligible for the analysis. The second part describes the coupling of the CPT's with the used work methods and the survey data. The last part describes the analysis of the CPT data. In paragraph 5.2 the statistical analysis is made on the retrieved relative densities from every CPT. The results of the statistical analysis are compared with the values that are mentioned in literature (i.a. Blommaart & Viergever [1995]; CROW [2004]; de Groot *et al.* [1988]; Heezen & van der Stap [1985, 1988]; Hoogeveen *et al.* [1987]; Lee [2001]; Lee *et al.* [1999]; Mastbergen & Bezuijen [1988]). The values from literature are based on field measurements, laboratory test and experience of the dredging companies. The work methods and correlations for the relative density are compared together in a statistical way. In the last paragraph 5.3, an analysis, of the hydrodynamic environment of the Maasvlakte II project, is made. This paragraph exists of two parts. The first part describes the wave environment and the last part describes the analysis of the measured hydrodynamic data of the Maasvlakte II.

5.1 CPT Data

The data of 278 CPT's, from the Maasvlakte II Project, are collected for analysis. 158 CPT's are made with the standard cone, 108 CPT's are made with the mini cone and for 12 CPT's it is unknown which type of cone is used. From the 12 unknown CPT's only the result is available. In total 182 CPT's are used for the analysis. The other 96 CPT's are not used because of the following reasons:

- CPT raw data is not available;
- CPT is taken in a dredging area such as a future port basin;
- CPT is made in the original seabed;
- Work methods are unknown;
- The sand body is constructed with stationary equipment and/or dry earthmoving equipment (area C1).

5. DATA ANALYSIS

In table [5.1], a list of the used CPT's per area (area's are shown in Appendix A) is shown. The CPT data is placed in a database with the following information namely, the CPT number, name, coordinates and the date of the CPT is made.

Table 5.1: CPT's analysed per area.

Area	Total CPT's	no. CPT's
D1 & D2	140	1 until 140
HZw, HZm & HZo	38	189, 190, 196, 197, 202, 204, 206 until 211, 213 until 216, 218 until 221, 223, 225, 226, 227, 229 until 238, 240, 241, 243 & 245
ZI	4	264 until 267

5.1.1 Work Methods and Survey Data

The work methods are specified with the help of the TSHD database. In the TSHD database the following information is stored. The name of the TSHD, the trip number, date, the load, discharge area, discharge method, d_{50} , % fines and remarks.

The Maasvlakte II Project area is divided in boxes of 500x500 m. These boxes are divided in sub boxes of 50x25 m (see also Appendix A). The big boxes are numbered as follows: Starting with the letter M then a number and then a letter, this is similar as a check board. The sub boxes have only a number. The TSHD database in this format is not very useful for the analysis so some adjustments have been made in this database.

The first adjustment is to assign, the coordinates of the centre of a dump box to every dump box. This is necessary to assign each TSHD trip to a CPT. The second adjustment is to change the discharge methods. On the Maasvlakte II project, three discharge methods are used in the project registration, namely rainbowing, dumping and pumping. This analysis discusses six discharge methods; rainbowing, dumping, pumping, back filling through suction pipe, spraying with the SD "Sliedrecht 27" and spraying with the "Coastal Discovery". The information of the other three discharge types is achieved from the remarks from the trip reports. The remarks in the trip reports give, in most of the time, the actual used discharged method. By making the analysis one of the work methods is lost, because of the fact that the date of the last CPT's is made, before the start date of spraying with multicat "Coatal Discovery".

The TSHD database has been converted with Matlab into a format that can be used for analysis. The CPT database and the TSHD database is added together by assigning to every CPT the TSHD trips that are fulfilled in a radius of 25 m around the CPT. The reason for using a 25 m radius, has to do with the Dutch engineering practice. The CPT is representative for this distance [NEN 6740, 2006]. Another reason is that for a greater radius, TSHD trips are taken into account that are not representative for that area. In

figure [5.2] the locations of the CPT's and the discharge locations of the TSHD trips are illustrated.

For each CPT, the associated TSHD trip is known. The next step is to add the survey data to each CPT. Two methods are used to determine the bed level of the TSHD trip. Method 1 is a search function, from each TSHD trip the date, time x and y coordinate is known. The survey database logs date, time x , y and z coordinate. In the survey database the nearest value for the x , y , date and time is searched, based on the TSHD trips. As a result, the value for z is now also known, because the values of z is linked to the date, time, x and y coordinate. This is also illustrated in figure [5.1]. Method 2 uses linear interpolation in time to achieve the z value from the survey database. The value of z is used in the analysis to divide the soil profile in layers in which different work methods have been used. Method 1 is used to check whether the results of method 2 are plausible.

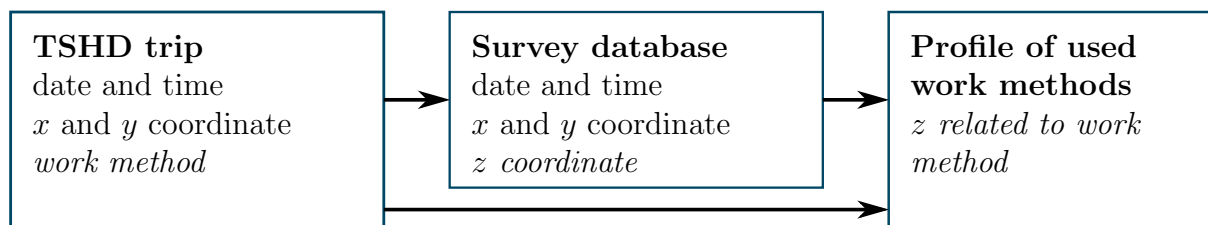


Figure 5.1: Scheme for TSHD trip, survey database and work method.

5.1.2 CPT Analysis

CPT measurement generates the following data; depth (z), cone resistance (q_c), pore pressure (u), sleeve friction (f_s) and the friction ratio (R_f). The pore pressure is not measured in all cases. The vertical effective stress (σ_v) needs to be computed in order to be able to use the relations of Baldi (equation [3.9]), Lunne and Christoffersen (equation [3.10]).

First the specific weight of soil (γ_s) needs to be determined for above groundwater level (GWS) and below GWS. A representative value of 18 kN/m^3 is assumed for above GWS and 20 kN/m^3 below GWS. A level of 0 m to NAP is assumed for the GWS. This value is around mean sea level (MSL) at Hoek van Holland. The MSL of Hoek van Holland is $+0.1 \text{ m}$ to NAP. The specific weight of water (γ_w) is computed with equation [3.1]. A value of 1025 kg/m^3 is assumed for the density of water (ρ_w), so, γ_w becomes 10.05 kN/m^3 .

The pore pressure (σ_w) is computed as follows. If the pore pressure is measured (u), then $\sigma_w = u$. In the other cases it is assumed that the pore pressure behaves hydrostatic. This assumption is based on the CPT's where the pore pressure is measured, in those cases the pore pressure behaves hydrostatic. The CPT's that also measures the pore pressure are given in Appendix D.1. The computed hydrostatic pore pressure is illustrated in the pore pressure graph. This assumption has a negligible influence for the relative density.

5. DATA ANALYSIS

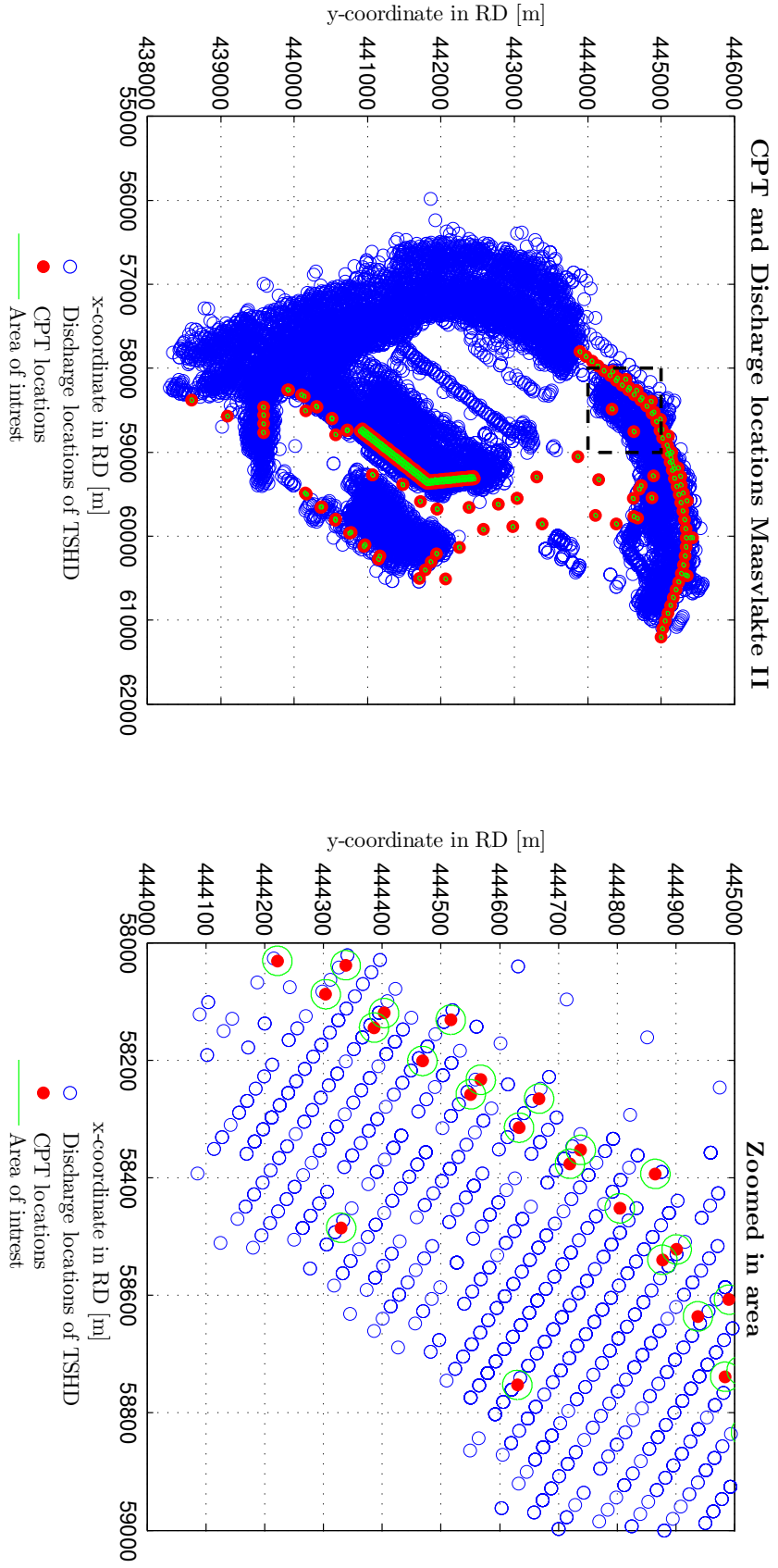


Figure 5.2: CPT and discharge locations Maasvlakte II project.

That can be seen in the CPT's of Appendix D.1. In the graph of the relative density, the relative density based on the measured pore pressure and on the computed hydrostatic pore pressure is illustrated. The differences are small. Some variation is visible in the relative density for above GWS. Those variations are small. So, it is a logic assumption to use the hydrostatic pore pressure in the cases that the pore pressure is not measured. The hydrostatic pore pressure is computed with equation [5.1].

$$\sigma_w = z \cdot \gamma_w \quad [5.1]$$

Equation [5.1] can only be used below GWS; above GWS the value of $\sigma_w = 0$. The ground pressure (σ_g) can be computed with equation [5.2].

$$\sigma_g = z \cdot \gamma_s \quad [5.2]$$

The value of γ_s depends on the value of z . Is the value of z above GWS then the values of γ_s above GWS is used otherwise the value for γ_s below GWS is used. Since σ_w and σ_g are known, σ_v can be computed with equation [5.3].

$$\sigma_v = \sigma_g - \sigma_w \quad [5.3]$$

Since σ_v is known, it can be used for the relative density (R_e) relation of Baldi (equation [3.9]) and for the relation of Lunne and Christoffersen (equation [3.10]).

The next step is the analysis of the TSHD trips to make a work method profile over the depth of the constructed sand body. A relation can be made between the R_e and the work method, with the work methods profile .

The last part of the analysis exist of the CPT Soil Behaviour Type (SBT) chart [Robertson *et al.*, 1986]. In figure [5.3] the SBT of CPT-001 is illustrated.

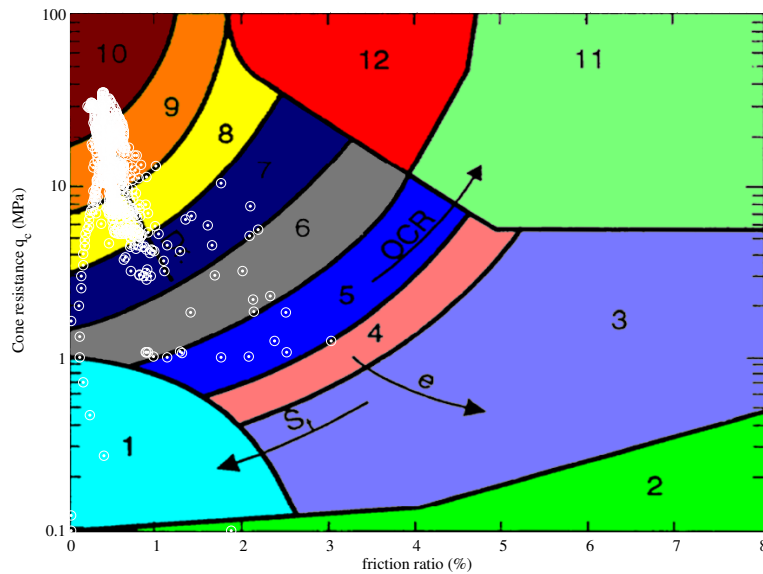


Figure 5.3: CPT Soil Behaviour Type (SBT) chart [Robertson *et al.*, 1986] for CPT-001.

5. DATA ANALYSIS

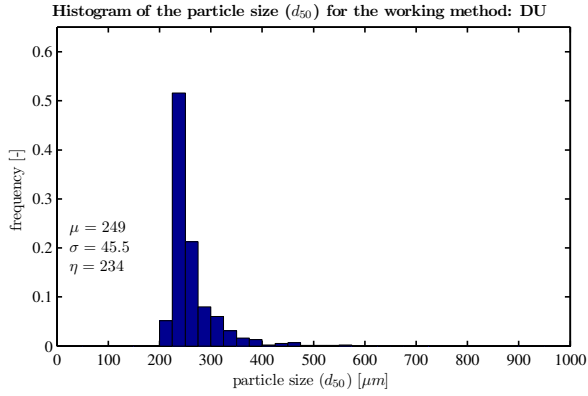
The numbers in figure [5.3] stand for a soil type, which is mentioned below.

1. Sensitive fine grained
2. Organic material
3. Clay
4. Silty clay to clay
5. Clayey silt to silty clay
6. Sandy silt to clayey silt
7. Silty sand to sandy silt
8. Sand to silty sand
9. Sand
10. Gravelly sand to sand
11. Very stiff fine grained*
12. Sand to clayey sand*
* over consolidated or cemented

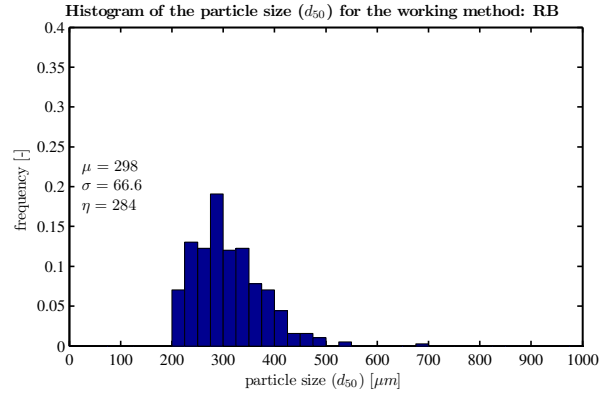
Figure [5.3] is not used in the way it is presented here. The information of this figure [5.3] is translated into a soil profile.

“It is often important to realize that classification charts are generalized global charts that provide a guide to SBT. The charts cannot be expected to provide accurate prediction of soil type for all soil conditions.” [Robertson *et al.*, 1986]

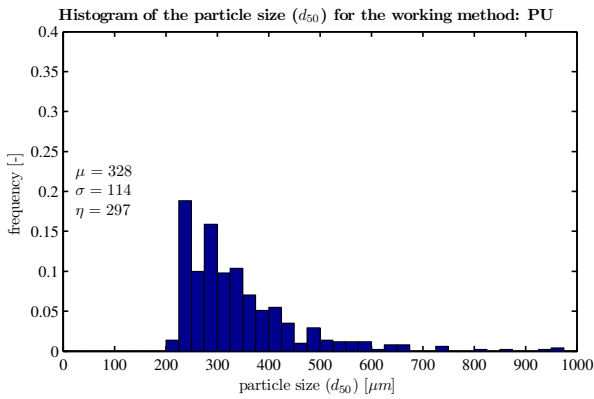
A text file has been made, for the analysis, starting the number and name of the CPT, execution date, RD-coordinates and work methods. The presented description of every work method includes; layer thickness, the minimum, maximum and mean value of the relative density R_e according to Baldi (BA), Lunne and Christoffersen (LU) and the minimum, maximum and mean value of the d_{50} and minimum, maximum and mean value of the % fines. For the d_{50} and % fines there is only a remark. This has to do with the fact that the d_{50} and % fines are measured in the hopper of the TSHD during suction with a CPA machine. In figure [5.4] are illustrated the measured d_{50} on-board of the TSHD by means of histograms. The results of the CPT analysis are illustrated in Appendix D.2. The different work methods are known for every CPT, so cross sections with indication of the applied work methods per area can be made. One cross section is made for area D1 & D2. One cross section is made for the area ZI. Four cross sections are made for the area HZw, HZm & HZo, namely for the offset 100 m, 130 m, 160 m and 185 m. The centre lines that are used to make the cross sections are displayed on the drawing in Appendix A. In Appendix E the cross sections are given for the different area's.



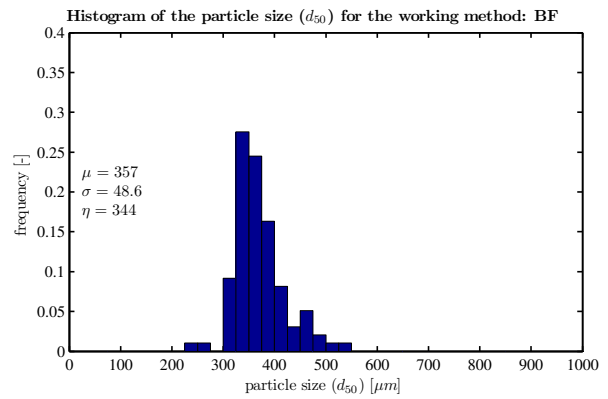
(a) d_{50} for work method: DU.



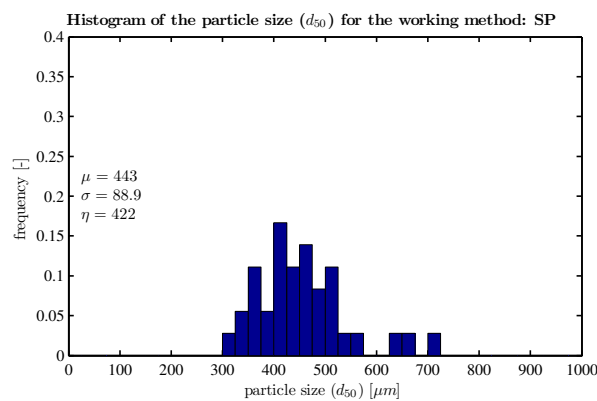
(b) d_{50} for work method: RB.



(c) d_{50} for work method: PU.



(d) d_{50} for work method: BF.



(e) d_{50} for work method: SP.

Figure 5.4: Histograms of the measured d_{50} on-board of the TSHD.

5.2 Statistical Analysis of Relative Density Data

The statistical analysis of the relative density data is necessary for the mutually comparison of the relative densities for the different work methods. After all, only with a good statistical analysis, it can be reliably shown whether there is a significant difference in relative density for different work methods.

Paragraph 5.2.1 mentions which statistical parameters are determined and explained which tests are used to determine the probability density distribution. In paragraph 5.2.2 the statistical testing of different statistical hypotheses is mentioned. Also the different types of the statistical test, used in this paragraph 5.2.2, are explained.

The work methods are mentioned with the following abbreviations:

- Dumping (DU);
- Rainbowing (RB);
- Pumping (PU);
- Back filling through suction pipe (BF);
- Spraying with SD “Sliedrecht 27” (SP).

5.2.1 Determination of the Probability Distributions and Statistical Parameters per Work Method

A dataset of the relative density (R_e) per work method is realized for every CPT. All those datasets are put together per area and for the entire Maasvlakte II project. This is called data pooling. The pooling of the data is possible because on the project Holocene and Pleistocene sand is used from the same borrow area, the same work methods are used and the same type of field measurements are used. After the data per relative density correlation, work method and area are added together. Histograms are made per relative density correlation, work method and area. A best fitting probability density distribution (PDF) is determined for each histogram. The PDF is an important tool to approximate the probability distribution of the average of independent random variables [Dekking *et al.*, 2005]. The reason that the PDF is determined is due to the fact that the PDF determines which statistical test can be used. The produced datasets (also called groups or populations) are analysed by using the computer program “Bestfit”. The computer program “Bestfit” determines which PDF fits best through the population based on three test methods, namely:

1. χ^2 Test;
2. Kolmogorov-Smirnov Test (K-S Test);
3. Anderson-Darling Test (A-D Test).

Also for each dataset the following statistical parameters are determined, per relative density correlation, per work method and area, mean (μ), standard deviation (σ), median (η) and variance (Var).

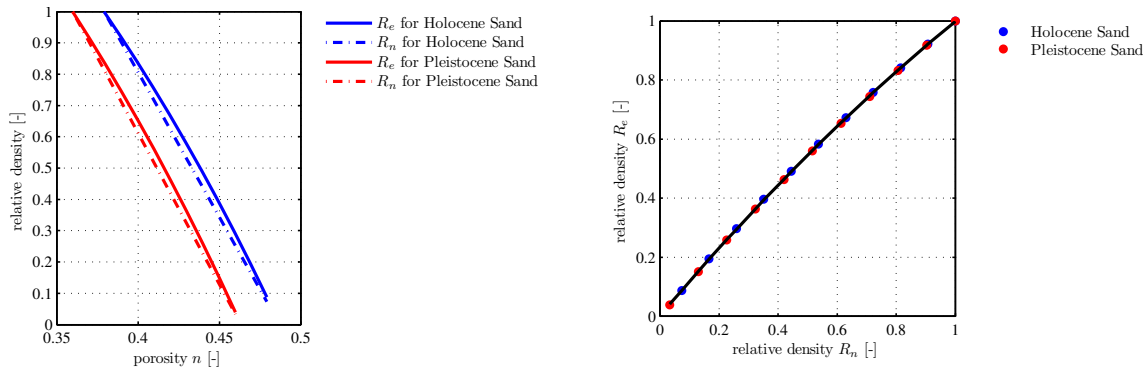
The χ^2 Test compares the histogram of the statistical material with the selected probability density function [CUR 190, 1997; Vrijling & van Gelder, 2006a].

The Kolmogorov-Smirnov Test is applicable to observations from given distributions which have not been classified. The K-S Test returns the maximum deviation from a point of the given distribution. This gives an indication of the fit with the observations surrounding the modal value (is the value that occurs most frequently in a population or a probability distribution) of the population if the approximation of the population is correct [Vrijling & van Gelder, 2006b].

The Anderson-Darling test [Anderson & Darling, 1952; Stephens, 1974] is used to test whether a sample of data came from a population with a specific distribution. It is a modification of the K-S test and gives more weight to the tails than the K-S test does. The K-S test is distribution free in the sense that the critical values do not depend on the specific distribution that is being tested. The A-D test makes use of the specific distribution in calculating critical values. This has the advantage of allowing a more sensitive test and the disadvantage that critical values must be calculated for each distribution [NIST/SEMATECH, 2010].

The computer program “Bestfit” runs those test for 18 different PDF’s. The distributions are mentioned in Appendix F.1. The result of the program “Bestfit” is a ranking per test method of which PDF fits the best through each given population per relative density correlation, work method and area. The best fitted PDF of the three statistical test methods is illustrated in table [F.1] in Appendix F.2. The histograms are illustrated in Appendix F.3. The results of these statistical analyses are given in table [F.2] in Appendix F.2.

The results in table [F.2] are compared with the results for R_n in the literature (table [3.4]). The mentioned values of μ in table [F.2] are the R_e values for the Maasvlakte II project. There is only one problem; the result of table [F.2] cannot be compared with table [3.4], because table [F.2] has values mentioned in R_e and table [3.4] has values mentioned in R_n . So, first the correlation between R_n and R_e needs to be determined.



(a) Relation between porosity and relative density.

(b) Correlation between R_n and R_e .

Figure 5.5: Comparison between porosity and the different kind of relative densities.

5. DATA ANALYSIS

The relation between porosity (n) and the relative density is computed, with the parameters from paragraph 2.6 and with equation [3.5] and equation [3.6]. The results are illustrated in figure [5.5a]. A scatter plot of the combination R_n and R_e for the same n can be made, from the data of R_e and R_n from figure [5.5a] to show the relation between R_n and R_e . This scatter plot is illustrated in figure [5.5b]. A trend line is fitted through those data points. The trend line has the following fitting equation [5.4].

$$R_e = -0.1805 \cdot R_n^2 + 1.1774 \cdot R_n + 0.0021 \quad [5.4]$$

The results in table [3.4] can be translated into values for R_e . The results are given in table [5.2]. The result from literature and from the statistical analysis can be compared now with each other, see table [5.2]. It is obvious from table [5.2] that the relative densities per work method for the Maasvlakte II project are much higher than the results from literature and higher than the two mentioned projects in Hong Kong. In chapter 6 physical hypotheses are drafted in order to try to explain why the relative densities of the Maasvlakte II project are higher than the values found in literature and the projects in Hong Kong.

5.2.2 Statistical Testing of the Statistical Hypotheses

The following step is to compare the different groups per work method and the groups per work method per CPT with each other. A group of a sample is part of a population. These comparisons can be made e.g. t-test, F-test or Analysis of variance (ANOVA). These tests are called parametric statistical tests [McClave *et al.*, 2005]. The only problem of these tests is that they are only applicable for groups that have distributions that are approximately normally distributed. From table [F.2] it is clear that not all the groups are normally distributed. Therefore non-parametric tests are needed to make the computations. These tests are called distribution-free tests. Distribution-free tests are statistical tests that do not rely on any underlying assumptions about the probability distribution of the sampled population (group) [McClave *et al.*, 2005]. One of the tests that can be used now is a kind of the Wilcoxon Rank Test [Wilcoxon, 1945]. But, the Wilcoxon Rank Test can only be used by comparing two groups. Comparing of multiple (more than two) groups the Kruskal-Wallis Test [Kruskal & Wallis, 1952, 1953] is used. The Kruskal-Wallis Test compares the medians of the groups, and returns the probability (p) for the null statistical hypothesis that all groups are from the same population. Sometimes it is preferable to perform a test to determine which groups are significantly different, and which are not. This is done by a Multiple Comparison Test (MC Test). The following statistical hypotheses are tested with the Kruskal-Wallis Test:

- I. *The probability distributions per work method according to the relative density (R_e) correlation of Lunne and Christoffersen are equivalent (figure [5.6a]).*
- II. *The probability distributions per work method according to the relative density (R_e) correlation of Baldi are equivalent (figure [5.6b]).*

Table 5.2: Relative densities for different kind of activities from literature, projects and Maasvlakte II.

Activity	Relative density from									
	Literature		West Kowloon		CLK	Maasvlakte II				$\frac{R_{e;Maasvlakte}}{R_{e;Literature}}$
	R_n	R_e	R_e	R_e	R_e	LU	BA	LU	BA	
Dumping under water (< 10 m)	0.50	0.55	0.43	0.37-0.45	0.62	0.69	1.13	1.25	-	-
Dumping under water (> 10 m)	0.60	0.64	0.62	0.50-0.60	-	-	-	-	-	-
Spraying under water	0.40 ¹	0.44	-	-	0.62	0.56	1.41	1.27	0.67	1.45
Back filling through the suction pipe	0.40 ¹	0.44	-	-	0.60	0.67	1.52	1.45	0.67	1.45
Rainbowing (below LAT)	0.40 ¹	0.44	0.50	0.37-0.45	0.60	0.67	1.36	1.52	0.85	1.28
Rainbowing (above LAT)	0.70	0.74	-	-	0.85	0.95	1.15	1.28	0.95	1.28
Hydraulic reclamation (below LAT)	0.40 ¹	0.44	-	0.37-0.45	0.55	0.60	1.25	1.36	0.60	1.36
Hydraulic reclamation (above LAT)	0.70	0.74	0.80	0.70-1.00	0.98	1.05	1.32	1.42	1.05	1.42

¹In literature the following methods are taken as equivalent: spraying under water, back filling through the suction pipe, rainbowing (below LAT) and hydraulic reclamation (below LAT)

5. DATA ANALYSIS

A boxplot and a Multiple Comparison Test per work method is made, for every Kruskal-Wallis Test, and are illustrated in figure [5.6]. In table [5.3] is presented the probability (p) and the conclusion which indicated that the tested distributions are equivalent.

Table 5.3: Test results of the Kruskal-Wallis Test.

	Probability (p) [-]	Conclusion
I.	0.0	the statistical hypothesis is rejected (figure [5.6a] and [5.6c])
II.	0.0	the statistical hypothesis is rejected (figure [5.6b] and [5.6d])

If the probability is near zero, this casts doubt on the statistical hypothesis and suggests that at least one sample median is significantly different from the others. If that is the case, than the figures [5.6c] and [5.6d] visualize this. In the figures [5.6c] and [5.6d] illustrates the x , the median value of the work method, the line through the x expresses the standard error. The magenta dashed lines illustrates the range, where the other work methods needs to fit. If the work method is coloured red then the work method does not fit, is the work method coloured green than it fits. The Kruskal-Wallis Test test all the possible combinations, only one is illustrated in figure [5.6c] and figure [5.6d].

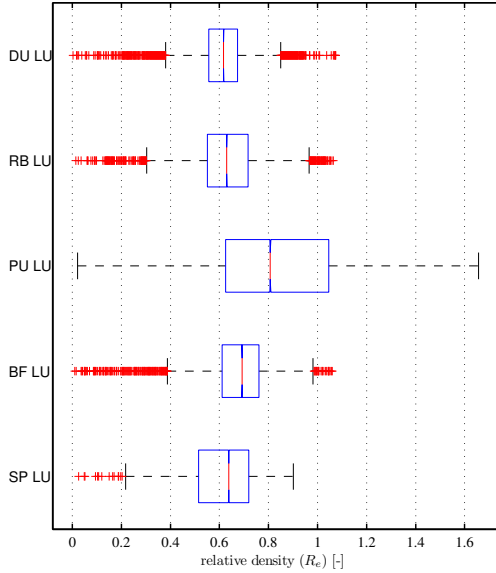
From table [5.3], statistical hypothesis (I.) and (II.), it is clear that the different work methods are not related to each other. So the relative densities achieved per work method have no statistical relation to another work method. Thus, for fulfilling contract requirements, based on the relative density, the choice of a work method determines the obtained relative density.

It is also possible to make a comparison between the different work methods and the used relative density correlations. This comparison can be made with the Friedman Test [Friedman, 1937, 1939, 1940]. This comparison is not made, because in this case it is better to test the difference between the relative density correlations per work method with the Wilcoxon Rank Sum Test. The following statistical hypothesis is tested with the Wilcoxon Rank Sum Test:

- III. *The probability distributions corresponding to the relative density (R_e) correlation of Baldi and Lunne-Christoffersen per work method are equivalent.*

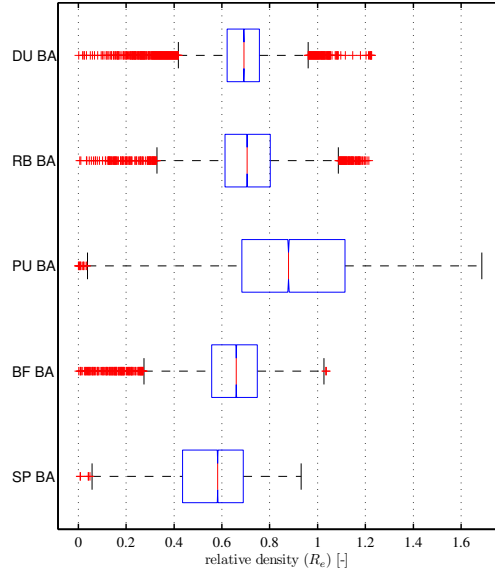
The result of the Wilcoxon Rank Sum Test are given in table [5.4]. The Wilcoxon Rank Sum Test is performed with a 0.05 significance level. So, if the probability is lower than 0.05, the statistical hypotheses will be rejected.

Comparison between the different CPTs by means of a Boxplot
 Work method: DU & RB & PU & BF & SP
 Relative density relation: Lunne (LU)



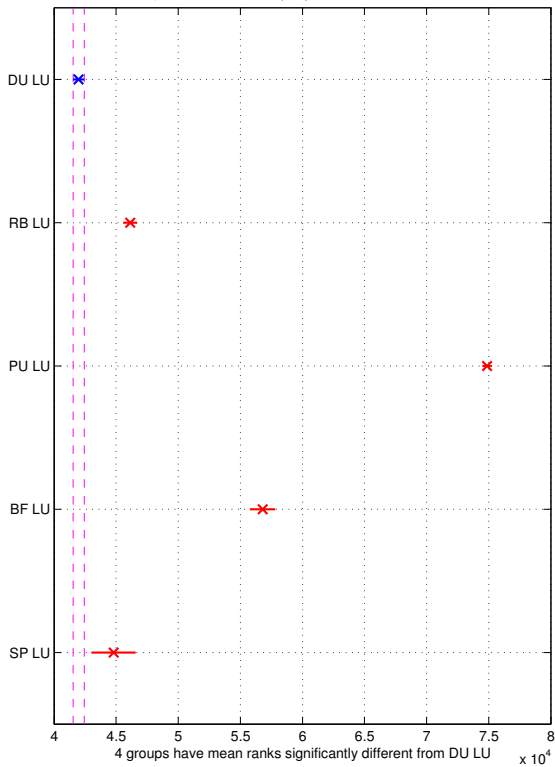
(a) Boxplot for the correlation of Lunne and Christoffersen.

Comparison between the different CPTs by means of a Boxplot
 Work method: DU & RB & PU & BF & SP
 Relative density relation: Baldi (BA)



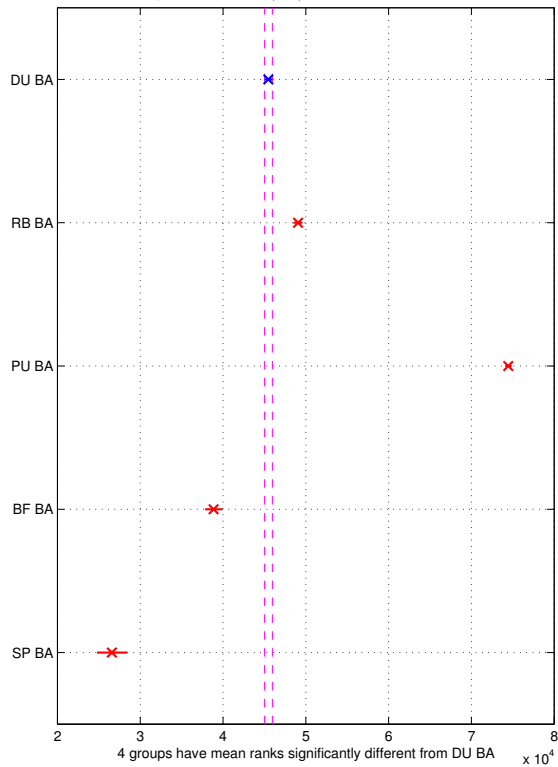
(b) Boxplot for the correlation of Baldi.

Comparison between the different CPTs by means of a MC-test
 Work method: DU & RB & PU & BF & SP
 Relative density relation: Lunne (LU)



(c) Results of the Multiple Comparison Test for the correlation of Lunne and Christoffersen.

Comparison between the different CPTs by means of a MC-test
 Work method: DU & RB & PU & BF & SP
 Relative density relation: Baldi (BA)



(d) Results of the Multiple Comparison Test for the correlation of Baldi.

Figure 5.6: Test results of the Kruskal-Wallis Test.

5. DATA ANALYSIS

Table 5.4: Test results of the Wilcoxon Rank Sum Test.

Hypotheses	Work method	Probability (p) [-]	Conclusion
III.	DU	0.0	the statistical hypothesis is rejected
	RB	0.0	the statistical hypothesis is rejected
	PU	0.0	the statistical hypothesis is rejected
	BF	$4.46 \cdot 10^{-26}$	the statistical hypothesis is rejected
	SP	$1.34 \cdot 10^{-28}$	the statistical hypothesis is rejected

From the result, in table [5.4], it is clear that there is no relation between the relative density correlations. It may be concluded that the choice of the correlation for the relative density relies on the conditions that are given for the correlations. The Pleistocene and Holocene sand fulfil those conditions, but it is better to determine the soil constants, that are mentioned in equation [3.9], for Pleistocene and Holocene sand to get a better prediction for the relative density.

5.3 Hydrodynamics

In this paragraph the hydrodynamic conditions at the Maasvlakte II project are mentioned. The first sub-paragraph treats the wave environment of the North Sea and the second sub-paragraph treats the measured hydrodynamic data of the Maasvlakte II project.

5.3.1 Wave Environments

Davies [1980] has identified four major deep water wave environments (figure [5.7]), namely:

- Storm wave environments;
- West coast swell environments;
- East coast swell environments;
- Protected sea environments.

Besides that, Davies also identified trade, monsoon and tropical cyclone influences. From figure [5.7] it is clear that the North Sea has a storm wave environment.

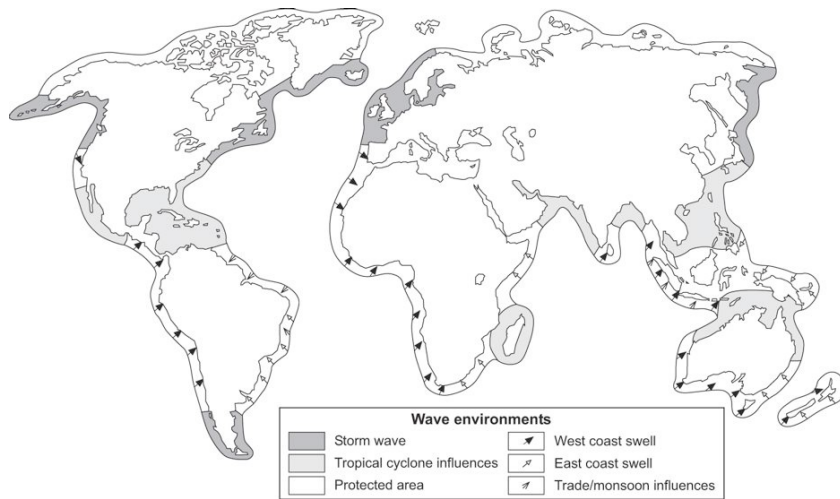


Figure 5.7: World wide distribution of wave environments.
 From Masselink *et al.* [2011] modified from Davies [1980].

A storm wave climate has the following characteristics [Bosboom & Stive, 2010] (see also Short [2005]):

- The most important and energetic wave environment;
- Located between 40° and 60° North and South;
- Operates in winter in the Northern hemisphere (NH);
- Locally generated by westerlies and associated mid-latitude cyclones;
- Waves are steep, short-crested, irregular and multi-directional (sea);
- Direction is predominantly westerly to south-westerly in the NH impacting west facing coasts (Dutch coast);
- Deep water wave heights are 2-3 m 90% of the time, 5-6 m 10% of the time;
- Wave periods are about 5 s, longer during storms.

5.3.2 Hydrodynamic Data of Maasvlakte II Project

The data is used from measurement spot “Stroommeetpaal Maasmond” and “Hoek van Holland” for the hydrodynamic analysis. The significant wave height (H_{m0}), mean wave energy period (T_{m-10}), flow velocity (SSV_{10}) and the flow direction (SRV_{10}) are measured at the ‘Stroommeetpaal Maasmond’. From measurement spot “Hoek van Holland” the predicted and measured astronomical tide are obtained.

The start date of construction, when the last CPT is made and the construction time is specified, for every area, see table [5.5] for the results. The construction periods are also plotted into the hydrodynamic graphs, which are illustrated in Appendix G.

5. DATA ANALYSIS

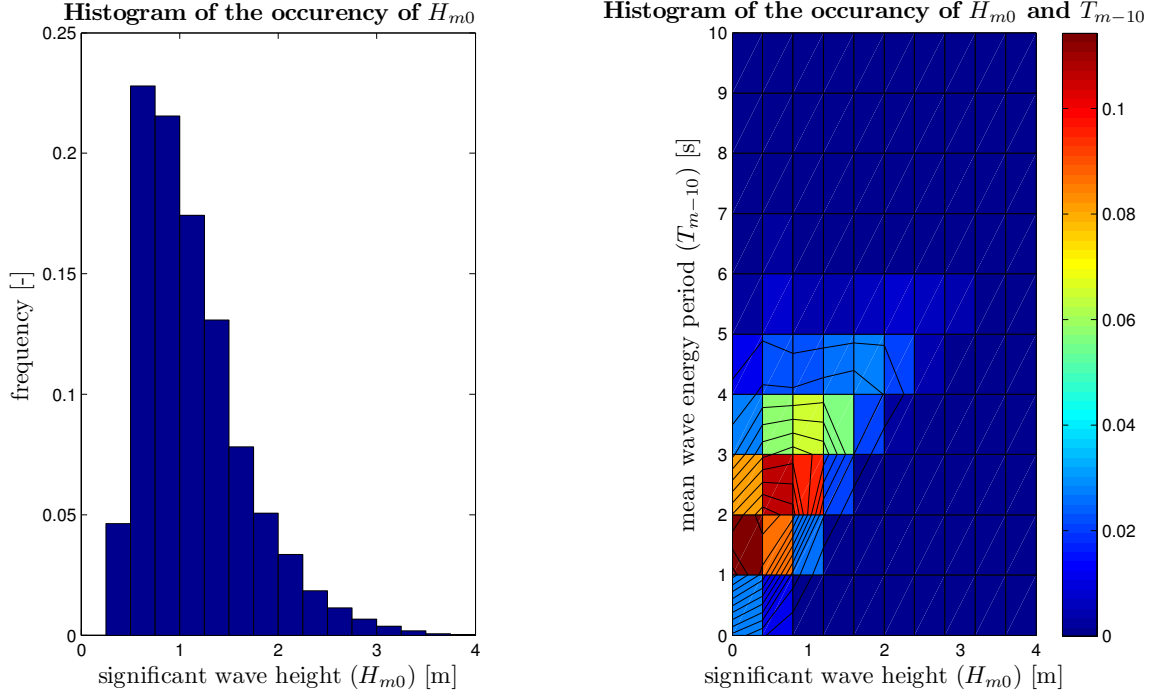


Figure 5.8: Wave statistics “Stroommeetpaal Maasmond”.

Table 5.5: Construction time per area.

Area	Start construction	Last CPT made	Construction time
D1 & D2	8-4-2009	18-8-2009	132 days
HZw, HZm & HZo	3-9-2009	13-4-2010	222 days
ZI	4-8-2009	11-5-2010	280 days

The hydrodynamic data of Maasvlakte II project is also analysed in a statistical way. The results are illustrated in figure [5.8]. For every area the maximum value of H_{m0} and SSV_{10} are obtained in the construction period. The results are displayed in table [5.6].

Table 5.6: Maximum hydrodynamic values per area.

Area	H_{m0} [m]	T_{m-10} [s]	SSV_{10} [m/s]	SRV_{10} [°]
D1 & D2	2.78	6.72	1.359	4.42
HZw, HZm & HZo	3.87	7.27	1.532	5.28
ZI	3.87	7.27	1.532	5.28

In Appendix H the progress of the construction of the Maasvlakte II is illustrated. From

this it is clear that area ZI is constructed in a sheltered area. This area does not suffer from storm conditions because of the sheltering, but the obtained relative densities for this area (table [F.2]) are also high.

The northern head of area D1 is only sheltered as the constructing is started in the areas HZw, HZm & HZo. So, the head of area D has to suffer under some storms during construction. A few times during construction the head of D1 is repaired, due to storm damage.

Another phenomenon is the outflow of the “Nieuwe Waterweg” into the North sea. This causes higher waves during storm. The increase of wave height is locally. Only the North part, the so called hard sea defence (area HZ) is partly affected by this phenomenon. This effect has not a visible influence for the relative density for the work methods dumping and rainbowing. This can be seen in table [F.2] by comparing the different areas with each other. It is remarkable that for the correlation of Baldi, the relative density for area HZ is the lowest and that for the correlation of Lunne and Christoffersen, the relative density for area HZ is the highest. This statement is only valid for the mean (μ) value of the relative density. By comparing the median (η) the same trend is visible as by the mean, but this is not the case for the correlation of Baldi with the work method rainbowing. For the work methods back filling through the suction pipe and Spraying with SD “Sliedrecht 27”, an influence cannot be determined, because these work methods are only used in the area HZ. Thus there is no further reference data available.

5. DATA ANALYSIS

Chapter 6

Physical Hypotheses

In this chapter the physical hypotheses are mentioned. A physical hypothesis is an assumed physical explanation for a phenomenon. In this case the physical hypotheses are used to explain the relation between physical processes and the relative density. The physical hypotheses are used to retrieve, the major/minor physical processes that influence the relative densities on the Maasvlakte II project. In this chapter the physical processes are described theoretical and in chapter 7, the computations are made belonging to the physical processes. The computations results of chapter 7 are used to check, the assertion of the physical hypotheses. The following physical hypotheses are further investigated:

- I. *If sand settles from a density flow with a low near bed sand concentration and therefore with a low effect of hindered settlement then the packing of the deposited sand layer depends mainly on the actual value of the bottom shear stress and turbulence. The relative density will increase with the bottom shear stress (e.g. van Rhee [2002a]). Because of the shear stress the particles will settle with a dynamic settling process ("shaking by turbulence") between the already settled particles.*

- II. *If sand settles from a flow with a high near bed sand concentration and therefore with a high effect of hindered settlement and increased viscosity then the packing of the deposited sand layer will increase less with increasing shear stress. This is due to the reduction of the dynamic behavior of the grains during settling, as a result of the high viscosity and the hindered settlement, by which the movement of the particles relative to each other is damped out. This prevents a good compaction of the settled sand particles and will allow the particles to settle into a loosely packed "card house" structure.*

- III. *When sand is settling at short distance resulting in a steep slope the sand is transported to the toe of the slope by flow slides. The sand-mass of the flow slide comes to a hold at the toe of the slope having a high viscosity and extreme effect of hindered settling. The sand settles then with a shear stress of zero into a loosely packed "card house" structure resulting in a low relative density.*

6. PHYSICAL HYPOTHESES

IV. *The hydrodynamic environment under storm conditions causes a high shear stress at the bed level that causes a high relative density in the bed level.*

Paragraph 6.1 explains how flow slides can occur and how the sedimentation length is computed. This information is required for physical hypothesis (I.), (II.) and (III.). Paragraph 6.2 describes the shear stress and the shear stress due to density currents, waves and currents. This information is required for physical hypothesis (I.), (II.), (III.) and (IV.). Paragraph 6.3, the influence of the sedimentation velocity on the relative density is described. This information is required for physical hypothesis (I.) and (II.).

Porosity and relative density are related to each other. First, it will be explained what is porosity and how the porosity influences the relative density. Porosity is the amount of pores in a particle skeleton. For a high relative density you need a low porosity (figure [3.1]). The particles are stacked in a cubic array, see figure [6.1a]. By placing a shear force on the spheres the spheres will move more close to each other and so the pores are decreased. In figure [6.1b] the most dense packing for spherical particles is illustrated. So, the packing changed from a loose packing to a dense packing. If we translate the phenomenon explained above to the cause of the high relative density, then a shear stress is required, to rearrange the particle skeleton in such a way that the porosity decreases. Besides shear stress as a compacting effect, there is also shear, whether or not after liquefaction as a dilatation effect.

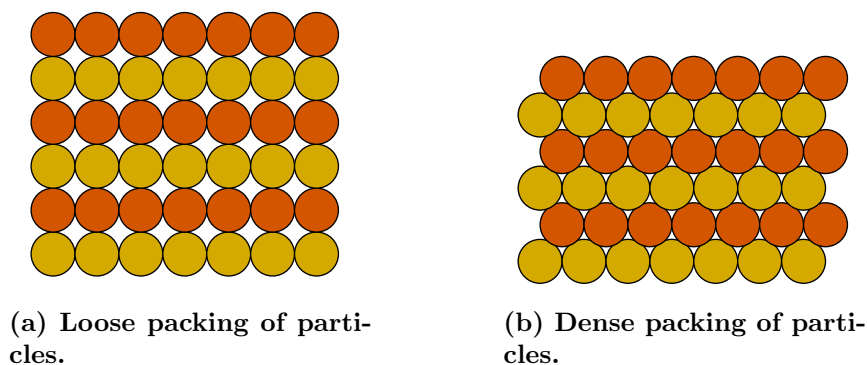


Figure 6.1: Different packings for particles.

Another possibility for a high relative density is the sedimentation of thin layers (≈ 0.5 m thick) on top of each other, see figure [6.2].

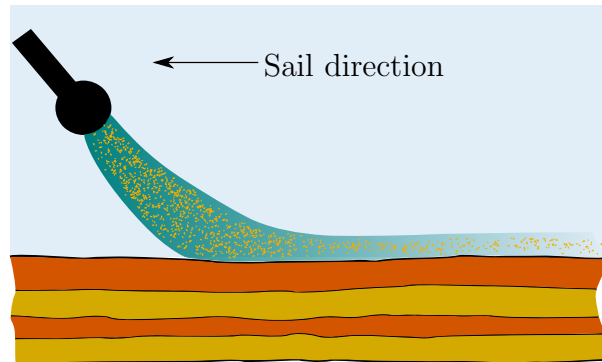


Figure 6.2: Spraying of thin layers.

On the Maasvlakte II project the thin layers are constructed with a low sailing speed, a high concentration (measured on-board of the TSHD), a high sand production and a low discharge velocity for the work methods back filling through the suction pipe and spraying with the SD “Slidrecht 27”. During sedimentation/deposition of thin layers the pore water can easily run off.

6.1 Under Water Slope built-up

The development of a sand body under water is the result of sedimentation processes. The sand settles according to two processes namely bed load transport and suspended load transport [CUR 152, 1991]. In the under water development of the slope, the geotechnical properties (e.g. liquefaction) have a greater influence than above water level. The deposited sand has a loose packing. So, it is sensitive to liquefaction. Under certain conditions, such as a large slope height (h), the slope is unstable. Therefore failure of slope stability can occur due to overloading by increasing the slope angle (β) or decreasing the slope length (l). Or the failure of slope stability can occur due to vibrations in the water by vessel movements or due to vibrations onshore by earthmoving equipment. As a result of the failure, liquefaction can occur followed by a flow slide (figure [6.3]) [CUR 152, 1991]. The specific mixture flow (q_m) above water level is governed by the mixture density. Once the flow gets under water, the driving force from gravity is reduced to the particles in the flow. Therefore, under water, the flow behaviour is predominantly defined by the specific sand production (s) instead of the specific mixture flow. The average value and the vertical distribution of the mixture density are both important. The Reynolds number determines whether the flow is turbulent or laminar. At low values for s ($s < 10$ kg/ms) and fine sands, both sediment transport processes occur in small layers. However, by high values for s ($s > 25$ kg/ms) the main process is a turbulent suspended load transport [CUR 152, 1991].

6. PHYSICAL HYPOTHESES

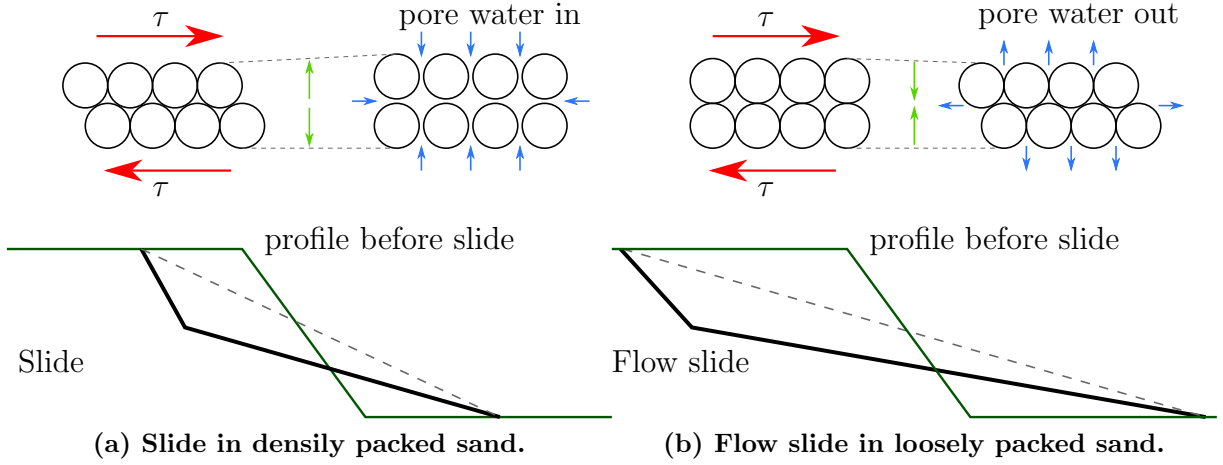


Figure 6.3: Slides and flow slides, modified from Schiereck [2004].

6.1.1 Slope Development

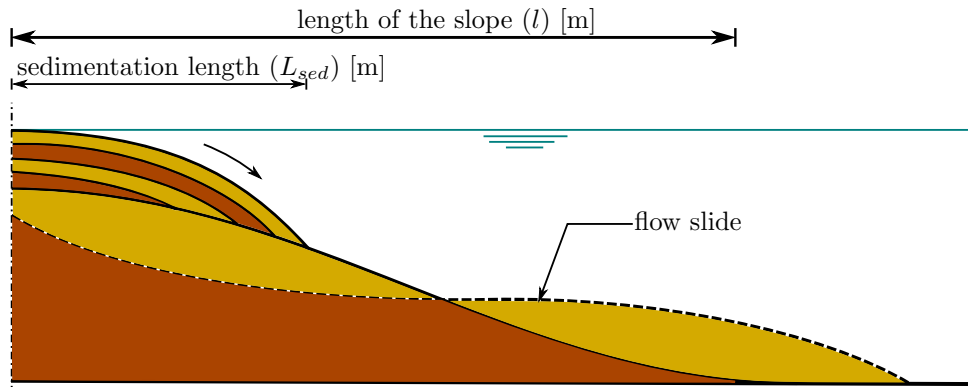
Three types of slope development under water are possible [CUR 152, 1991], see figure [6.4] for the outline of each type. When applying low and medium values of specific sand production ($s < 25$ kg/ms) and fine sand, the development of the slope under water in shallow to deep water will take place in a discontinuous manner. First, increasing slope caused by depositing of sand followed by flow slides that transport the deposited sand to deeper parts. This is observed in field measurements [de Groot *et al.*, 1988] and by experiments in a test flume [Mastbergen *et al.*, 1988].

When discharging sand, bed and suspended load transport takes place. Locally the slope height is increasing, so a critical situation is created that leads to a flow slide (figure [6.4a]). This is a continuous process which is dominated by flow slides transporting the sand to the toe of the slope. The process of flow slides is less frequently observed by coarser sand, with the same specific sand production and shallow water. However, in both cases the sand is loosely packed and the settled sand has a porosity (n_{situ}) that is higher than the critical porosity (n_{cr}).

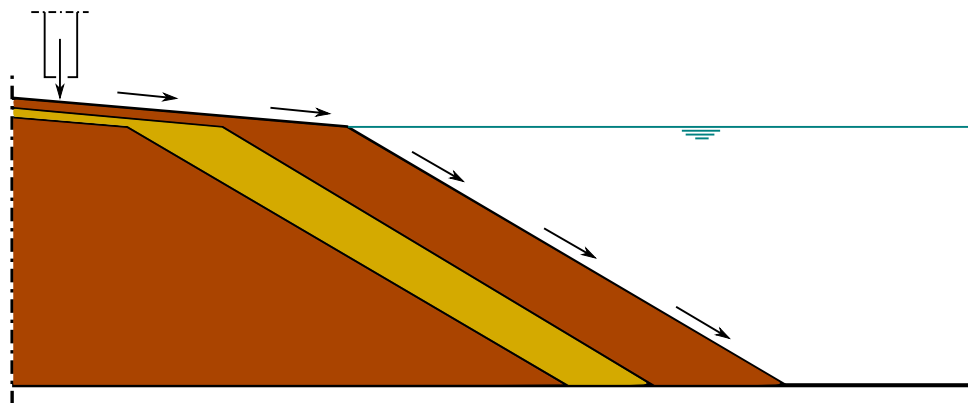
Existence of a critical slope height (h_{cr}) of the deposited sand appears at the top of the sand body near the waterline. This critical slope height provides the development of the slope in horizontal direction, that is defined by the water depth. To estimate the critical slope height (h_{cr}), equation [6.1] is derived. Equation [6.1] is based on experience of building underwater sand bodies with particle sizes between $100 \mu\text{m}$ and $500 \mu\text{m}$ [CUR 152, 1991]. Also the slope angle and porosity of the first sedimentation have influence on the slope height.

$$h_{cr} = 0.075 \cdot d_{50} - 8.5 \quad [6.1]$$

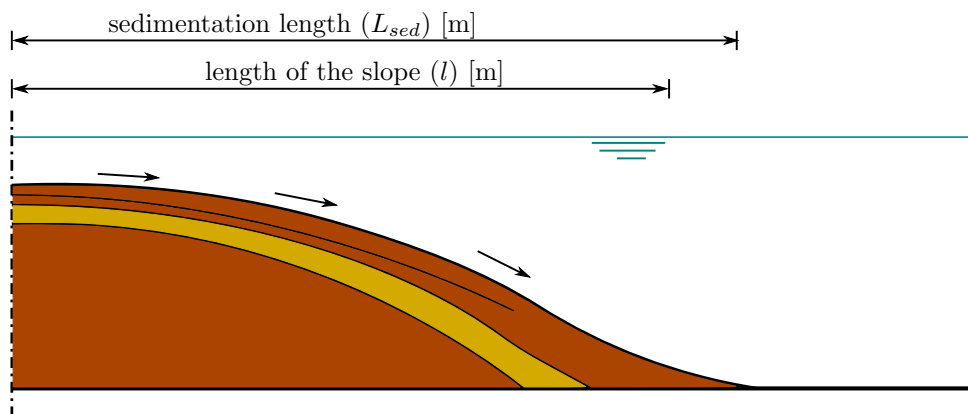
For high values for s ($s > 25$ kg/ms) the behaviour of fine and coarser sand is a turbulent suspension flow with a mixture jump that moves in upstream direction. The suspension



(a) low specific sand production; discontinuous slope development; increasing slope followed by flow slides ($L^* < 1$).



(b) continuous slope development ($L^* \approx 1$).



(c) high specific sand production; decreasing slope ($L^* > 1$).

Figure 6.4: Development of sand slopes, modified from CUR 152 [1991].

6. PHYSICAL HYPOTHESES

flow can continue after the toe of the slope, that results in a gentler slope (figure [6.4c]). Flow slides can occur but are not the dominant sediment transport process.

To classify the above described slope developments, three dimensionless parameters can be derived, namely:

- Dimensionless hydraulic sedimentation length (L^*)

$$L^* = \frac{\text{sedimentation length}}{\text{slope length}} = \frac{L_{sed}}{l} \quad [6.2]$$

- Ratio between occurring porosity (n_{situ}) and critical porosity (n_{cr})

$$N^* = \frac{\text{occurring porosity}}{\text{critical porosity}} = \frac{n_{situ}}{n_{cr}} \quad [6.3]$$

- Ratio between occurring slope height (h) and critical slope height (h_{cr})

$$H^* = \frac{\text{occurring slope height}}{\text{critical slope height}} = \frac{h}{h_{cr}} \quad [6.4]$$

The determination of the sedimentation length (L_{sed}) is given in paragraph 6.1.2. For $L^* < 1$ the situation of figure [6.4a] is occurring, so flow slides are the dominant transport mechanism. For $L^* > 1$ the situation of figure [6.4c] is occurring in this situation the main transport mechanism is the turbulent suspension flow. For the situation that $L^* \approx 1$ the slope is constant, see figure [6.4b]. If L^* is much larger then 1, the sand flows beyond the toe of the slope and the gradient of the slope decreases. From the field measurements [de Groot *et al.*, 1988] and the test flume [Mastbergen *et al.*, 1988] is observed that when the occurring porosity is higher than the critical porosity, so $N^* > 1$, the sand body is sensitive for liquefaction. In the case that $H^* > 1$ the slope is unstable and for $H^* < 1$ the slope is stable.

6.1.2 Sedimentation Length

This paragraph describes how to compute the sedimentation length. The sedimentation length is used in equation [6.2] to compute L^* . This parameter is used to determine the slope type. The slope types are mentioned in figure [6.4]. As the slope type is known, it is also known if flow slides occur. A flow slide results in mostly flat slopes and it decreases the porosity [CUR 152, 1991; CUR 157, 1993], with an increase in relative density.

The length over which a turbulent flow of a sand-water mixture may extend is determined by the degree of turbulence of the flow and the fall velocity of the particles. The sedimentation length for a suspension flow can be estimated without the degree of turbulence [Mastbergen & Bezuijen, 1988]:

$$L_{sed} = \frac{q_m}{w_s} = \frac{q_m}{w_0(1 - c_v)^m} \quad [6.5]$$

With:

$$c_v = \frac{\rho_m - \rho_w}{\rho_s - \rho_w} \quad [6.6]$$

Where:

- c_v = volume concentration [-];
- w_s = particle fall velocity in suspension [m/s];
- w_0 = particle fall velocity [m/s];
- ρ_m = mixture density [kg/m³].

The approach of Mastbergen & Bezuijen [1988] is a similar approach as the Camp model for sedimentation in settling tanks [Camp, 1936, 1946; Camp & Estrada, 1953], see also figure [6.5]. The sedimentation length is defined as the length over which 90% of the

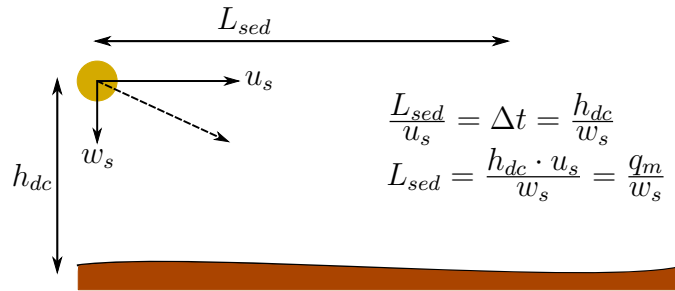


Figure 6.5: Definition sketch for the sedimentation length according to Mastbergen & Bezuijen [1988].

sand is settled. The comparison is drawn up for a particle diameter of 225 μm and is accurate for a concentration of 30%. As a result of the experiments of Mastbergen & Bezuijen [1988], Mastbergen & Bezuijen [1988] derived a value of 4 for the exponent m . Burgmans [2003] has verified if equation [6.5] can be used for larger particles. Burgmans [2003] conclude that it is possible to use equation [6.5] for particle diameters $> 225 \mu\text{m}$. Equation [6.7] is used for computing w_0 [van Rhee, 2002a]:

$$w_0 = \sqrt{\frac{4 \cdot g \cdot \Delta \cdot d_{50} \cdot \Psi}{3 \cdot C_D}} \quad [6.7]$$

Where:

- Δ = specific density defined as $\frac{\rho_s - \rho_w}{\rho_w}$ [-];
- Ψ = shape factor (≈ 0.7) [-];
- C_D = drag coefficient [-].

The drag coefficient (C_D) depends on the particle Reynolds number (Re_p), defined with:

$$Re_p = \frac{w_0 \cdot d_{50}}{\nu} \quad [6.8]$$

6. PHYSICAL HYPOTHESES

Where:

ν = kinematic viscosity ($\approx 1.33 \cdot 10^{-6}$ m²/s by a temperature of 10°C.) [m²/s].

The most common equations for the laminar (or Stokes), transitional and turbulent regime are respectively [van Rhee, 2002a].

$$\begin{aligned} C_D &= \frac{24}{Re_p} && \text{for } Re_p \leq 1 \\ C_D &= \frac{24}{Re_p} + \frac{3}{\sqrt{Re_p}} + 0.34 && \text{for } 1 < Re_p < 2000 \\ C_D &= 0.4 && \text{for } Re_p \geq 2000 \end{aligned} \quad [6.9]$$

The coefficient m is a function of the particle Reynolds number. Based on experiments with concentrations $0.05 < c < 0.65$ and Reynold numbers $0.000185 < Re_p < 7150$ Richardson & Zaki [1954] found:

$$\begin{aligned} m &= 4.65 && \text{for } Re_p < 0.2 \\ m &= 4.35 \cdot Re_p^{-0.03} && \text{for } 0.2 \leq Re_p < 1 \\ m &= 4.45 \cdot Re_p^{-0.1} && \text{for } 1 \leq Re_p < 200 \\ m &= 2.39 && \text{for } Re_p > 200 \end{aligned} \quad [6.10]$$

In paragraph 7.4 the sedimentation length is defined with the above described method. The slope type follows from this computation.

Another method to determine the sedimentation length is to solve a convection equation for the concentration (c_v). The convection equation for the concentration (c_v) is as follows:

$$\frac{\partial}{\partial t} \left(\frac{c_v q_m}{u} \right) + \frac{\partial c_v q_m}{\partial x} + w_s \cdot c_v = 0 \quad [6.11]$$

By assumption that u and q_m are constant and that $\frac{\partial c_v}{\partial t} = 0$, the differential equation becomes:

$$\frac{\partial c_v}{\partial x} + \frac{w_s \cdot c_v}{q_m} = 0 \quad [6.12]$$

If w_s is constant, then the analytical solution becomes:

$$c_v(x) = c_{v;0} \cdot e^{-\frac{w_s \cdot x}{q_m}} \quad [6.13]$$

Zanke [1977] proposed for particles between the 100 μm and 1000 μm the following equation:

$$w_s = 10 \cdot \frac{\nu}{d_{50}} \cdot \left(\sqrt{1 + \frac{0.01 \cdot \Delta \cdot g \cdot d_{50}^3}{\nu^2}} - 1 \right) \quad [6.14]$$

Only w_s is not constant. In this case it has a dependency on the concentration (c_v). This has to do with the high concentrations and the hindered settling. Therefore, the following equation is used for the fall velocity (w_s). The Richardson & Zaki [1954] equation [6.15] predicts accurately the hindered settling velocity (w_s) [Baldock *et al.*, 2004].

$$w_s = w_0 \cdot (1 - c_v)^m \quad [6.15]$$

By substituting equation [6.15] in differential equation [6.12], this differential equation [6.16] is not linear any more.

$$\frac{\partial c_v}{\partial x} + \frac{w_0 \cdot (1 - c_v)^m \cdot c_v}{q_m} = 0 \quad [6.16]$$

The non-linear differential equation [6.16] is solved by using an explicit numerical scheme. The explicit numerical scheme becomes:

$$c_{j+1} = c_j + \Delta x \cdot \left(-\frac{w_0 \cdot (1 - c_j)^m \cdot c_j}{q_m} \right) \quad [6.17]$$

6.2 Shear Stress

Fluids moving along a solid boundary will encounter a shear stress (τ) on that boundary. The no-slip condition [Day, 1990] prescribes that the velocity of the fluid relative to the boundary is zero, but at some height above the boundary the flow velocity must equal that of the fluid. For all Newtonian fluids in laminar flow the shear stress is proportional to the strain rate in the fluid where the viscosity is the constant of proportionality. However for Non Newtonian fluids, this is no longer the case as for these fluids the viscosity is not constant. The shear stress is imparted onto the boundary as a result of this loss of velocity. The shear stress, for a Newtonian fluid, at a surface element parallel to a flat plate is given by:

$$\tau(z) = \rho \cdot \nu \cdot \frac{\partial u}{\partial z} = \mu_d \cdot \frac{\partial u}{\partial z} \quad [6.18]$$

Where:

μ_d = dynamic viscosity [Pa · s].

Commonly the following equation for the relation between the shear stress (τ) and the Chézy roughness (C) is used (e.g. Jansen *et al.* [1979]; van Rijn [1993]):

$$\tau = \frac{\rho_w \cdot g \cdot u_f^2}{C^2} \quad [6.19]$$

6. PHYSICAL HYPOTHESES

With:

$$C = 18 \cdot \log \left(\frac{12 \cdot z}{k_s} \right) \quad [6.20]$$

Where:

- u_f = flow velocity [m/s];
- z = water depth [m];
- k_s = equivalent sand roughness (Nikuradse roughness) [m].

Shields [1936] gives a relation between a dimensionless shear stress (θ) (also called Shields parameter) and the so called particle Reynolds number (Re_*). In Appendix J the critical Shields parameter is described.

$$\theta = \frac{\tau}{(\rho_s - \rho_w) \cdot g \cdot d_{50}} = \frac{u_*^2}{\Delta \cdot g \cdot d_{50}} = f(Re_*) = f \left(\frac{u_* \cdot d_{50}}{\nu} \right) \quad [6.21]$$

Where:

- u_* = shear velocity [m/s].

In this case the particle Reynolds number (Re_*) is defined by:

$$Re_* = \frac{u_* \cdot d_{50}}{\nu} \quad [6.22]$$

This looks similar to equation [6.8] but is not the same because $u_* \neq w_0$. Both are velocities by dimension but are not the same, u_* is defined by:

$$u_* = \sqrt{\frac{\tau}{\rho_w}} \quad [6.23]$$

From equation [6.23] it is now obvious that u_* is not a real velocity.

The Nikuradse roughness height (k_s) is determined with the following equations of van Rijn [1993].

$$k_s = 3 \cdot \theta \cdot d_{90} \quad [6.24]$$

The d_{90} is as follows defined:

$$d_{90} = \sigma^{1.3} \cdot d_{50} \quad [6.25]$$

Substituting equation [6.21] and equation [6.25] into equation [6.24], the equation becomes:

$$k_s = \frac{3 \cdot \tau \cdot \sigma^{1.3}}{(\rho_s - \rho_w) \cdot g} \quad [6.26]$$

With $\sigma = 1.75$ (σ is the standard deviation of the PSD), this value comes from table [2.3]. Dohmen-Janssen [1999] mentioned also other relations for k_s , then the relation of van Rijn [1993]. The Nikuradse roughness height of van Rijn [1993] is used for the reason that for the other computations of the different kind of shear stresses also van Rijn [1993] is used.

In further detail is looked at the shear stress caused by the density current (paragraph 6.2.1) and the shear stress caused by the hydrodynamics (paragraph 6.2.2).

6.2.1 Shear Stress as a Result of a Density Current

In this paragraph the theory is discussed about a density current in relation to the shear stress. There are two flow conditions described, namely: the initial condition and the stationary condition. In paragraph 6.2.1.1 the initial condition is described and in paragraph 6.2.1.2 the stationary condition is described.

6.2.1.1 Shear Stress as a Result of a Density Current for the Initial Condition

The density current related bed shear stress ($\tau_{dc;ic}$) for the initial condition is defined as:

$$\tau_{dc;ic} = \frac{\rho_m \cdot g \cdot u_{dc;ic}^2}{C^2} \quad [6.27]$$

With:

For smooth flow $\left(\frac{\sqrt{\tau_{dc;ic}} \cdot k_s}{\nu \cdot \sqrt{\rho_m}} \leq 5 \right)$:

$$C = 18 \cdot \log \left(\frac{12 \cdot h_{dc}}{\frac{3.3 \cdot \nu \cdot \sqrt{\rho_m}}{\sqrt{\tau_{dc;ic}}}} \right) \quad [6.28a]$$

For transitional flow $\left(5 < \frac{\sqrt{\tau_{dc;ic}} \cdot k_s}{\nu \cdot \sqrt{\rho_m}} < 70 \right)$:

$$C = 18 \cdot \log \left(\frac{12 \cdot h_{dc}}{k_s + \frac{3.3 \cdot \nu \cdot \sqrt{\rho_m}}{\sqrt{\tau_{dc;ic}}}} \right) \quad [6.28b]$$

For rough flow $\left(\frac{\sqrt{\tau_{dc;ic}} \cdot k_s}{\nu \cdot \sqrt{\rho_m}} \geq 70 \right)$:

$$C = 18 \cdot \log \left(\frac{12 \cdot h_{dc}}{k_s} \right) \quad [6.28c]$$

6. PHYSICAL HYPOTHESES

Where:

$u_{dc;ic}$ = density current velocity for initial conditions [m/s].

h_{dc} = layer thickness of the density current [m].

In figure [6.6] are the parameters illustrated for the computation of the density current with initial conditions. Equation [6.27] is a similar expression as Jansen *et al.* [1979] and van Rijn [1993] uses.

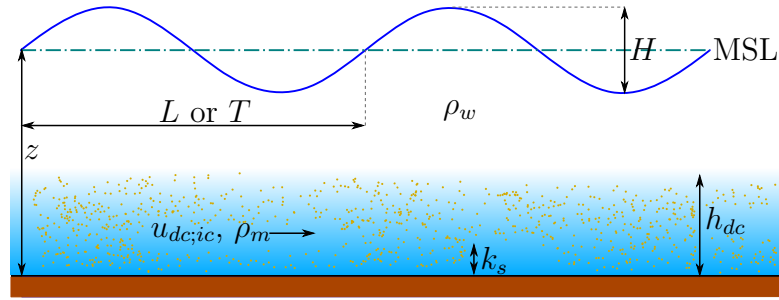


Figure 6.6: Definition sketch for the density current with initial conditions.

If the density current comes to a hold, the particles will settle, also the particles will settle during flow. The shear stress related to the density current goes to zero, thus no compaction occurs any more by the density current related shear stress. The particle structure that arises in such a way has the stability of a card house (see figure [6.1a]). Due to the card house structure, the risk of the occurrence of flow slides increases. The card house structure has a high porosity thus a low relative density. The computations results are given in paragraph 7.5 and Appendix J.

6.2.1.2 Shear Stress as a Result of a Density Current for the Stationary Condition

The flow velocity ($u_{dc;sc}$) for a stationary density current can be defined as:

$$u_{dc;sc} = C \cdot \sqrt{h_{dc} \cdot i \cdot \frac{\rho_m - \rho_w}{\rho_m}} \quad [6.29]$$

Where:

i = slope ($\beta = \tan i$) [-].

Substituting equation [6.29] into equation [6.27] results in:

$$\tau_{dc;sc} = \rho_m \cdot g \cdot h_{dc} \cdot i \cdot \frac{\rho_m - \rho_w}{\rho_m} \quad [6.30]$$

In figure [6.7] are the parameters illustrated for the computation of the density current with stationary conditions.

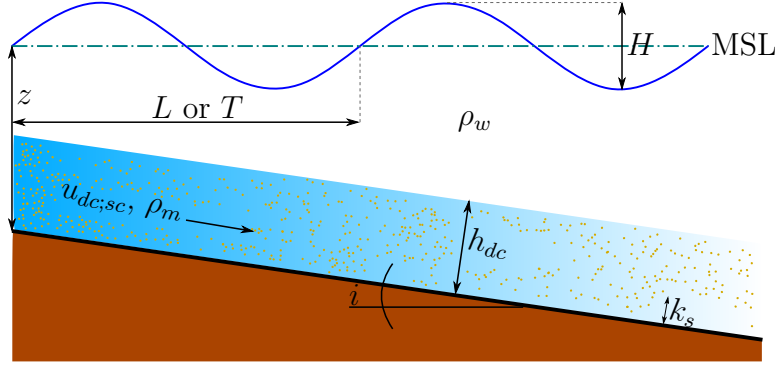


Figure 6.7: Definition sketch for the density current with stationary conditions.

The computations results are given in paragraph 7.5 and Appendix J.

6.2.2 The influence of Hydrodynamic Conditions on the Relative Density

In this paragraph the theory on the relation of waves and current in relation to the shear stress is discussed. van Rijn [1993] has defined the total bed shear stress ($\tau_{b,cw}$) for current and waves as follows:

$$\tau_{b,cw} = \tau_{b,c} + \tau_{b,w} \quad [6.31]$$

The current related bed shear stress ($\tau_{b,c}$) is defined by van Rijn [1993] as:

$$\tau_{b,c} = \frac{\rho_w \cdot g \cdot \bar{u}_c^2}{C^2} \quad [6.32]$$

With:

For smooth flow $\left(\frac{\sqrt{\tau_{b,c}} \cdot k_s}{\nu \cdot \sqrt{\rho_w}} \leq 5 \right)$:

$$C = 18 \cdot \log \left(\frac{12 \cdot z}{\frac{3.3 \cdot \nu \cdot \sqrt{\rho_w}}{\sqrt{\tau_{b,c}}}} \right) \quad [6.33a]$$

For transitional flow $\left(5 < \frac{\sqrt{\tau_{b,c}} \cdot k_s}{\nu \cdot \sqrt{\rho_w}} < 70 \right)$:

6. PHYSICAL HYPOTHESES

$$C = 18 \cdot \log \left(\frac{12 \cdot z}{k_s + \frac{3.3 \cdot \nu \cdot \sqrt{\rho_w}}{\sqrt{\tau_{b,c}}}} \right) \quad [6.33b]$$

For rough flow $\left(\frac{\sqrt{\tau_{b,c}} \cdot k_s}{\nu \cdot \sqrt{\rho_w}} \geq 70 \right)$:

$$C = 18 \cdot \log \left(\frac{12 \cdot z}{k_s} \right) \quad [6.33c]$$

Where:

$\overline{u_c}$ = depth averaged current velocity [m/s].

The near-bed orbital velocities are required, for the computation of wave related bed shear stress ($\tau_{b,w}$). By applying linear wave theory, this is rather well explained by Holthuijsen [2010]. The peak value of the orbital excursion amplitude (\hat{A}_δ) and velocity (\hat{U}_δ) at the edge of the wave boundary layer can be expressed as:

$$\hat{A}_\delta = \frac{H}{2 \cdot \sinh(k \cdot z)} \quad [6.34]$$

$$\hat{U}_\delta = \frac{\pi \cdot H}{T \cdot \sinh(k \cdot z)} \quad [6.35]$$

With:

$$L = \frac{g \cdot T^2}{2 \cdot \pi} \cdot \tanh(k \cdot z) \quad [6.36]$$

Where:

H = wave height [m];

T = wave period [s];

k = wave number defined by $\frac{2\pi}{L}$ [m^{-1}];

L = wave length [m];

In figure [6.8] are the parameters illustrated of equation [6.34], equation [6.35] and equation [6.36]. The wave related bed shear stress ($\tau_{b,w}$) is defined by van Rijn [1993] as:

$$\tau_{b,w} = 0.25 \cdot \rho_w \cdot f_w \cdot \hat{U}_\delta^2 \quad [6.37]$$

With:

For laminar flow $\left(\frac{\hat{U}_\delta \cdot \hat{A}_\delta}{\nu} < 10^4 \right)$ [Jonsson, 1966]:

$$f_w = \frac{2}{\sqrt{\frac{\hat{U}_\delta \cdot \hat{A}_\delta}{\nu}}} \quad [6.38a]$$

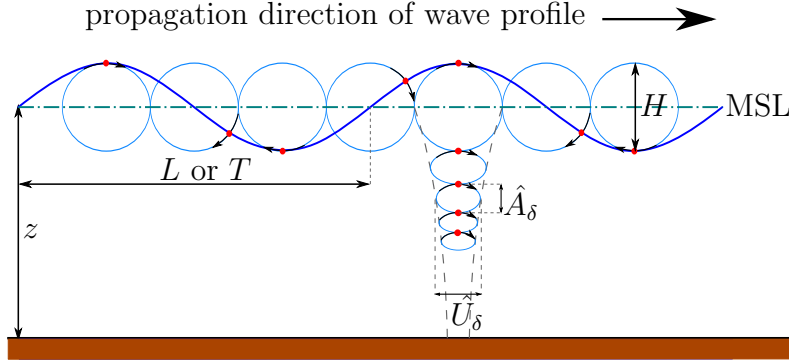


Figure 6.8: Definition sketch for the orbital motion of the water particles under a harmonic wave. Modified from Holthuijsen [2010].

For smooth turbulent flow $\left(10^4 < \frac{\hat{U}_\delta \cdot \hat{A}_\delta}{\nu} < 10^6 \text{ and } \frac{\hat{A}_\delta}{k_s} > 10^3\right)$ [Jonsson, 1966, 1980]:

$$\frac{\sqrt{f_w}}{4} + 2 \cdot \log\left(\frac{1}{4 \cdot \sqrt{f_w}}\right) = -1.55 + \log\left(\frac{\hat{U}_\delta \cdot \hat{A}_\delta}{\nu}\right) \quad [6.38b]$$

van Rijn [1993] mentioned an approximation for equation [6.38b]. In the computations this approximation is used.

$$f_w = \frac{0.09}{\left(\frac{\hat{U}_\delta \cdot \hat{A}_\delta}{\nu}\right)^{0.2}} \quad [6.38c]$$

For rough turbulent flow $\left(\frac{\hat{U}_\delta \cdot \hat{A}_\delta}{\nu} > 10^5 \text{ and } \frac{\hat{A}_\delta}{k_s} < 10^2\right)$, with $f_{w,max} = 0.3$ for $\frac{\hat{A}_\delta}{k_s} \leq 1.57$ [Swart, 1976]:

$$f_w = \exp\left(-6 + 5.2 \cdot \left(\frac{\hat{A}_\delta}{k_s}\right)^{-0.19}\right) \quad [6.38d]$$

For transitional flow $\left(10^4 < \frac{\hat{U}_\delta \cdot \hat{A}_\delta}{\nu} < 10^5 \text{ and } 10^2 < \frac{\hat{A}_\delta}{k_s} < 10^3\right)$, van Rijn [1993] suggests:

$$f_w = \exp\left(-6 + 5.2 \cdot \left(\frac{\hat{A}_\delta}{k_s + \frac{3.3 \cdot \nu \sqrt{\rho_w}}{\sqrt{\tau_{b,w}}}}\right)^{-0.19}\right) \quad [6.38e]$$

Where:

f_w = friction factor [-].

In paragraph 7.6 and Appendix L the computation results are given.

6. PHYSICAL HYPOTHESES

6.2.3 Relation between Shear Stress and Porosity

The response of the bed surface to a fluid forcing such as a shear stress depends on a number of bed properties, namely: particle size, sorting, density, porosity, surface roughness, consolidation and cohesion.

Mitchener & Torfs [1996] describes a relation between the critical bed shear stress and the bulk density, but this relation can not be used. It describes namely the erosion of a bed surface that exists of a mixture of sand/mud.

If the bed surface has a dense packing, then at increasing shear stress dilatancy occurs. The phenomena of dilatancy was first described by Reynolds [1885, 1886]. Dilatancy is the increase in volume that may occur during shear [van Rhee, 2010b; Verruijt & van Baars, 2005]. This can also be explained by figure [6.1]. The bed has the particle skeleton of figure [6.1b] by increasing shear the particle skeleton is changing into figure [6.1a]. By dilatancy the porosity is increasing, so, the relative density is decreasing. The opposite of dilatancy is contractancy/compaction, Contractancy is the decrease in volume that may occur during shear.

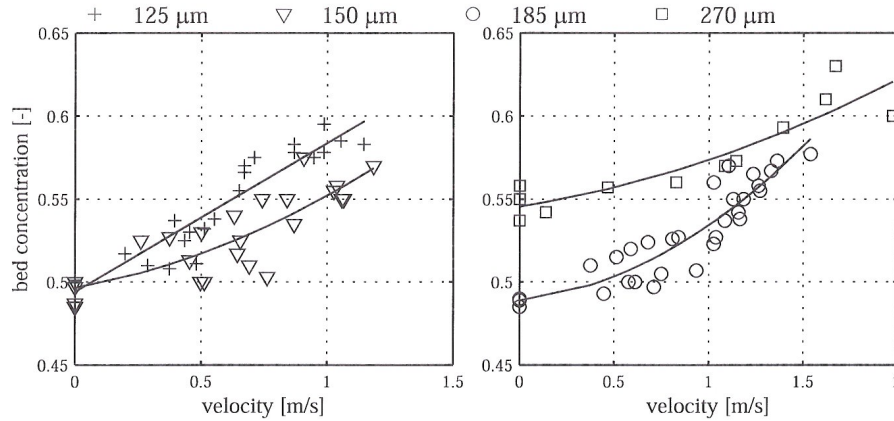


Figure 6.9: Bed concentration versus velocity for all sands, from van Rhee [2002a].

van Rhee [2002a,b] has researched the influence of the bed shear stress on the sedimentation of sand. Van Rhee has observed a relation between the shear stress and the sedimentation velocity. In a subsequent research about this subject, van Rhee [2004] observed a porosity difference between the loosest and densest state of approximately 10%. The research was done with four types of sand with a d_{50} of 125, 150, 185 and 270 μm . van Rhee [2002a] observed an influence of the flow velocity at which sedimentation takes place and the packing of particles in the bed (figure [6.9]). From figure [6.9] it is obvious that there is a relation between the flow velocity and the bed concentration ($1 - n$). If the bed concentration increase then the porosity decrease and the relative density increase. When the particles settle at zero velocity the loosest state of the bed is reached. With increasing flow velocity, also the shear stress increases, because the flow velocity and the shear stress are related to each other (e.g. equation [6.19]). So, at increasing flow velocity,

the packing of the bed becomes denser. van Rhee [2002a] provides a possible explanation for this phenomenon that states, that a settling particle under flow conditions can only stay inside a bed when it finds a more or less sheltered place between other grains (figure [6.10]). This results in a higher density of the bed and also in a higher relative density.

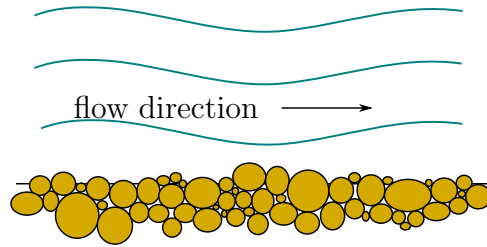


Figure 6.10: Sheltering and interlocking of particles into the bed.

6.3 The influence of the Sedimentation Velocity on the Relative Density

In the settling sand layer there is more damping of the motion caused by the shear stress. So the particles settle more like a card house structure, with a lower relative density, rather than be pushed into the bed through the shear stress.

The bed shear stress affects sedimentation velocity. The sedimentation velocity (v_{sed}) is often expressed as the difference between sedimentation and erosion flux [van Rhee & Talmon, 2010]:

$$v_{sed} = \frac{S - E}{\rho_s \cdot (1 - n - c_b)} \quad [6.39]$$

Where:

- v_{sed} = sedimentation velocity [m/s];
- S = sedimentation flux [kg/m²s];
- E = erosion flux [kg/m²s];
- c_b = near-bed volumetric concentration [-].

The sedimentation flux is as follows defined:

$$S = \rho_s \cdot w_s \cdot c_b = \rho_s \cdot w_0 \cdot c_b \cdot (1 - c_b)^m \quad [6.40]$$

Where:

- β = slope angle [°].

The erosion flux is commonly presented in dimensionless form. It is also called the pick-up flux:

$$\phi_p = \frac{E}{\rho_s \cdot \sqrt{g \cdot \Delta \cdot d_{50}}} \quad [6.41]$$

6. PHYSICAL HYPOTHESES

Where:

ϕ_p = pick-up flux [-].

During the used work methods of the Maasvlakte II project the erosion flux is zero or $S > E$, such that sedimentation takes place in stead of erosion. In figure [6.11] the relation between the sedimentation velocity and the near-bed volumetric concentration is illustrated, with $E = 0$ and the d_{50} from table [2.3], for the Pleistocene sand and paragraph 2.6 for the Holocene sand. The commonly used pick-up functions a.o. van Rijn

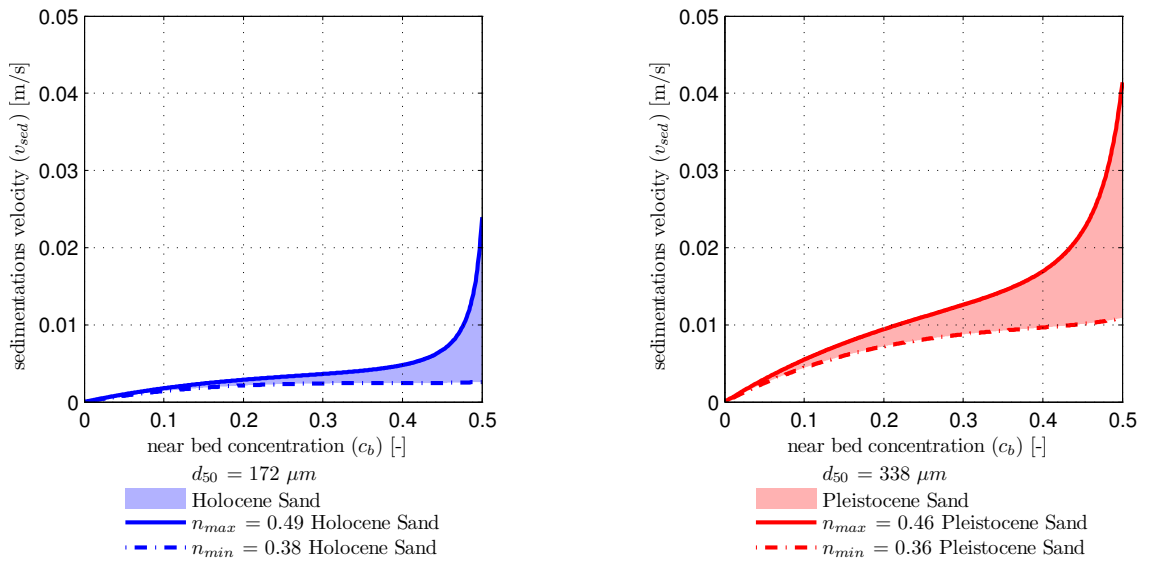


Figure 6.11: Relation between the sedimentation velocity and the near-bed volumetric concentration.

[1984a] are based on experiments with very low sediment concentrations. van Rhee & Talmon [2010] uses the concept of sediment entrainment by turbulent eddies for including the influence of the near bed concentration into the pick-up.

“It is assumed that turbulent eddies pick up particles at the bed where a concentration of $1 - n$ is present. If an eddy transports a volume of water and sediment from the bed, due to continuity the same volume of water must be transported back to the bed surface. If the sediment concentration is low, the back flow will contain few particles. For higher values of the near-bed concentration the back flow will transport particles back to the bed. In a limit situation where the near bed concentration is almost equal to the bed concentration, net sediment transport from the bed to the flow due to turbulent eddies will not occur. Following this reasoning, the effect of the near-bed concentration on the pick-flux can be written as a reduction factor.” [van Rhee & Talmon, 2010]

The net pick up flux (ϕ_{pn}) is as follows defined:

$$\phi_{pn} = \frac{1 - n - c_b}{1 - n} \cdot \phi_p \quad [6.42]$$

Finally van Rhee & Talmon [2010] derives an empirical function (equation [6.43]) for the pick-up flux, which includes the reduction factor of equation [6.42], the particle diameter (D^*) and the shear stress through the Shields parameter.

$$\phi_p = 0.0025 \cdot (D^* - 2.4)^{0.3} \cdot \frac{1 - n - c_b}{1 - n} \cdot \theta \quad [6.43]$$

Equation [6.43] is calibrated on experiments with high concentration and large Shields parameters. The influence of the particle size in equation [6.43] is small. It should be possible to use equation [6.43] for the Maasvlakte II project, but it is better to calibrate and validate equation [6.43] for the Maasvlakte II project.

6. PHYSICAL HYPOTHESES

Chapter 7

Physical Processes and Parameter Calculations of a Sand Fill

In this chapter each physical hypothesis of chapter 6 will be verified by making calculations for different work methods with different physical phenomena. Resulting in values for the parameters that possibly influence the relative density according to the physical hypothesis under investigation.

Also in this chapter the physical processes are described that are not mentioned in chapter 6, but are needed to execute the calculations mentioned in this chapter.

In paragraph 7.1 the input parameters are mentioned for the different kind of computations. In paragraph 7.2 the fall processes of a sand water mixture through water are explained and the computation results are mentioned. In paragraph 7.3 the processes are described for the work method pumping also the computation results are mentioned for the work method pumping. In paragraph 7.4 the computations results are mentioned for the sedimentation length (L_{sed}), critical slope height (h_{cr}) and the associated slope type. The relation between those parameters and the relative density is described qualitative, because a mathematical relation between the parameters and the relative density is not found in literature. In paragraph 7.5 the computation results for the density current are mentioned. Also, for the shear stress a qualitative description about the relation with the relative density exists, because also for this no mathematical relation is found in literature.

7.1 Input Parameters for the Computations

A characteristic value for each work method is selected to achieve the input parameters for the different kind of the computations. The required parameters are mentioned in tables [7.1]. Further it is assumed that $\rho_w = 1025 \text{ kg/m}^3$ and $\rho_s = 2650 \text{ kg/m}^3$.

The sand production (P_s) of a TSHD:

$$P_s = \frac{V_{load}}{t_{discharge}} \cdot \frac{\rho_{m;0} - \rho_w}{\rho_s - \rho_w} \cdot \rho_s = P \cdot \frac{\rho_{m;0} - \rho_w}{\rho_s - \rho_w} \cdot \rho_s \quad [7.1]$$

7. PHYSICAL PROCESSES AND PARAMETER CALCULATIONS OF A SAND FILL

Where:

V_{load} = volume of sand (incl. pores) in TSHD [m^3];

$t_{discharge}$ = discharge time of a TSHD [s];

P = Production of a TSHD [m^3/s].

Table 7.1: The input parameters for the different kind of computations.

Parameter	Unit	Work methods				
		DU	RB	PU	BF	SP
$d_{50;min}$	μm	189	197	204	235	297
$d_{50;average}$	μm	249	298	328	357	443
$d_{50;max}$	μm	552	669	957	521	699
d_0	mm	-	$\varnothing 800$	$\varnothing 1000$	$\varnothing 900$	$\varnothing 1000$
b_0^a	m	2.170	-	-	0.850	0.350
A^b	m^2	244	-	-	2.87	3.33
u_0	m/s	0.1	7	6	4	5
P	m^3/s	6.80	3.52	3.30	2.54	3.93
$\rho_{m;0}$	kg/m^3	1700	1500	1700	1600	1600
P_s	kg/s	7485	2726	3633	2382	3685
H_{wd}^c	m	4.0	-	-	3.5	3.0
z	m	11	5	10	18	9
h	m	1.0	1.9	6.0	0.5	2.9
l for $d_{50;min}^d$	m	175	490	700	36	81
l for $d_{50;average}$	m	150	420	600	32	72
l for $d_{50;max}$	m	125	350	500	28	63

^awidth of discharge opening [m].

^bsurface of discharge area [m^2].

^crequired water depth under discharge point (see figure [7.1]).

^dslope length (see figure [6.4]).

The slope lengths (l) are based on experience figures from the Maasvlakte II project. The following slopes angles are used, for the work methods dumping, rainbowing and pumping:

- slope 1:35 for the lowest measured value of the d_{50} ;
- slope 1:30 for the averaged value of the d_{50} ;
- slope 1:25 for the highest measured value of the d_{50} .

For the other two work methods, the following slopes angles are used. The steepest slope is used for the coarsest particle size. So, the following slope, are used for back filling through suction pipe and spraying with the SD “Sliedrecht 27”:

- slope 1:9 for the lowest measured value of the d_{50} ;
- slope 1:8 for the averaged value of the d_{50} ;
- slope 1:7 for the highest measured value of the d_{50} .

7.2 Fall Processes of a Sand-Water Mixture

The fall process for the various work methods can be described with a plume/jet mechanism, with exception of the work method pumping. The work method pumping is described in paragraph 7.3. In figure [7.1] all the types of fall processes are illustrated. The fall process lump-like dumping (figure [7.1c]) is not further described because this process has not occurred during the construction of the Maasvlakte II project. The following

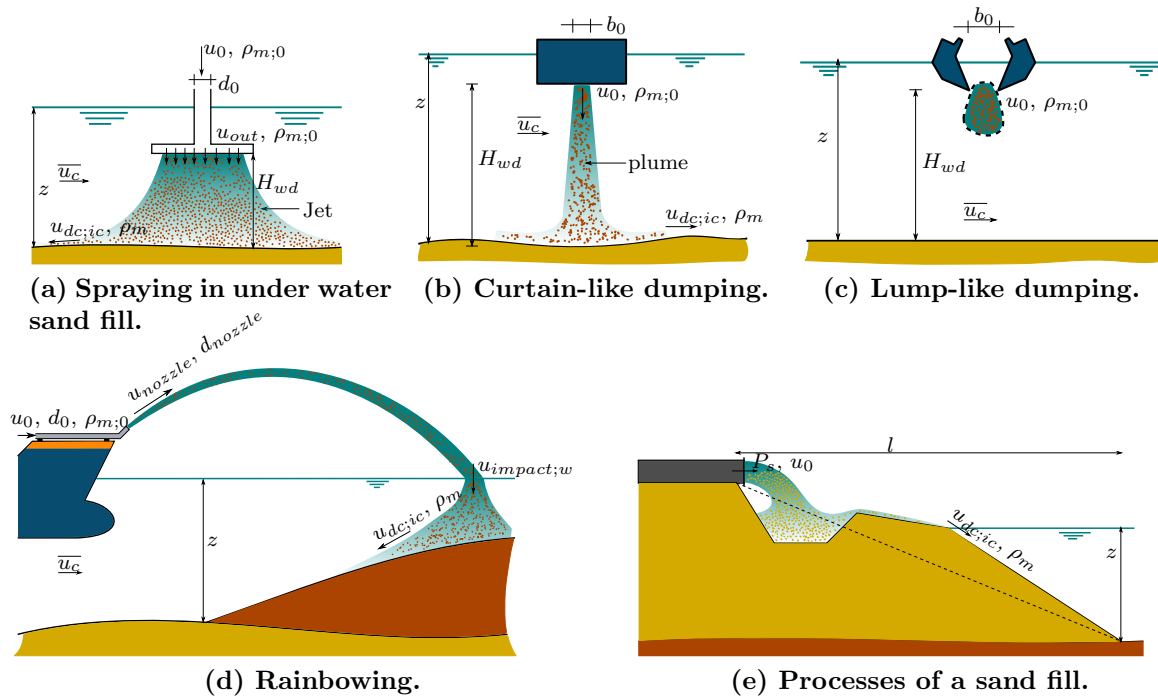


Figure 7.1: Types of fall processes, modified from CUR 152 [1991].

parameters have influence on the fall process of a sand-water mixture through water:

- Dump/spray height (H_{wd});
- Density of the sand-water mixture ($\rho_{m;0}$, ρ_m);
- Cross-section of the discharge opening (b_0 , d_0);
- Flow velocity (u_0 , u_{out} and $u_{dc;ic}$);
- Current ($\overline{u_c}$);

The program JET is used to compute the bottom process parameters (jet/plume mechanism) for the input in the hypotheses from chapter 6. This program is originally developed by Oostinga in 1983 for Volker Stevin Dredging and van Rhee has improved it in 1992 for the HAM. The program JET computes the flow in a jet/plume mechanism on base of Delvigne [1979]. The program JET has 2 computation modes, namely: JET2D and JET3D. JET2D is used to compute curtain-like dumping, because it can be modelled as a flat plume flow and the other work methods are computed with JET3D.

7. PHYSICAL PROCESSES AND PARAMETER CALCULATIONS OF A SAND FILL

van Rhee [2002a] has also developed a 2DV-model to compute the sedimentation processes in a hopper of a TSHD. With this model it is also possible to make a simulation for the jet/plume mechanism to retrieve the bottom process parameters for the input in the hypotheses from chapter 6. This model is not used.

Recently van Rhee [2010a, 2011] has developed a model to compute the bottom discharge process (dumping) of a TSHD, this model is based on the 2DV-model of van Rhee [2002a].

The value for u_0 for RB, PU, BF and SP is the measured value on-board of the TSHD. In figure [7.2] the physical processes of rainbowing are illustrated. The outgoing velocity at the end of the rainbow nozzle (d_{nozzle}) $\varnothing 400$ mm, becomes u_{nozzle} 28 m/s. The area of impact has a diameter of $d_{impact} \approx 1.25$ m, this value is based on visual observations. With the aid of figure [7.3] and figure [7.4] and an assumption that the mixture density 1300 kg/m^3 is at impact on the water surface, the flow velocity of impact ($u_{impact;w}$) becomes 5 m/s.

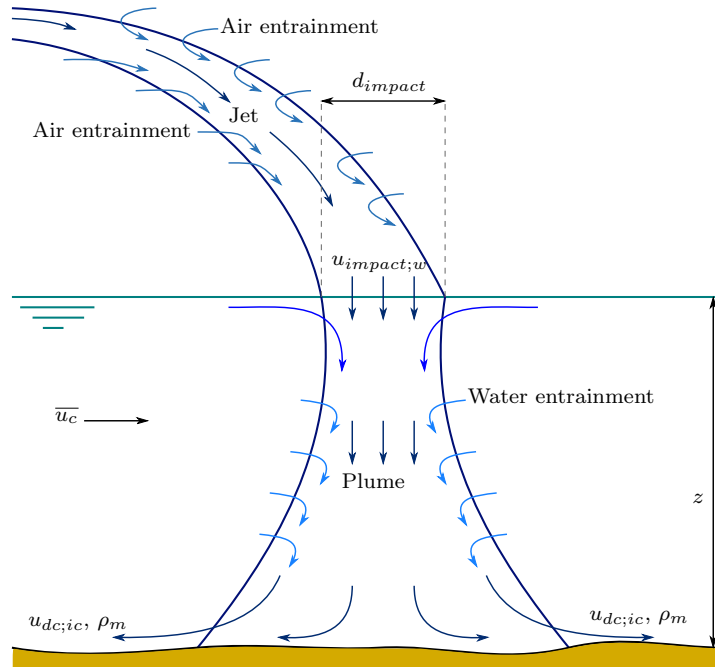


Figure 7.2: Physical processes of the work method rainbowing.

From the sand balance, the specific sand production (s) can be described as:

$$s = \rho_s \cdot \frac{u_0 \cdot \pi \cdot d_0^2}{4} \cdot \frac{\rho_{m;0} - \rho_w}{\rho_s - \rho_w} \quad [7.2]$$

The flow velocity ($u_{impact;w}$) at impact on the water surface is computed with:

$$u_{impact;w} = \frac{4 \cdot s \cdot (\rho_s - \rho_w)}{\rho_s \cdot \pi \cdot d_{impact}^2 \cdot (\rho_{m;impact} - \rho_w)} \quad [7.3]$$

A velocity reduction, for the work methods BF and SP, because of the large outflow

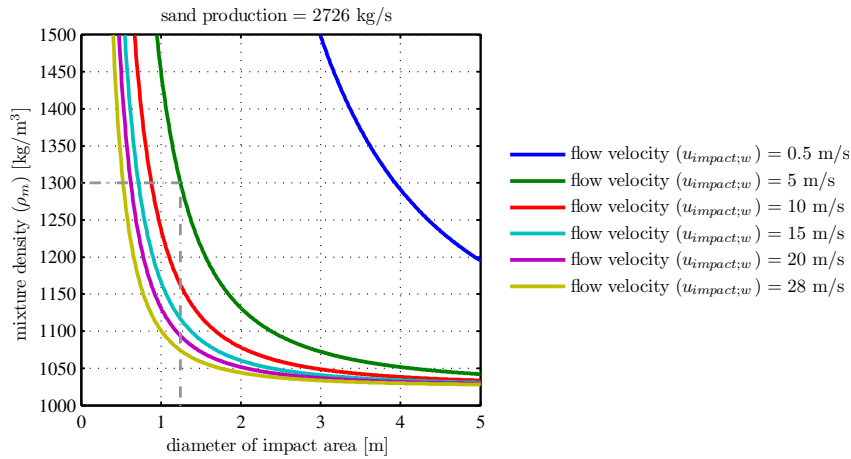


Figure 7.3: Relation between the mixture density and the diameter of the impact area.

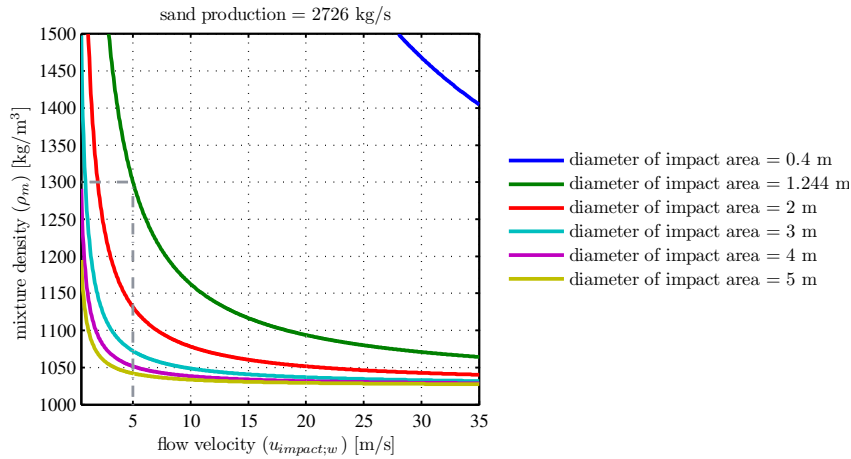


Figure 7.4: Relation between the mixture density and the flow velocity on impact of the rainbow jet.

opening. So the flow velocity (u_{out}) for BF becomes 0.9 m/s and for SP becomes the flow velocity (u_{out}) 1.2 m/s. In table [7.2], the computations results from the JET 2D or 3D computations are mentioned. The results mentioned in table [7.2] are at the sea bottom. These results are used in the computations of paragraph 7.4 and paragraph 7.5.

7. PHYSICAL PROCESSES AND PARAMETER CALCULATIONS OF A SAND FILL

Table 7.2: The output parameters at sea bottom from JET computations.

		Work methods			
		DU	RB	BF	SP
JET		2D	3D	3D	3D
u_{out}	m/s	0.1	-	0.9	1.2
u_{nozzle}	m/s	-	28	-	-
$u_{impact;w}$	m/s	-	5	-	-
$\rho_{m;impact}$	kg/m ³	-	1300	-	-
ρ_m	kg/m ³	1103	1153	1182	1121
$u_{dc;ic}$	m/s	2.41	4.80	3.53	2.42
q_m	m ² /s	0.87	4.39	1.45	0.73
s	kg/ms	110	917	371	114

7.3 Sand-Water Mixture Flow on a Sand Fill

For the computations of the parameters for the work method pumping, the literature is used of Mastbergen & Leeuwestein [1986]. Further, it is assumed that the average load of the TSHD is 11,880 m³ of sand, the discharge time is 3,600 s, the width of the sand fill (W) is 20 m and the total height of the sand fill is 14 m. The height of the sand fill can be divided into two parts. The part above MSL is 6 m high and the part below MSL is 8 m high. The sand production can be divided as $\frac{3}{7}$ settles above MSL and $\frac{4}{7}$ below MSL. In figure [7.1e] and figure [7.5] the parameters are illustrated for the work method pumping. Equation [7.4] and equation [7.6] comes from continuity, with the assumption

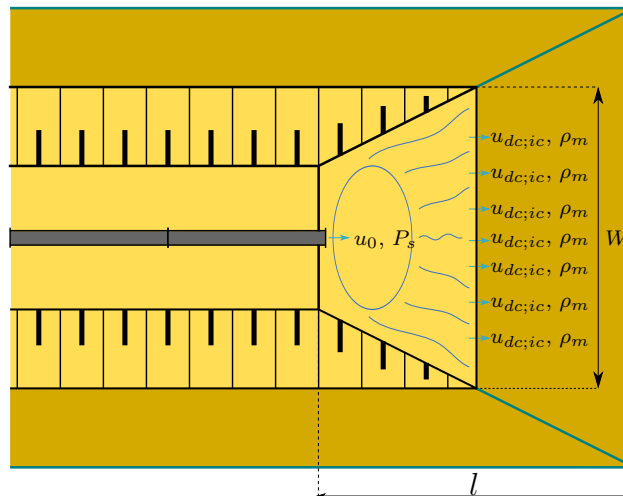


Figure 7.5: Physical processes of the work method pumping.

that W is constant.

$$q_m = \frac{Q}{W} \quad [7.4]$$

With:

$$Q = \frac{\pi \cdot d_0^2 \cdot u_0}{4} \quad [7.5]$$

$$q_m = u_{dc;ic} \cdot h_{dc} \quad [7.6]$$

Equation [7.7] is based on the assumption that the specific sand production (s) takes place as suspended transport.

$$s = \rho_s \cdot q_m \cdot c_v \quad [7.7]$$

Equation [7.8] comes from the derivation of a turbulent logarithmic velocity profile. Based on observations Mastbergen & Leeuwestein [1986] assumed that the Darcy-Weisbach friction (f_0) is 0.15.

$$u = u_* \cdot \sqrt{\frac{8}{f_0}} \quad [7.8]$$

Equation [7.9] is valid for the shear velocity (u_*).

$$u_* = \sqrt{g \cdot i \cdot h_{dc}} \quad [7.9]$$

Equation [7.10] gives the specific sand production as function of the flow velocity (u_s). Mastbergen & Leeuwestein [1986] uses an Engelund-Hansen based equation, because with out adjustments this equation [7.10] gives quiet reliable results.

$$s = \frac{\rho_s}{20} \cdot \left(\frac{8}{f_0}\right)^{1.5} \cdot \frac{u^5}{\Delta^2 \cdot g^2 \cdot d_{50}} \quad [7.10]$$

From equation [7.4] until equation [7.10], Mastbergen & Leeuwestein [1986] derived the following equations for the flow velocity ($u_{dc;ic}$), slope (i) and the layer thickness (h_{dc}) of the destiny current. Equation [7.11] presents the slope (i).

$$i = \left(\frac{f_0}{8}\right)^{0.1} \cdot \frac{(20 \cdot \Delta \cdot c_v \cdot \Delta \cdot d_{50})^{0.6} \cdot g^{0.2}}{q_m^{0.4}} \quad [7.11]$$

7. PHYSICAL PROCESSES AND PARAMETER CALCULATIONS OF A SAND FILL

Equation [7.12] presents the flow velocity ($u_{dc;ic}$).

$$u_{dc;ic} = (20 \cdot q_m \cdot c_v \cdot d_{50})^{0.2} \cdot \left(\frac{8}{f_0}\right)^{0.3} \cdot \Delta^{0.4} \cdot g^{0.4} \quad [7.12]$$

Equation [7.13] presents the layer thickness (h_{dc}) of the mixture flow.

$$h_{dc} = \frac{q_m}{u_{dc;ic}} = \left(\frac{q_m^2}{\Delta \cdot g}\right)^{0.4} \cdot \left(\frac{1}{20 \cdot c_v \cdot d_{50}}\right)^{0.2} \cdot \left(\frac{f_0}{8}\right)^{0.3} \quad [7.13]$$

With equation [7.1], equation [7.4] until equation [7.13] is it possible to compute c_v , ρ_m , $u_{dc;ic}$, h_{dc} and q_m . From continuity the following mass balance is derived. With $\epsilon = \frac{4}{7}$, the ratio of the sand production that settles below MSL.

$$\frac{\epsilon \cdot P_s}{W} = \rho_s \cdot u_{dc;ic} \cdot h_{dc} \cdot c_v \quad [7.14]$$

Substitution of equation [7.1], equation [7.6], equation [7.4] and equation [7.5] into equation [7.14], the mass balance becomes:

$$\frac{\epsilon \cdot V_{load} \cdot (\rho_{m;0} - \rho_w) \cdot \rho_s}{t_{discharge} \cdot (\rho_s - \rho_w) \cdot W} = \rho_s \cdot c_v \cdot \frac{\pi \cdot d_0^2 \cdot u_0}{4 \cdot W} \quad [7.15]$$

An expression for c_v can be derived from equation [7.15]. Equation [7.16] presents the expression for c_v .

$$c_v = \frac{4 \cdot \epsilon \cdot V_{load} \cdot (\rho_{m;0} - \rho_w)}{t_{discharge} \cdot (\rho_s - \rho_w) \cdot \pi \cdot d_0^2 \cdot u_0} \quad [7.16]$$

The concentration (c_v) can also be presented as:

$$c_v = \frac{\rho_m - \rho_w}{\rho_s - \rho_w} \quad [7.17]$$

The mixture density (ρ_m) can be derived from equation [7.16] and equation [7.17]. Equation [7.18] presents the mixture density.

$$\rho_m = \frac{\rho_w \cdot t_{discharge} \cdot \pi \cdot d_0^2 \cdot u_0 + 4 \cdot \epsilon \cdot V_{load} \cdot \rho_{m;0} - 4 \cdot \epsilon \cdot V_{load} \cdot \rho_w}{t_{discharge} \cdot \pi \cdot d_0^2 \cdot u_0} \quad [7.18]$$

The flow velocity ($u_{dc;ic}$) for the density current is computed with equation [7.12] and the mixture flow is computed with equation [7.4]. The computation results are given in table [7.3]. These results are used in the computations of paragraph 7.4 and paragraph 7.5.

Table 7.3: The output parameters at sea bottom for the work method: pumping.

		Work method
		PU
ρ_m	kg/m ³	1295
$u_{dc;ic}$	m/s	1.89
q_m	m ² /s	0.24
s	kg/ms	104

7.4 Computation Results for the Sedimentation Length and Slope Type

In this paragraph the phenomena of paragraph 6.1 are verified by making the computations. For these computations the equations of paragraph 6.1.1 and 6.1.2 are used. For the input table [7.1] and table [7.2] is used. In table [7.6] it is not possible to use the parameter H^* , for describing the slope stability. Due to the fact that the particle size is larger than 500 μm , equation [6.1] cannot be used. Equation [6.1] is only valid for particle sizes between 100 μm and 500 μm . In the table [7.4] and table [7.5] the parameter H^* can be used. It can be concluded that according to the definition of H^* the slopes are stable. Flat slopes are more stable than steep slopes [Verruijt & van Baars, 2005]. But if the dimensionless hydraulic sedimentation length (L^*) is considered, it is clear that for the following work methods DU, RB, PU and SP the slope type is A, thus sensitive for flow slides. For the work method BF the slope type is C.

In figure [7.6] the solution of the convection equation is illustrated. The sedimentation length mentioned in table [7.4], table [7.5] and table [7.6] is based on Mastbergen & Bezuijen [1988]. The effect of hindered settling causes a longer sedimentation length than by neglecting the effect of hindered settling. This can be seen by the difference in figure [7.6] between the solution of the numerical scheme (equation [6.17]) and the analytical solution (equation [6.13]) with w_s computed according to equation [6.14]. Flow slides have a compacting effect, see for instance figure [7.7]. A flow slide occurred at every peak for increased pore pressure in the lowest graph. The porosity is illustrated in the upper graph. During the flow slide the porosity decreases and so the relative density increases. The porosity (n) decreases, in the displayed time series, with a value of ≈ 0.025 . This results in an increase of the relative density (R_e) with a value of ≈ 0.25 . From this it is clear that a small variation in the porosity has a large influence on the relative density. So, computations for the relative density (R_e) based on the porosity (n) are quite sensitive for disturbances.

7. PHYSICAL PROCESSES AND PARAMETER CALCULATIONS OF A SAND FILL

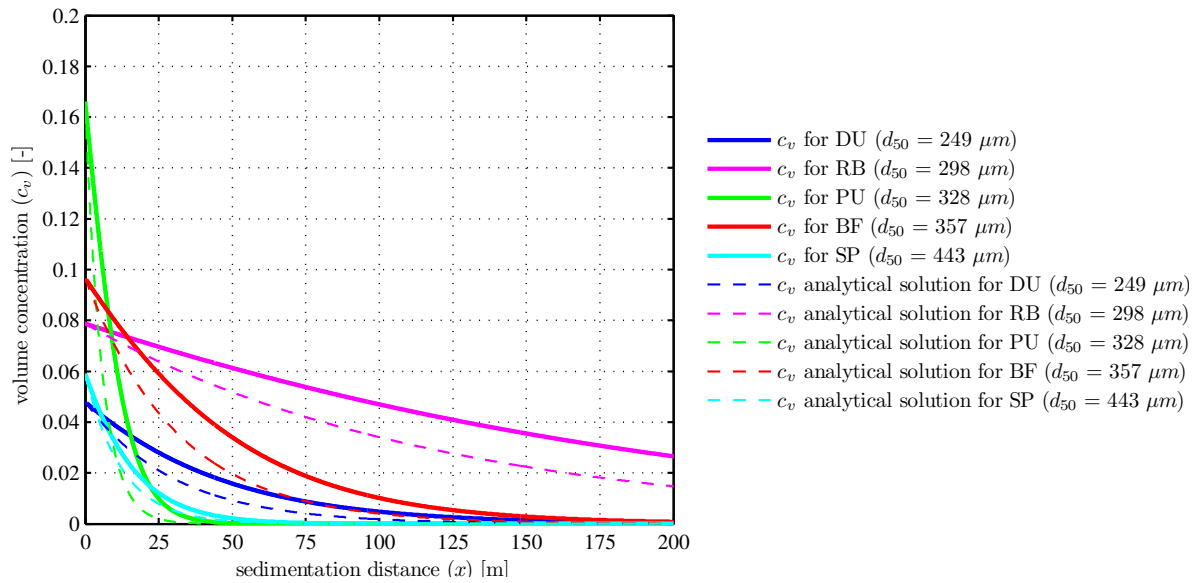


Figure 7.6: Sedimentation length and concentration development for the different work methods.

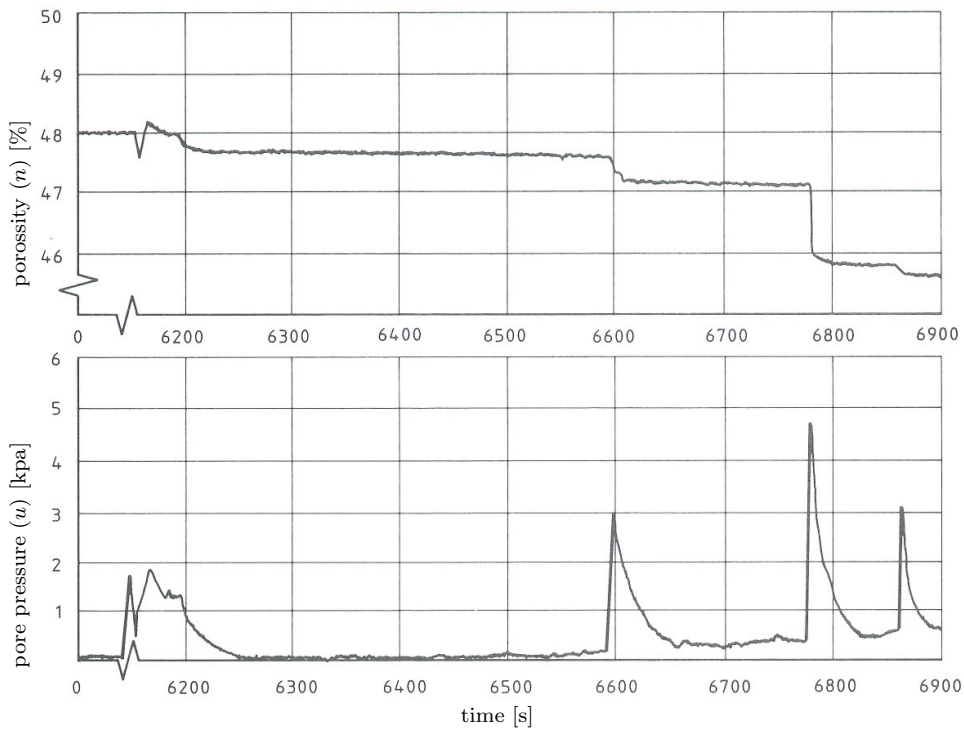


Figure 7.7: Example of increases of the pore pressure and decrease of the porosity during a flow slide [CUR 152, 1991], from Mastbergen *et al.* [1988].

Table 7.4: Computation results for sedimentation length, critical slope height and slope type, with lowest measured value of d_{50} .

		Work methods				
		DU	RB	PU	BF	SP
w_0	m/s	0.014	0.015	0.015	0.020	0.029
Re_p	-	1.923	2.153	2.368	3.462	6.372
h_{cr}	m	5.7	6.3	6.8	9.1	13.8
H^*	-	0.176	0.303	0.882	0.055	0.211
L_{sed}	m	78	432	27	110	32
L^*	-	0.450	0.865	0.039	3.059	0.393
slope type		A	A	A	C	A

Table 7.5: Computation results for sedimentation length, critical slope height and slope type, with average value of d_{50} .

		Work methods				
		DU	RB	PU	BF	SP
w_0	m/s	0.022	0.029	0.033	0.038	0.051
Re_p	-	4.035	6.427	8.187	10.100	16.942
h_{cr}	m	10.2	13.9	16.1	18.3	24.8
H^*	-	0.098	0.137	0.373	0.027	0.117
L_{sed}	m	44	207	12	55	18
L^*	-	0.295	0.494	0.020	1.721	0.243
slope type		A	A	A	C	A

Table 7.6: Computation results for sedimentation length, critical slope height and slope type, with highest measured value of d_{50} .

		Work methods				
		DU	RB	PU	BF	SP
w_0	m/s	0.067	0.084	0.122	0.063	0.088
Re_p	-	27.958	42.399	87.768	24.573	46.502
h_{cr}	m	32.9	41.7	63.3	30.6	44
H^*	-	0.030	0.046	0.095	0.016	0.066
L_{sed}	m	15	67	3	32	10
L^*	-	0.121	0.191	0.006	1.144	0.157
slope type		A	A	A	C	A

7. PHYSICAL PROCESSES AND PARAMETER CALCULATIONS OF A SAND FILL

The dimensionless hydraulic sedimentation length (L^*) is computed per work method for three different values of the d_{50} and for every work method the relative density (R_e) is derived from the statistics. In figure [7.8] is illustrated the relation between the relative density (R_e) and dimensionless hydraulic sedimentation length (L^*). The correlations are

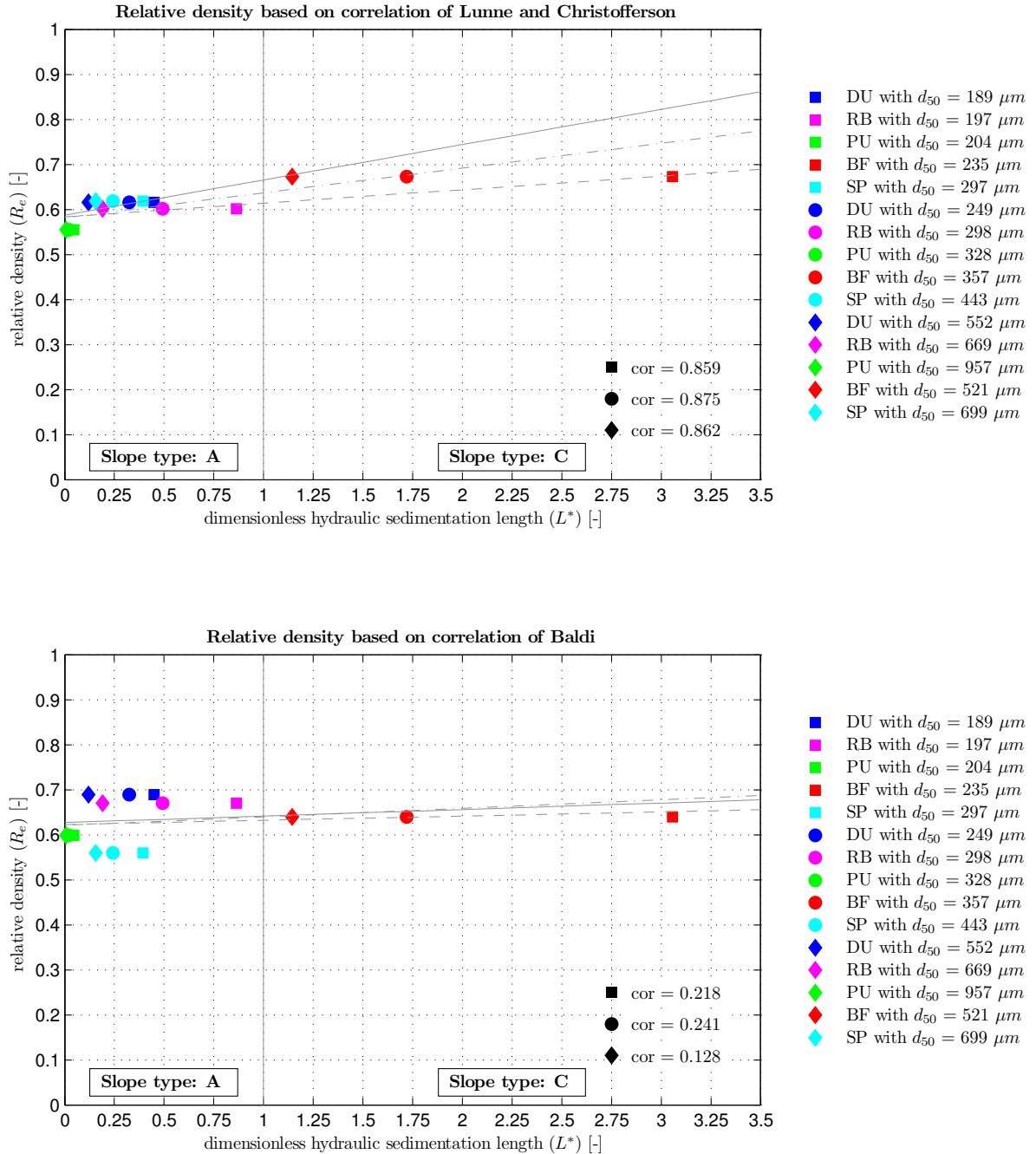


Figure 7.8: Relation between the relative density and the dimensionless hydraulic sedimentation length.

also computed. Table [7.7] presents the interpretation of correlation coefficients based on Guilford & Fruchter [1973].

Table 7.7: Guilford & Fruchter [1973] suggested interpretation for correlation coefficient values.

Value	Interpretation
< 0.2	Slight, almost negligible relationship.
0.2 - 0.4	Low correlation; definite but small relationship.
0.4 - 0.7	Moderate correlation; substantial relationship.
0.7 - 0.9	High correlation; marked relationship.
0.9 - 1.0	Very high correlation; very dependable relationship.

In the upper part of figure [7.8] the relative density based on equation [3.10] of Lunne and Christofferson is illustrated. The correlation coefficients are quiet high (correlation coefficient > 0.85), thus this suggests that there is a high correlation, according to table [7.7], thus a marked relationship between the relative density (R_e) based on Lunne and Christofferson and the dimensionless hydraulic sedimentation length (L^*). From the figure it is obvious that if $L^* < 1$, the achieved relative density based on Lunne and Christofferson is ≈ 0.6 for the work methods DU, RB and SP. In the lower part of figure [7.8] the relative density based on equation [3.9] of Baldi is illustrated. The correlation coefficients for the relative density (R_e) based on Baldi are quiet low (correlation coefficient < 0.25), so this suggest that there is a low correlation, according to table [7.7], thus a definite but small relationship between the relative density (R_e) based on Baldi and the dimensionless hydraulic sedimentation length (L^*).

Flow slides can occur in two types, see figure [6.3]. If the flow slide of figure [6.3a] occurs then the relative density decreases. If the flow slide of figure [6.3b] occurs then the relative density increases. In figure [7.7] the pore pressure is measured during laboratory test of Mastbergen *et al.* [1988]. The pore pressure increases until a flow slide occurs, this is a flow slide of figure [6.3b], so the relative density is increased. The statement of physical hypothesis (III.) is partly true. If the flow slide of figure [6.3a] occurs, the statement is true. If the flow slide of figure [6.3b] occurs, the statement is false. From figure [7.8] it is clear that the work methods DU, RB, PU and SP are sensitive for flow slides, but the relative density are between 0.55 and 0.70. Thus the statement of physical hypothesis (III.) is false.

7.5 Computation Results for the Density Current

In this paragraph the influence of the different mixture densities and suspension flow velocity regarding to the Shields parameter are compared. Furthermore, the parameters from table [7.1] and table [7.2] are used. Four computations have been made, namely:

7. PHYSICAL PROCESSES AND PARAMETER CALCULATIONS OF A SAND FILL

Table 7.8: Computation results for the density current.

Work methods										
DU		RB		PU		BF		SP		
τ	θ	τ	θ	τ	θ	τ	θ	τ	θ	
[N/m ²]	[-]	[N/m ²]	[-]	[N/m ²]	[-]	[N/m ²]	[-]	[N/m ²]	[-]	
<i>Initial conditions</i>										
1.	2.944	0.779	14.310	3.270	2.916	0.206	8.680	1.688	3.236	0.487
2.	2.944	0.388	14.310	1.949	2.916	0.135	8.680	1.206	3.236	0.432
<i>Stationary conditions</i>										
3.	9.182	2.430	38.298	8.751	11.000	2.523	40.141	7.808	16.139	2.429
4.	9.182	1.210	38.298	5.216	11.000	1.655	40.141	5.575	16.139	2.152

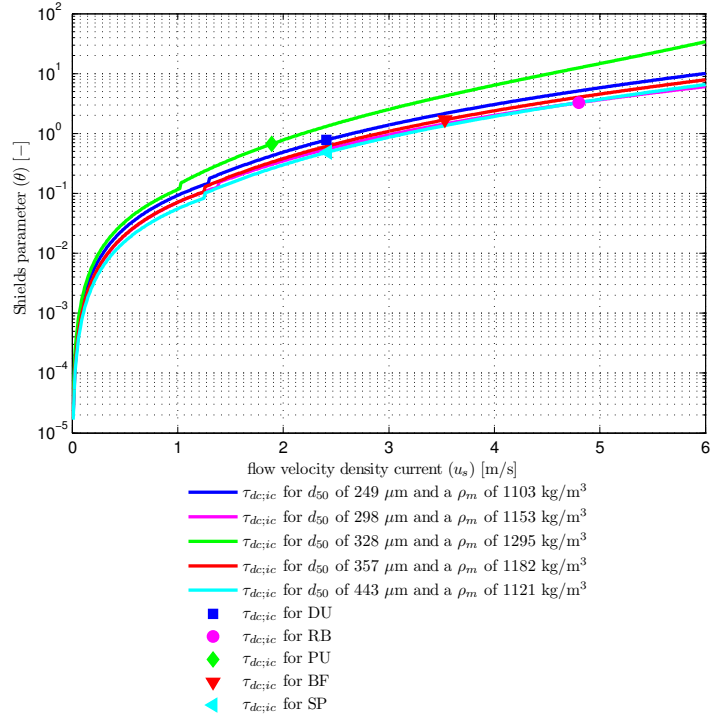
1. No variations, the equations from paragraph 6.2.1.1 are used;
2. Fixed particle diameter of 500 μm and the equations from paragraph 6.2.1.1 are used;
3. No variations, the equations from paragraph 6.2.1.2 are used;
4. Fixed particle diameter of 500 μm and the equations from paragraph 6.2.1.2 are used;

Computation (1.) and computation (2.) are computations based on the initial conditions and computation (3.) and computation (4.) are based on the stationary condition. In table [7.8] the results per work method are mentioned. In the figure [7.9a] and figure [7.9b] the computation results are illustrated for computation (1.). In the figure [7.10a] and figure [7.10b] the computation results are illustrated for computation (3.). In Appendix K the results are illustrated for all the computations. From the figure [7.9a] or figure [K.1] and figure [K.2], it is clear that by increasing suspension flow velocity the Shields parameter increases. From the figure [7.9b] or figure [K.3] and figure [K.4] it is clear that the mixture density has an influence on the Shields parameter. By increasing mixture density also the Shields parameter increases. The influence of the mixture density is the same for each work method. The difference between the mixture densities (ρ_m) are small, so the main influencing parameter for the density current is the flow velocity ($u_{dc;ic}$). The particle size has no influence on the shear stress, but the shear stress is presented in Shields values, so therefore there is an influence. By increasing particle size the Shields parameter decrease. That the particle size has no influence on the shear stress, comes due to the Nikuradse roughness height (k_s). The Nikuradse roughness height according to equation [6.26] has only an influence on the PSD, by means of the standard deviation (σ) that is mentioned in equation [6.26] and not any more an influence about the particle size.

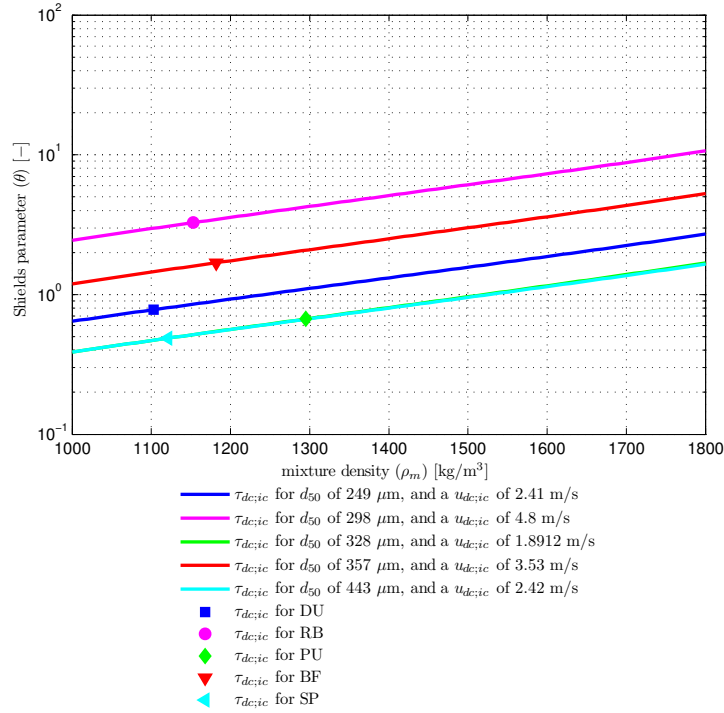
For the stationary conditions it is clear that the Shields value per work method are higher then for the initial conditions. From the figure [7.10a] or figure [K.5] and figure [K.6] it is

clear that by increasing flow velocity the shear stress decrease. Equation [6.30] has only a dependency with the flow velocity through the layer thickness of the density current (h_{dc}). The layer thickness is compute by dividing the mixture flow (q_m) through the flow velocity. For the mixture flow the values are used that are mentioned in table [7.2] and table [7.3]. So they mixture flow is kept constant and the flow velocity is increased and thus the layer thickness decreases. For the stationary density current there is an influence of the mixture density on the shear stress. If the mixture density increases also the shear stress increases. The particle size has no influence on the shear stress, because equation [6.30] has no dependency on the particle size. The dependency between the particle size and the shear stress is introduced by rewriting the shear stresses into Shield values. So, by increasing particle size the Shields values decrease.

7. PHYSICAL PROCESSES AND PARAMETER CALCULATIONS OF A SAND FILL

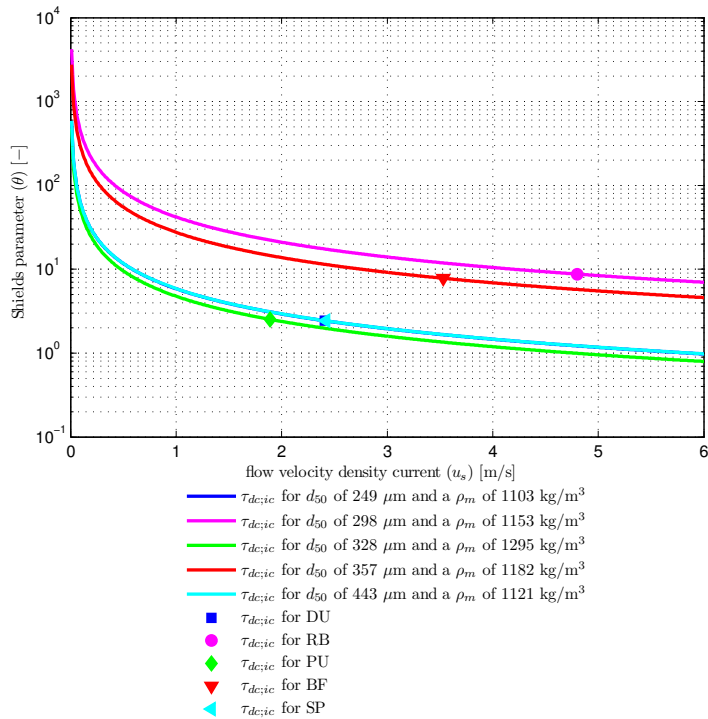


(a) Relation between Shields parameter and the flow velocity of a density current.

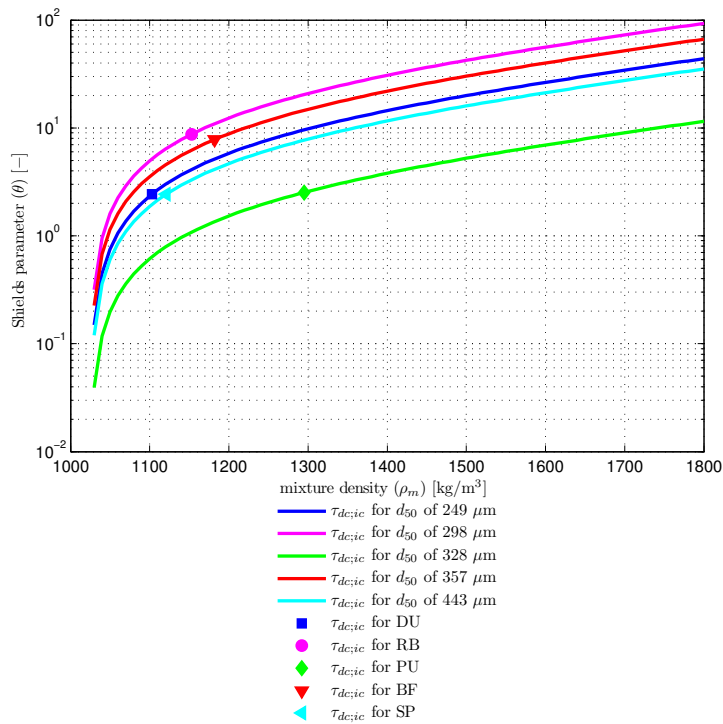


(b) Relation between Shields parameter and mixture density of a density current.

Figure 7.9: Computation results for the initial condition.



(a) Relation between Shields parameter and the flow velocity of a density current.



(b) Relation between Shields parameter and mixture density of a density current.

Figure 7.10: Computation results for the stationary condition.

7. PHYSICAL PROCESSES AND PARAMETER CALCULATIONS OF A SAND FILL

The Shields parameter (θ) is computed per work method for all four computations, the relative density (R_e) per work method is derived from the statistics. In figure [7.11] is illustrated the relation between the relative density (R_e) based on Lunne and Christofferson and the Shields parameter (θ). In figure [7.12] is illustrated the relation between the relative density (R_e) based on Baldi and the Shields parameter (θ). The correlations are also computed. With the aid of table [7.7] is it possible to say something about the correlations of the different computations. Computation (1.) of figure [7.11] has a slight correlation, thus an almost negligible relationship. The correlation of computation (2.) of figure [7.11] is low, thus a definite but small relationship. The correlation of computation

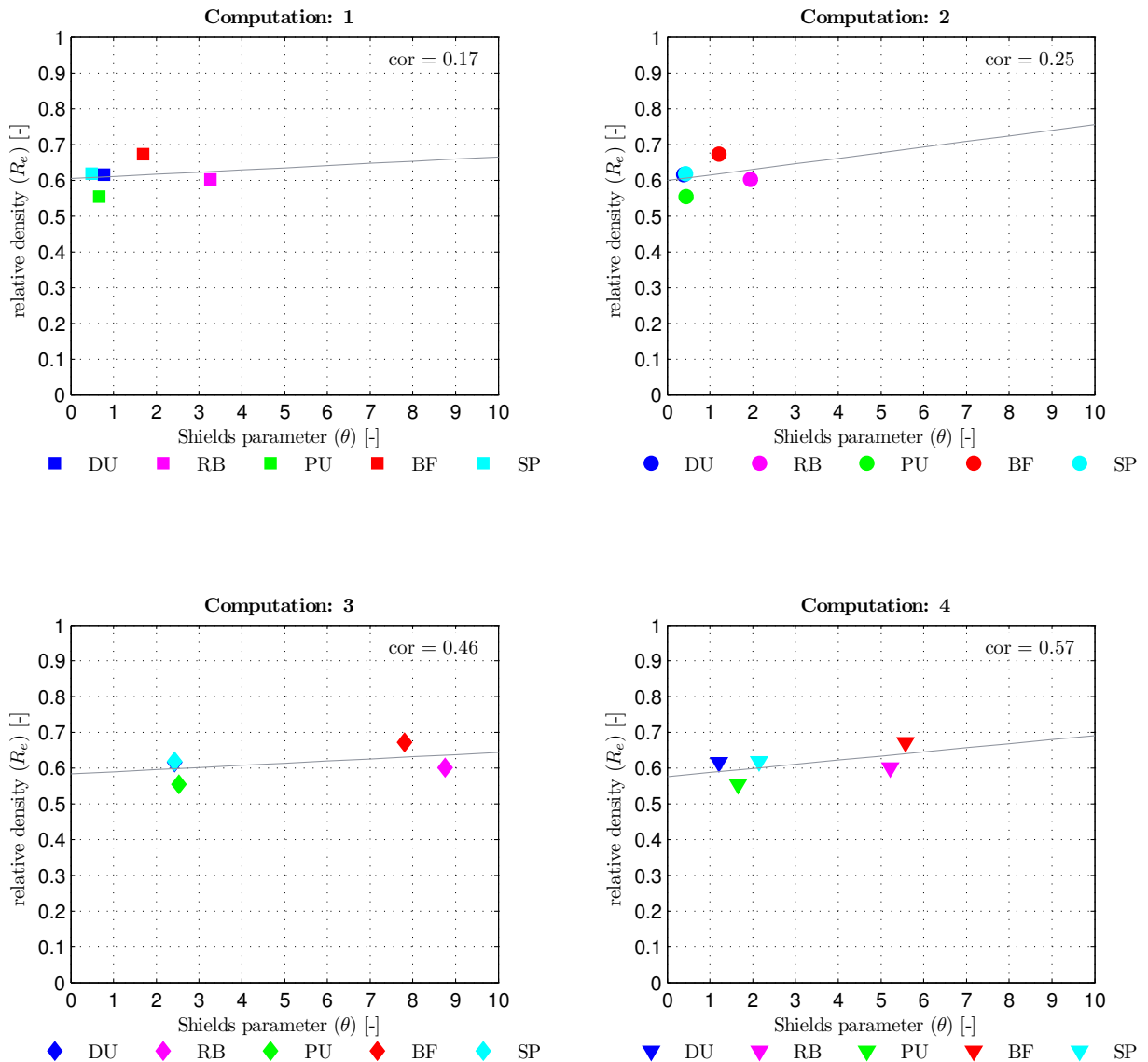


Figure 7.11: Relation between the relative density based on Lunne and Christofferson and the Shields parameter.

(3.) and computation (4.) of figure [7.11] are moderate, thus a substantial relationship. Computation (1.), computation (2.) and computation (3.) of figure [7.12] have a moder-

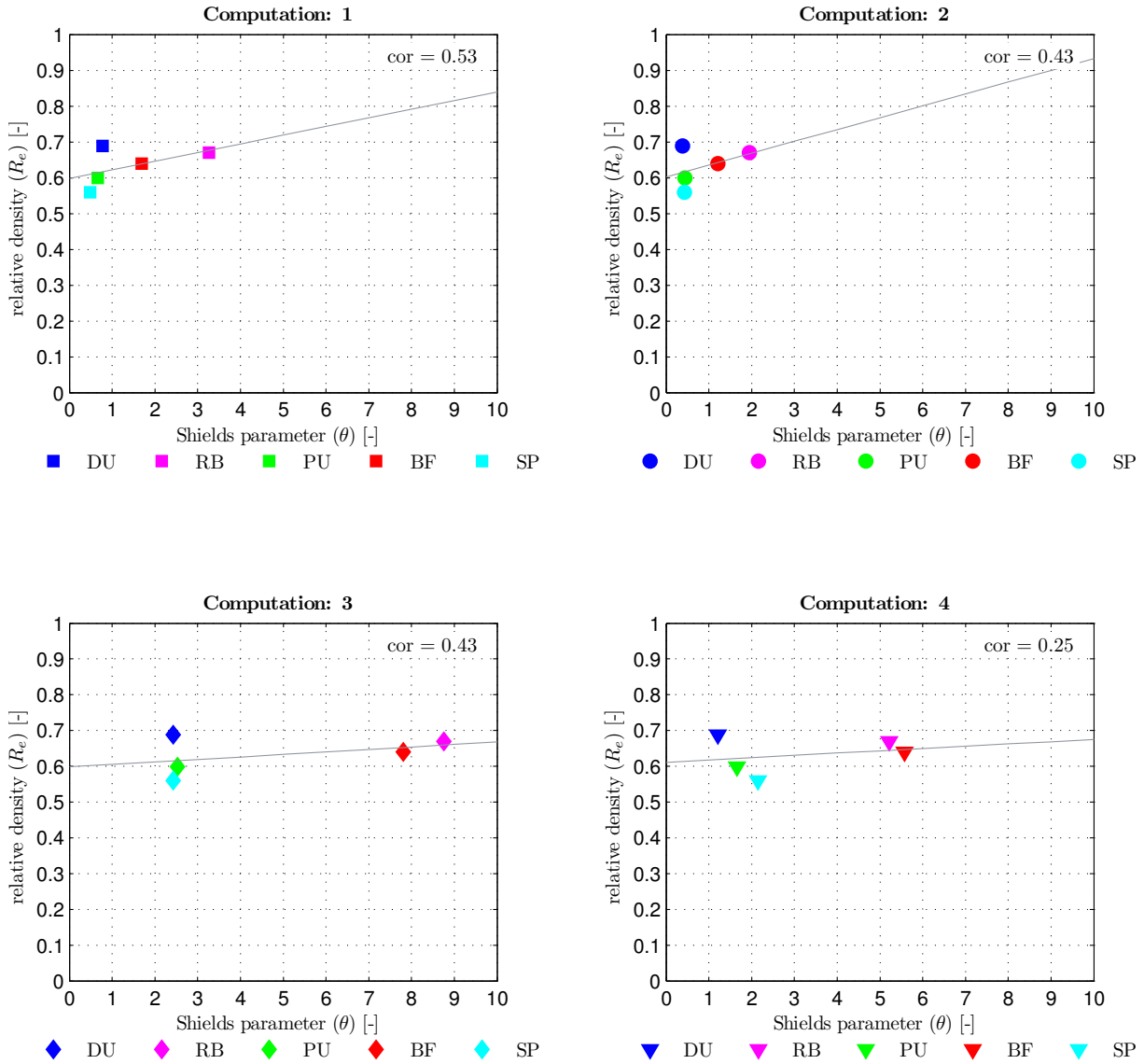


Figure 7.12: Relation between the relative density based on Baldi and the Shields parameter.

ate correlation, thus a substantial relationship. The correlation of computation (4.) of figure [7.12] is low, thus a definite but small relationship.

The correlations of figure [7.11] and figure [7.12] are positive thus this indicates that if the shear stress increase then also the relative density increase. Thus physical hypothesis (I.) is true. Physical hypothesis (II.) cannot be checked, because the concentrations of the different work methods are low. The values of the concentrations lie between the 0.04 and the 0.17.

7.6 Computation Results for the Hydrodynamics

In this paragraph the influence, of the different significant wave heights, wave periods and current velocities regarding to the Shields parameter, are computed. These computations are made to check the influence of the hydrodynamics on the relative density.

After construction, the hydrodynamics have, a small influence on the relative density of the top layer of the constructed sand body.

For the computations belonging to this paragraph, the hydrodynamic input from table [7.9] is used. This table illustrates real measured significant wave heights and periods from the Maasvlakte II project. For the current velocity also the dataset of the Maasvlakte II project is used. Furthermore, the parameters from table [7.1] and table [7.2] are used. Four computations have been made, namely:

1. No variations, input parameters from table [7.1], table [7.2] and table [7.9] are used;
2. Fixed water depth of 10 m and a particle diameter belonging to the corresponding work method;
3. Fixed particle diameter of 300 μm and a water depth belonging to the corresponding work method;
4. Fixed water depth of 10 m and a particle diameter of 300 μm .

Table 7.9: Hydrodynamic data used for computations

H_{m0}	T_{m-10}	H_{m0}	T_{m-10}
[m]	[s]	[m]	[s]
0.25	3.57	2.25	6.17
0.50	5.12	2.50	5.86
0.75	5.03	2.75	6.90
1.00	4.07	3.00	7.82
1.25	4.63	3.25	7.00
1.50	5.38	3.49	7.10
1.75	5.57	3.76	7.74
2.00	6.30	3.87	7.27

The computation results, for computation (1.), are illustrated in figure [7.14] and figure [7.13]. In Appendix L the results are illustrated for all four computations. In figure [7.14a] or figure [L.1] the relation between the significant wave height and the Shields parameter is illustrated. In figure [7.14b] or figure [L.2] the relation between the mean wave energy period and Shields parameter is illustrated. From the figures it is clear that by increasing wave height or period the Shields parameter also increases. Influence of the water depth on the Shields parameter can also be seen in the figures. By increasing water depth the Shields parameter is decreasing. This can be explained by using linear wave theory. The orbital motions are decreasing by increasing water depth. So, if the water depth is large enough, the Shields parameter is zero at the bottom. In figure [L.3] and figure [L.4] the

water depth variation is removed. From this it is clear that the variation between the work methods is small. The variation that is visible for the different work methods has to do with the mentioned friction factor in equation [6.37]. The differences into the friction factor are related to the boundary conditions for the different oscillatory flow regimes. In figure [7.13] the relation between the current velocity and Shields parameter related to currents is illustrated. From the graph it is clear that by increasing current velocity the bed shear stress related to currents also increases. The variation between the different work methods are negligible.

It can be concluded that for physical hypothesis (IV.) the influence of the hydrodynamics is small. For storm conditions the Shield values lie between 0.4 and 1.2, this are values by a water depth of 5 m, by increasing water depth the shear stress decreases. It only influences the workability during construction. During and after construction, it has an influence on the cross shore and long shore sediment transport [Bosboom & Stive, 2010]. The influence of the current is negligible.

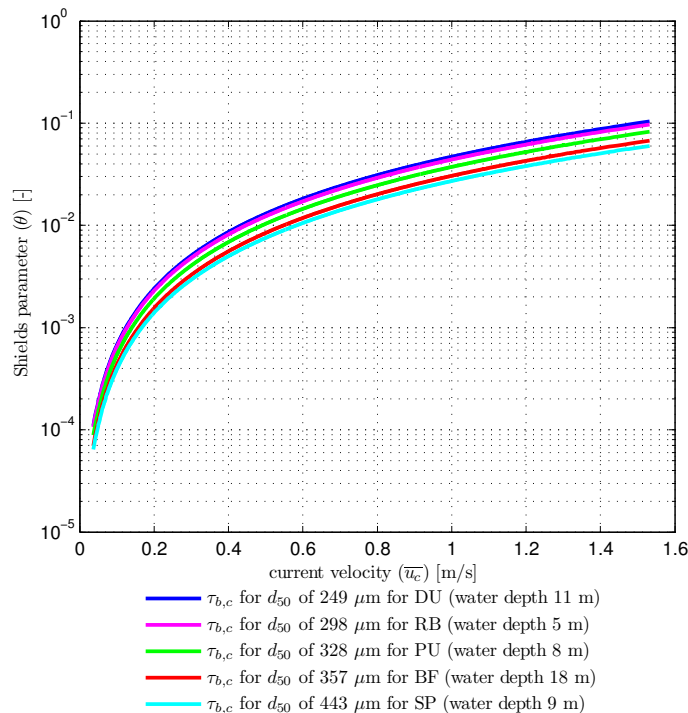
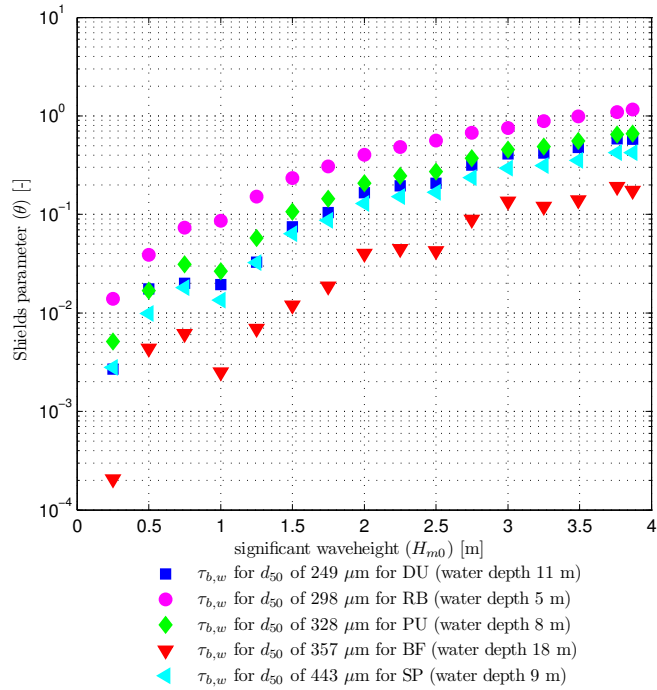
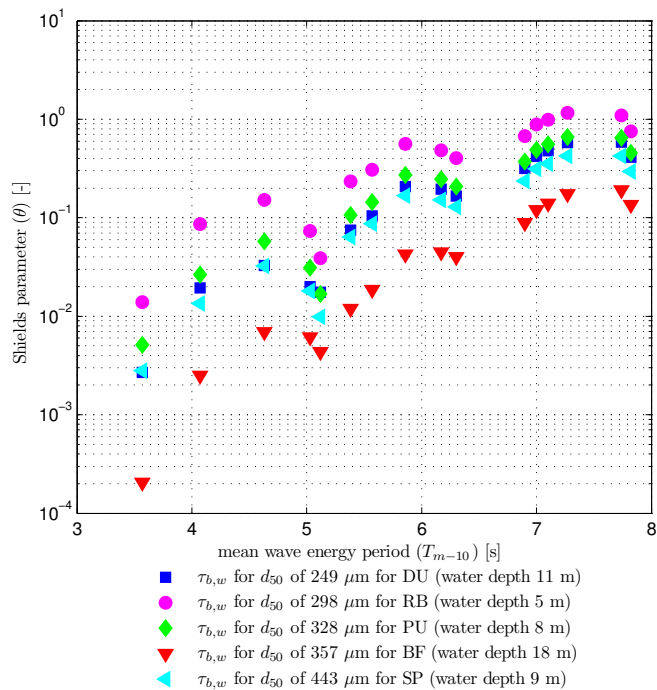


Figure 7.13: Relation between current velocity and the Shields parameter.

7. PHYSICAL PROCESSES AND PARAMETER CALCULATIONS OF A SAND FILL



(a) Relation between Shields parameter and significant wave height.



(b) Relation between Shields parameter and mean wave energy period.

Figure 7.14: Relation between Shields parameter and waves.

Chapter 8

Conclusions and Recommendations

In this chapter the conclusions and the recommendations are mentioned.

8.1 Conclusions

The aim of this research is to verify which processes influence the relative density of placed sand underwater by various techniques. The following question is central to the research:

What are the influencing and determining processes for achieving the relative density of dumped or sprayed sand underwater?

The work methods used for the hydraulic placement, the discharge conditions, the layer thickness, the water depth and the soil properties of the borrow area are all important in the achieved relative densities.

- In literature equal values for the relative density ($R_e = 0.44$) are taken for the different work methods spraying under water, back filling through the suction pipe, rainbowing (below LAT) and hydraulic reclamation (below LAT). This research reveals that, these different work methods (in practice) results in different values for the relative density. This means that there is a relation between the relative density and the used work method;
- For the work method pumping (hydraulic reclamation (above LAT)) the results of the relative density are comparable with the results of literature and other projects;
- Statistical testing, with the Kruskal-Wallis Test and Wilcoxon Rank Sum Test, prove that the used work method has an influence on the achieved relative densities;
- The used correlations, for cone resistance and relative density, have an influence on the results of the achieved relative density. From statistical testing, with the Kruskal-Wallis Test and Wilcoxon Rank Sum Test, the used correlations in this thesis are not equivalent;

8. CONCLUSIONS AND RECOMMENDATIONS

- The relative density based on Lunne and Christofferson in relation with the dimensionless hydraulic sedimentation length results in the highest correlation and shows that there is a relationship. For the work methods DU, RB, PU and SP the dimensionless hydraulic sedimentation length is smaller than 1 and the resulting relative density is ≈ 0.6 ;
- The flow velocity ($u_{dc;ic}$) of the density current is the major influencing parameter for the shear stress caused by the initial conditions for the density current. If the flow velocity increases then the shear stress increases and so the relative density increases;
- The influence of the mixture density (ρ_m) on the shear stress caused by the initial conditions for the density current, is small in comparison with the flow velocity ($u_{dc;ic}$).

8.2 Recommendations

- The registration of the TSHD trips can be improved by taking into account the spreading of the discharged load. Thus by registering several dump boxes per TSHD trip;
- The registration of the used work method per TSHD trip can be improved, by registering every chosen work method separately;
- It is important to obtain the soil constants of equation [3.9] or deriving a complete new fit for the Bligh Bank Formation (Holocene sand) and Kreftenheye Formation (Pleistocene Sand) by laboratory research based on Calibration Chamber Tests. This research results into a better correlation between the relative density and the used sands from the Bligh Bank Formation (Holocene sand) and Kreftenheye Formation (Pleistocene Sand);
- Research about the development of the velocity and concentration profile due to air and water entrainment for rainbowing a sand-water mixture at the point of impact on the water surface. Also the influence of the water depth needs to be taken into account. Probably by a small water depth the sand-water mixture behaves as a jet flow and by a large water depth there is first a jet flow and then the jet flow transforms to a plume flow. This has an influence on the velocity and concentration profile;
- For the work methods spraying and back filling through the suction pipe, the relative densities are higher than from literature. This is confirmed by physical hypothesis (I.). The work methods have a low concentration (0.04-0.17) at the bed and a high shear stress, which result in a higher relative density than mentioned in literature.

These work methods have a great accuracy and precision of placing the sand within the required slope tolerances, due to the controllable discharge processes. A positive side effect of these work methods is a constant relative high flow velocity that gives a high shear stress with higher values of the relative density. The last statement needs to be checked by executing laboratory research. A laboratory test can be set up with a large test flume with a movable discharge pipe, that can be equipped with a draghead, a dustpan or a T-shaped spray nozzle and the possibility to change the spray angle. The varying test parameters are discharge velocity, mixture density, stand off distance of the discharge pipe and the moving speed of the discharge pipe. These tests are almost identical to the tests that have been carried out by Mastbergen *et al.* [1988].

8. CONCLUSIONS AND RECOMMENDATIONS

References

- ALLEN, J.R.L. (1994). Fundamental properties of fluids and their relation to sediment transport. In *Sediment Transport and Depositional Processes*, pp. 25–60, Blackwell Scientific Publications, Oxford, United Kingdom.
- ANDERSON, T.W. & DARLING, D.A. (1952). Asymptotic theory of certain goodness-of-fit criteria based on stochastic processes. *Annals of Mathematical Statistics*, **23**, pp. 193–212.
- ASTM D1557 (2009). Standard Test Method for Laboratory Compaction Characteristics of Soil Using Standard Effort (2700 kN – m/m³).
- ASTM D2167 (2008). Standard Test Method for Density and Unit Weight of Soil in Place by the Rubber Balloon Method.
- ASTM D4253 (2006). Standard Test Methods for Maximum Index Density and Unit Weight of Soils Using a Vibratory Table.
- ASTM D4254 (2006). Standard Test Methods for Minimum Index Density and Unit weight of Soils and Calculation of Relative Density.
- ASTM D6938 (2010). Standard test method for In-Place Density and Water Content of Soil and Soil-Aggregate by Nuclear Methods (Shallow Depth).
- ASTM D698 (2007). Standard Test Method for Laboratory Compaction Characteristics of Soil Using Standard Effort (600 kN – m/m³).
- BAGNOLD, R.A. (1966). An approach to the sediment transport problem from general physics. Geological survey professional paper 422-i, United States Department of the Interior.
- BALDI, G., BELLOTTI, R., GHIONNA, M., V. JAMIOLKOWSKI & PASQUALINI, E. (1982). Design parameters for sands from CPT. In *Proceedings of the 2nd European Symposium on Penetration Testing*, vol. 2, pp. 425–432, ESOPTII, Balkema, Rotterdam, the Netherlands, Amsterdam, the Netherlands.

REFERENCES

- BALDOCK, T., TOMKINS, M., NIELSEN, P. & HUGHES, M. (2004). Settling velocity of sediments at high concentrations. *Coastal Engineering*, **51**, pp. 91–100.
- BLOMMAART, P.J.L. & VIERGEVER, M.A. (1995). Density of Cohesionless Soils. Tech. Rep. CO-354260/17, Delft Geotechnics (nowadays Deltares), Delft, the Netherlands.
- BOOSTER, L., LOMAN, G., DYKSTRA, C. & VAN DER MEER, J. (2008). Maasvlakte 2: Geotechnische beoordeling van aanleggebied. Ontwerpnota puma-q-lb-onb01, Projectorganisatie Uitbreiding Maasvlakte (PUMA).
- BOSBOOM, J. & STIVE, M.J.F. (2010). *Coastal Dynamics I, Lecture notes CT4305*. Delft University of Technology, Faculty of Civil Engineering and Geosciences, Section Hydraulic Engineering, VSSD, Delft, The Netherlands, v0.2 edn.
- BS 1377 (1990). Methods of test for soils for civil engineering purpose.
- BURGMANS, S. (2003). *Rainbowen van medium en grof zand*. Master's thesis, Delft University of Technology, Faculty of Civil Engineering and Geosciences, Section Hydraulic Engineering,
- CAMP, T.R. (1936). A study of the rational design of settling tanks. *Sewage Works Journal*, **8**, pp. 742–758.
- CAMP, T.R. (1946). Sedimentation and the design of settling tanks. *Transactions of the American Society of Civil Engineers*, **111**, pp. 895–958.
- CAMP, T.R. & ESTRADA, A.A. (1953). Studies of sedimentation basin design. *Sewage and Industrial Wastes*, **25**, pp. 1–14.
- CROW (2004). *Handboek Zandboek*. Publicatie 599, CROW, Ede, the Netherlands, Ede, the Netherlands,
- CROW (2011). Standaard RAW Bepalingen 2010.
- CUR 152 (1991). *CUR Repport 152: kunstmatig in water opgebouwde zandlichamen*. 152, W.D. Meinema B.V.
- CUR 157 (1993). *CUR Report 157: Sand Closures*. 157, A.A. Balkema, Rotterdam, The Netherlands.
- CUR 190 (1997). *CUR report 190: Probability in Civil Engineering*. 190, CUR.
- DAVIES, J.L. (1980). *Geographical Variation in Coastal Development*. Longman, London, 2nd edn.
- DAY, M.A. (1990). The no-slip condition of fluid dynamics. *Erkenntnis*, **33**, pp. 285–296.

REFERENCES

- DEKKING, F.M., KRAAIKAMP, C., LOPUHAÄ, H.P. & MEESTER, L.E. (2005). *A Modern Introduction to Probability and Statistics: Understanding Why and How (Springer Texts in Statistics)*. Springer.
- DELVIGNE, G.A.L. (1979). Round buoyant jet with three dimensional trajectory in ambient flow. Tech. Rep. Publication 228, WL|Delft Hydraulics (nowadays Deltares).
- DOHMEN-JANSSEN, M. (1999). *Grain size influence on sediment transport in oscillatory sheet flow*. Ph.D. thesis, Delft University of Technology.
- EMSAGG (2010). Maasvlakte 2 project: reclaiming future land with historical sand. *EMSAGG*, Issue 21, pp. 3–5.
- ENGELUND, F. (1965). A criterion for the occurrence of suspended load. *La Houille Blanche*, 8.
- FRIEDMAN, M. (1937). The Use of Ranks to Avoid the Assumption of Normality Implicit in the Analysis of Variance. *Journal of the American Statistical Association*, 32, pp. 675–701.
- FRIEDMAN, M. (1939). A correction: The use of ranks to avoid the assumption of normality implicit in the analysis of variance. *Journal of the American Statistical Association*, 34.
- FRIEDMAN, M. (1940). A comparison of alternative tests of significance for the problem of m rankings. *The Annals of Mathematical Statistics*, 11, pp. 86–92.
- DE GROOT, M.B., HEEZEN, F.T., MASTBERGEN, D.R. & STEFESS, H. (1988). Slopes and densities of hydraulically placed sands. In *Hydraulic Fill Structures*, ASCE Geotechnical Division Specialty Conference, Colorado State University, Fort Collins, USA.
- GUILFORD, J.P. & FRUCHTER, B. (1973). *Fundamental statistics in psychology and education*. McGraw-Hill, New York, 5th edn.
- HEEZEN, F.T. & VAN DER STAP, A.C.M. (1985). *Onderwater gestorte zandlichamen Deel I: Fysische processen*. Master's thesis, Delft University of Technology, Faculty of Civil Engineering and Geosciences, Section Hydraulic Engineering,
- HEEZEN, F.T. & VAN DER STAP, A.C.M. (1988). An engineering approach to under water dumped sandbodies. In *International Symposium on Modelling Sand-Water-Structure Interactions*, Balkema, Rotterdam, the Netherlands, Delft, the Netherlands.
- HOLTHUIJSEN, L.H. (2010). *Waves in Oceanic and Coastal Waters*. Cambridge University Press.

REFERENCES

- HOOGVEEEN, R., DE GROOT, M.B. & LUBKING, P. (1987). Literatuurstudie naar het storten van zand onder water. Tech. Rep. Bagt. 396CO-284460/11, Grondmechanica Delft (nowadays Deltares), Delft, The Netherlands.
- JANSEN, P.P., VAN BENDEGOM, L., VAN DEN BERG, J., DE VRIES, M. & ZANEN, A. (1979). *Principles of river engineering: the non-tidal alluvial river*. Water Resources Engineering Series, Pitman.
- JONSSON, I.G. (1966). Wave Boundary Layers and Friction Factors. In *Proceedings of 10th Conference on Coastal Engineering*, vol. 2, pp. 127–148, Tokyo, Japan.
- JONSSON, I.G. (1980). A new approach to oscillatory rough turbulent boundary layers. *Ocean Engineering*, **7**, pp. 109–152.
- KRUSKAL, W.H. & WALLIS, W.A. (1952). Use of Ranks in One-Criterion Variance Analysis. *Journal of the American Statistical Association*, **47**, pp. 583–621.
- KRUSKAL, W.H. & WALLIS, W.A. (1953). Errata: Use of ranks in one-criterion variance analysis. *Journal of the American Statistical Association*, **48**, pp. 907–911.
- LEE, K.M. (2001). Influence of placement method on the cone penetration resistance of hydraulically placed sand fills. *Canadian Geotechnical Journal*, **38**, pp. 592–607.
- LEE, K.M., SHEN, C.K., LEUNG, D.H.K. & MITCHELL, J.K. (1999). Effects of Placement Method on Geotechnical Behavior of Hydraulic Fill Sands. *Journal of Geotechnical and Geoenvironmental Engineering*, **125**, pp. 832–846.
- LUNNE, T. (2006). Correlation CPT to Relative Density. Tech. Rep. 20041367-3, NGI.
- LUNNE, T. & CHRISTOFFERSEN, H.P. (1983). Interpretation of Cone Penetrometer Data for Offshore Sands. In *Proceedings 15th Annual Offshore Technology Conference*, Offshore Technology Conference, Houston, Texas, USA.
- LUNNE, T., ROBERTSON, P.K. & POWELL, J.J.M. (1997). *Cone Penetration Testing in Geotechnical Practice*. E & FN Spon, London, United Kingdom.
- MARINE SAMPLING HOLLAND (2009). *Method Statement CPT Testing*.
- MASSELINK, G., HUGHES, M.G. & KNIGHT, J. (2011). *An Introduction to Coastal Processes and Geomorphology*. Hodder Education, 2nd edition edn.
- MASTBERGEN, D.R. & BEZUIJEN, A. (1988). Het storten van zand onder water 5: Zand-waterstromingen, Verslag experimentele vervolgstudie middelgrof zand. Tech. Rep. Bagt. 420 / Z261 / CO-294750, Grondmechanica Delft, WL|Delft Hydraulics (nowadays Deltares).

REFERENCES

- MASTBERGEN, D.R. & LEEUWESTEIN, W. (1986). Het gedrag van zandwatermengselstromingen bij zandsluitingen. Tech. rep., Technische Universiteit Delft, Faculteit Civiele Techniek, Delft, the Netherlands.
- MASTBERGEN, D.R., BEZUIJEN, A. & WINTERWERP, J.C. (1988). On the construction of sand fill dams, Part I and II. In *International Symposium on Modelling Sand-Water-Structure Interactions*, Balkema, Rotterdam, the Netherlands, Delft, the Netherlands.
- MCClave, J.T., BENSON, P.G. & SINCICH, T. (2005). *Statistics for Business and Economics*. Prentice Hall, 9th edn.
- MIEDEMA, S.A. (2008). An analytical method to determine scour. In *WEDA XXVIII/Texas A/M 39*, WEDA/TAMU, St. Louis, USA, June 2008.
- MIEDEMA, S.A. (2010). Constructing the Shields curve, a new theoretical approach and its applications. In *WODCON XIX*, WODA, Beijing.
- MITCHENER, H. & TORFS, H. (1996). Erosion of mud/sand mixtures. *Coastal Engineering*, **29**, pp. 1–25.
- NEN 6740 (2006). Geotechniek - TGB 1990 - Basiseisen en belastingen .
- NEN-EN-ISO 14688-1 (2002). Geotechnical investigation and testing - Identification and classification of soil - Part 1: Identification and description.
- NIST/SEMATECH (2010). e-Handbook of Statistical Methods. <http://www.itl.nist.gov/div898/handbook/>.
- POWERS, M.C. (1953). A new roundness scale for sedimentary particles. *Journal of Sedimentary Petrology*, **23**, pp. 117–119.
- REYNOLDS, O. (1885). On the dilatancy of media composed of rigid particles in contact, with experimental illustrations. *Phil. Mag.*, **Series 5**, pp. 469–481.
- REYNOLDS, O. (1886). Experiments showing dilatancy, a property of granular material, possibly connected with gravitation. *Proc. Royal Institution of Great Britain*, pp. 217–227.
- VAN RHEE, C. (2002a). *On the sedimentation process in a Trailing Suction Hopper Dredger*. Ph.D. thesis, Delft University of Technology.
- VAN RHEE, C. (2002b). The influence of the bed shear stress on the sedimentation of sand. In *11th Int. Symposium on Transport and Sedimentation of Solid Particles*, Ghent, Belgium.
- VAN RHEE, C. (2004). Sediment settling and Pick-up at a flow velocity below the deposition limit. In *16th Int Conference on Hydrotransport*.

REFERENCES

- VAN RHEE, C. (2010a). Numerical Simulation of the Bottom Discharge Process of a Trailing Suction Hopper Dredger. In *WODCON XIX*.
- VAN RHEE, C. (2010b). Sediment Entrainment at High Flow Velocity. *Journal of Hydraulic Engineering-Asce*, **136**, pp. 572–582.
- VAN RHEE, C. (2011). Numerical Simulation of the Backfilling Process of a Trench using a Trailing Suction Hopper Dredger. In *Proceedings of the ASME 30th International Conferences On Ocean, Offshore and Arctic Engineering OMAE 2011*, ASME, Rotterdam, the Netherlands.
- VAN RHEE, C. & TALMON, A.M. (2010). Sedimentation and Erosion of sediment at high solids concentration. In N. Heywood, ed., *18th international conference on hydro-transport*, pp. 211–222, BHR Group limited, Bedfordshire, United Kingdom.
- RICHARDSON, J.F. & ZAKI, W.N. (1954). Sedimentation and fluidisation: Part i. *Chemical Engineering Research and Design*, **75**, S82–S100.
- VAN RIJN, L.C. (1984a). Sediment pickup functions. *Journal of Hydraulic Engineering*, **110**, pp. 1494–1502.
- VAN RIJN, L.C. (1984b). Sediment Transport, Part I: Bed Load Transport. *Journal of Hydraulic Engineering*, **110**, pp. 1431–1456.
- VAN RIJN, L.C. (1984c). Sediment Transport, Part II: Suspended Load Transport. *Journal of Hydraulic Engineering*, **110**, pp. 1613–1641.
- VAN RIJN, L.C. (1993). *Principles of sediment transport in rivers, estuaries, and coastal seas*. Aqua Publications.
- ROBERTSON, P.K., CAMPANELLA, R.G., GILLESPIE, D. & GREIG, J. (1986). Use of Piezometer Cone Data. In *Proceedings of the ASCE Specialty Conference In Situ '86: Use of In Situ Test in Geotechnical Engineering*, pp. 1263–1280, American Society of Engineers (ASCE), Blacksburg.
- SCHIERECK, G. (2004). *Introduction to Bed, Bank and Shore protection*. Delft University of Technology, Faculty of Civil Engineering and Geosciences, Section Hydraulic Engineering, VSSD, Delft, The Netherlands.
- SHIELDS, A. (1936). *Anwendung der Ähnlichkeitsmechanik und der Turbulenzforschung auf die Geschiebebewegung*. Ph.D. thesis, Technischen Hochschule Berlin, Mitteilungen der Preussischen Versuchsanstalt für Wasserbau und Schiffbau, Berlin.
- SHIELDS, A., OTT, W.P. & VAN UCHELEN, J.C. (1936). Application of similarity principles and turbulence research to bed-load movement. Tech. Rep. 167, California

REFERENCES

- Institute of Technology, Hydrodynamics Laboratory, Pasadena, California, USA, anwendung der Ähnlichkeitsmechanik und der Turbulenzforschung auf die Geschiebebewegung. [English title: Application of similarity principles and turbulence research to bed-load movement / by Ing. A. Shields; translated by W.P. Ott and J.C. van Uchelen Hydrodynamics Laboratory publication ; 167.
- SHORT, A.D. (2005). Wave Environment. In *Encyclopedia of Coastal Science*, Springer.
- STEPHENS, M.A. (1974). EDF Statistics for Goodness of Fit and Some Comparisons. *Journal of the American Statistical Association*, **69**, pp. 730–737.
- SWART, D.H. (1976). Predictive equations regarding Coast Transport. In *Proceedings of 15th Conference on Coastal Engineering*, vol. 1, pp. 1113–1132, Honolulu, Hawaii.
- TUFENKJIAN, M.R., YEE, E. & THOMPSON, D.J. (2010). Comparison of cone and minicone penetration resistance for sand at shallow depth. In *2nd International Symposium on Cone Penetration Testing*, Huntington Beach, CA, USA.
- UNSÖELD, G. (1984). Der Transportbeginn rolligen Sohlmaterials in gleichförmigen turbulenten Strömungen - Eine kritische Überprüfung der Shields-Funktion und ihre experimentelle Erweiterung auf feinkörnige, nichtbindige Sedimente. Tech. rep., Universität Kiel, Germany.
- VBKO (1998). *Voortgezette Opleiding Uitvoering Baggerwerken: Grondmechanica*, vol. 1. The Dutch Association of Contractors in Dredging, Shore and Bank Protection, Leidschendam, The Netherlands.
- VAN DE VELDE, M. (2008). Captain of TSHD "Leiv Eiriksson". <http://www.theartofdredging.com>.
- VELDHUIS, A. (1992). *Uitlevering van Zand*. Master's thesis, Delft University of Technology, Faculty of Civil Engineering and Geosciences, Section Hydraulic Engineering.
- VERRUIJT, A. & VAN BAARS, S. (2005). *Grondmechanica*. VSSD, Delft, The Netherlands.
- VOUW (2010a). *Advanced Training in Hydraulic Engineering Works: Soil Mechanics*, vol. 1. Dutch Association of Dredging Contractors, Gouda, The Netherlands, 2010th edn.
- VOUW (2010b). *Advanced Training in Hydraulic Engineering Works: Trailing Suction Hopper Dredgers*, vol. 5b. Dutch Association of Dredging Contractors, Gouda, The Netherlands, 2010th edn.
- VRIJLING, J.K. & VAN GELDER, P.H.A.J.M. (2006a). *CT4130 Probability in civil Engineering (Lecture notes)*. Delft University of Technology, Faculty of Civil Engineering and Geosciences, Section Hydraulic Engineering.

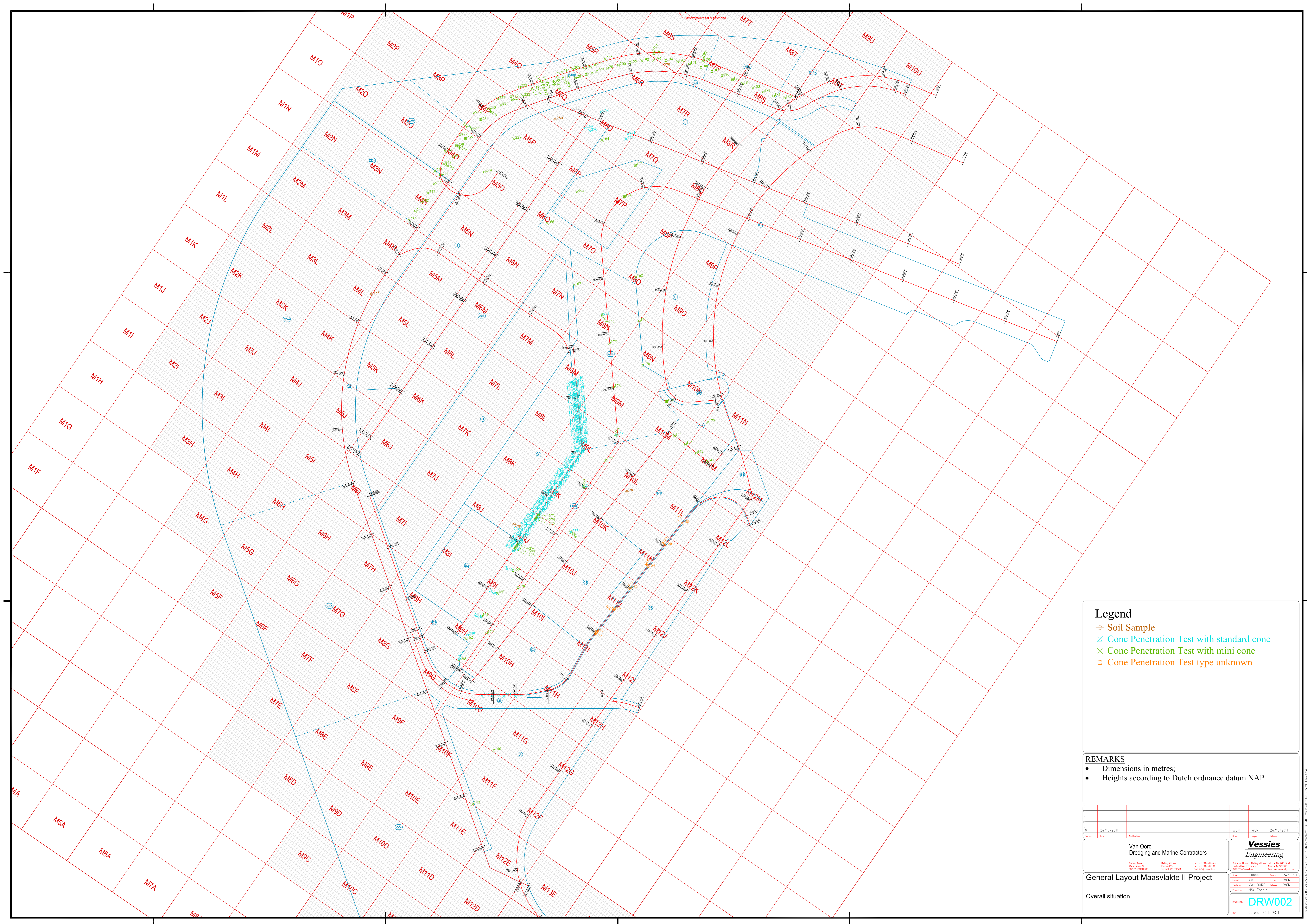
REFERENCES

- VRIJLING, J.K. & VAN GELDER, P.H.A.J.M. (2006b). *CT5310 Probabilistic Design in Hydraulic Engineering (Lecture notes)*. Delft University of Technology, Faculty of Civil Engineering and Geosciences, Section Hydraulic Engineering.
- WILCOXON, F. (1945). Individual comparisons by ranking methods. *Biometrics Bulletin*, **1**, pp. 80–83.
- WL|DELFT HYDRAULICS (1969). Begin van beweging van bodemmateriaal. Tech. Rep. S159-1, WL|Delft Hydraulics (nowadays Deltares).
- YALIN, M.S. (1977). *Mechanics of Sediment Transport*. Pergamon Press, 2nd edn.
- YOON, S. & TUMAY, M.T. (2010). Field application of continuous intrusion miniature CPT system in South Korea. In *2nd International Symposium on Cone Penetration Testing*, Huntington Beach, CA, USA.
- YOUNG, T.L. (1973). Factors controlling maximum and minimum densities of sands. In *Evaluation of Relative Density and Its Role in Geotechnical Projects Involving Cohesionless Soils*, vol. 523, pp. 98–112, ASTM Special Technical Publication, ASTM, Philadelphia, USA.
- ZANKE, U.C.E. (1977). *Berechnung der Sinkgeschwindigkeiten von Sedimenten*. No. Heft 46, Seite 243 in Mitteilungen des Franzius-Instituts für Wasserbau und Küsteningenieurwesen der Technischen Universität Hannover, EV.
- ZANKE, U.C.E. (2001). *Zum Einfluss der Turbulenz auf den Beginn der Sedimentbewegung*. Institut für Wasserbau und Wasserwirtschaft, Technische Universität Darmstadt.
- ZANKE, U.C.E. (2003). On the influence of turbulence on the initiation of sediment motion. *International Journal of Sediment Research*, **18**, pp. 17–31.

Appendices

Appendix A: General Overview of Maasvlakte II Project

Appendix A: General Overview of Maasvlakte II Project



Legend

- Soil Sample
- Cone Penetration Test with standard cone
- Cone Penetration Test with mini cone
- Cone Penetration Test type unknown

REMARKS

- Dimensions in metres;
- Heights according to Dutch ordnance datum NAP

24/10/2011 <small>Rev. No. Date</small>	WCN <small>Drawn</small>	WCN <small>Checked</small>	24/10/2011 <small>Date</small>
Van Oord Dredging and Marine Contractors		Vessies Engineering	
<small>Van Oord Address: ...</small>		<small>Vessies Address: ...</small>	
General Layout Maasvlakte II Project			
Overall situation			
<small>Scale: 1:10000</small>		<small>Date: 24/10/11</small>	
<small>Author: VAN OORD</small>		<small>Drawn: WCN</small>	
<small>Program: MSc Thesis</small>		<small>Drawn: WCN</small>	
<small>Drawings: DRW002</small>		<small>Date: October 24th, 2011</small>	

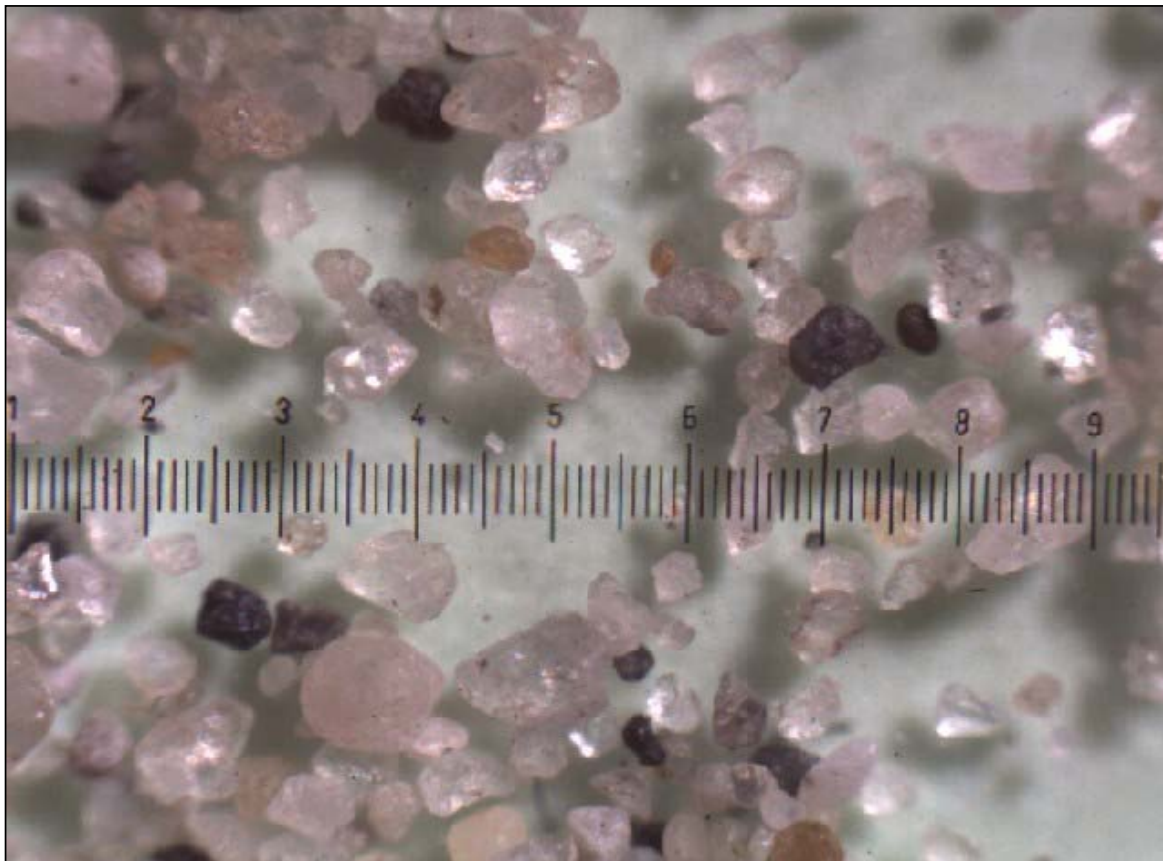
Appendix B: Results Grains Shape Analyse

Appendix B: Results Grains Shape Analyse

Grain Shape

Project: **Maasvalkte II**
 Project no.:
 Title:














Location: **Rotterdam**
 Date: **19-01-12**
 Prep.: **RDH**



Magnified 7X

Distance between major ticks: 450 micron

Sample 01

Sphericity	High						
	Low						
		Very Angular 0.15	Angular 0.20	Sub-Angular 0.30	Sub-Rounded 0.40	Rounded 0.60	Well Rounded 0.85
							

Estimated according Powers:
 Quartz Content (Estimated):

Sub Angular to Sub Rounded

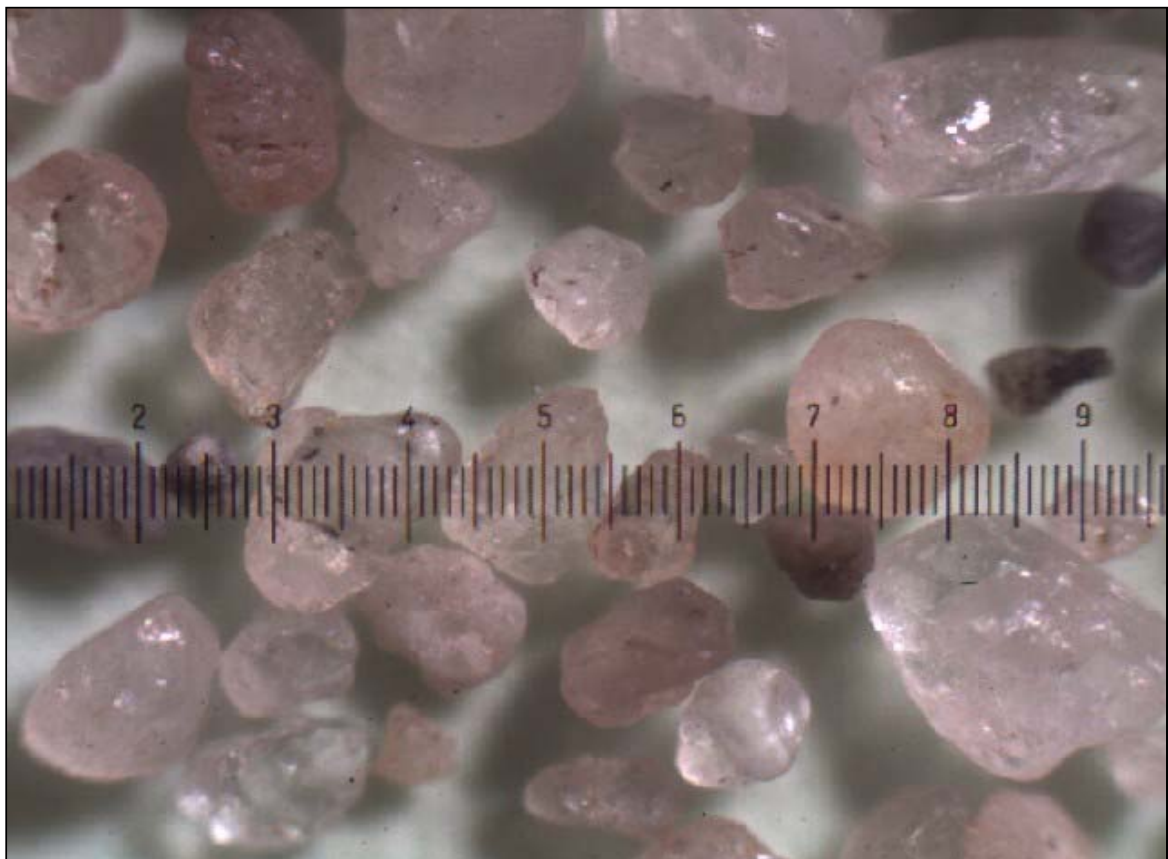
Appendix B: Results Grains Shape Analyse

Grain Shape



Project: **Maasvalkte II**
 Project no.:
 Title:

Location: **Rotterdam**
 Date: **19-01-12**
 Prep.: **RDH**



Magnified 7X

Distance between major ticks: 450 micron

Sample 02

Sphericity	High						
	Low						
		Very Angular 0.15	Angular 0.20	Sub-Angular 0.30	Sub-Rounded 0.40	Rounded 0.60	Well Rounded 0.85
				←→			

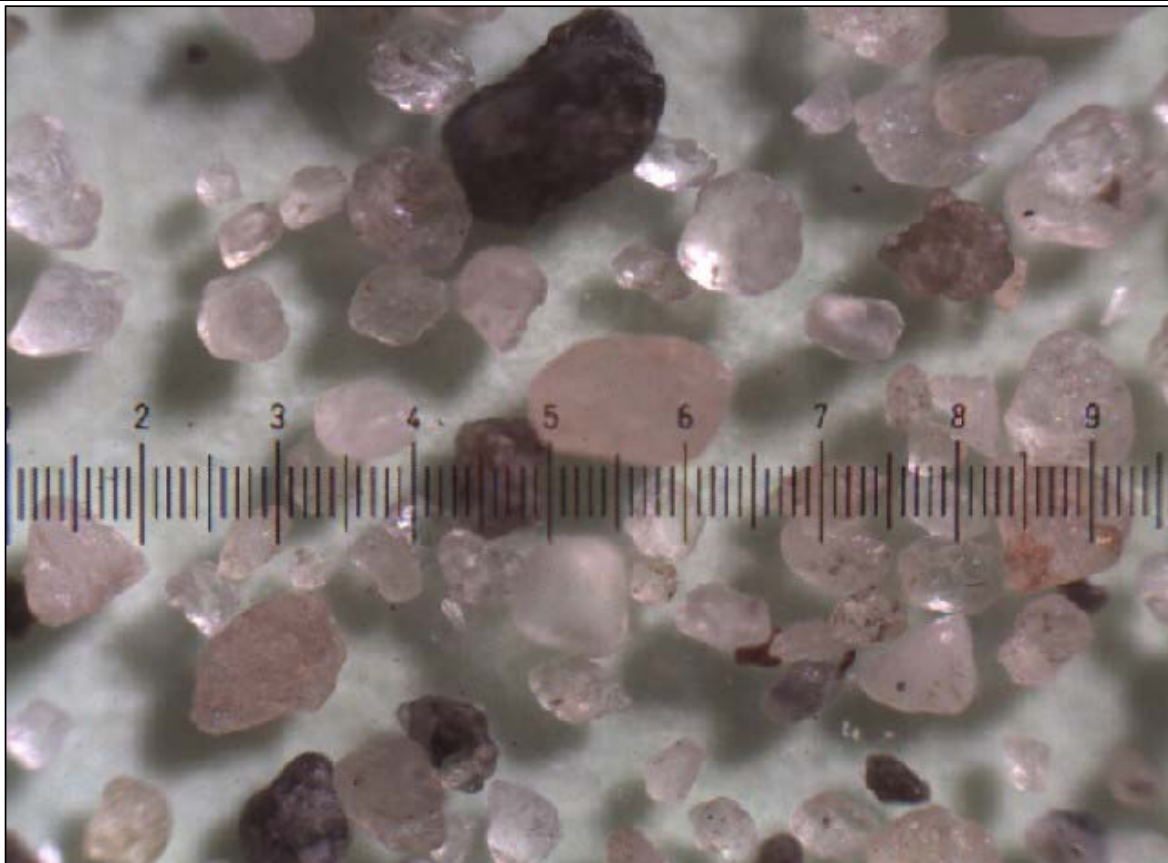
Estimated according Powers:
 Quartz Content (Estimated):

Sub Angular to Sub Rounded

Grain Shape

Project: **Maasvalkte II**
 Project no.:
 Title:





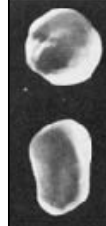







Location: **Rotterdam**
 Date: **19-01-12**
 Prep.: **RDH**



Magnified 7X

Distance between major ticks: 450 micron

Sample 03

Sphericity	High						
	Low						
		Very Angular 0.15	Angular 0.20	Sub-Angular 0.30	Sub-Rounded 0.40	Rounded 0.60	Well Rounded 0.85
				←→			

Estimated according Powers:
 Quartz Content (Estimated):

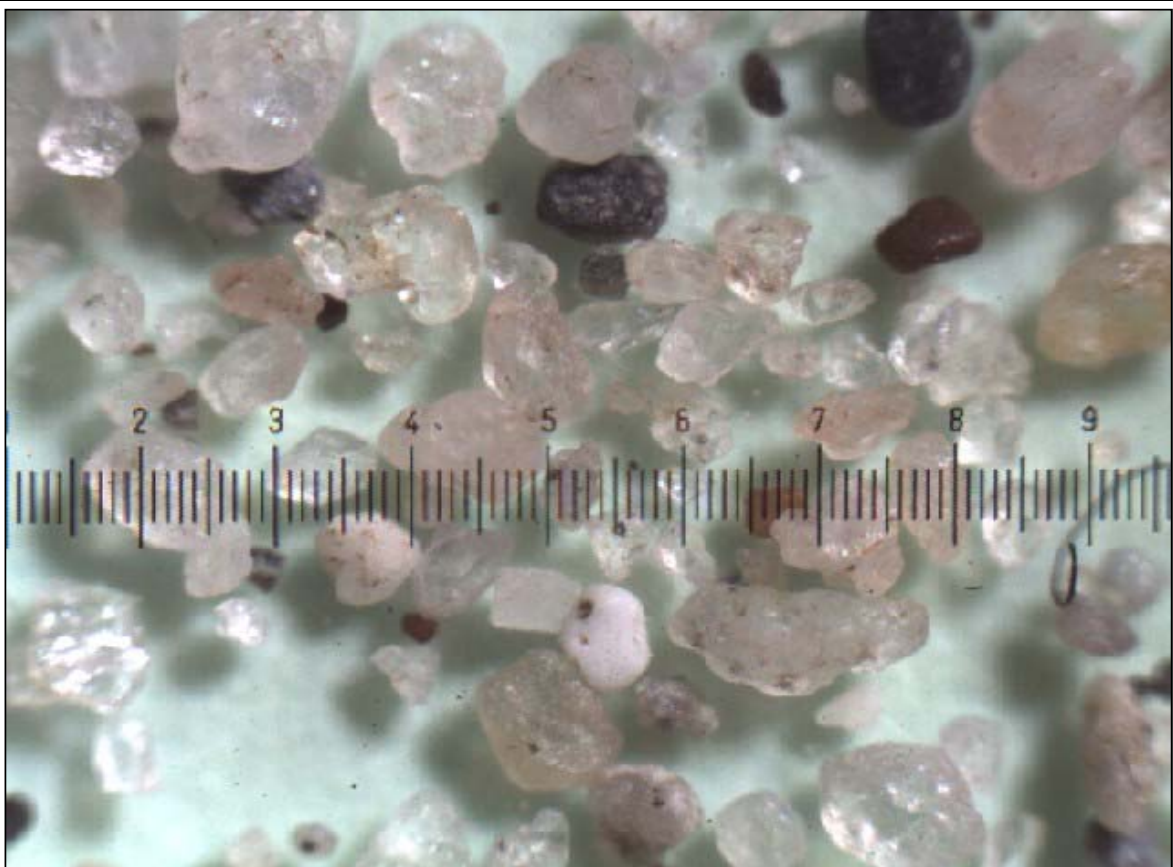
Sub Angular to Sub Rounded

Grain Shape



Project: **Maasvalkte II**
 Project no.:
 Title:

Location: **Rotterdam**
 Date: **19-01-12**
 Prep.: **RDH**



Magnified 7X

Distance between major ticks: 450 micron

Sample 04

Sphericity	High						
	Low						
		Very Angular 0.15	Angular 0.20	Sub-Angular 0.30	Sub-Rounded 0.40	Rounded 0.60	Well Rounded 0.85
				←→			

Estimated according Powers:
 Quartz Content (Estimated):

Sub Angular to Sub Rounded

Grain Shape

Project: **Maasvalkte II**
 Project no.:
 Title:







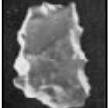






Location: **Rotterdam**
 Date: **19-01-12**
 Prep.: **RDH**



Magnified 7X

Distance between major ticks: 450 micron

Sample 05

Sphericity	High						
	Low						
		Very Angular 0.15	Angular 0.20	Sub-Angular 0.30	Sub-Rounded 0.40	Rounded 0.60	Well Rounded 0.85
							

Estimated according Powers:
 Quartz Content (Estimated):

Sub Angular to Sub Rounded

Appendix B: Results Grains Shape Analyse

Appendix C: Comparison between Standard CPT's and Mini-CPT's

Appendix C: Comparison between Standard CPT's and Mini-CPT's

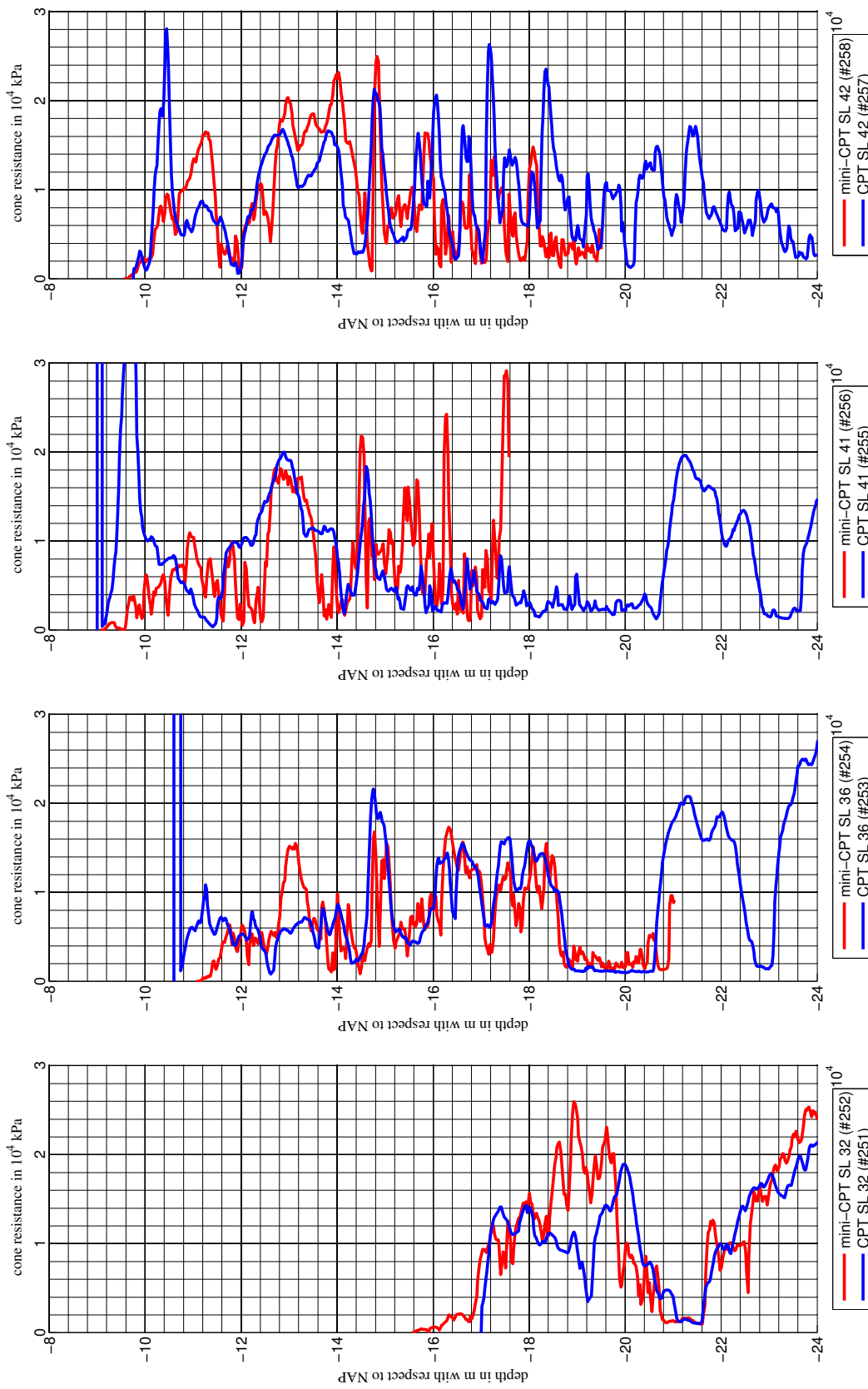


Figure C.1: Comparison between standard CPT's and mini-CPT's (offshore).

Appendix C: Comparison between Standard CPT's and Mini-CPT's

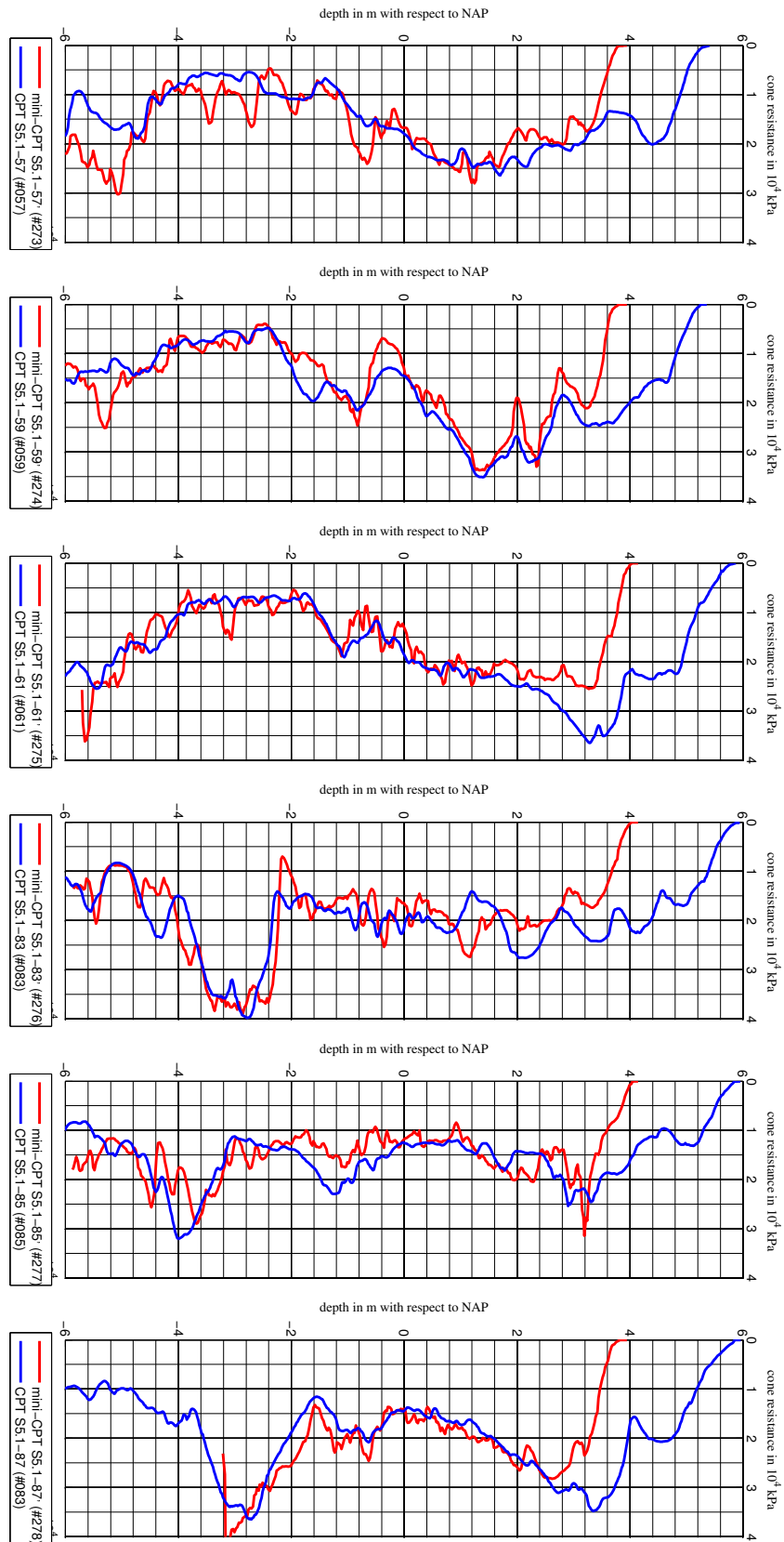


Figure C.2: Comparison between standard CPT's and mini-CPT's (onshore).

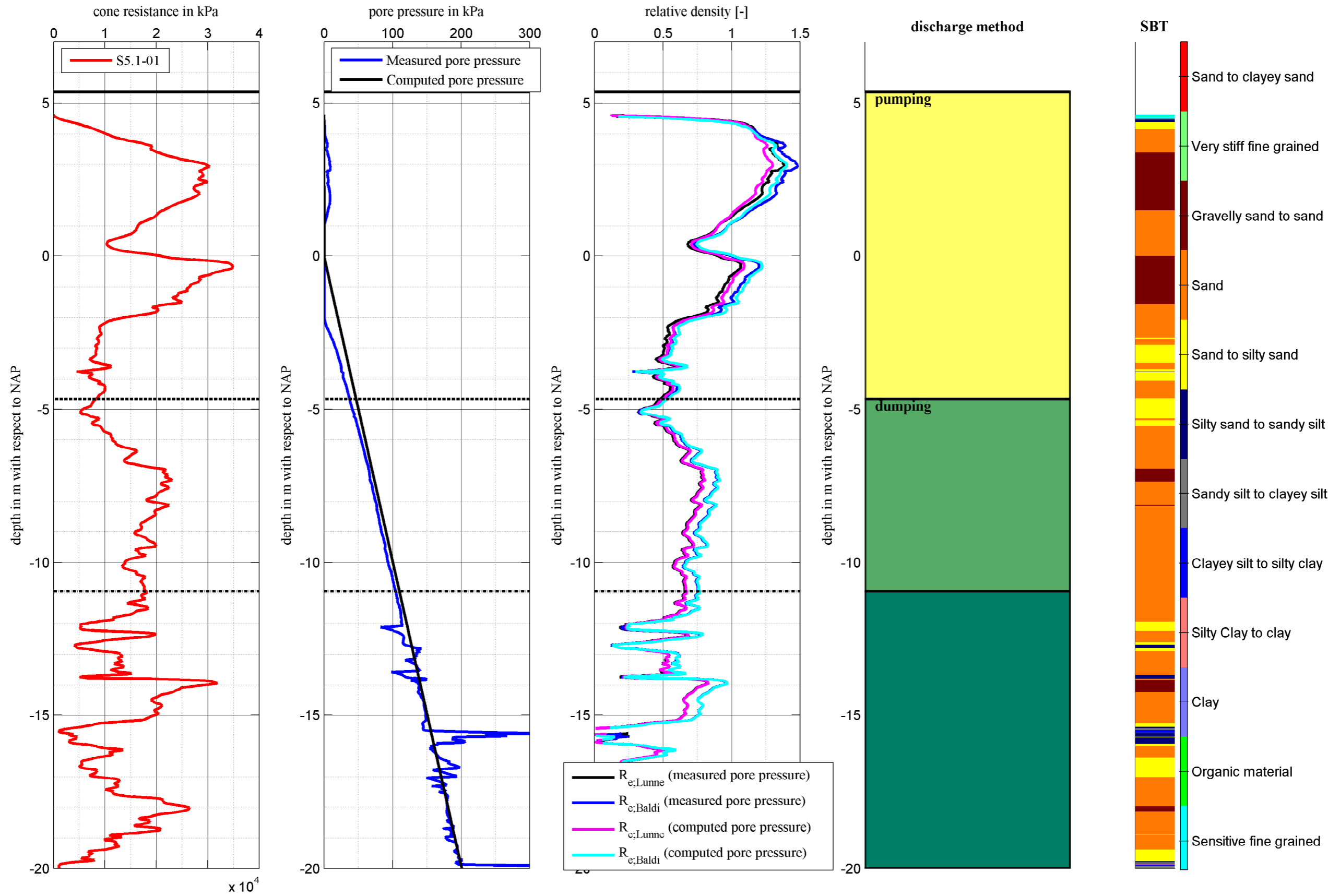
Appendix D: CPT Analysis

Appendix D: CPT Analysis

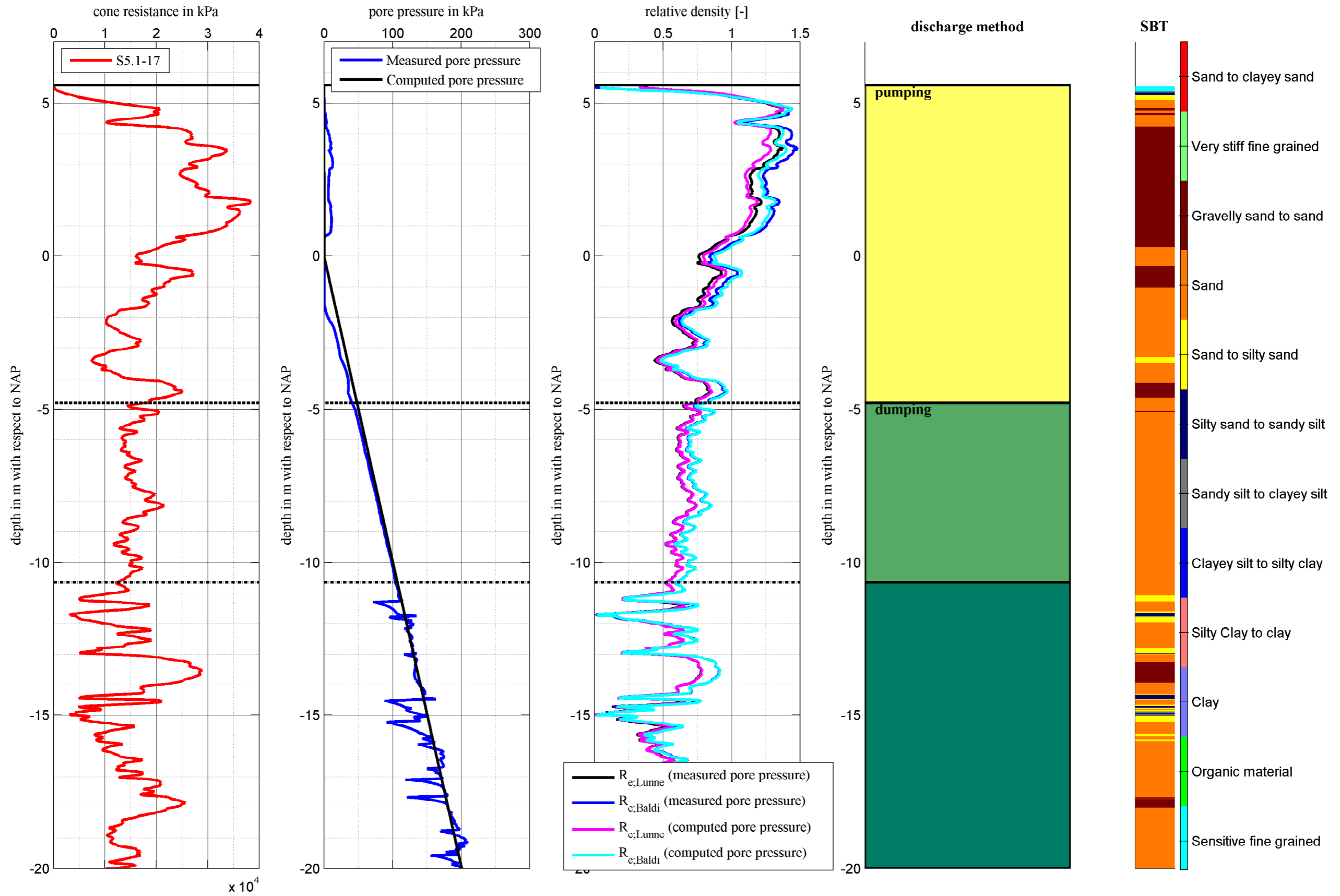
D.1 Comparison between Measured Pore Pressure and Hydrostatic Pore Pressure

Appendix D: CPT Analysis

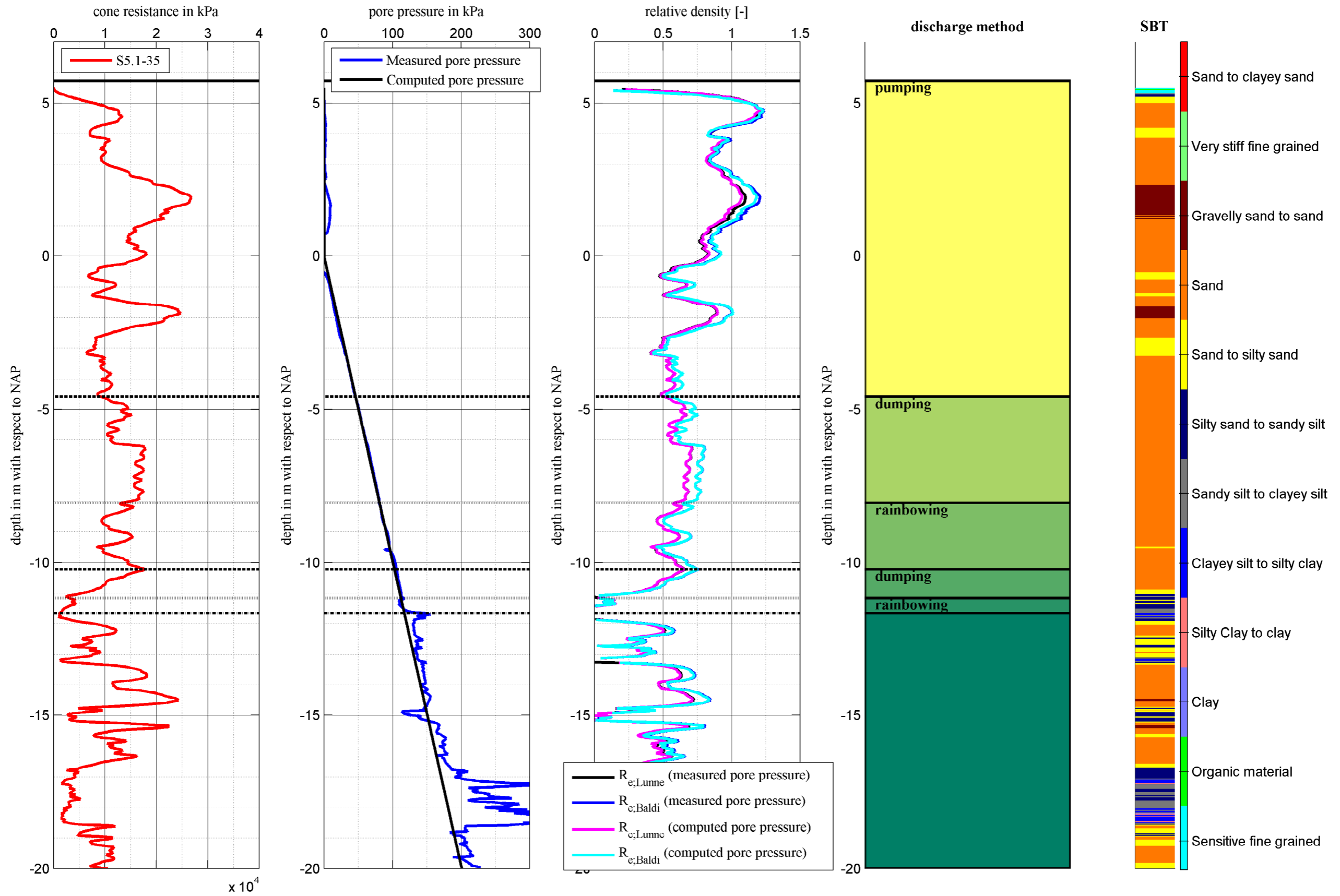
CPT 1 - S5.1-01 made on: 11-8-2009



CPT 17 - S5.1-17 made on: 11-8-2009



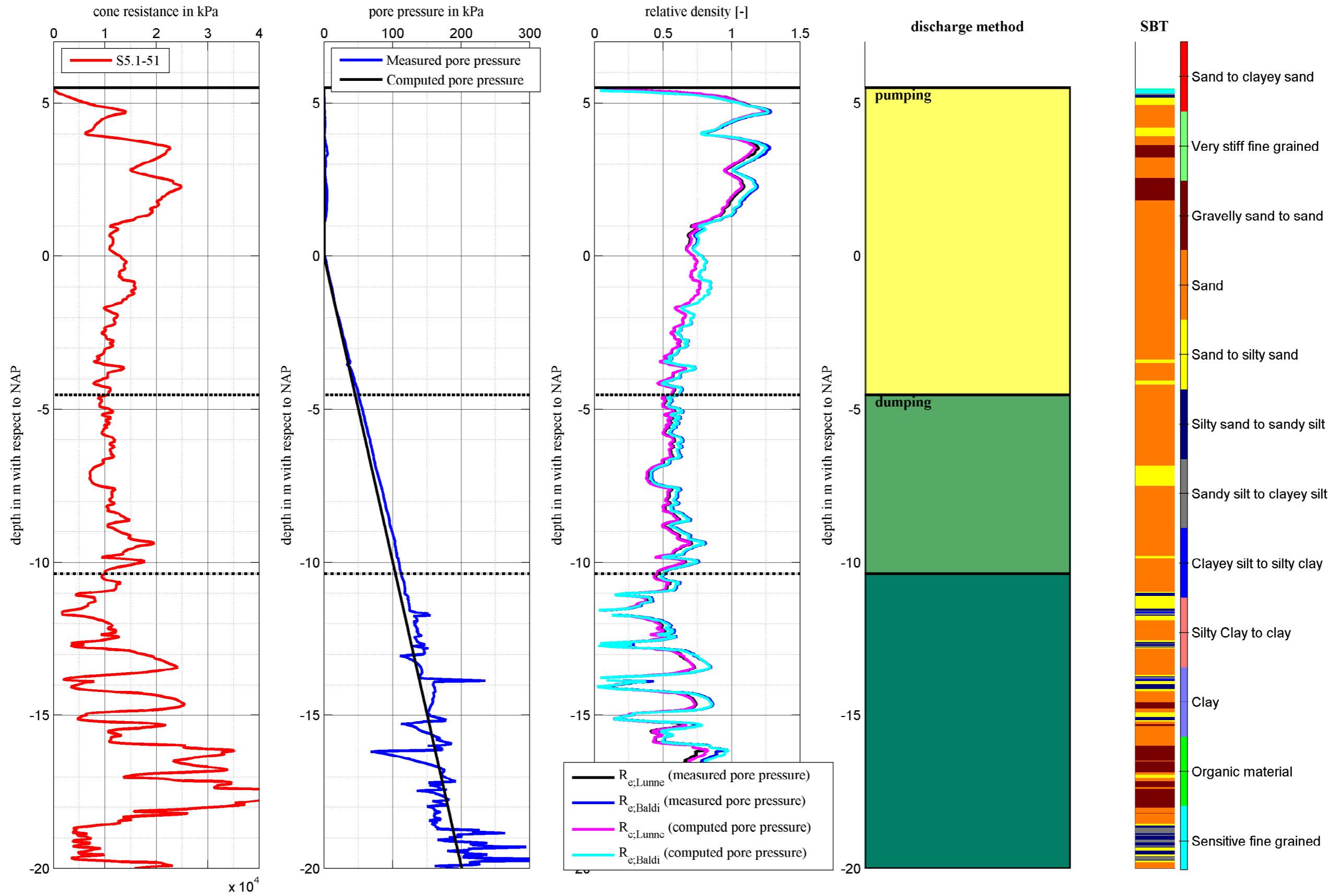
CPT 35 - S5.1-35 made on: 11-8-2009



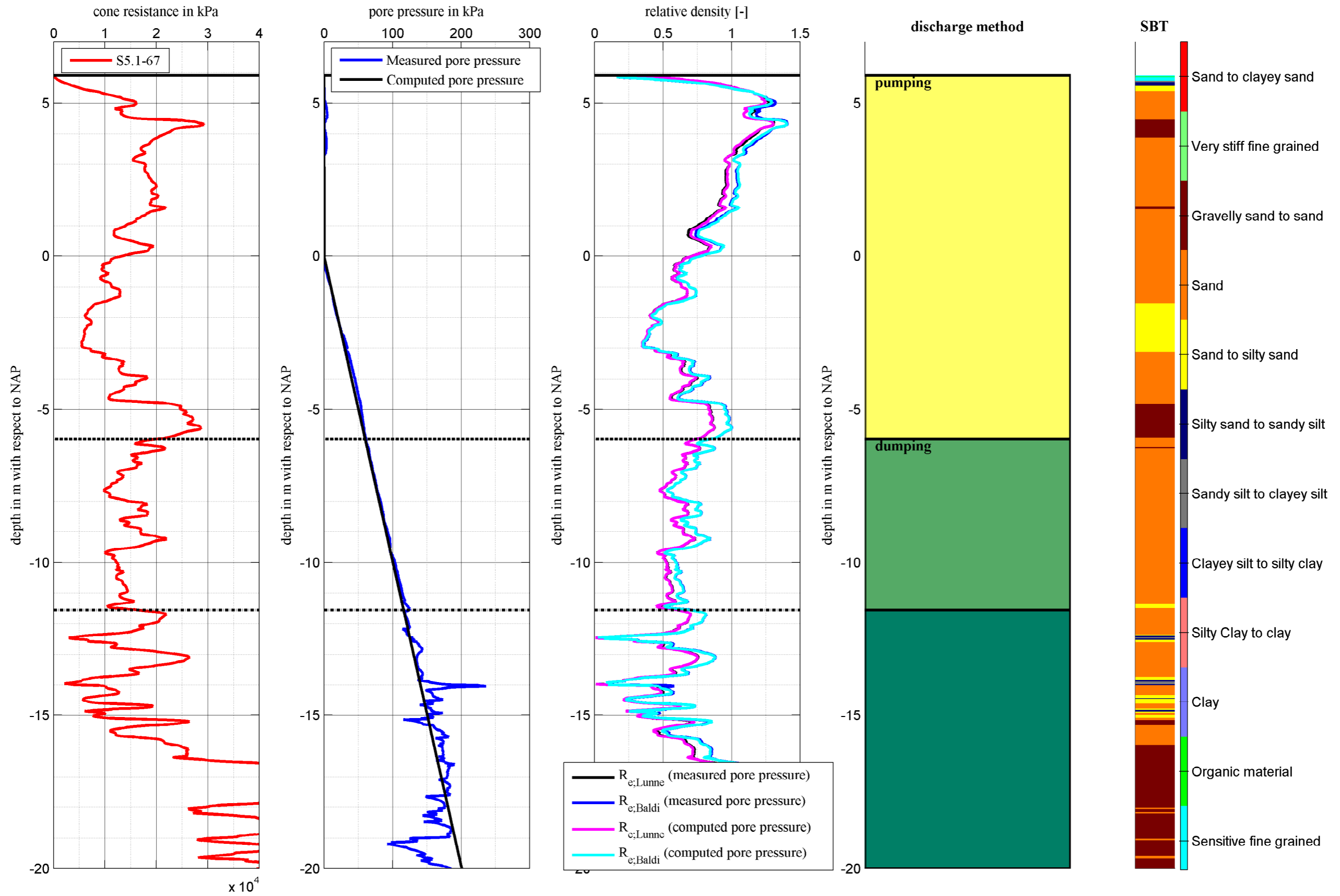
— $R_{e;Lunne}$ (measured pore pressure)
 — $R_{e;Baldi}$ (measured pore pressure)
 — $R_{c;Lunne}$ (computed pore pressure)
 — $R_{c;Baldi}$ (computed pore pressure)

$\times 10^4$

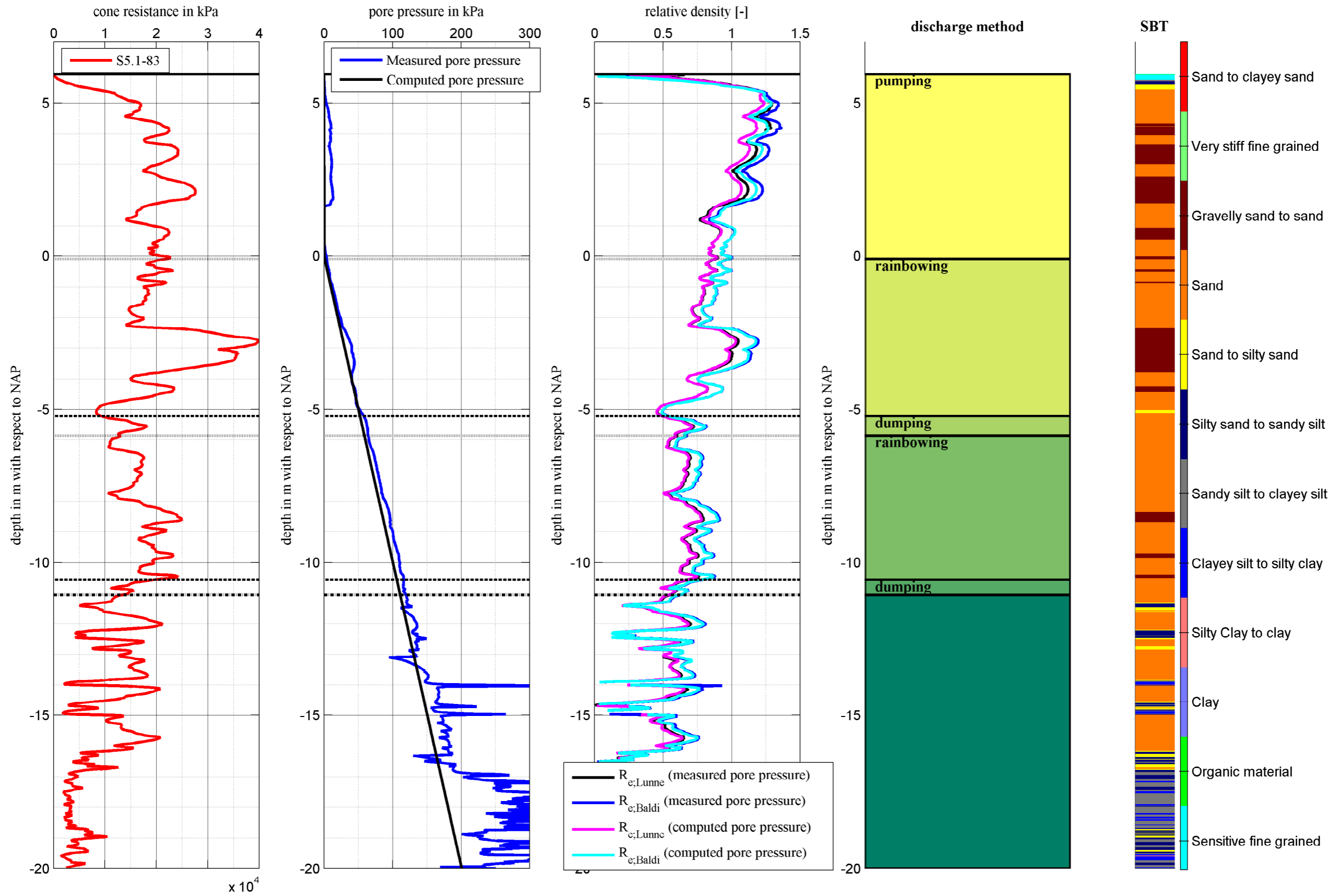
CPT 51 - S5.1-51 made on: 12-8-2009



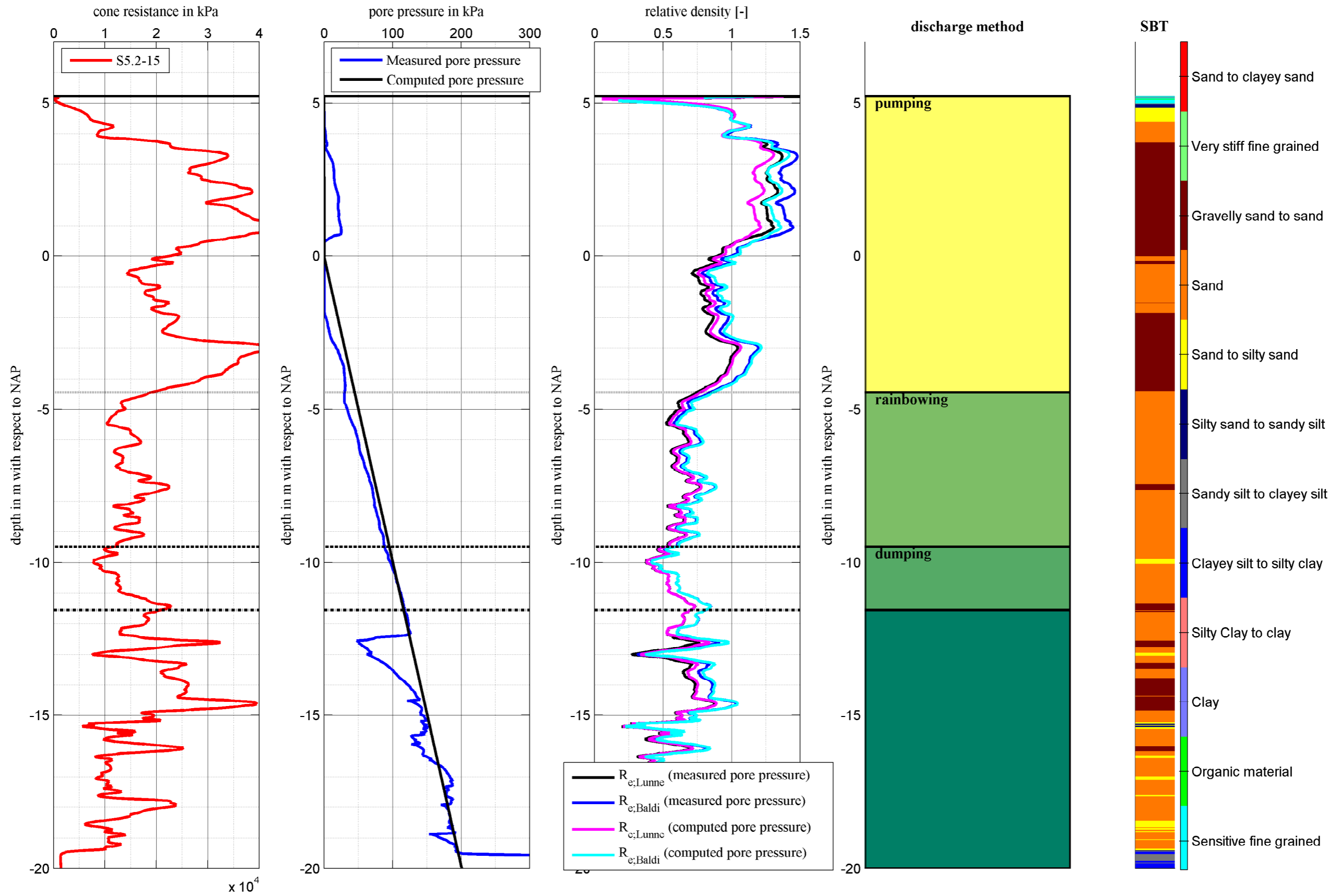
CPT 67 - S5.1-67 made on: 13-8-2009



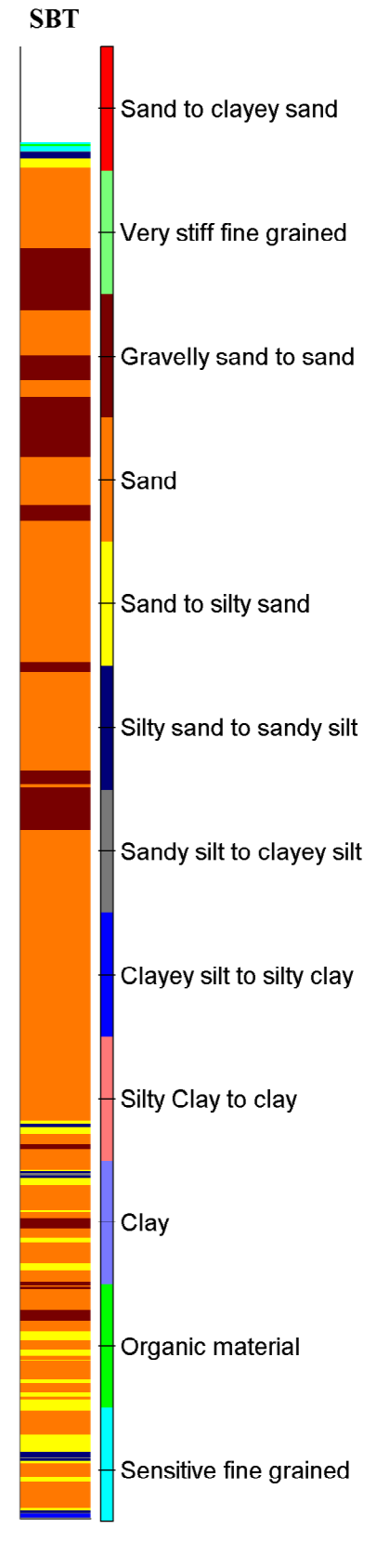
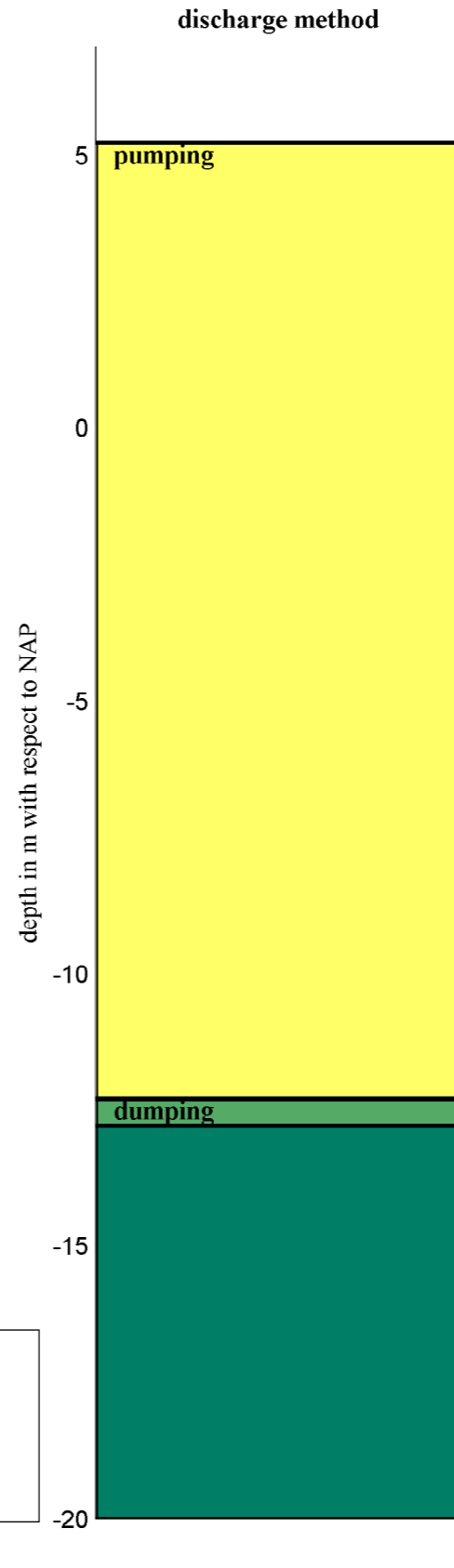
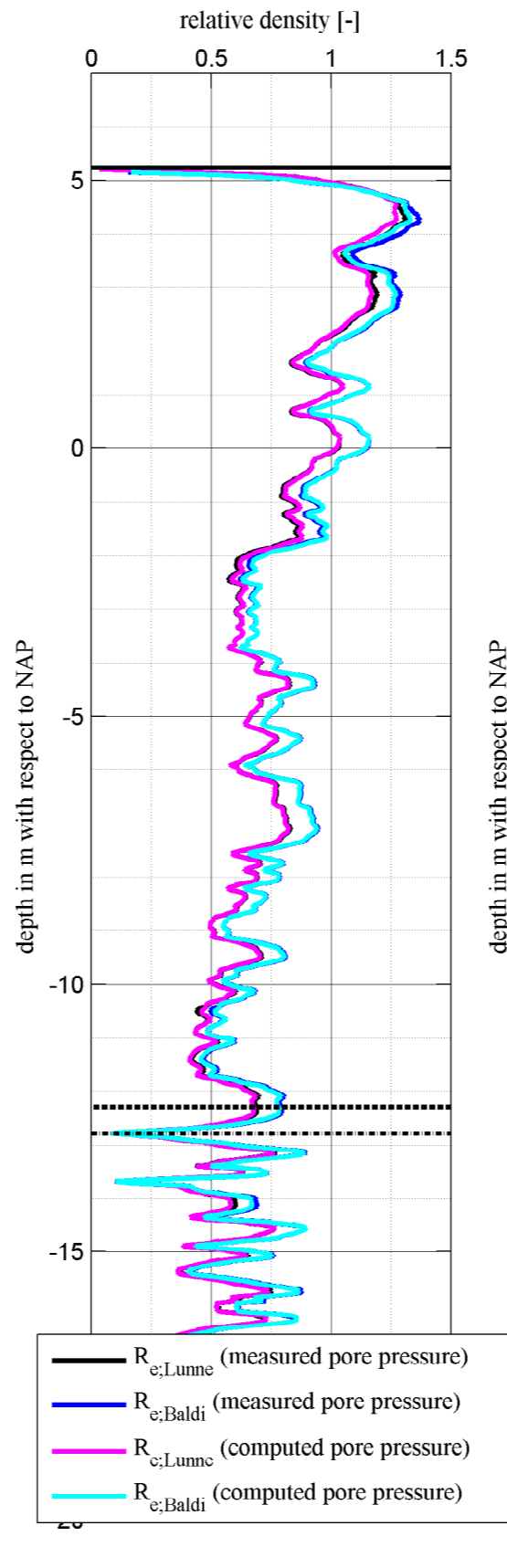
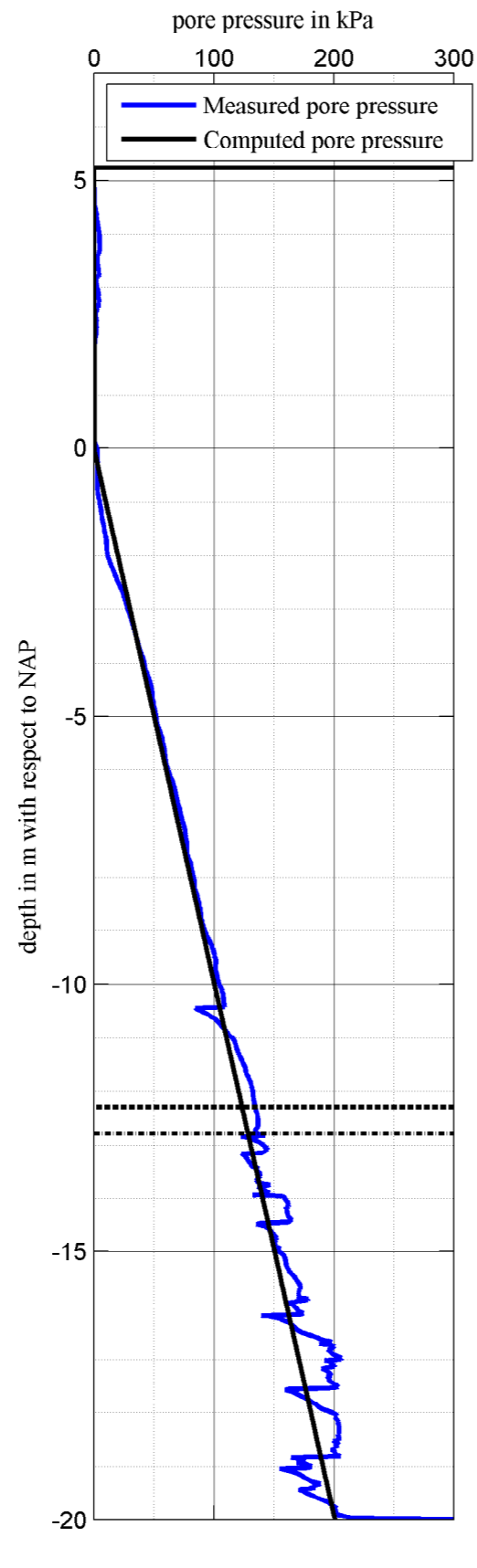
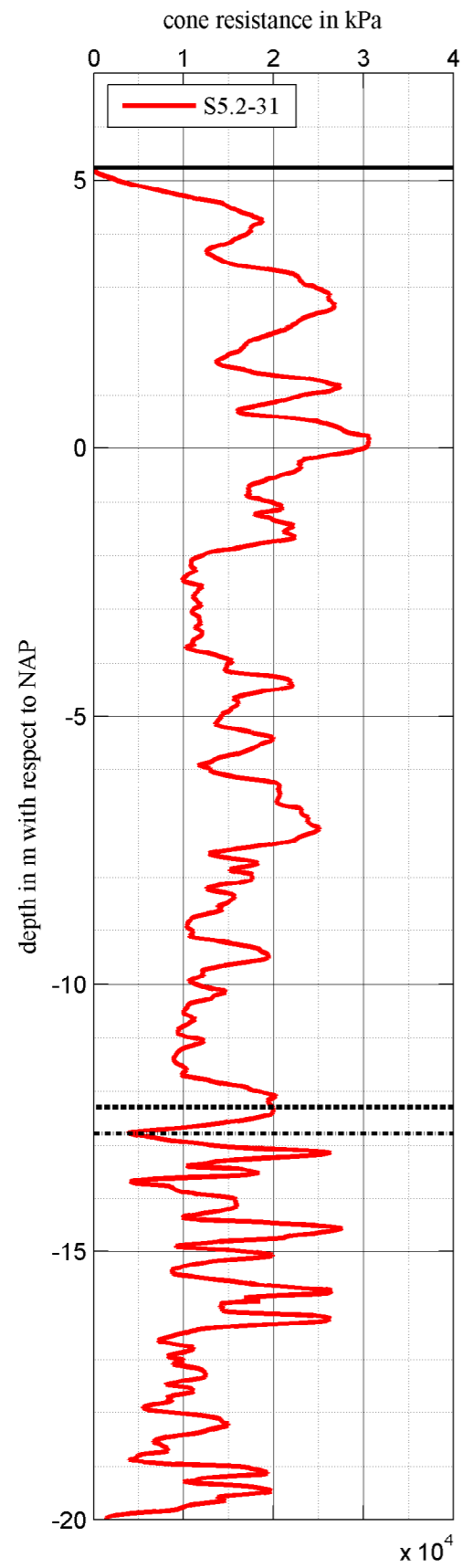
CPT 83 - S5.1-83 made on: 13-8-2009



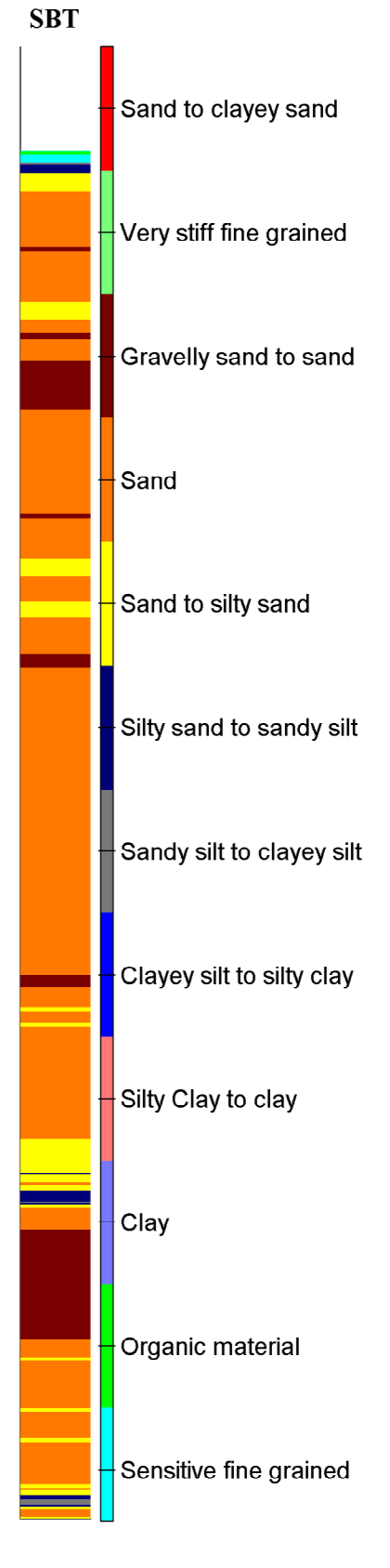
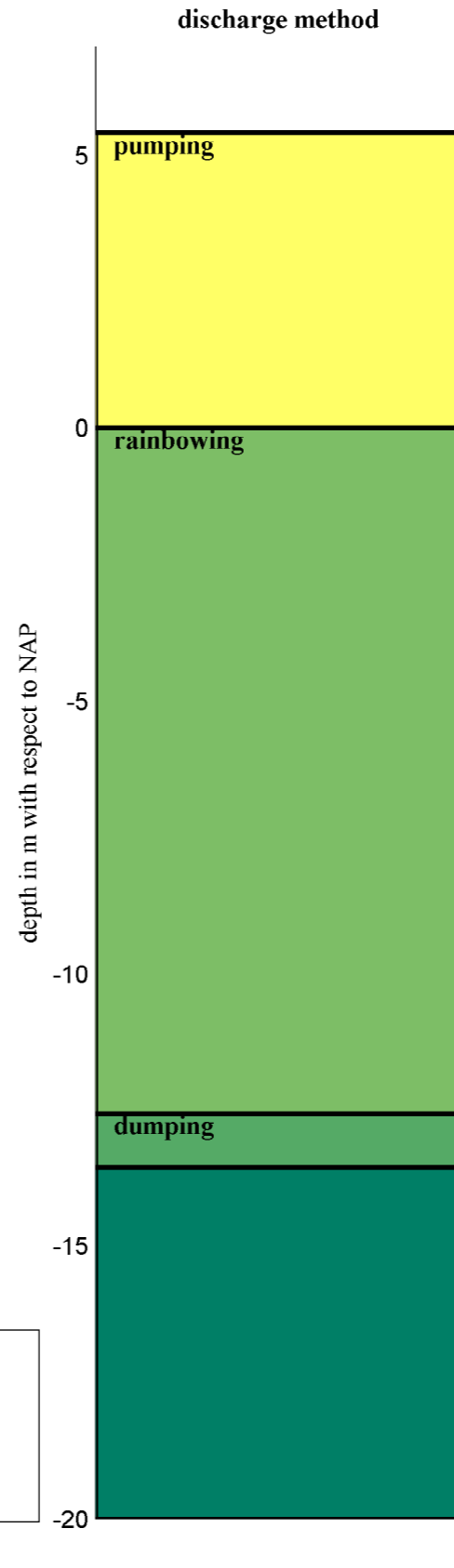
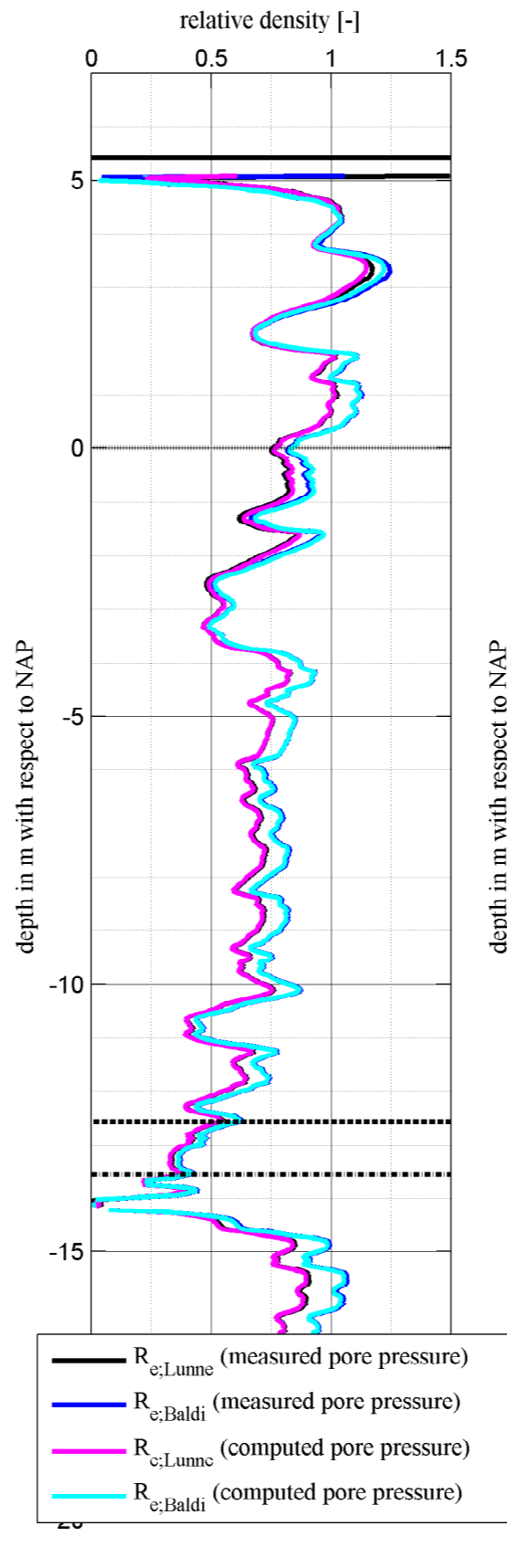
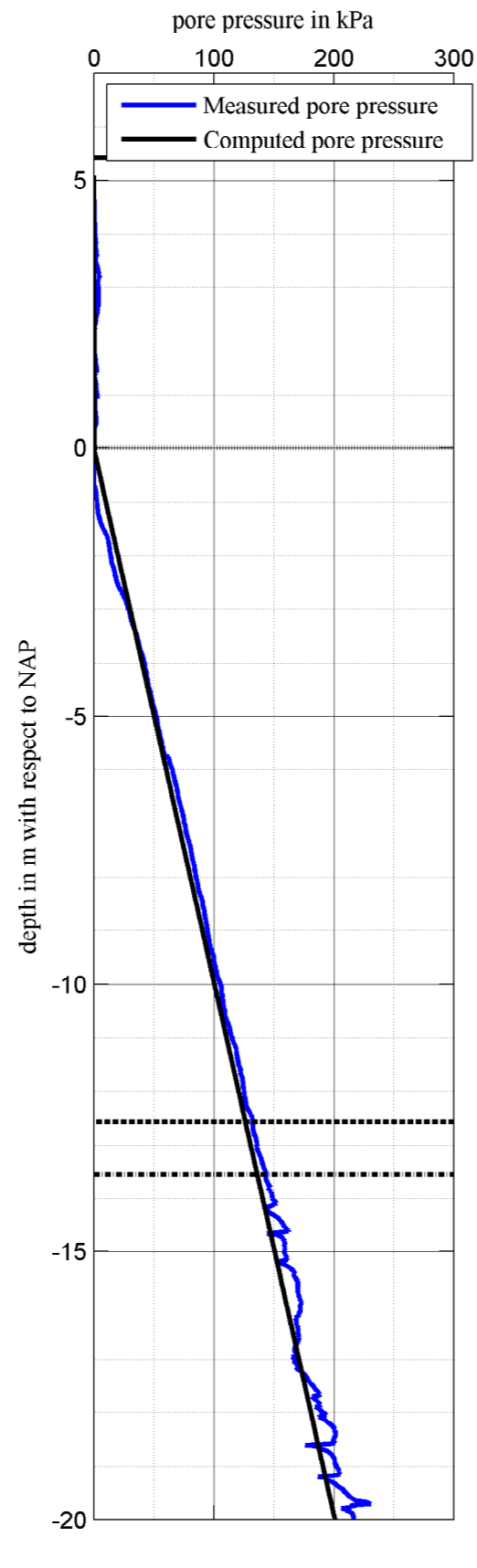
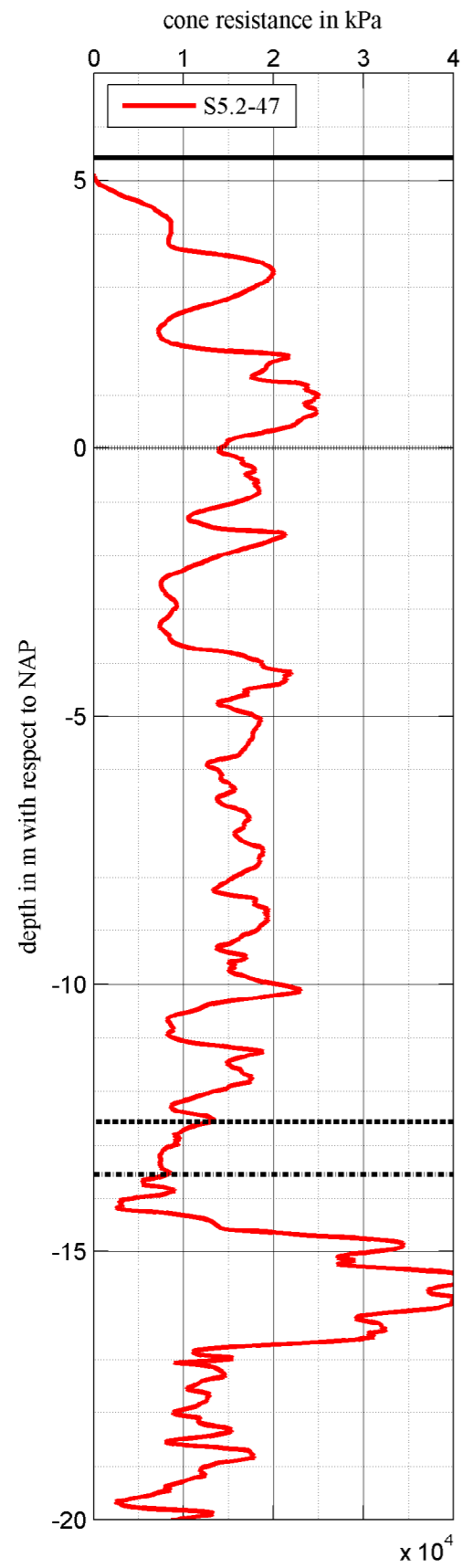
CPT 104 - S5.2-15 made on: 14-8-2009



CPT 120 - S5.2-31 made on: 14-8-2009



CPT 136 - S5.2-47 made on: 17-8-2009



D.2 Results of the CPT Analysis

Appendix D: CPT Analysis

CPT 1 - S5.1-01

CPT made on: 11-8-2009

RD-Coordinate
x = 59372.690 m
y = 441806.160 m

Working method: Pumping

Top layer : 4.630 m NAP
Bottom layer : -4.670 m NAP
Layer thickness : 10.025 m

Re according to Lunne: Re according to Baldi:
Re min = 0.170 Re min = 0.159
Re mean = 0.889 Re mean = 0.957
Re max = 1.383 Re max = 1.482

d50 and fines:
d50 min = 270 mu percentage fines min = 1.450
d50 mean = 270 mu percentage fines mean = 1.450
d50 max = 270 mu percentage fines max = 1.450

Working method: Dumping layer 1

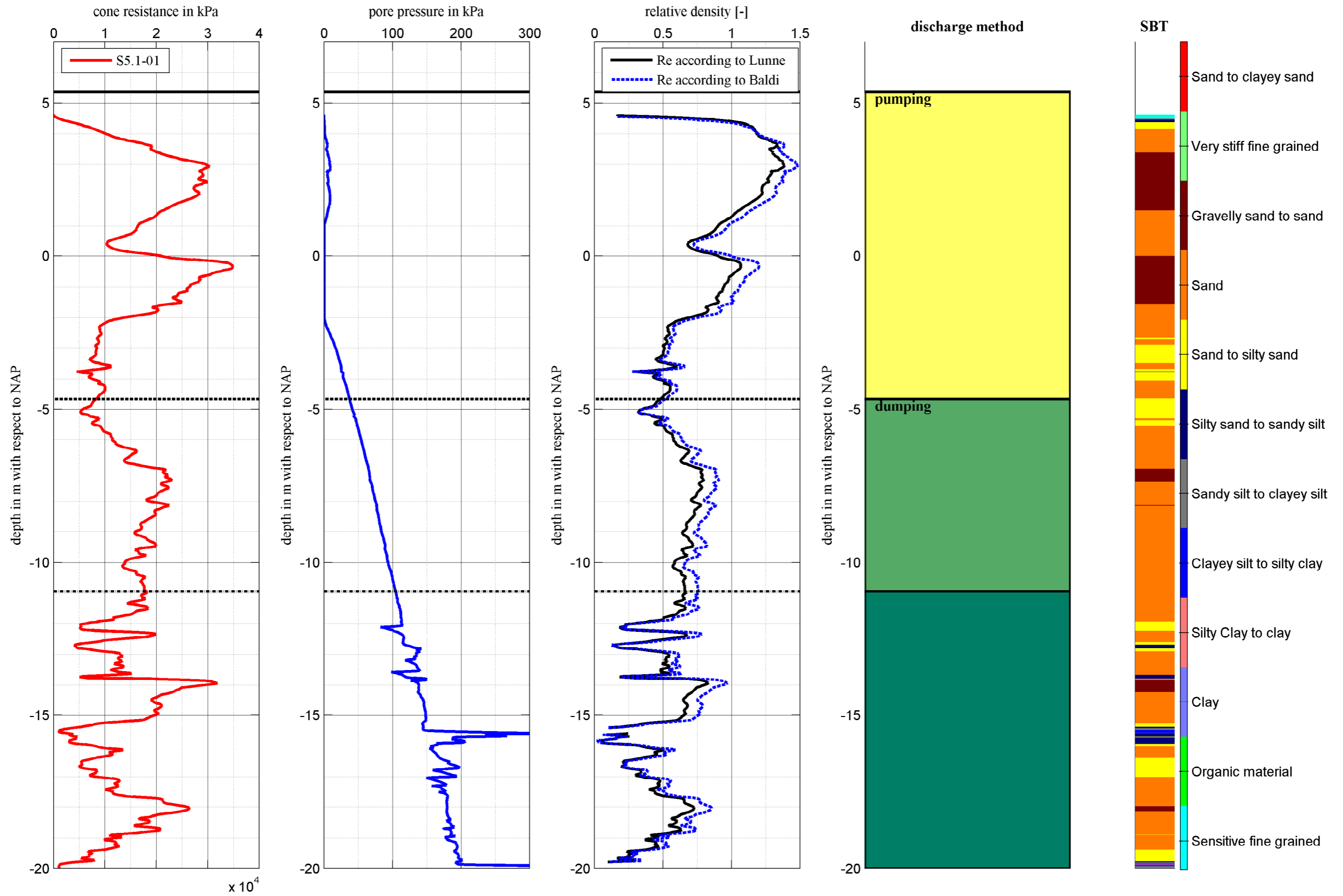
Top layer : -4.670 m NAP
Bottom layer : -10.946 m NAP
Layer thickness : 6.276 m

Re according to Lunne: Re according to Baldi:
Re min = 0.320 Re min = 0.324
Re mean = 0.639 Re mean = 0.719
Re max = 0.796 Re max = 0.907

d50 and fines:
d50 min = 208 mu percentage fines min = 1.160
d50 mean = 229 mu percentage fines mean = 1.630
d50 max = 287 mu percentage fines max = 2.310

REMARK: The values of the d50 and the percentage fines are measured on board of the TSHD with a CPA machine.

CPT 1 - S5.1-01 made on: 11-8-2009



CPT 4 - S5.1-04

CPT made on: 10-8-2009

RD-Coordinate
x = 59320.536 m
y = 441796.543 m

Working method: Pumping

Top layer : 5.160 m NAP
Bottom layer : -7.277 m NAP
Layer thickness : 12.588 m

Re according to Lunne: Re according to Baldi:
Re min = 0.324 Re min = 0.333
Re mean = 0.825 Re mean = 0.889
Re max = 1.242 Re max = 1.287

d50 and fines:
d50 min = 362 mu percentage fines min = 1.290
d50 mean = 362 mu percentage fines mean = 1.290
d50 max = 362 mu percentage fines max = 1.290

Working method: Dumping layer 1

Top layer : -7.277 m NAP
Bottom layer : -9.184 m NAP
Layer thickness : 1.907 m

Re according to Lunne: Re according to Baldi:
Re min = 0.485 Re min = 0.532
Re mean = 0.648 Re mean = 0.732
Re max = 0.747 Re max = 0.854

d50 and fines:
d50 min = 216 mu percentage fines min = 1.070
d50 mean = 249 mu percentage fines mean = 1.353
d50 max = 294 mu percentage fines max = 1.600

Working method: Rainbowing layer 1

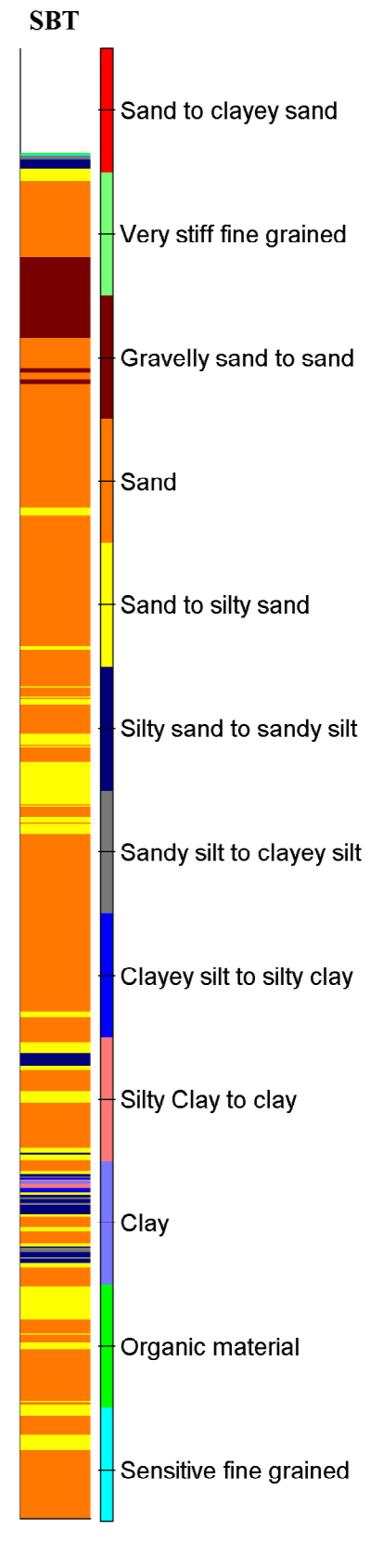
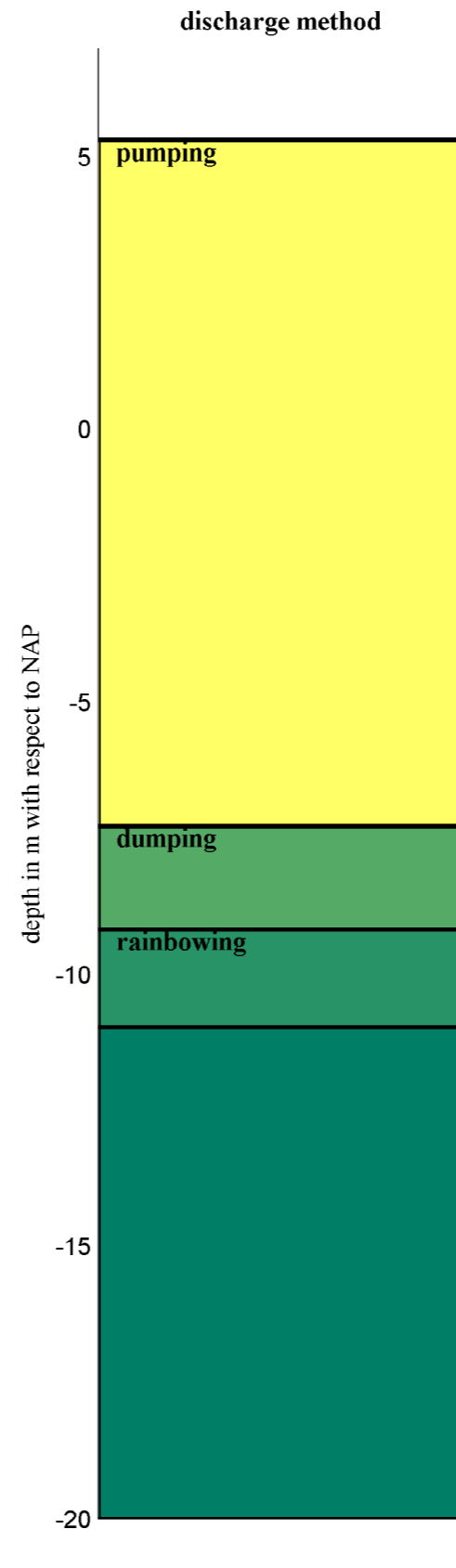
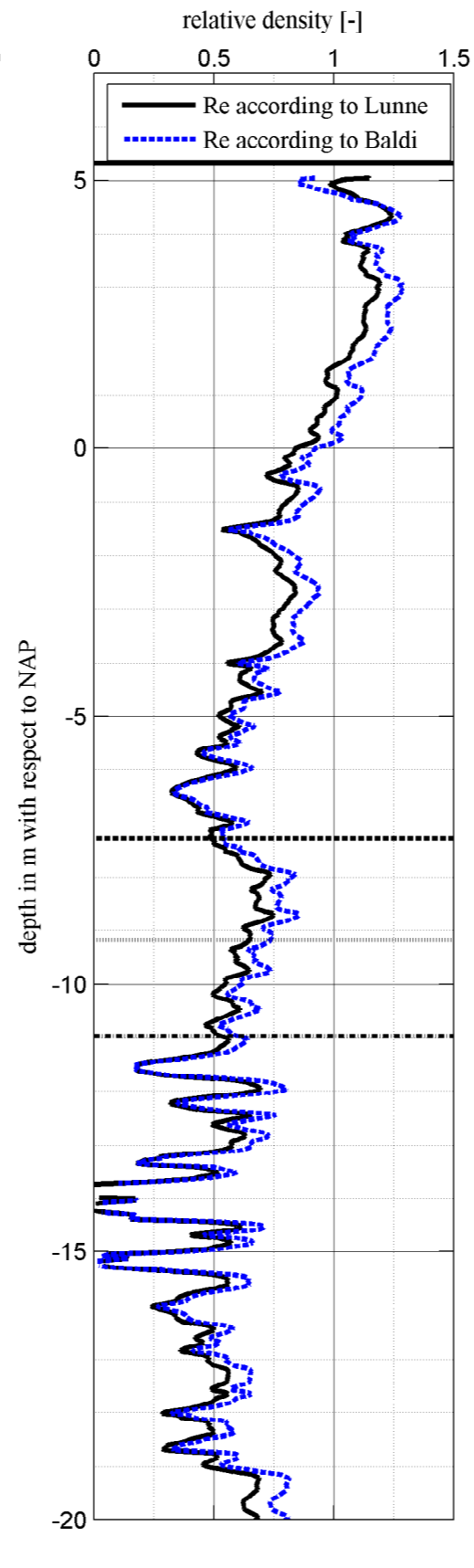
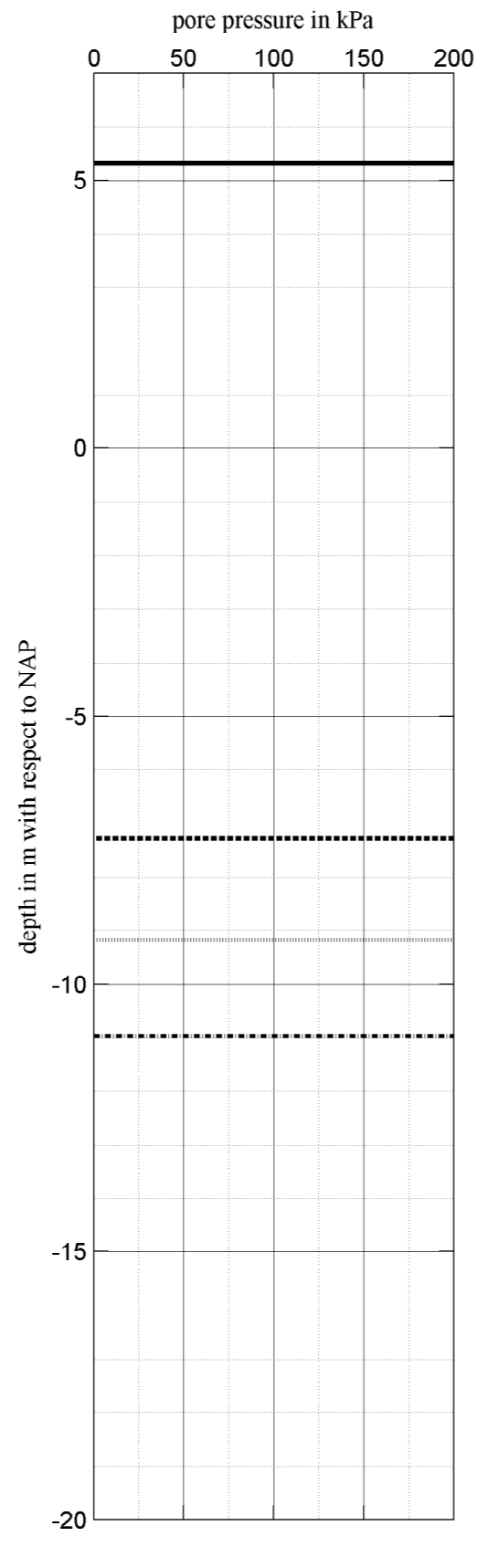
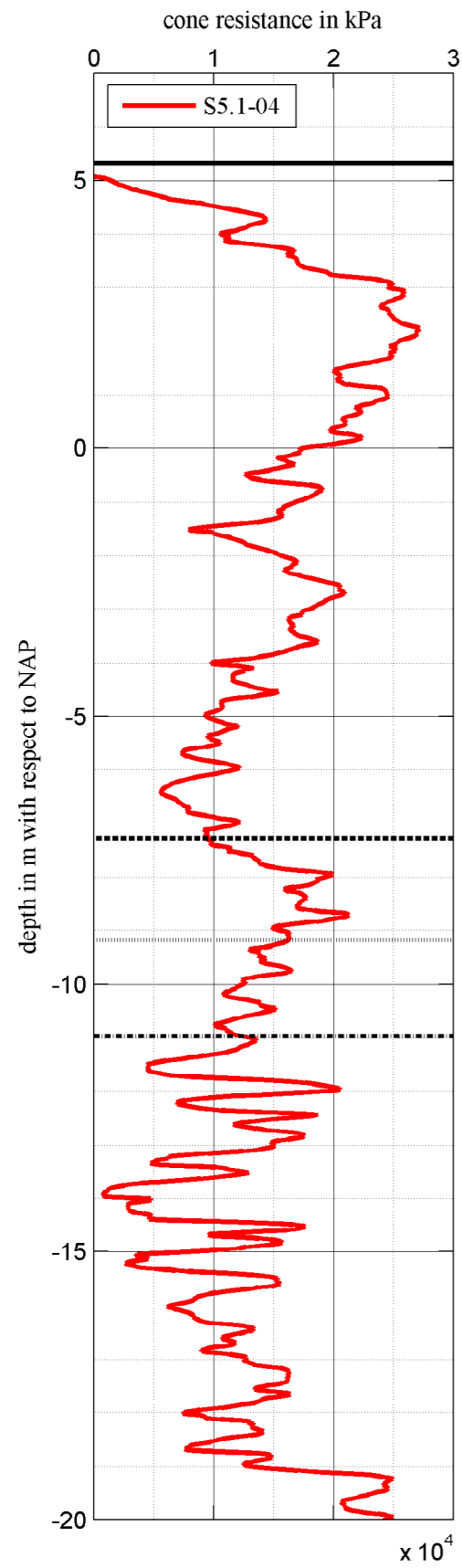
Top layer : -9.184 m NAP
Bottom layer : -10.968 m NAP
Layer thickness : 1.784 m

Re according to Lunne: Re according to Baldi:
Re min = 0.463 Re min = 0.519
Re mean = 0.562 Re mean = 0.635
Re max = 0.647 Re max = 0.737

d50 and fines:
d50 min = 232 mu percentage fines min = 1.320
d50 mean = 239 mu percentage fines mean = 1.415
d50 max = 246 mu percentage fines max = 1.510

REMARK: The values of the d50 and the percentage fines are measured on board of the TSHD with a CPA machine.

CPT 4 - S5.1-04 made on: 10-8-2009



CPT 89 - S5.1-89

CPT made on: 13-8-2009

RD-Coordinate
x = 58748.811 m
y = 440900.194 m

Working method: Pumping

Top layer : 6.120 m NAP
Bottom layer : 0.000 m NAP
Layer thickness : 6.120 m

Re according to Lunne: Re according to Baldi:
Re min = 0.717 Re min = 0.783
Re mean = 1.111 Re mean = 1.193
Re max = 1.444 Re max = 1.383

d50 and fines:
d50 min = 305 mu percentage fines min = 1.000
d50 mean = 305 mu percentage fines mean = 1.000
d50 max = 305 mu percentage fines max = 1.000

Working method: Rainbowing layer 2

Top layer : 0.000 m NAP
Bottom layer : -6.882 m NAP
Layer thickness : 6.882 m

Re according to Lunne: Re according to Baldi:
Re min = 0.306 Re min = 0.320
Re mean = 0.733 Re mean = 0.821
Re max = 0.949 Re max = 1.078

d50 and fines:
d50 min = 201 mu percentage fines min = 1.170
d50 mean = 243 mu percentage fines mean = 1.538
d50 max = 318 mu percentage fines max = 2.170

Working method: Dumping layer 1

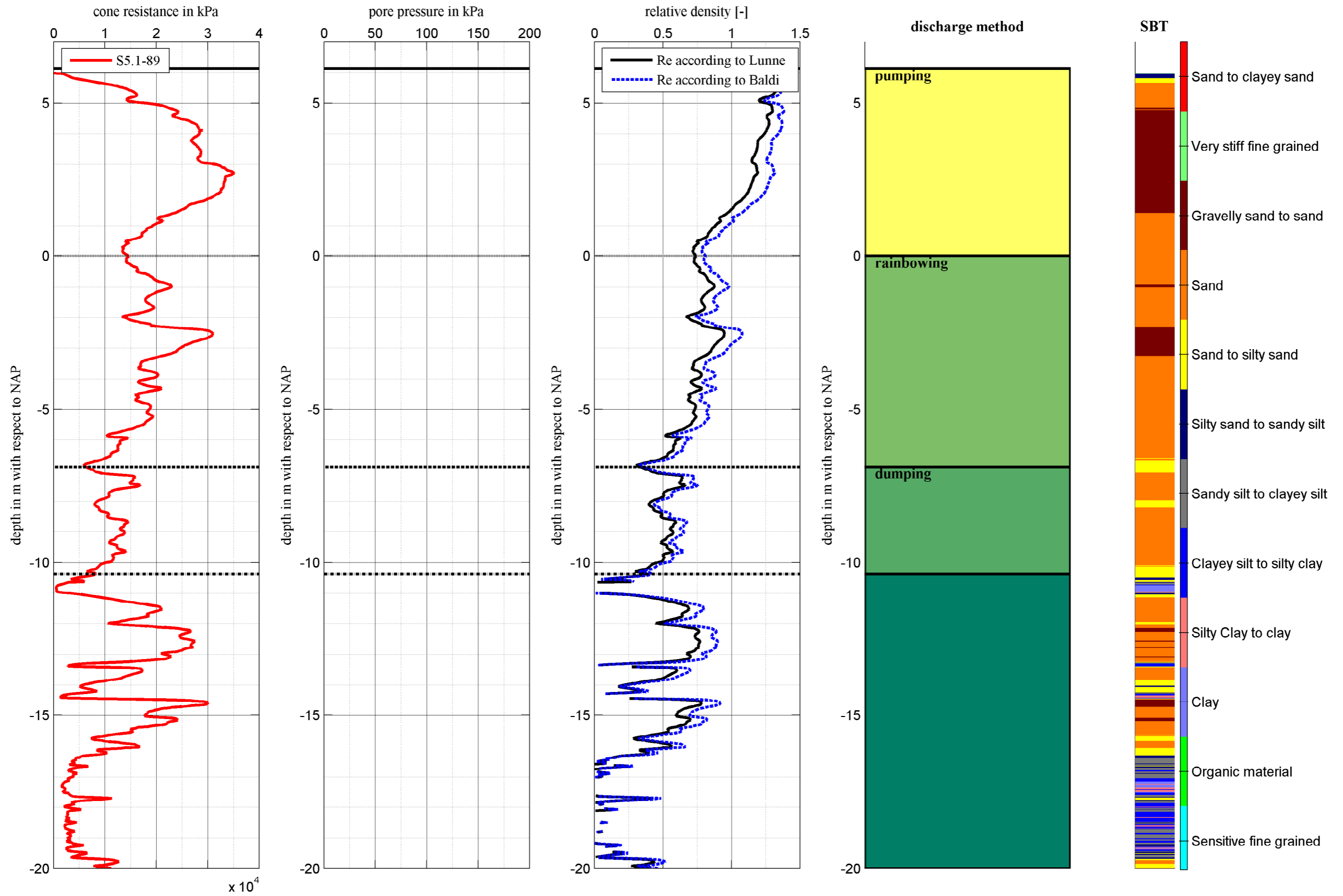
Top layer : -6.882 m NAP
Bottom layer : -10.387 m NAP
Layer thickness : 3.505 m

Re according to Lunne: Re according to Baldi:
Re min = 0.299 Re min = 0.323
Re mean = 0.504 Re mean = 0.566
Re max = 0.662 Re max = 0.752

d50 and fines:
d50 min = 189 mu percentage fines min = 1.240
d50 mean = 229 mu percentage fines mean = 2.467
d50 max = 300 mu percentage fines max = 4.620

REMARK: The values of the d50 and the percentage fines are measured on board of the TSHD with a CPA machine.

CPT 89 - S5.1-89 made on: 13-8-2009



CPT 120 - S5.2-31

CPT made on: 14-8-2009

RD-Coordinate
x = 59337.896 m
y = 442204.644 m

Working method: Pumping

Top layer : 5.230 m NAP
Bottom layer : -12.288 m NAP
Layer thickness : 17.518 m

Re according to Lunne: Re according to Baldi:
Re min = 0.036 Re min = 0.167
Re mean = 0.777 Re mean = 0.855
Re max = 1.276 Re max = 1.333

d50 and fines:
d50 min = 216 mu percentage fines min = 1.600
d50 mean = 216 mu percentage fines mean = 1.600
d50 max = 216 mu percentage fines max = 1.600

Working method: Dumping layer 1

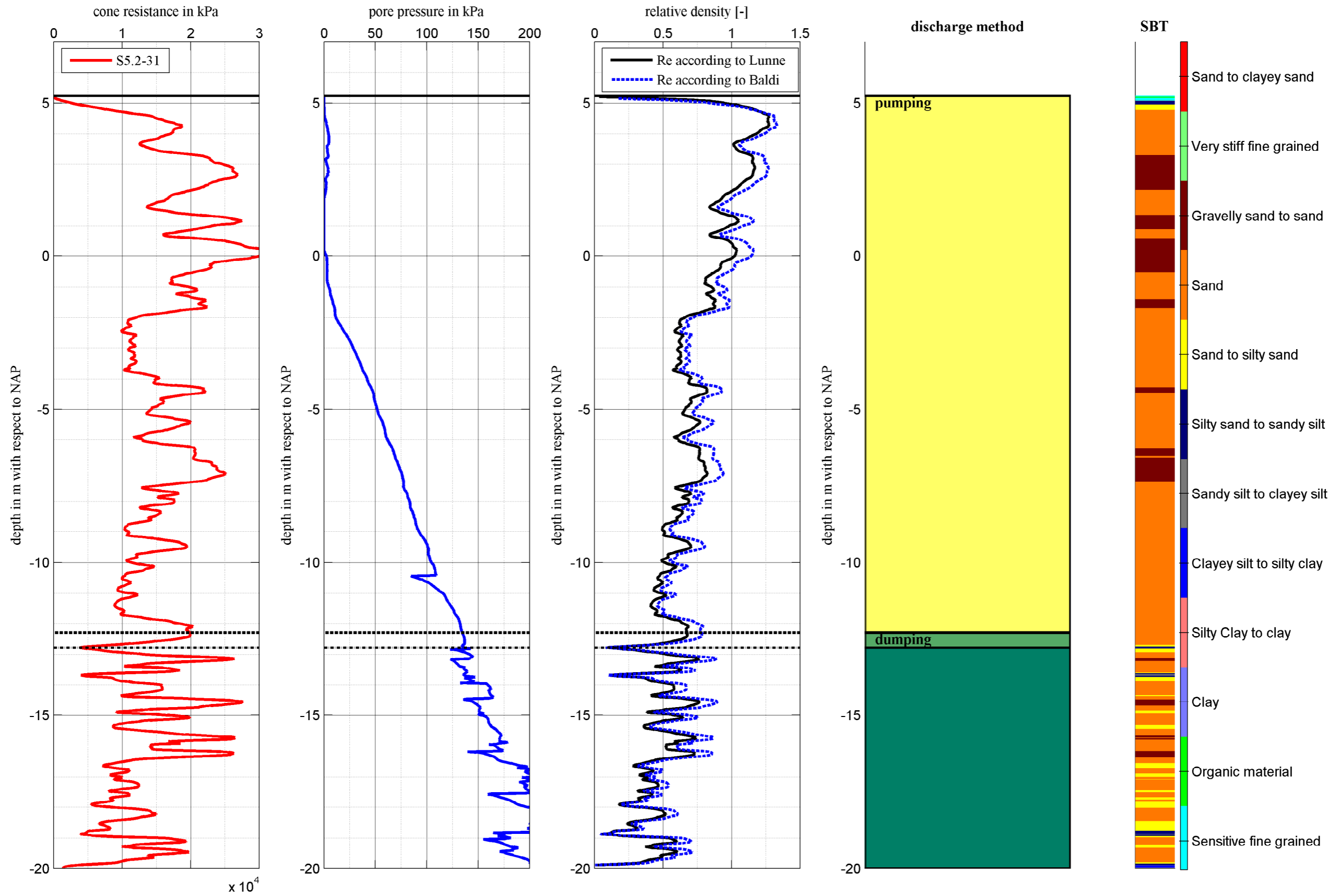
Top layer : -12.288 m NAP
Bottom layer : -12.788 m NAP
Layer thickness : 0.500 m

Re according to Lunne: Re according to Baldi:
Re min = 0.112 Re min = 0.101
Re mean = 0.542 Re mean = 0.620
Re max = 0.678 Re max = 0.783

d50 and fines:
d50 min = 280 mu percentage fines min = 0.850
d50 mean = 332 mu percentage fines mean = 1.490
d50 max = 435 mu percentage fines max = 2.130

REMARK: The values of the d50 and the percentage fines are measured on board of the TSHD with a CPA machine.

CPT 120 - S5.2-31 made on: 14-8-2009



CPT 214 - S-HZ-2200

CPT made on: 14-12-2009

RD-Coordinate
x = 59118.849 m
y = 445119.981 m

Working method: Dumping layer 2

Top layer : -12.294 m NAP
Bottom layer : -16.235 m NAP
Layer thickness : 3.941 m

Re according to Lunne: Re according to Baldi:
Re min = 0.197 Re min = 0.149
Re mean = 0.778 Re mean = 0.741
Re max = 1.006 Re max = 1.038

d50 and fines:
d50 min = 210 mu percentage fines min = 2.040
d50 mean = 210 mu percentage fines mean = 2.040
d50 max = 210 mu percentage fines max = 2.040

Working method: Back Fill layer 1

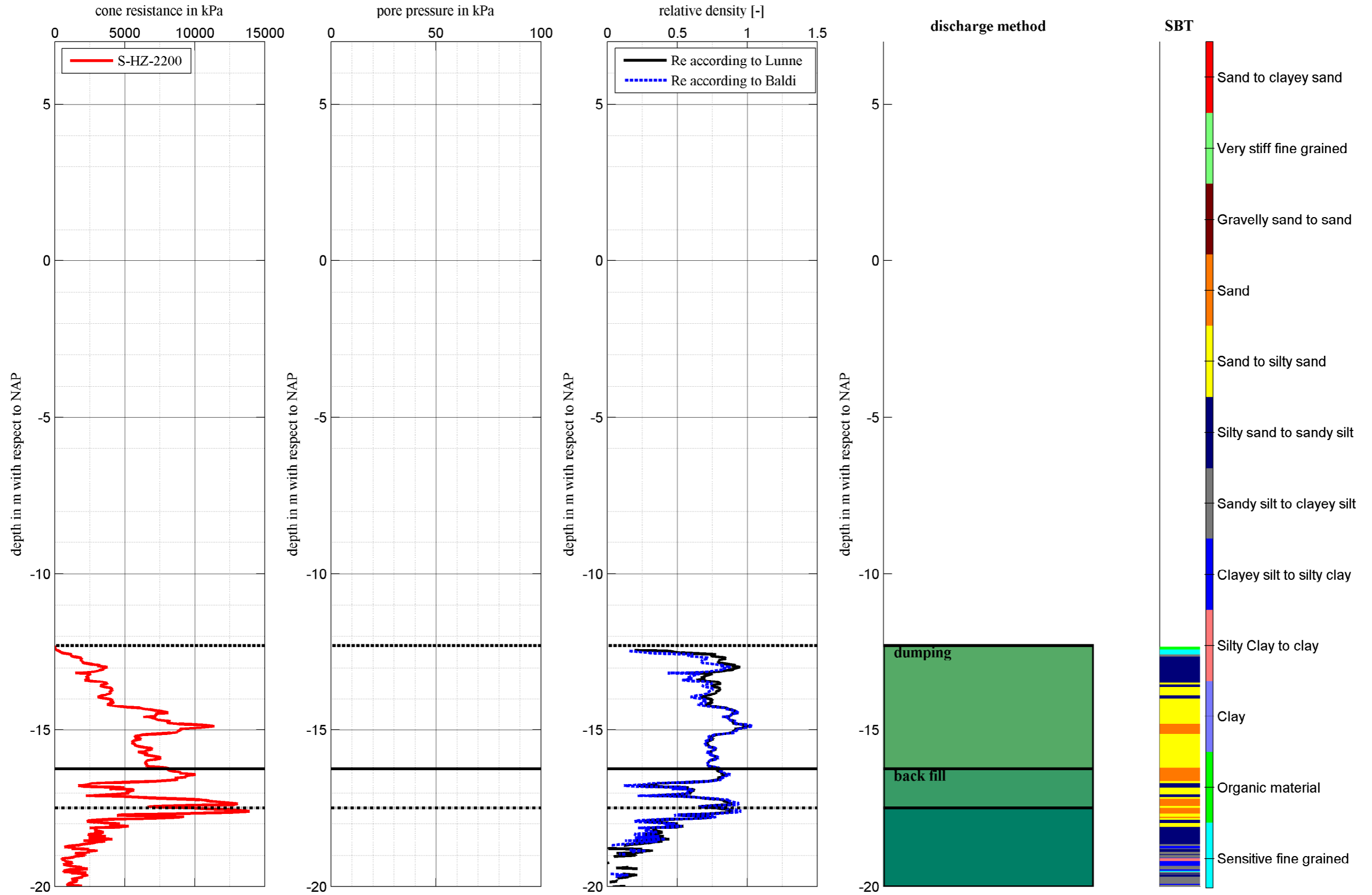
Top layer : -16.235 m NAP
Bottom layer : -17.498 m NAP
Layer thickness : 1.263 m

Re according to Lunne: Re according to Baldi:
Re min = 0.215 Re min = 0.120
Re mean = 0.667 Re mean = 0.666
Re max = 0.889 Re max = 0.941

d50 and fines:
d50 min = 305 mu percentage fines min = 1.040
d50 mean = 368 mu percentage fines mean = 1.262
d50 max = 430 mu percentage fines max = 1.440

REMARK: The values of the d50 and the percentage fines are measured on board of the TSHD with a CPA machine.

CPT 214 - S-HZ-2200 made on: 14-12-2009



CPT 238 - S-HZ-3200-130

CPT made on: 13-4-2010

RD-Coordinate
x = 58233.317 m
y = 444567.676 m

Working method: Spraying with Slidrecht 27

Top layer : -6.347 m NAP
Bottom layer : -9.590 m NAP
Layer thickness : 3.243 m

Re according to Lunne: Re according to Baldi:
Re min = 0.049 Re min = 0.009
Re mean = 0.585 Re mean = 0.496
Re max = 0.867 Re max = 0.876

d50 and fines:
d50 min = 453 mu percentage fines min = 1.250
d50 mean = 467 mu percentage fines mean = 1.320
d50 max = 481 mu percentage fines max = 1.390

Working method: Dumping layer 1

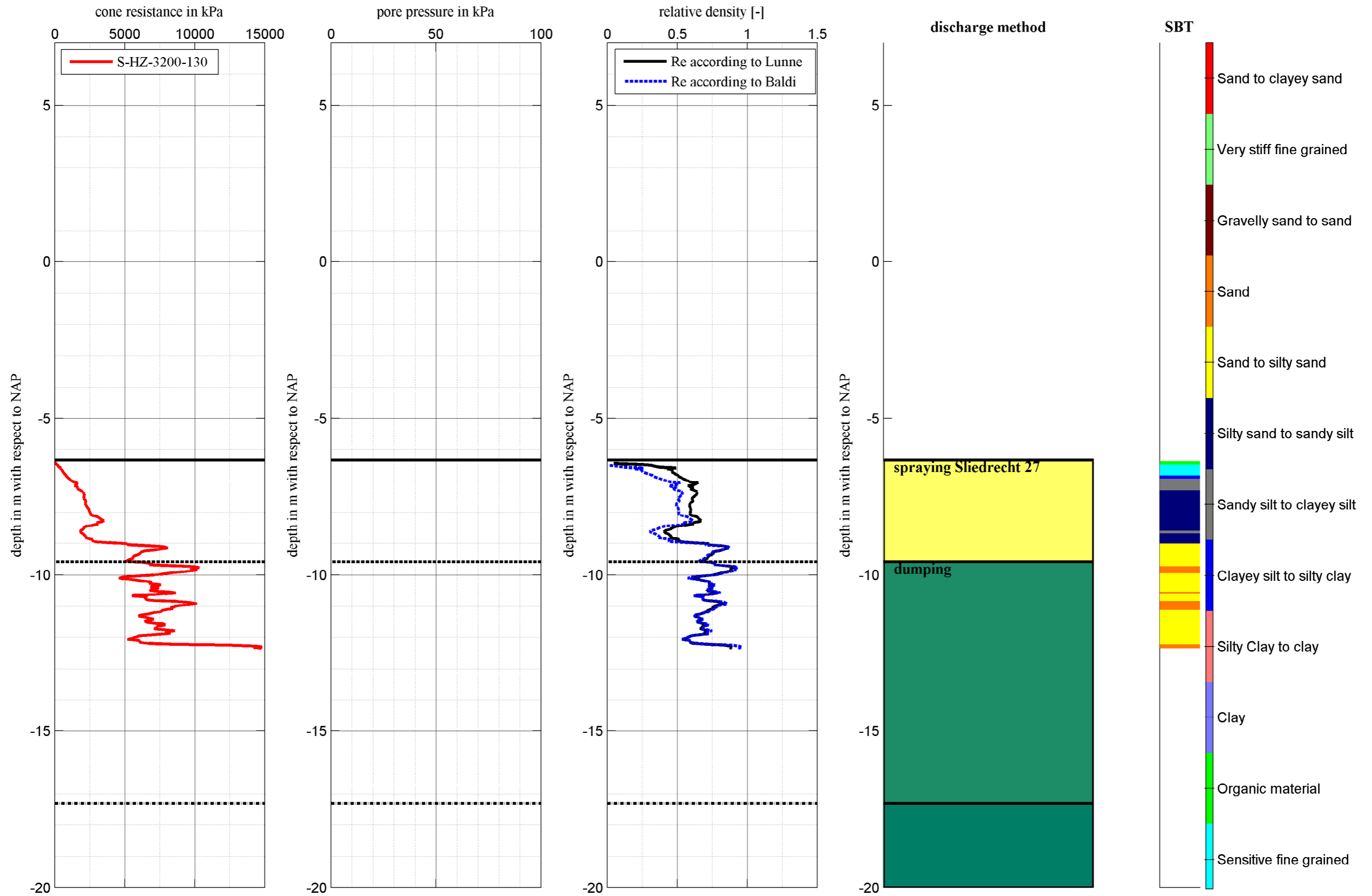
Top layer : -9.590 m NAP
Bottom layer : -17.311 m NAP
Layer thickness : 7.721 m

Re according to Lunne: Re according to Baldi:
Re min = 0.541 Re min = 0.529
Re mean = 0.717 Re mean = 0.727
Re max = 0.903 Re max = 0.955

d50 and fines:
d50 min = 229 mu percentage fines min = 1.210
d50 mean = 260 mu percentage fines mean = 1.615
d50 max = 291 mu percentage fines max = 2.020

REMARK: The values of the d50 and the percentage fines are measured on board of the TSHD with a CPA machine.

CPT 238 - S-HZ-3200-130 made on: 13-4-2010



CPT 265 - S-SZ002

CPT made on: 11-5-2010

RD-Coordinate
x = 58662.000 m
y = 439584.000 m

Working method: Pumping

Top layer : 6.040 m NAP
Bottom layer : -4.957 m NAP
Layer thickness : 10.997 m

Re according to Lunne: Re according to Baldi:
Re min = 0.379 Re min = 0.395
Re mean = 0.886 Re mean = 0.959
Re max = 1.314 Re max = 1.472

d50 and fines:
d50 min = 404 mu percentage fines min = 1.110
d50 mean = 404 mu percentage fines mean = 1.110
d50 max = 404 mu percentage fines max = 1.110

Working method: Dumping layer 1

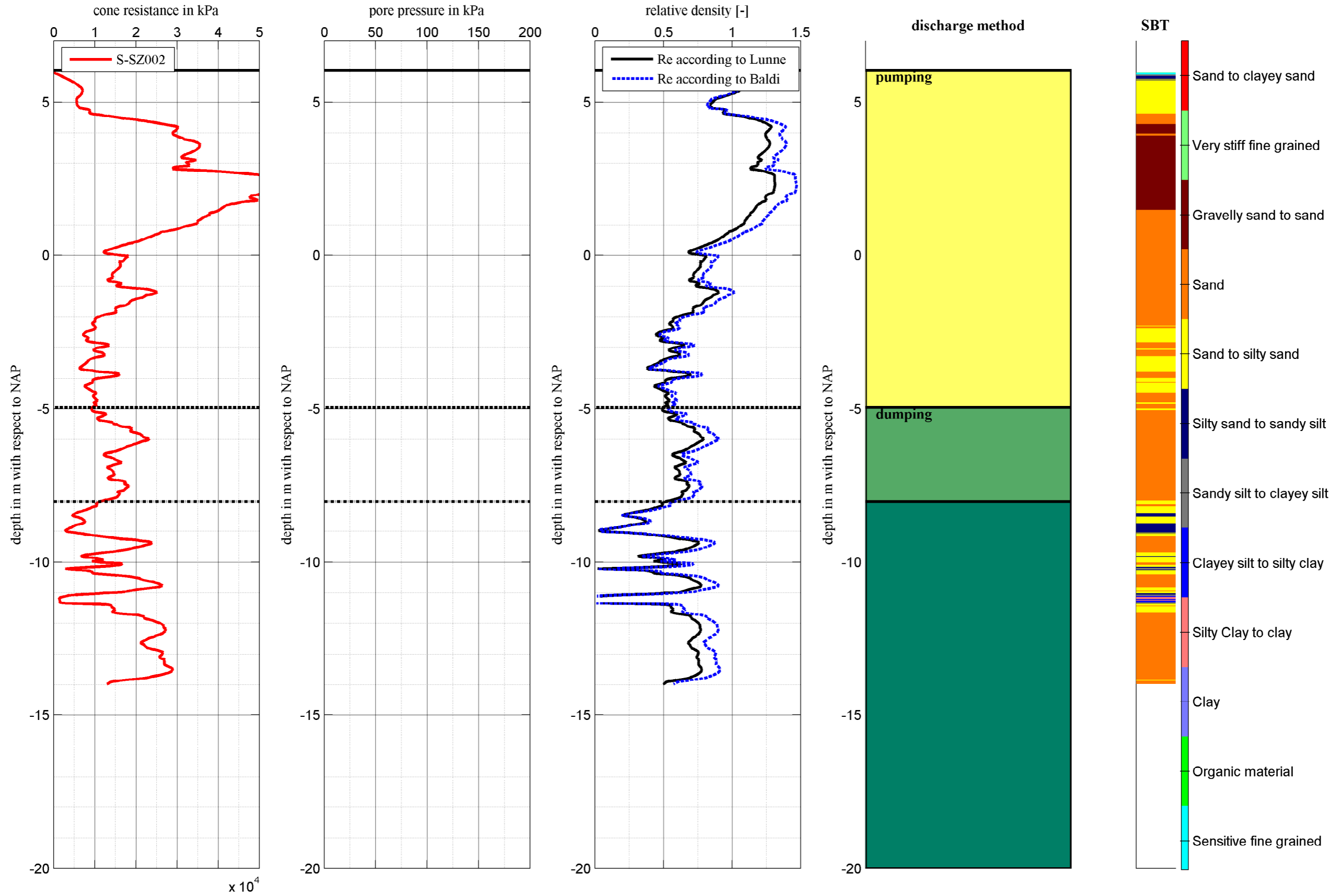
Top layer : -4.957 m NAP
Bottom layer : -8.022 m NAP
Layer thickness : 3.065 m

Re according to Lunne: Re according to Baldi:
Re min = 0.489 Re min = 0.534
Re mean = 0.640 Re mean = 0.722
Re max = 0.793 Re max = 0.904

d50 and fines:
d50 min = 198 mu percentage fines min = 1.160
d50 mean = 272 mu percentage fines mean = 1.614
d50 max = 450 mu percentage fines max = 2.340

REMARK: The values of the d50 and the percentage fines are measured on board of the TSHD with a CPA machine.

CPT 265 - S-SZ002 made on: 11-5-2010



Appendix E: Cross Sections

Appendix E: Cross Sections

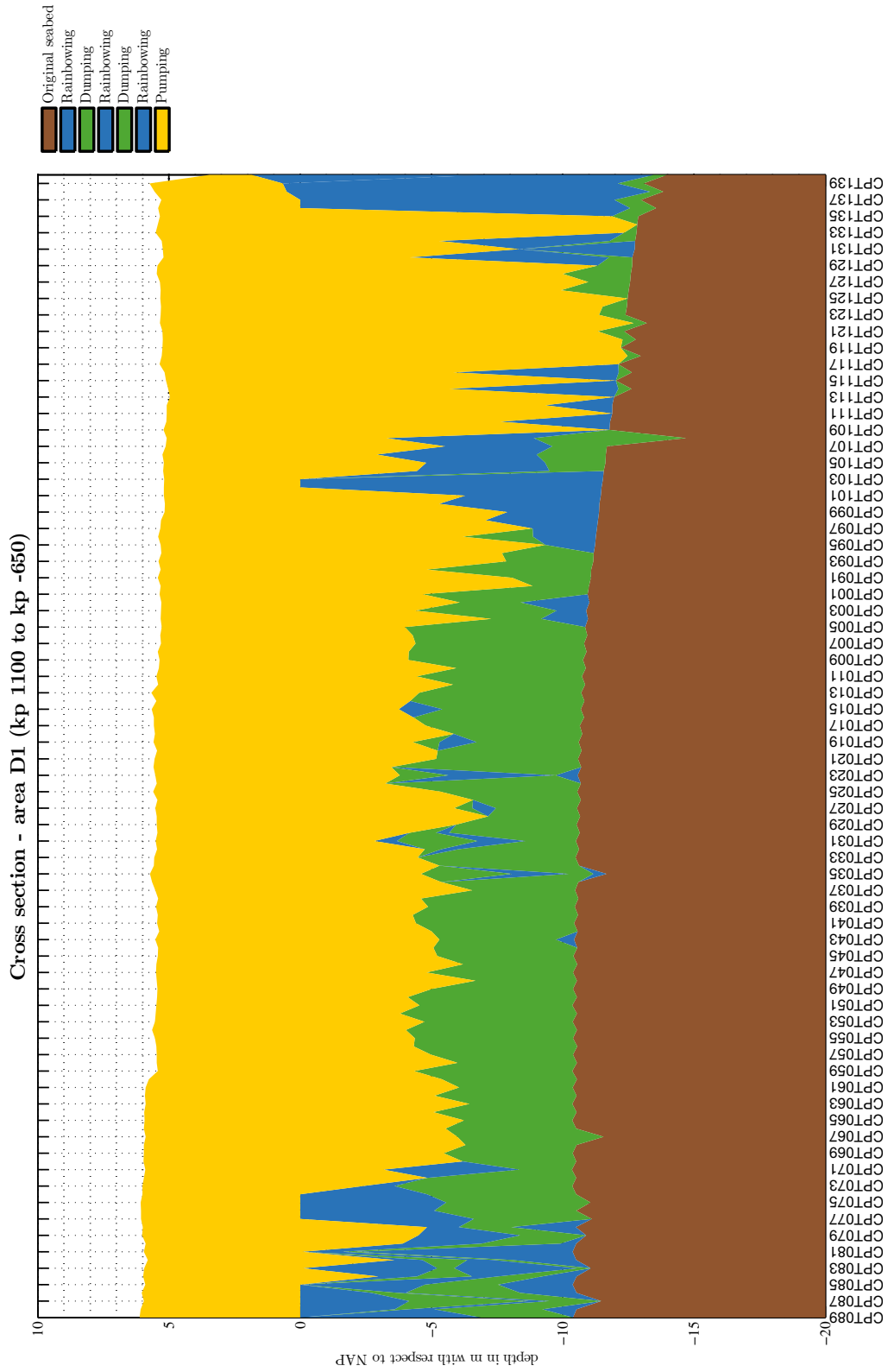


Figure E.1: Cross section - area D1 & D2 (CPT001 untill CPT140).

Appendix E: Cross Sections

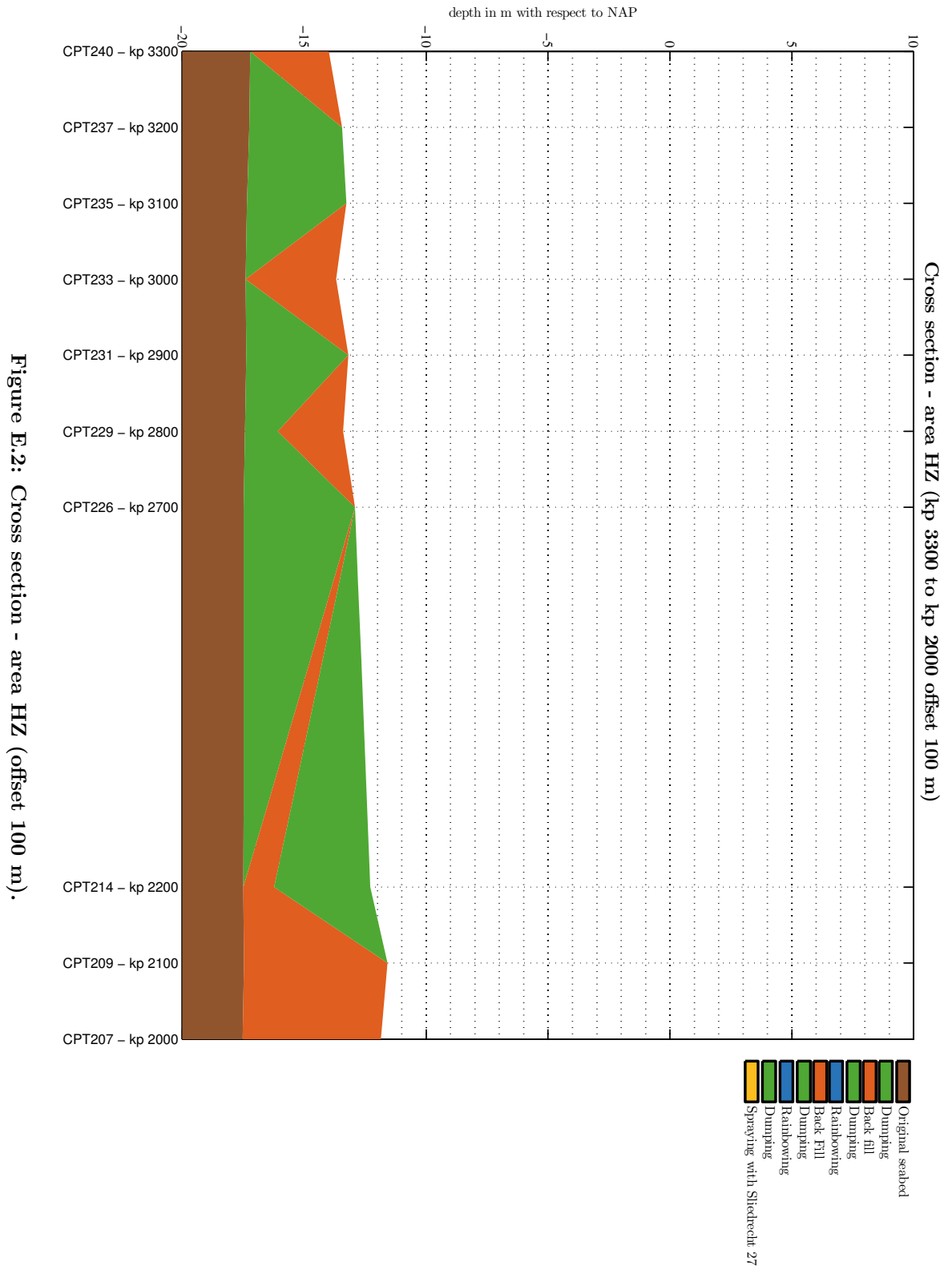


Figure E.2: Cross section - area HZ (offset 100 m).

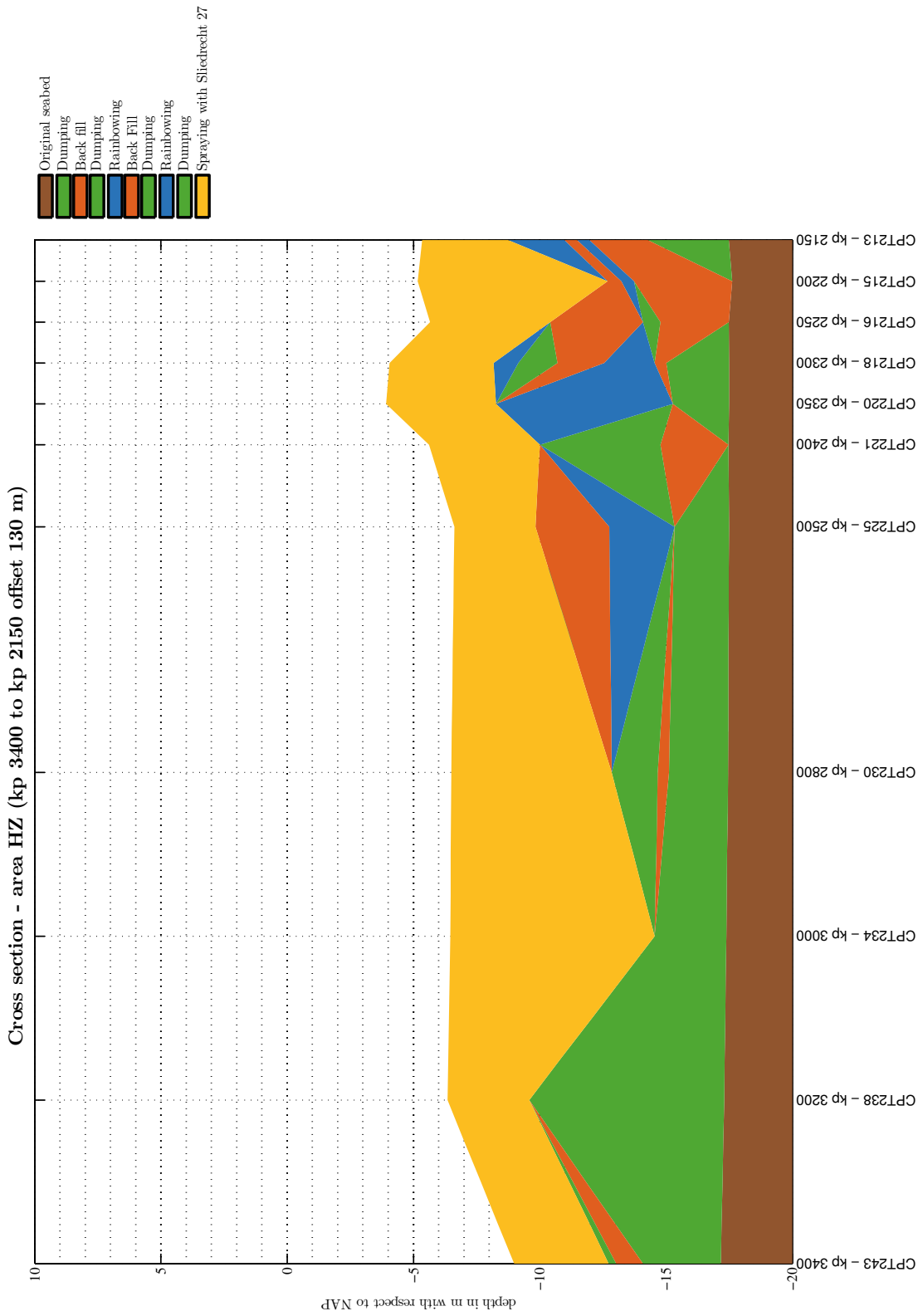


Figure E.3: Cross section - area HZ (offset 130 m).

Appendix E: Cross Sections

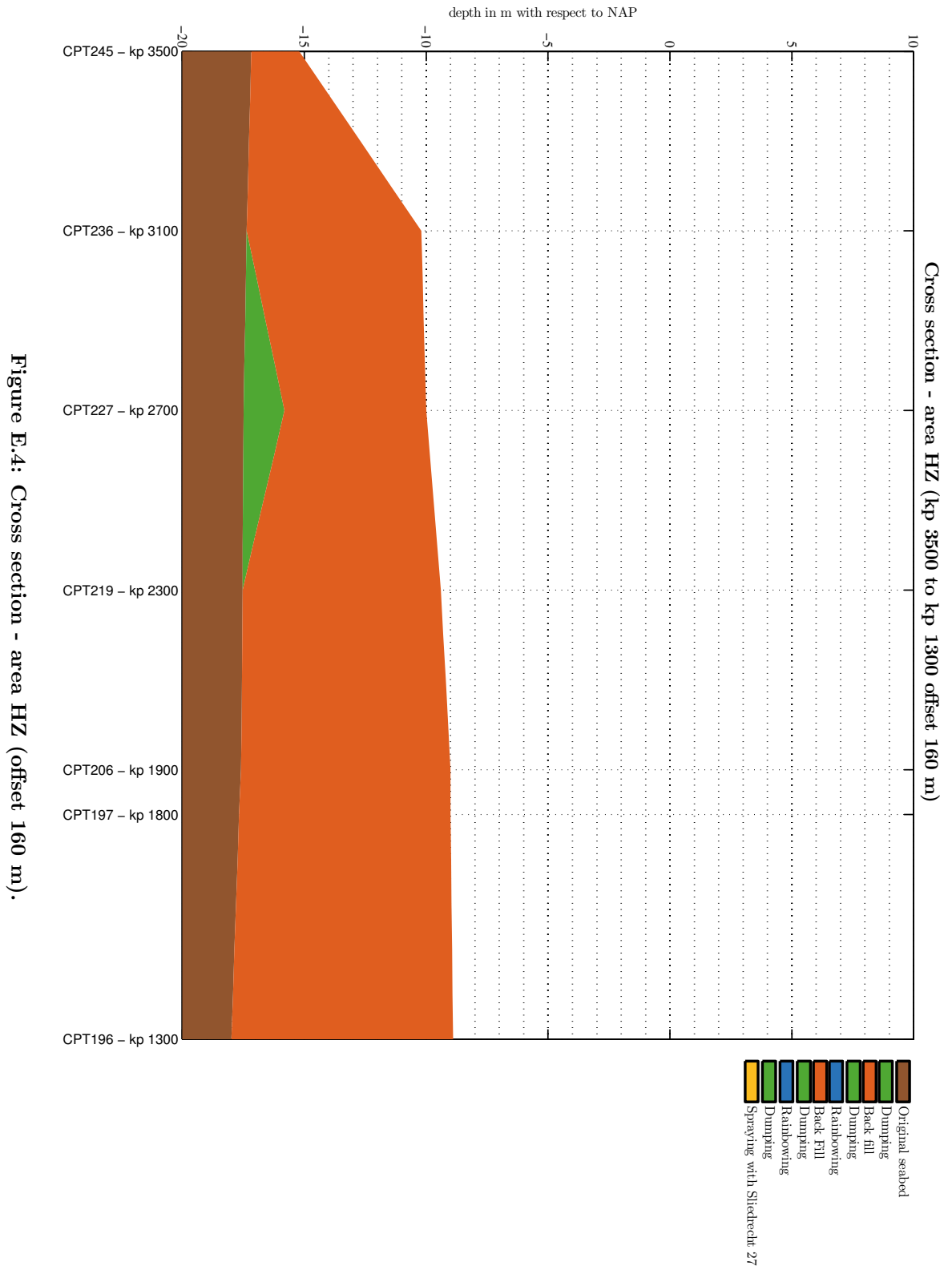


Figure E.4: Cross section - area HZ (offset 160 m).

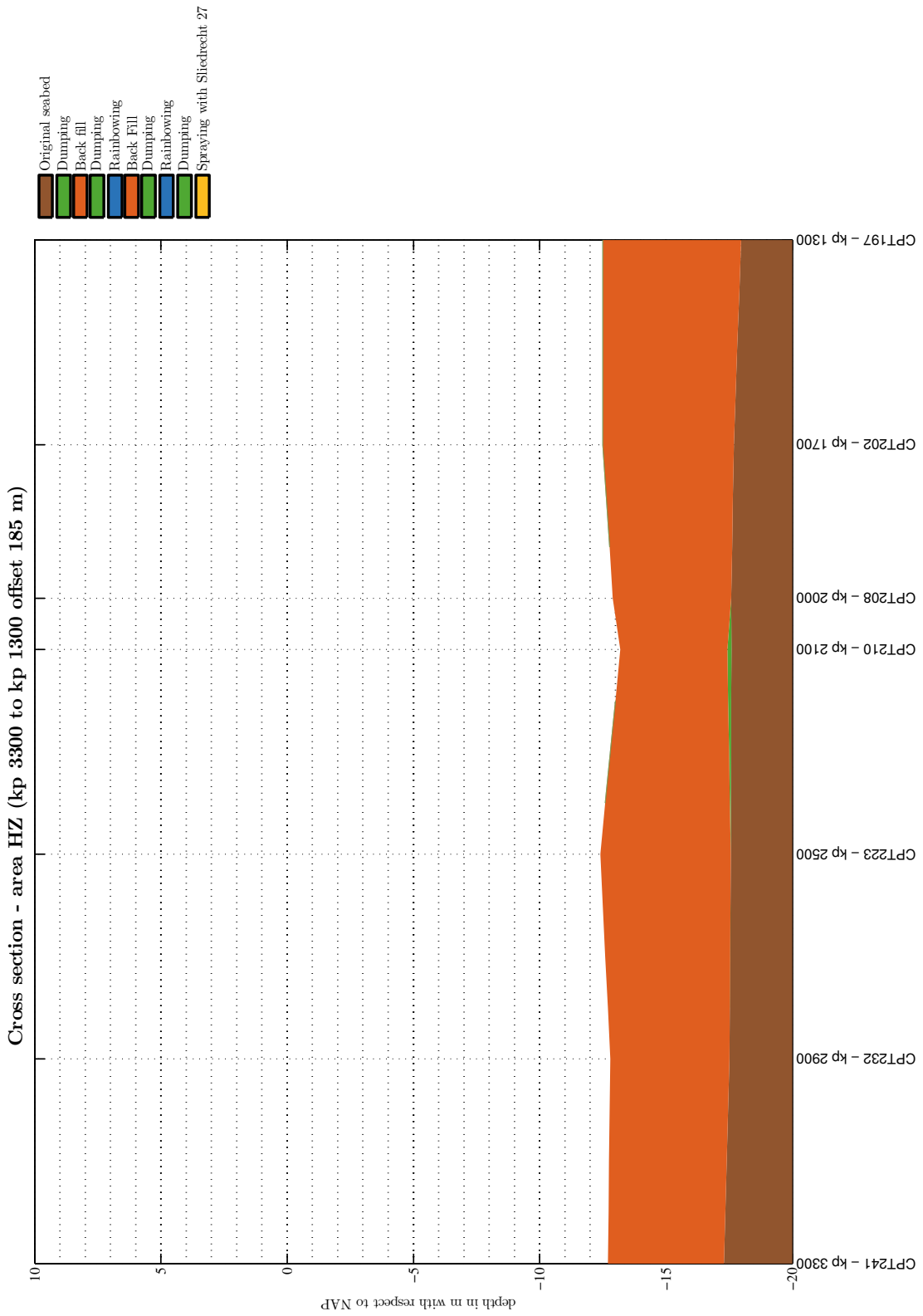


Figure E.5: Cross section - area HZ (offset 185 m).

Appendix E: Cross Sections

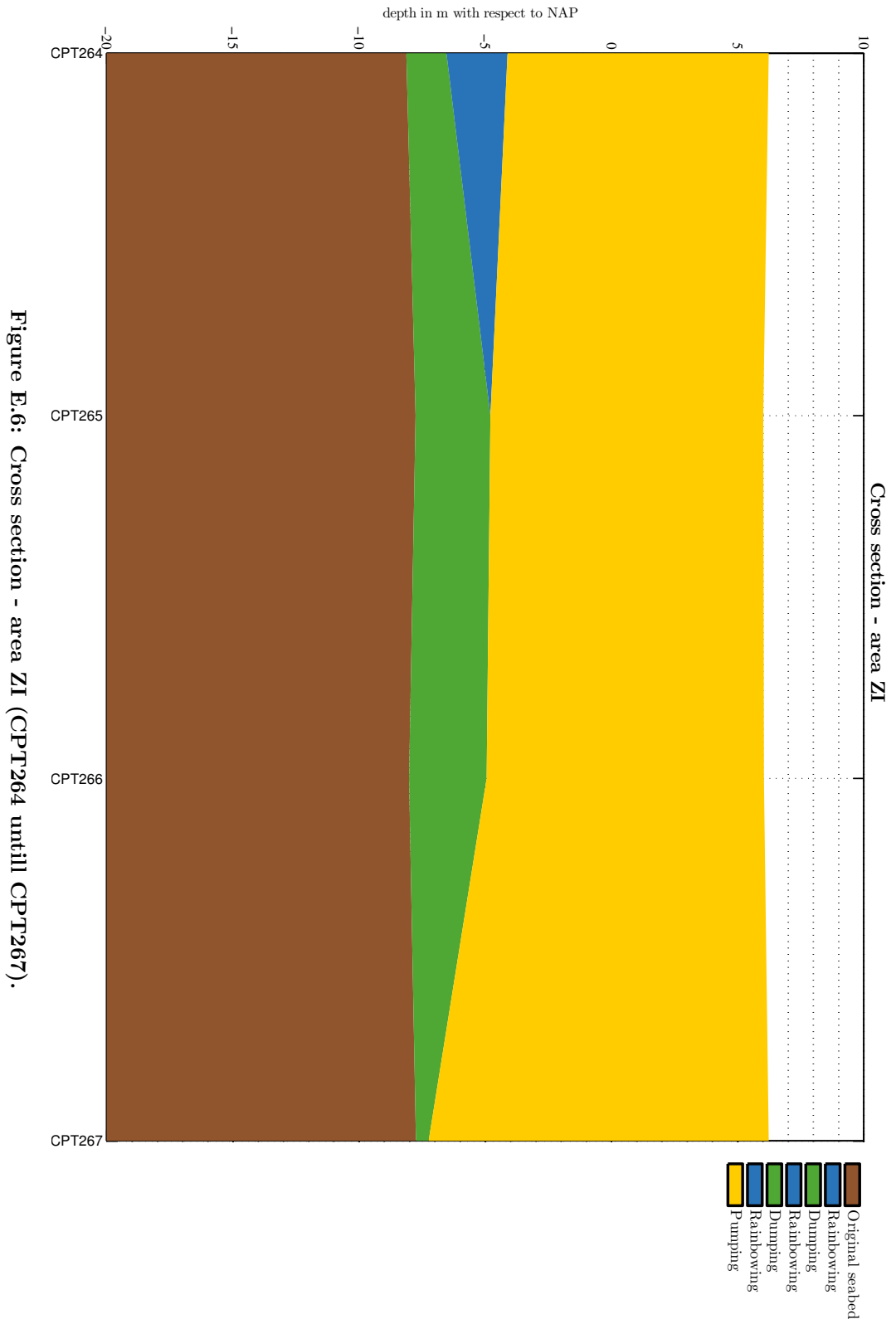


Figure E.6: Cross section - area ZI (CPT264 untill CPT267).

Appendix F: Statistical Analysis of Relative Density Data Histograms

Appendix F: Statistical Analysis of Relative Density Data Histograms

F.1 Probability Density Distributions

The 18 different probability density distributions (PDF) of “Bestfit”:

1. Beta Distribution;
2. Binomial Distribution;
3. χ^2 Distribution;
4. Error Function;
5. Erlang Distribution;
6. Exponential Distribution;
7. Gamma Distribution;
8. Geometric Distribution;
9. Hypergeometric Distribution;
10. Logistic Distribution;
11. Lognormal Distribution;
12. Lognormal2 Distribution;
13. Negative BinomialDistribution;
14. Normal Distribution;
15. Pareto Distribution;
16. Poisson Distribution;
17. Triangular Distribution;
18. Weibull Distribution.

F.2 Results of Statistical Analysis

Table F.1: The different distributions per work method and area.

Work method	Correlation	Area	χ^2 – Test	K-S Test	A-D Test	
Dumping (DU)	Baldi	D	Logistic	Logistic	Logistic	
		HZ	Logistic	Logistic	Logistic	
		ZI	Logistic	Weibull	Weibull	
		ZI	Logistic	Logistic	Logistic	
	Lunne and Christoffersen	D	Logistic	Logistic	Logistic	Logistic
		HZ	Logistic	Logistic	Logistic	Logistic
		ZI	Logistic	Weibull	Weibull	Weibull
		ZI	Lognormal	Lognormal	Lognormal	Logistic
Rainbowing (RB)	Baldi	D	Logistic	Logistic	Logistic	
		HZ	Logistic	Logistic	Logistic	
		ZI	Triangular	Weibull	Weibull	
		ZI	Triangular	Lognormal	Erlang	
	Lunne and Christoffersen	D	Logistic	Normal	Normal	Normal
		HZ	Logistic	Normal	Normal	Normal
		ZI	Triangular	Weibull	Weibull	Weibull
		ZI	Triangular	Lognormal2	Erlang	
Pumping (PU)	Baldi	D	Beta	Normal	Normal	
		HZ	Normal	Normal	Normal	
		ZI	-	-	-	
		ZI	Beta	Beta	Beta	
	Lunne and Christoffersen	D	Beta	Beta	Beta	Beta
		HZ	Weibull	Normal	Normal	
		ZI	-	-	-	
		ZI	Beta	Beta	Beta	
Back filling through suction pipe (BF)	Baldi	D	Logistic	Logistic	Logistic	
		HZ	-	-	-	
		ZI	Logistic	Logistic	Logistic	
		ZI	-	-	-	
	Lunne and Christoffersen	D	Logistic	Weibull	Weibull	
		HZ	-	-	-	
		ZI	Logistic	Weibull	Weibull	
		ZI	-	-	-	
Spraying with SD “Sliedrecht 17” (SP)	Baldi	D	Logistic	Weibull	Weibull	
		HZ	-	-	-	
		ZI	Logistic	Weibull	Weibull	
		ZI	-	-	-	
	Lunne and Christoffersen	D	Logistic	Weibull	Weibull	
		HZ	-	-	-	
		ZI	Logistic	Weibull	Weibull	
		ZI	-	-	-	

Appendix F: Statistical Analysis of Relative Density Data Histograms

Table F.2: Results of the mean (μ), standard deviate (σ), median (η) and variance (Var).

WM	Correlation	Area	PDF	μ	σ	η	Var
DU	Baldi		Logistic	0.68873	0.11825	0.6922	0.01398
		D	Logistic	0.68877	0.11675	0.69134	0.01363
		HZ	Weibull	0.66762	0.14782	0.68477	0.02185
		ZI	Logistic	0.74907	0.08637	0.74865	0.00746
	Lunne and Christoffersen		Logistic	0.61571	0.10174	0.61671	0.01035
		D	Logistic	0.61091	0.08945	0.61269	0.00969
		HZ	Weibull	0.69886	0.1325	0.71148	0.01756
		ZI	Lognormal	0.66163	0.07189	0.66186	0.00517
RB	Baldi		Logistic	0.70574	0.1519	0.70585	0.02307
		D	Logistic	0.7062	0.15267	0.70575	0.02331
		HZ	Weibull	0.67341	0.10835	0.70878	0.01174
		ZI	Lognormal	0.71392	0.12168	0.73704	0.01481
	Lunne and Christoffersen		Normal	0.63301	0.13109	0.6299	0.17184
		D	Normal	0.63232	0.13179	0.62887	0.01737
		HZ	Weibull	0.67357	0.08969	0.70473	0.00804
		ZI	Lognormal2	0.63586	0.09859	0.65429	0.00972
PU	Baldi		Normal	0.89202	0.26995	0.87849	0.07287
		D	Normal	0.89177	0.26857	0.87805	0.07213
		HZ	-	-	-	-	-
		ZI	Beta	0.90036	0.31263	0.89156	0.09774
	Lunne and Christoffersen		Beta	0.83042	0.25647	0.80739	0.06578
		D	Normal	0.83025	0.25557	0.80697	0.06532
		HZ	-	-	-	-	-
		ZI	Beta	0.83607	0.28491	0.82892	0.08117
BF	Baldi		Logistic	0.64	0.16267	0.65981	0.02646
		D	-	-	-	-	-
		HZ	Logistic	0.64	0.16267	0.65981	0.02646
		ZI	-	-	-	-	-
	Lunne and Christoffersen		Weibull	0.6725	0.14308	0.69183	0.02047
		D	-	-	-	-	-
		HZ	Weibull	0.6725	0.14308	0.69183	0.02047
		ZI	-	-	-	-	-
SP	Baldi		Weibull	0.56	0.17131	0.58169	0.02935
		D	-	-	-	-	-
		HZ	Weibull	0.56	0.17131	0.58169	0.02935
		ZI	-	-	-	-	-
	Lunne and Christoffersen		Weibull	0.61823	0.14376	0.63796	0.02067
		D	-	-	-	-	-
		HZ	Weibull	0.61823	0.14376	0.63796	0.02067
		ZI	-	-	-	-	-

F.3 Histograms of the Statistical Analysis

Appendix F: Statistical Analysis of Relative Density Data Histograms

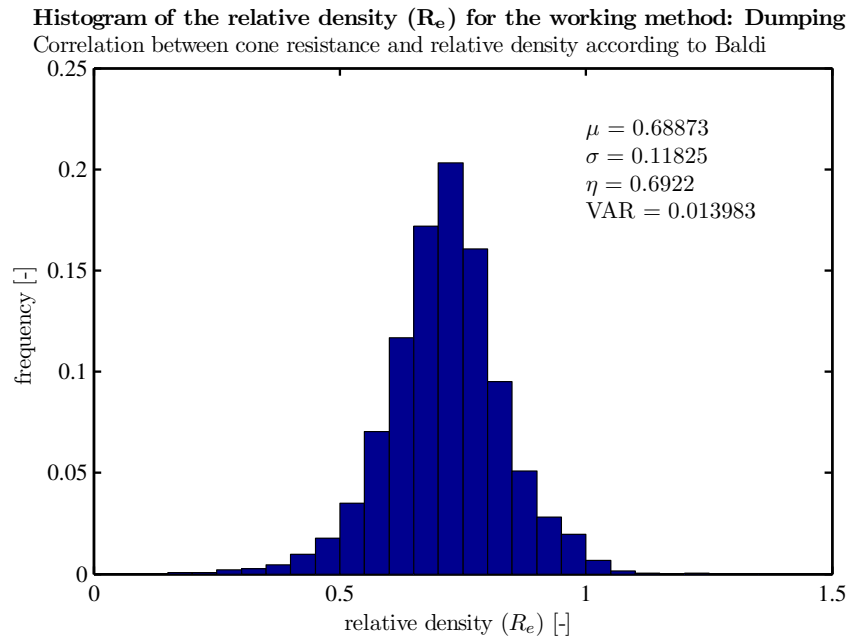


Figure F.1: Histogram for dumping, with the correlation of Baldi for all the data.

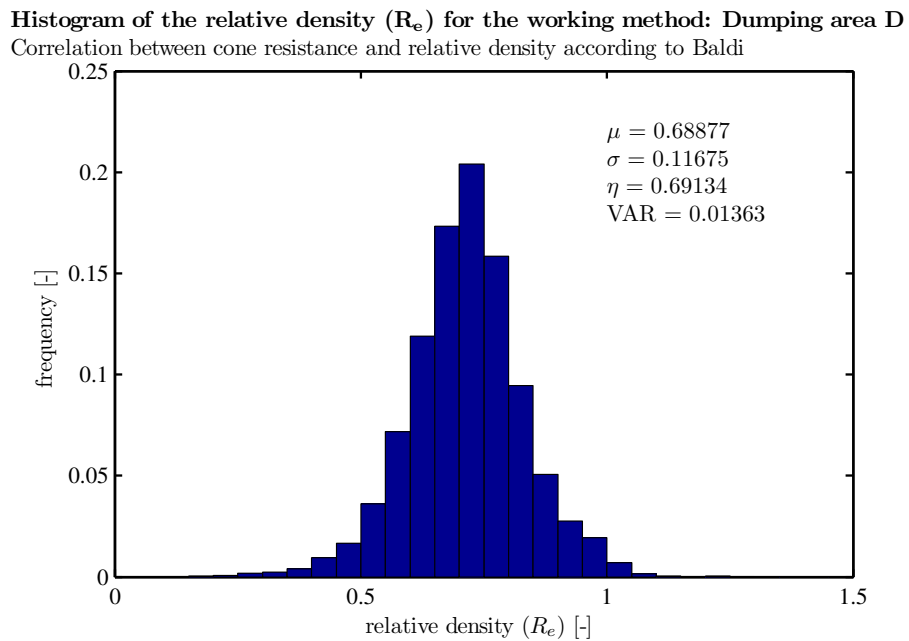


Figure F.2: Histogram for dumping, with the correlation of Baldi for area D1 & D2.

Histogram of the relative density (R_e) for the working method: Dumping area HZ
 Correlation between cone resistance and relative density according to Baldi

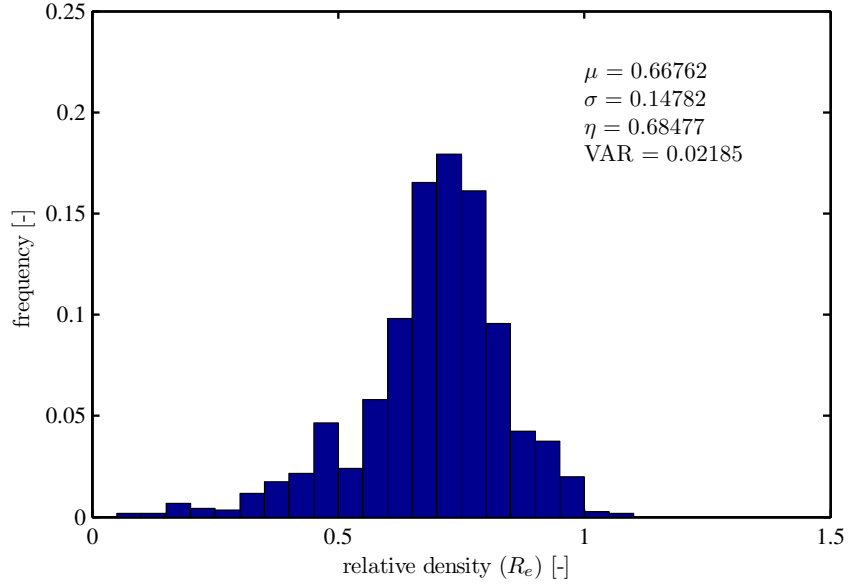


Figure F.3: Histogram for dumping, with the correlation of Baldi for area HZw, HZm & HZo.

Histogram of the relative density (R_e) for the working method: Dumping area ZI
 Correlation between cone resistance and relative density according to Baldi

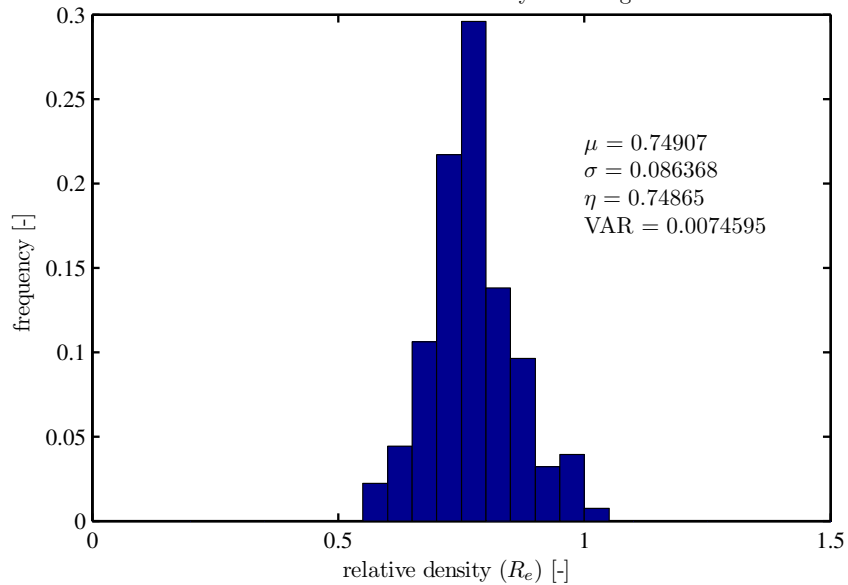


Figure F.4: Histogram for dumping, with the correlation of Baldi for area ZI.

Appendix F: Statistical Analysis of Relative Density Data Histograms

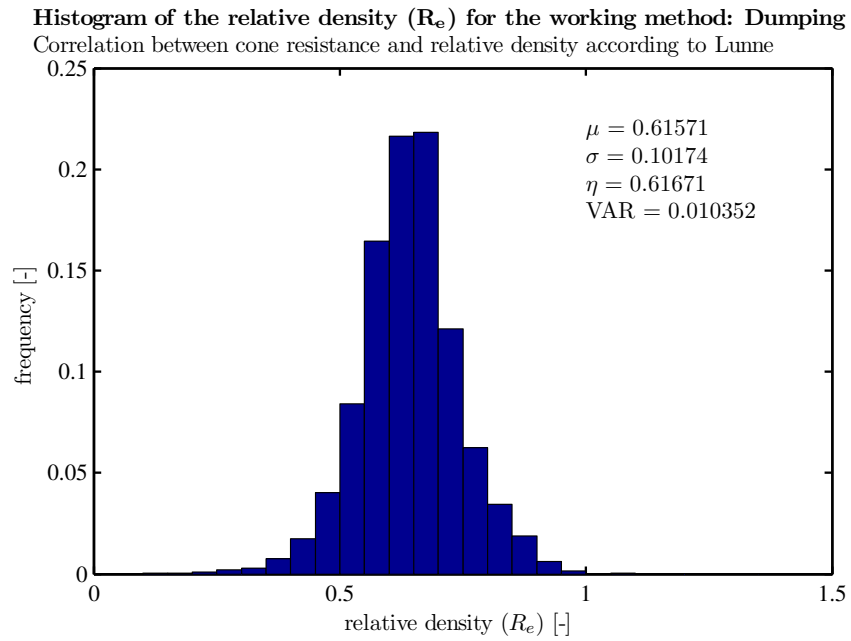


Figure F.5: Histogram for dumping, with the correlation of Lunne for all the data.

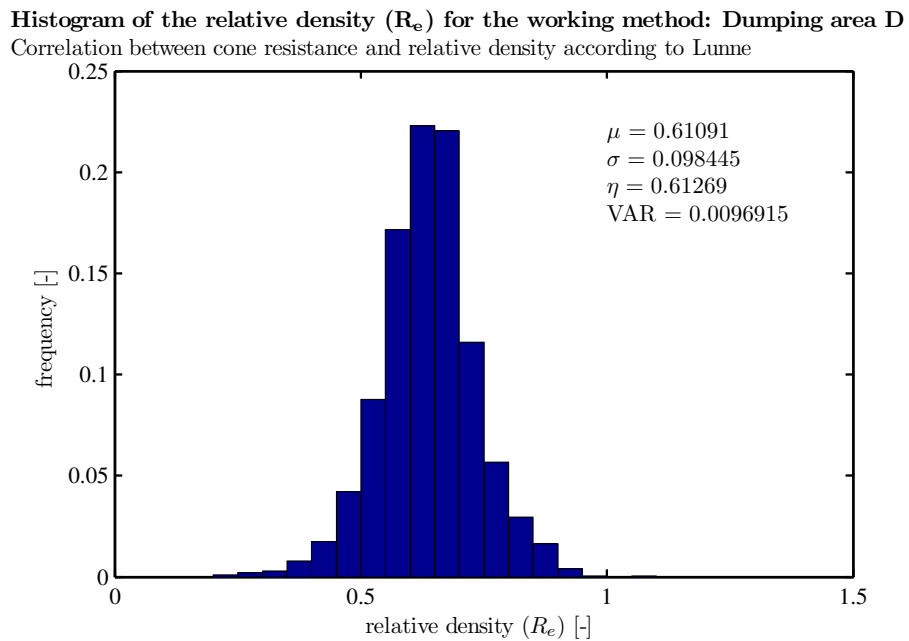


Figure F.6: Histogram for dumping, with the correlation of Lunne for area D1 & D2.

Histogram of the relative density (R_e) for the working method: Dumping area HZ
 Correlation between cone resistance and relative density according to Lunne

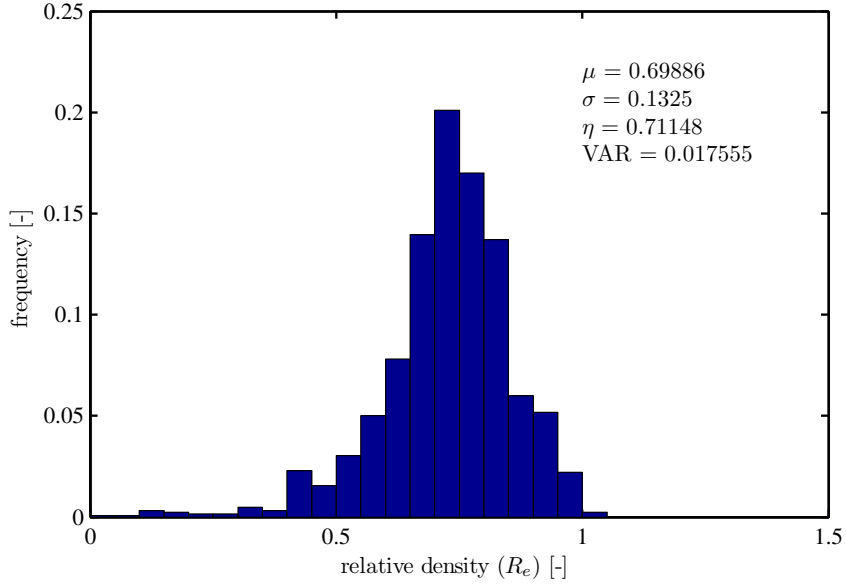


Figure F.7: Histogram for dumping, with the correlation of Lunne for area HZw, HZm & HZo.

Histogram of the relative density (R_e) for the working method: Dumping area ZI
 Correlation between cone resistance and relative density according to Lunne

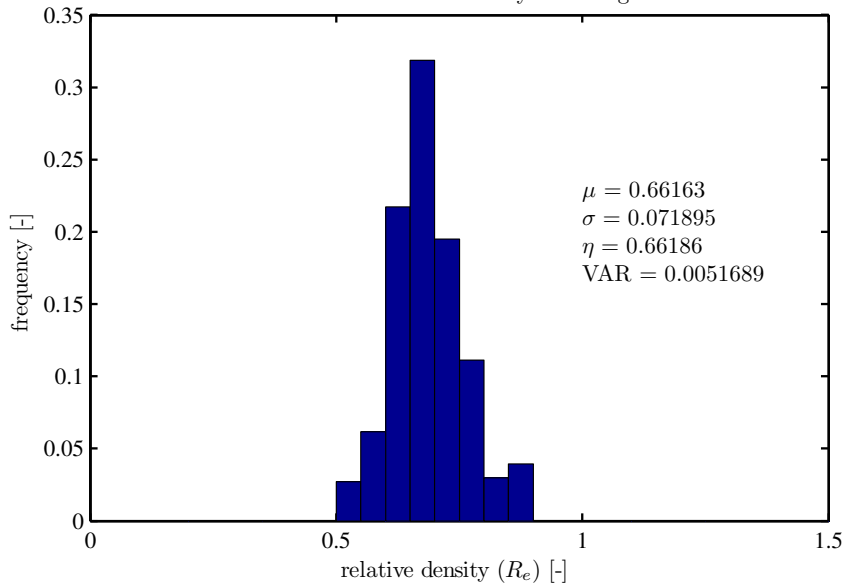


Figure F.8: Histogram for dumping, with the correlation of Lunne for area ZI.

Appendix F: Statistical Analysis of Relative Density Data Histograms

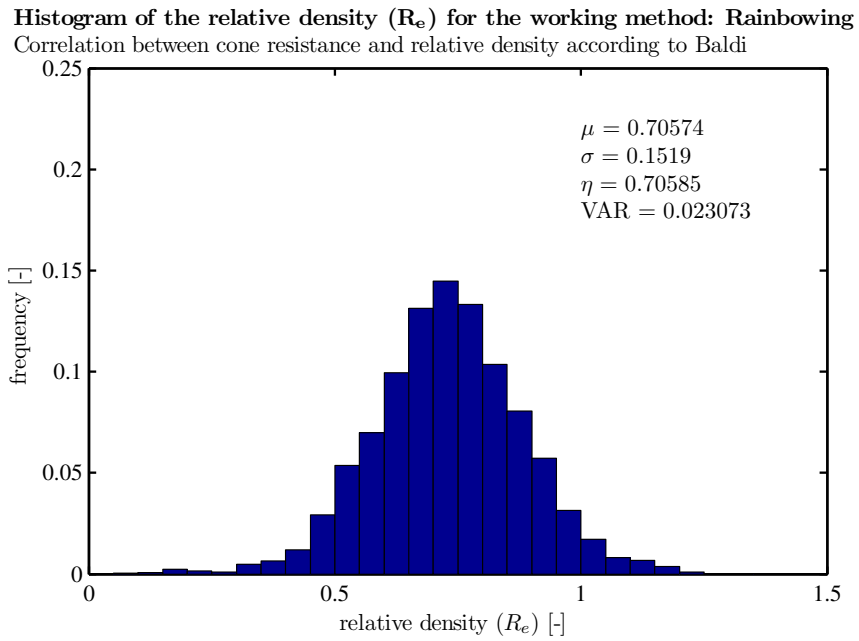


Figure F.9: Histogram for rainbowing, with the correlation of Baldi for all the data.

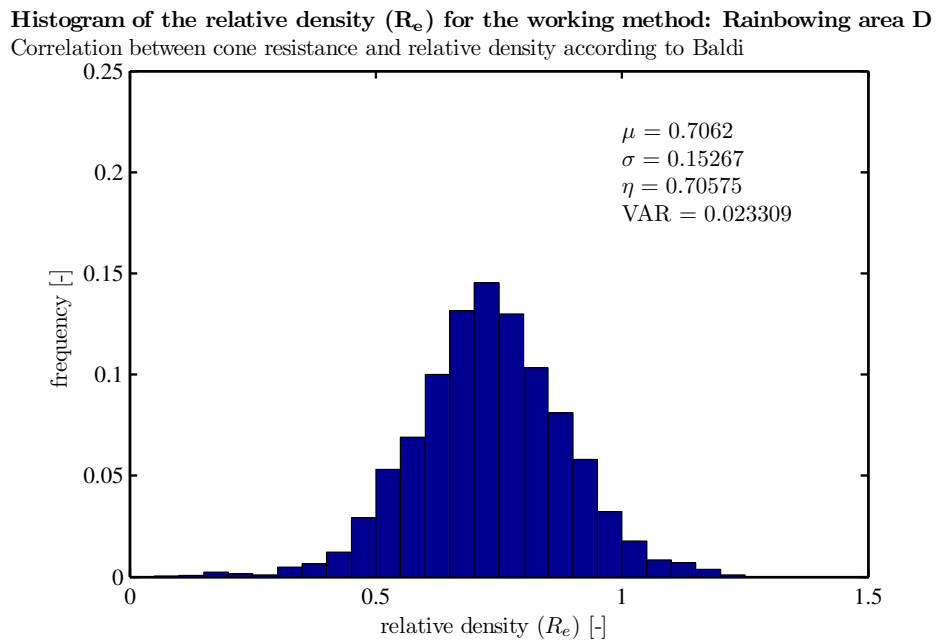


Figure F.10: Histogram for rainbowing, with the correlation of Baldi for area D1 & D2.

Histogram of the relative density (R_e) for the working method: Rainbowing area HZ
 Correlation between cone resistance and relative density according to Baldi

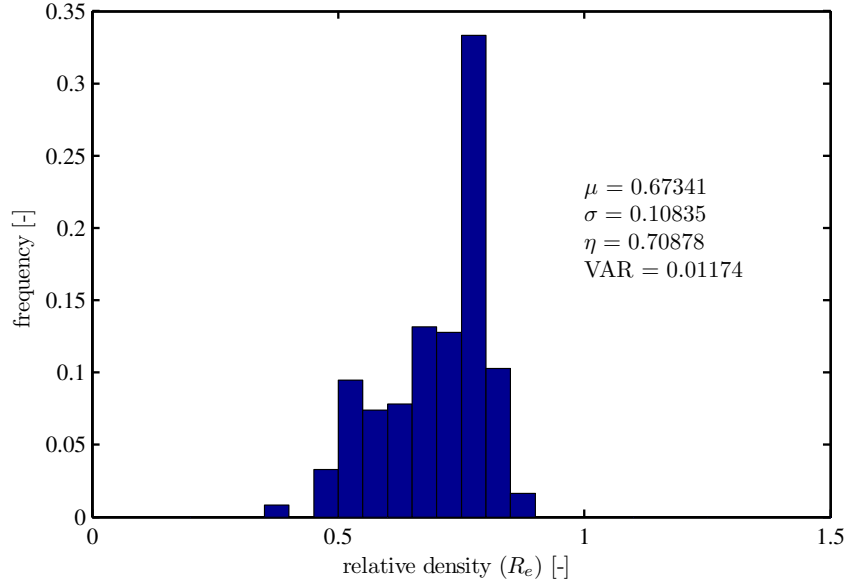


Figure F.11: Histogram for rainbowing, with the correlation of Baldi for area HZw, HZm & HZo.

Histogram of the relative density (R_e) for the working method: Rainbowing area ZI
 Correlation between cone resistance and relative density according to Baldi

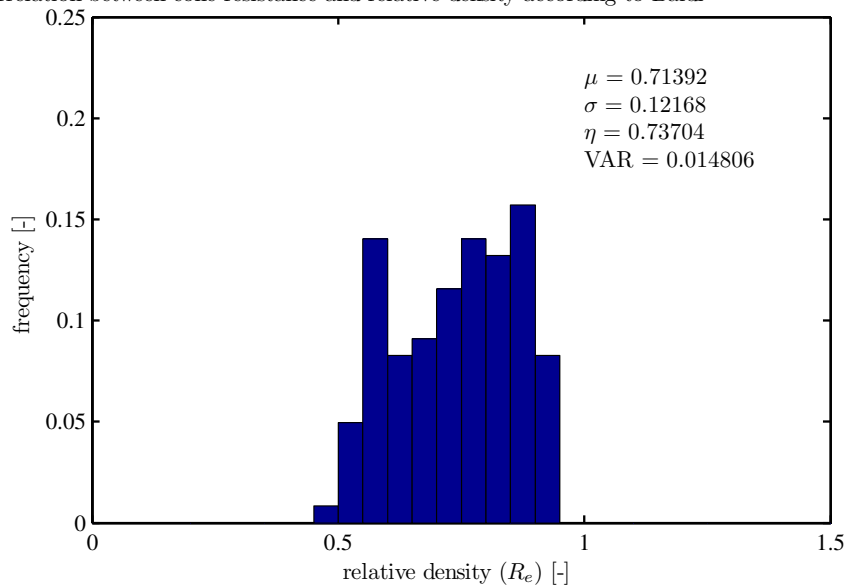


Figure F.12: Histogram for rainbowing, with the correlation of Baldi for area ZI.

Appendix F: Statistical Analysis of Relative Density Data Histograms

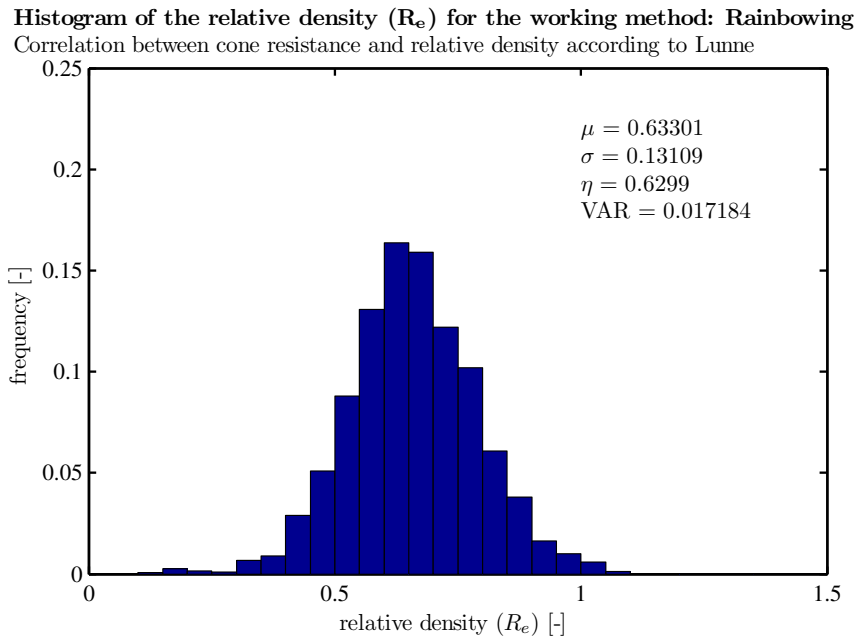


Figure F.13: Histogram for rainbowing, with the correlation of Lunne for all the data.

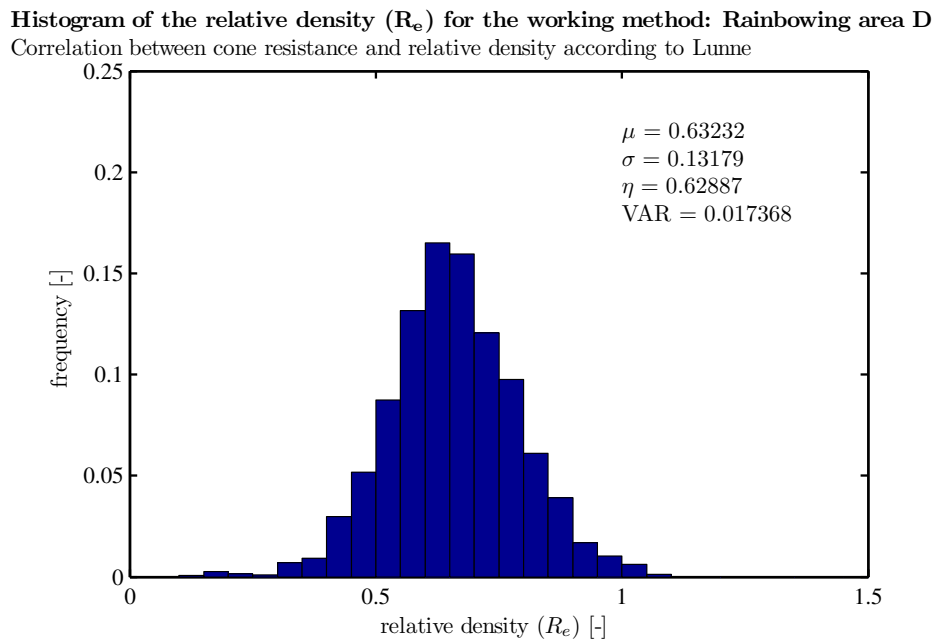


Figure F.14: Histogram for rainbowing, with the correlation of Lunne for area D1 & D2.

Histogram of the relative density (R_e) for the working method: Rainbowing area HZ

Correlation between cone resistance and relative density according to Lunne

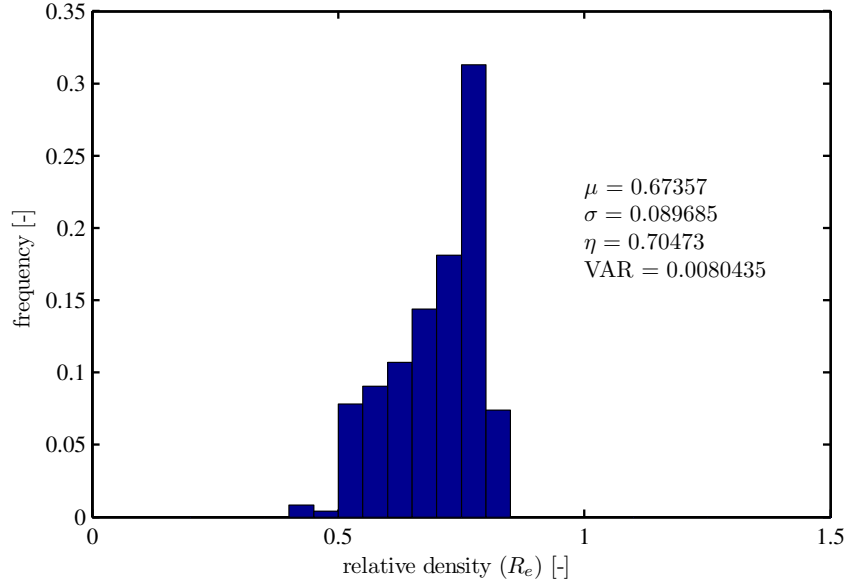


Figure F.15: Histogram for rainbowing, with the correlation of Lunne for area HZw, HZm & HZo.

Histogram of the relative density (R_e) for the working method: Rainbowing area ZI

Correlation between cone resistance and relative density according to Lunne

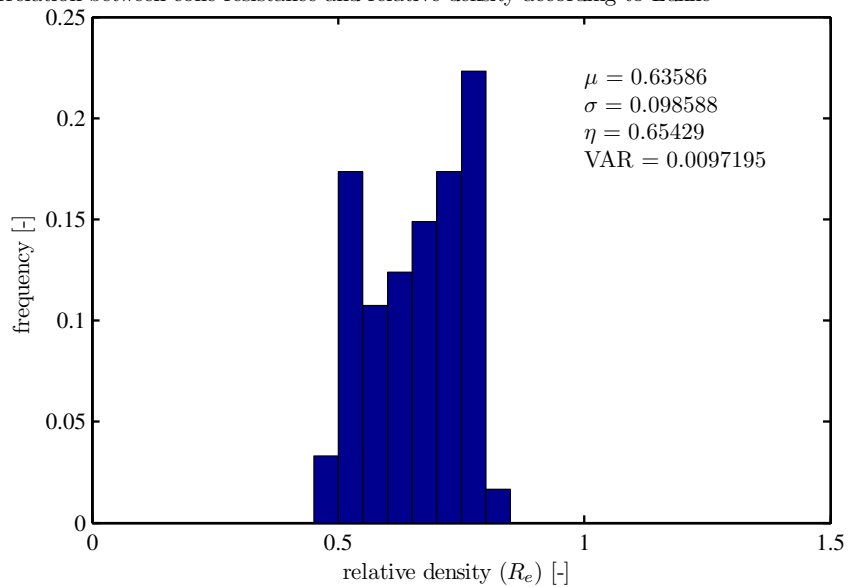


Figure F.16: Histogram for rainbowing, with the correlation of Lunne for area ZI.

Appendix F: Statistical Analysis of Relative Density Data Histograms

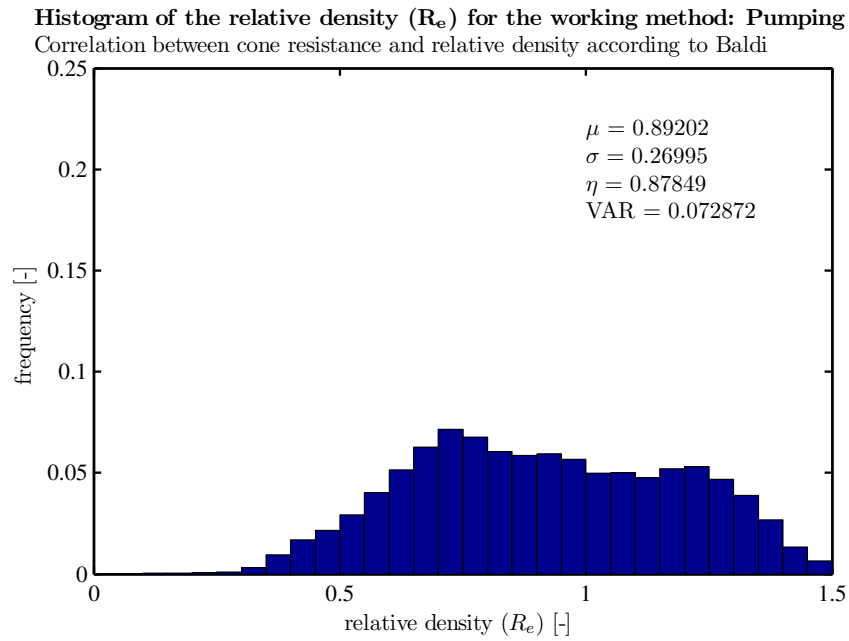


Figure F.17: Histogram for pumping, with the correlation of Baldi for all the data.

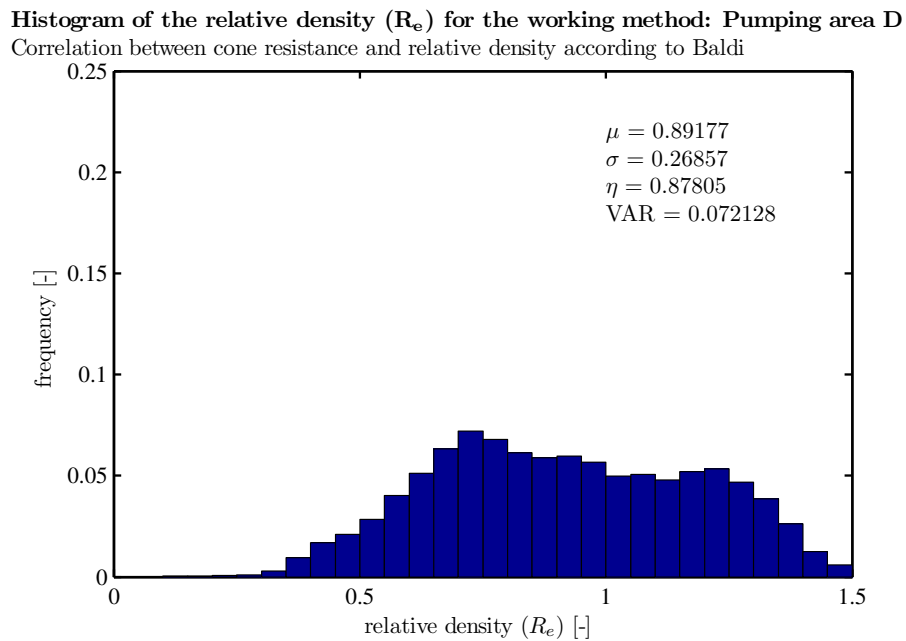


Figure F.18: Histogram for pumping, with the correlation of Baldi for area D1 & D2.

Histogram of the relative density (R_e) for the working method: Pumping area ZI
Correlation between cone resistance and relative density according to Baldi

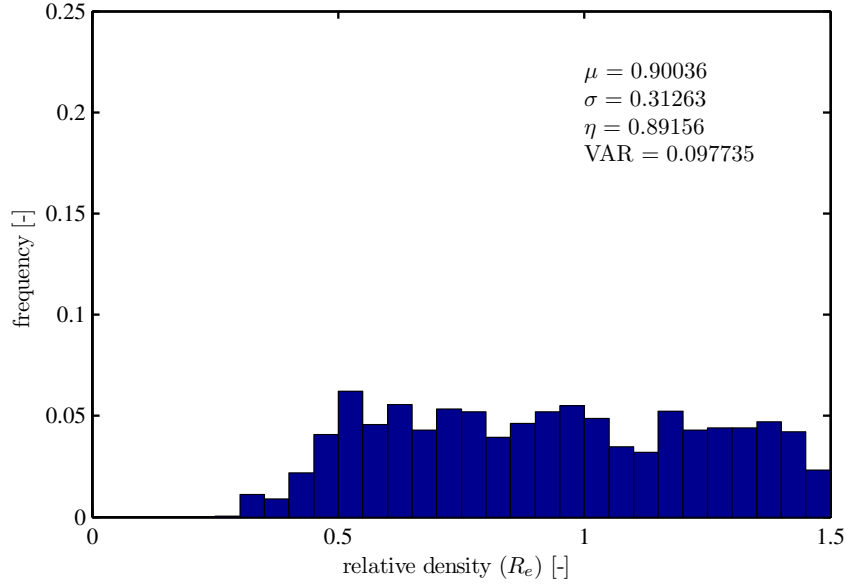


Figure F.19: Histogram for pumping, with the correlation of Baldi for area ZI.

Histogram of the relative density (R_e) for the working method: Pumping
Correlation between cone resistance and relative density according to Lunne

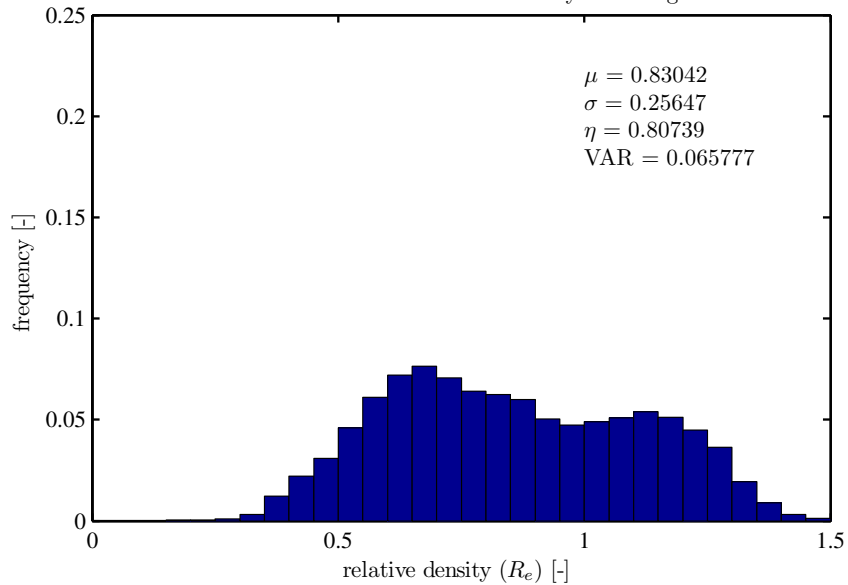


Figure F.20: Histogram for pumping, with the correlation of Lunne for all the data.

Appendix F: Statistical Analysis of Relative Density Data Histograms

Histogram of the relative density (R_e) for the working method: Pumping area D

Correlation between cone resistance and relative density according to Lunne

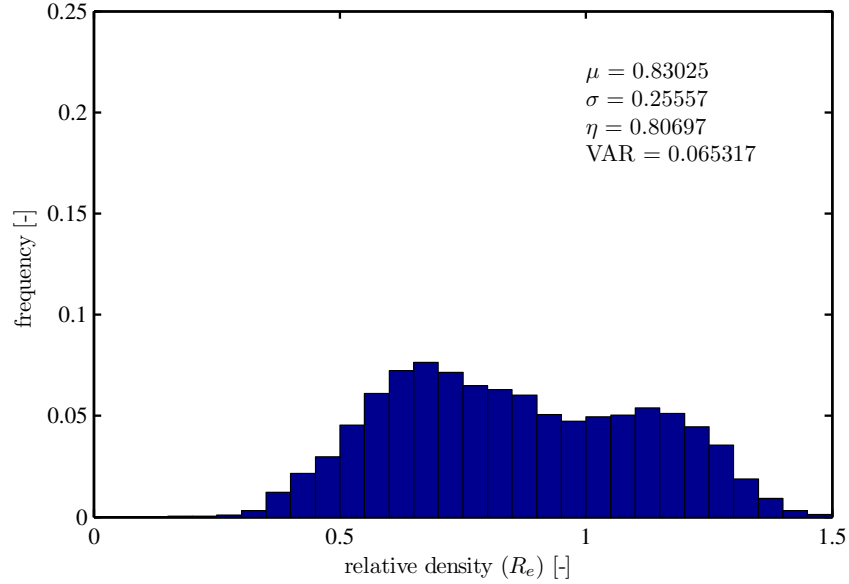


Figure F.21: Histogram for pumping, with the correlation of Lunne for area D1 & D2.

Histogram of the relative density (R_e) for the working method: Pumping area ZI

Correlation between cone resistance and relative density according to Lunne

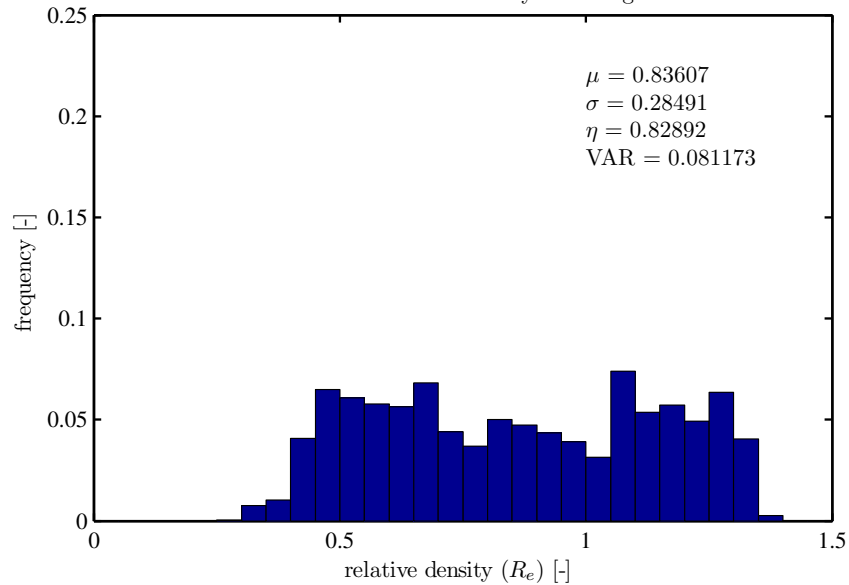


Figure F.22: Histogram for pumping, with the correlation of Lunne for area ZI.

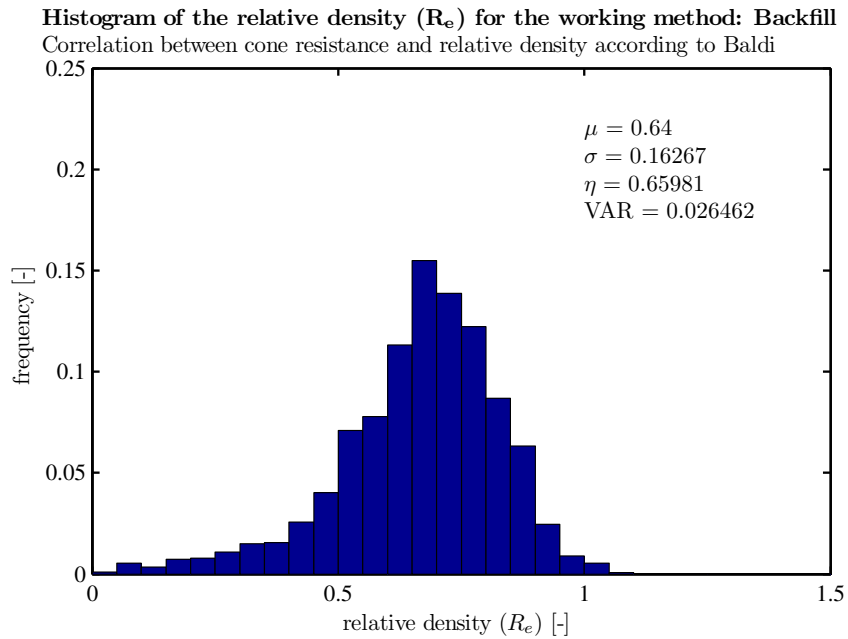


Figure F.23: Histogram for back filling through the suction pipe, with the correlation of Baldi for area HZ.

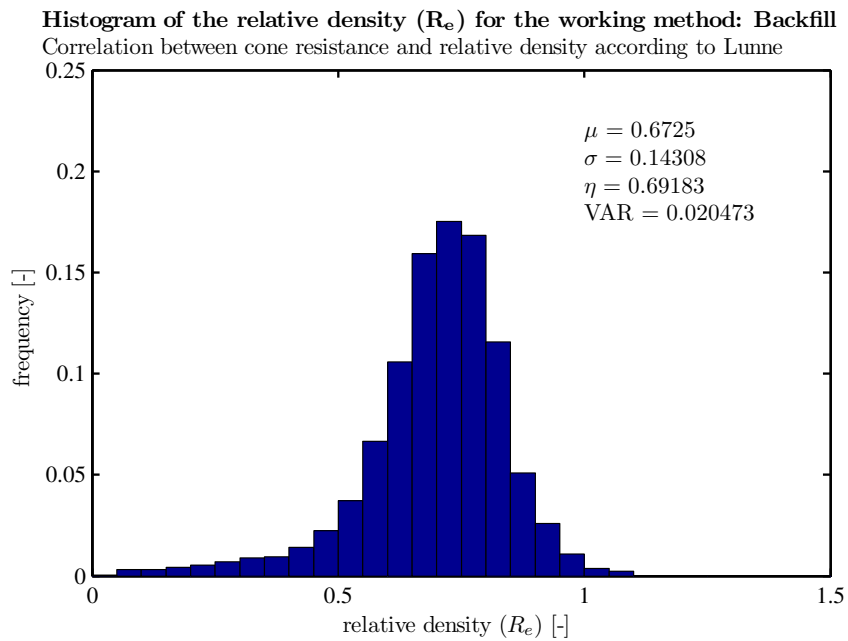


Figure F.24: Histogram for back filling through the suction pipe, with the correlation of Lunne for area HZ.

Appendix F: Statistical Analysis of Relative Density Data Histograms

Histogram of the relative density (R_e) for the working method: Spraying SL27
Correlation between cone resistance and relative density according to Baldi

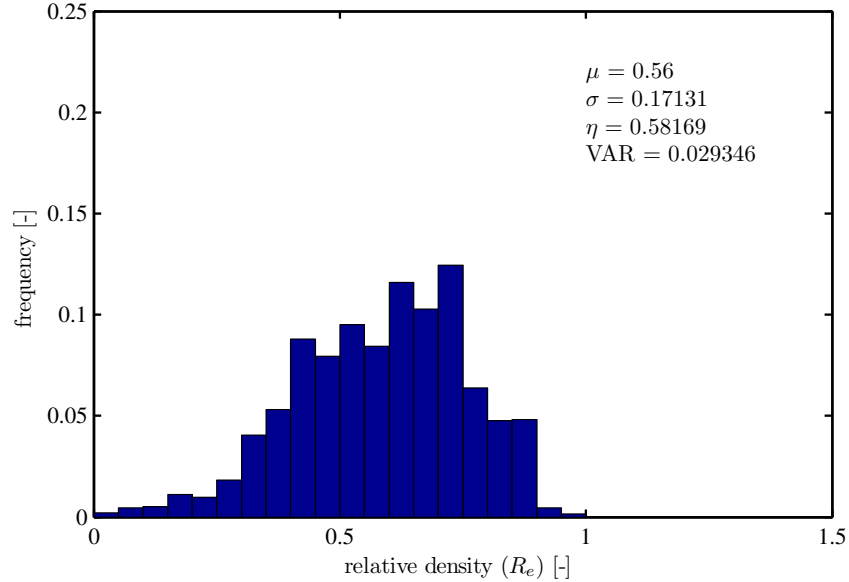


Figure F.25: Histogram for spraying with SD “Sliedrecht 17”, with the correlation of Baldi for area HZ.

Histogram of the relative density (R_e) for the working method: Spraying SL27
Correlation between cone resistance and relative density according to Lunne

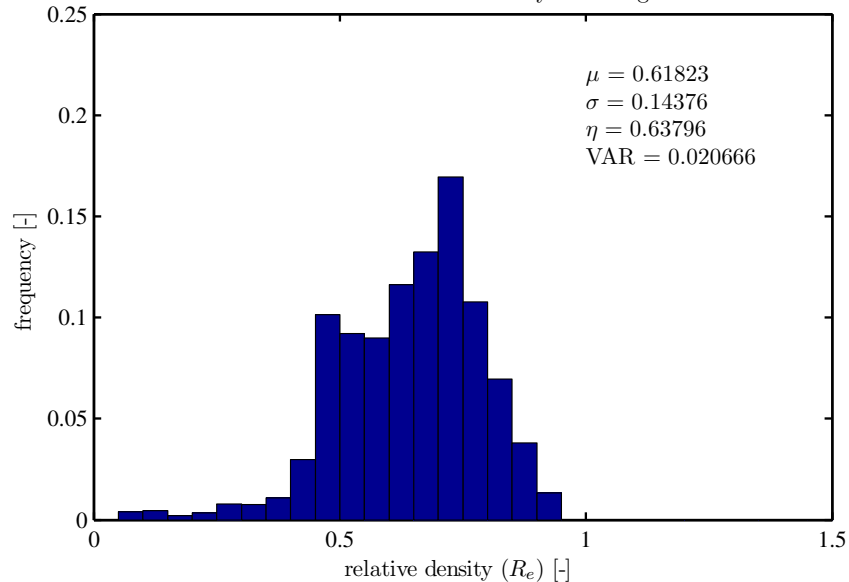


Figure F.26: Histogram for spraying with SD “Sliedrecht 17”, with the correlation of Lunne for area HZ.

Appendix G: Hydrodynamics

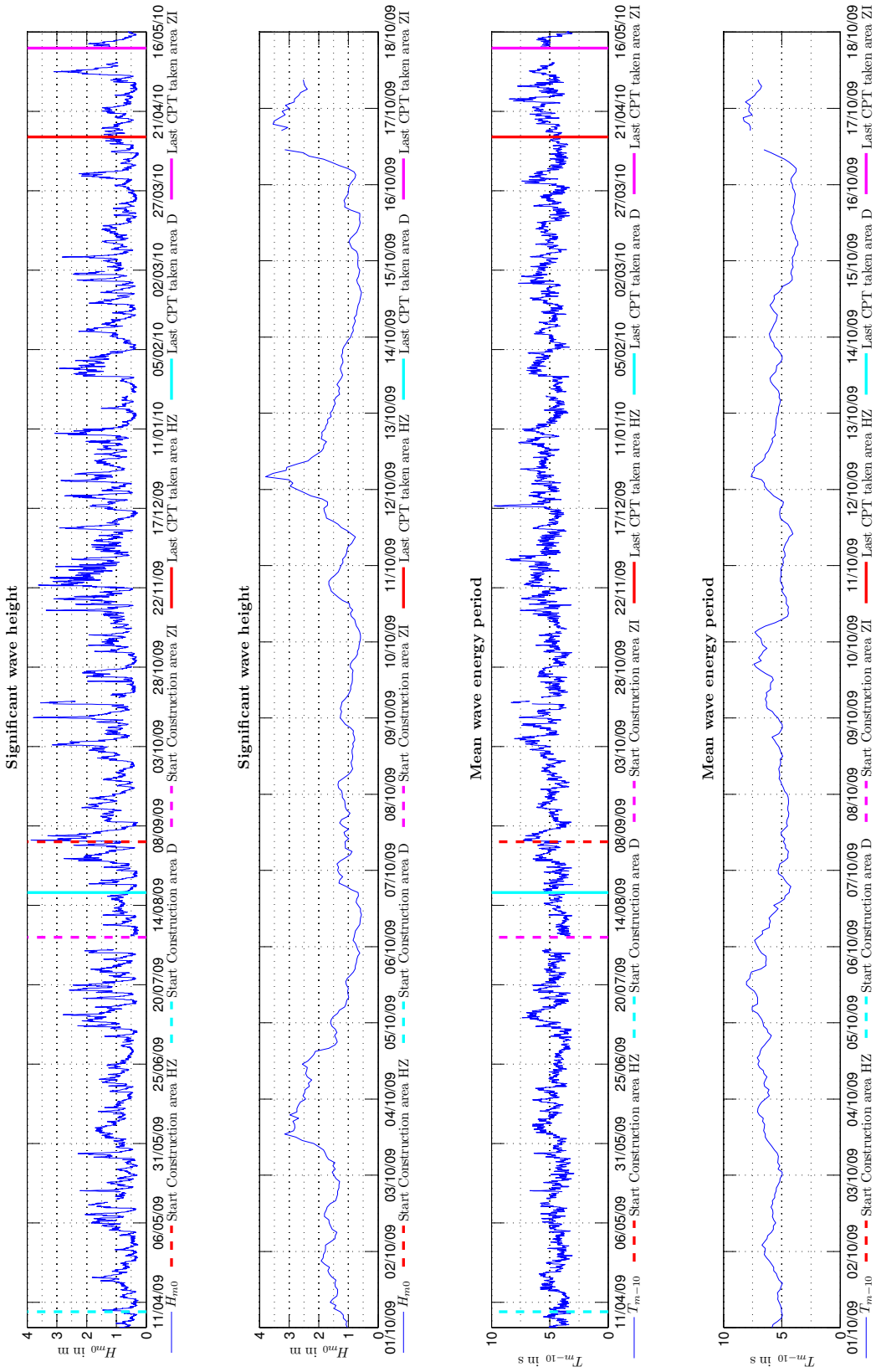


Figure G.1: Measured significant wave height and mean wave energy period.

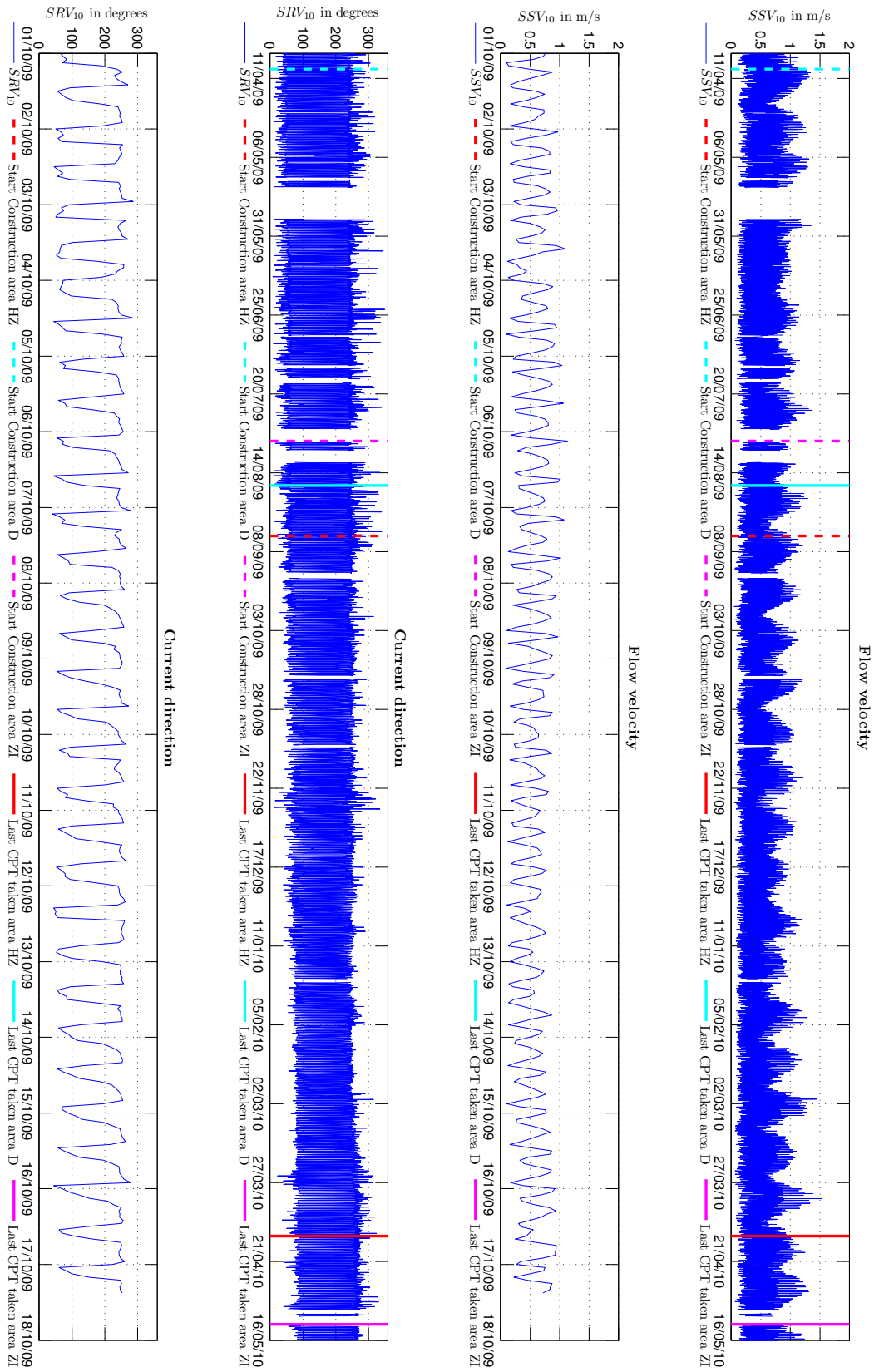


Figure G.2: Measured current velocity and direction.

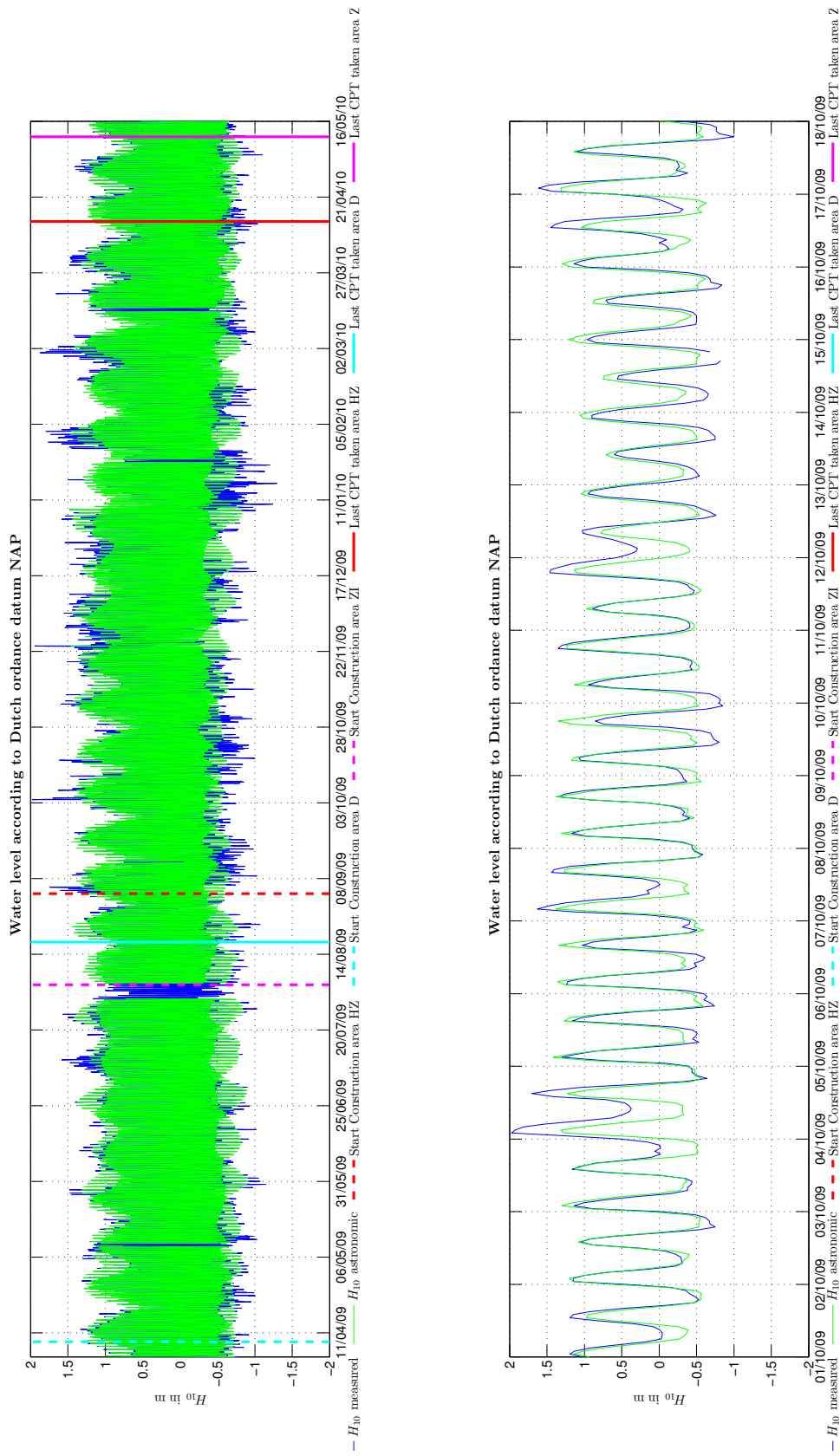


Figure G.3: Measured and astronomic water level, Hoek van Holland.

Appendix H: Progress of The Maasvlakte II Project

Appendix H: Progress of The Maasvlakte II Project



Figure H.1: Overview of the Maasvlakte II project. Survey data of April 1st, 2009.

Appendix H: Progress of The Maasvlakte II Project



Figure H.2: Overview of the Maasvlakte II project. Survey data of April 29th, 2009.



Figure H.3: Overview of the Maasvlakte II project. Survey data of June 2nd, 2009.

Appendix H: Progress of The Maasvlakte II Project

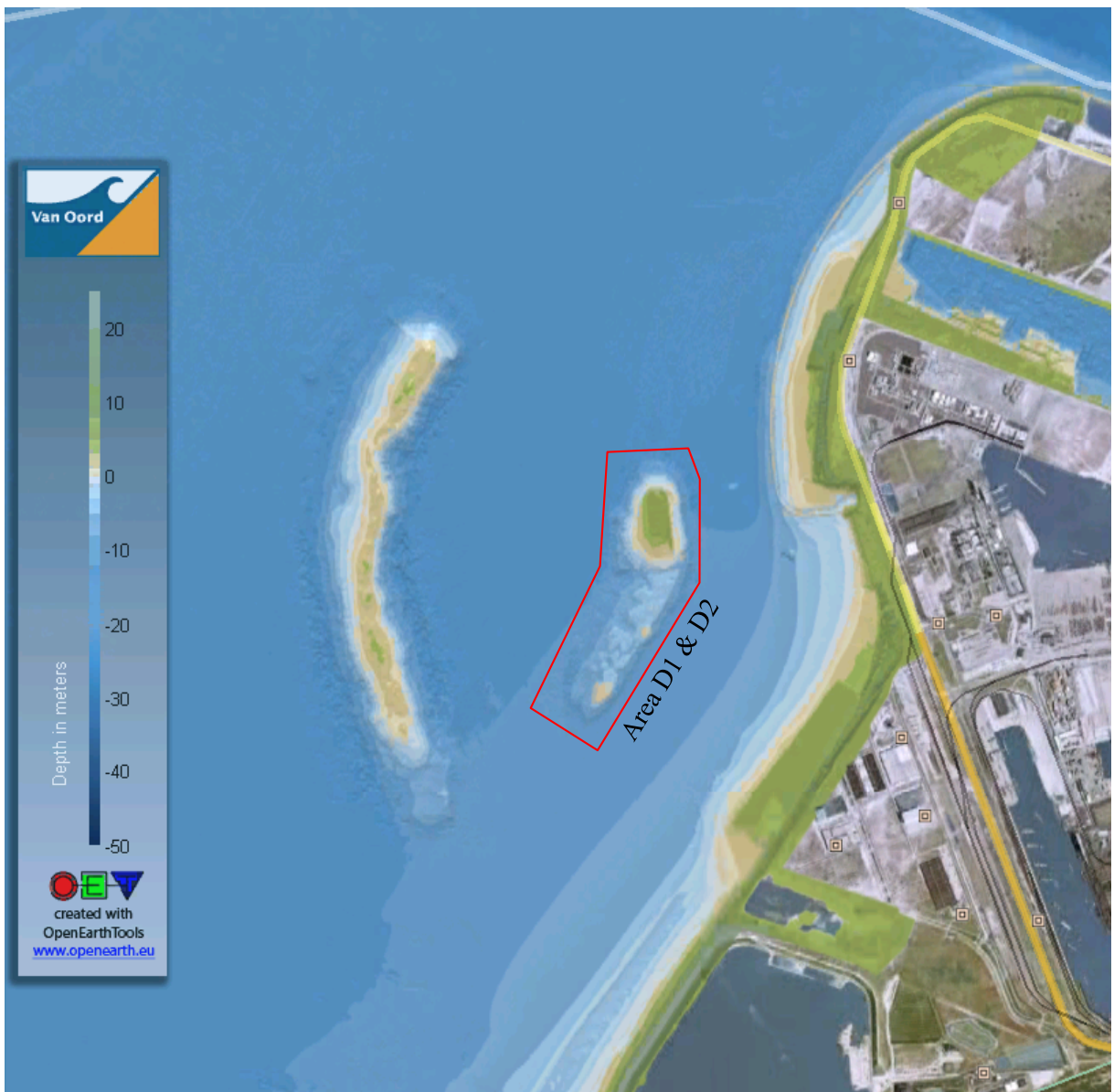


Figure H.4: Overview of the Maasvlakte II project. Survey data of July 2nd, 2009.



Figure H.5: Overview of the Maasvlakte II project. Survey data of August 4th, 2009.

Appendix H: Progress of The Maasvlakte II Project



Figure H.6: Overview of the Maasvlakte II project. Survey data of August 30th, 2009.



Figure H.7: Overview of the Maasvlakte II project. Survey data of October 2nd, 2009.

Appendix H: Progress of The Maasvlakte II Project



Figure H.8: Overview of the Maasvlakte II project. Survey data of November 1st, 2009.



Figure H.9: Overview of the Maasvlakte II project. Survey data of November 30th, 2009.

Appendix H: Progress of The Maasvlakte II Project



Figure H.10: Overview of the Maasvlakte II project. Survey data of December 30th, 2009.



Figure H.11: Overview of the Maasvlakte II project. Survey data of February 2nd, 2010.

Appendix H: Progress of The Maasvlakte II Project



Figure H.12: Overview of the Maasvlakte II project. Survey data of March 2th, 2010.



Figure H.13: Overview of the Maasvlakte II project. Survey data of April 2nd, 2010.

Appendix H: Progress of The Maasvlakte II Project



Figure H.14: Overview of the Maasvlakte II project. Survey data of May 1st, 2010.



Figure H.15: Overview of the Maasvlakte II project. Survey data of May 31th, 2010.

Appendix H: Progress of The Maasvlakte II Project

Appendix I: Bathymetry and Profiles

Appendix I: Bathymetry and Profiles

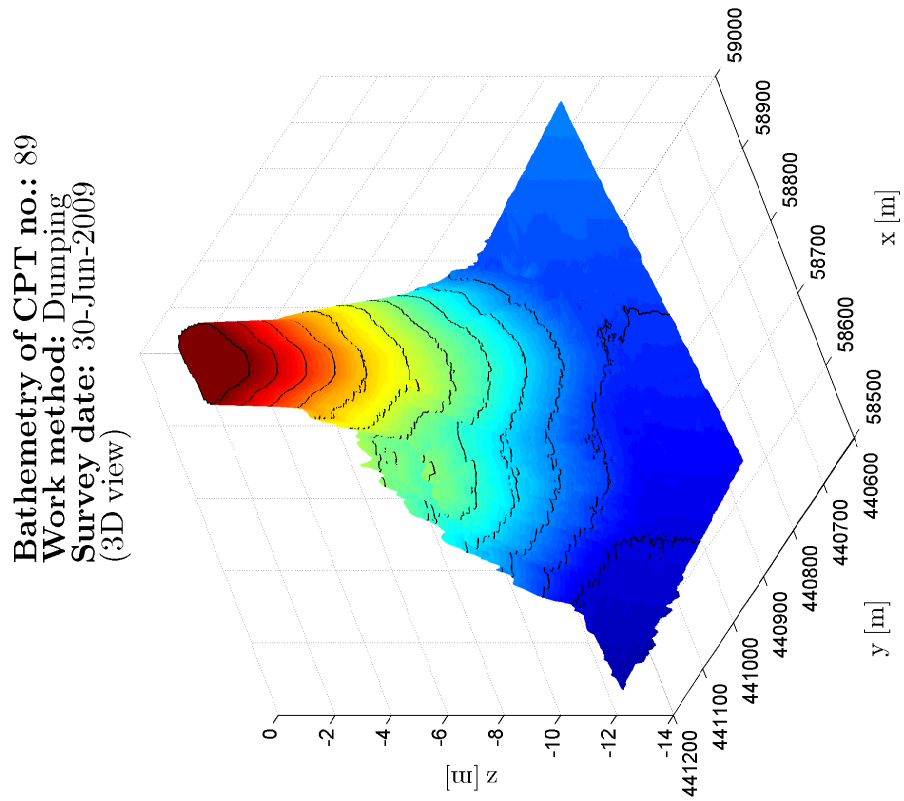
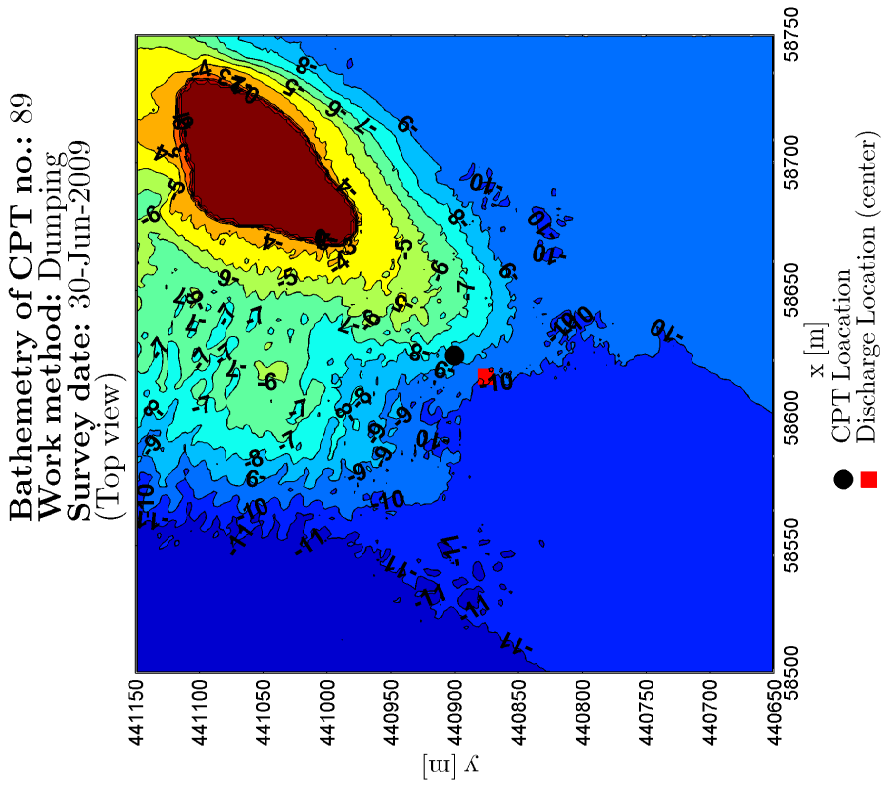


Figure I.1: Bathymetry of CPT no. 89 for work method: Dumping.

Appendix I: Bathymetry and Profiles

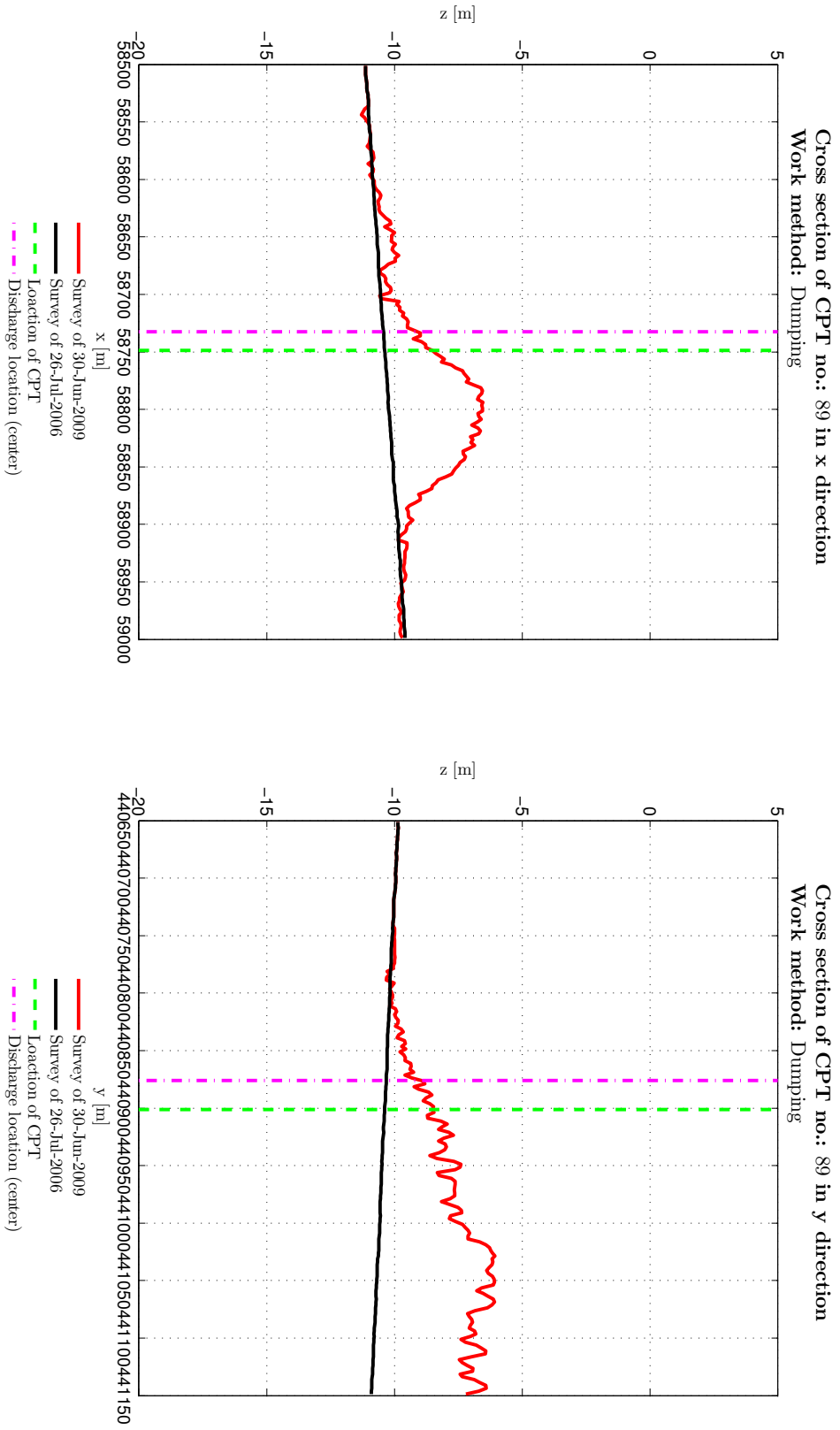


Figure I.2: Profiles of CPT no. 89 for work method: Dumping.

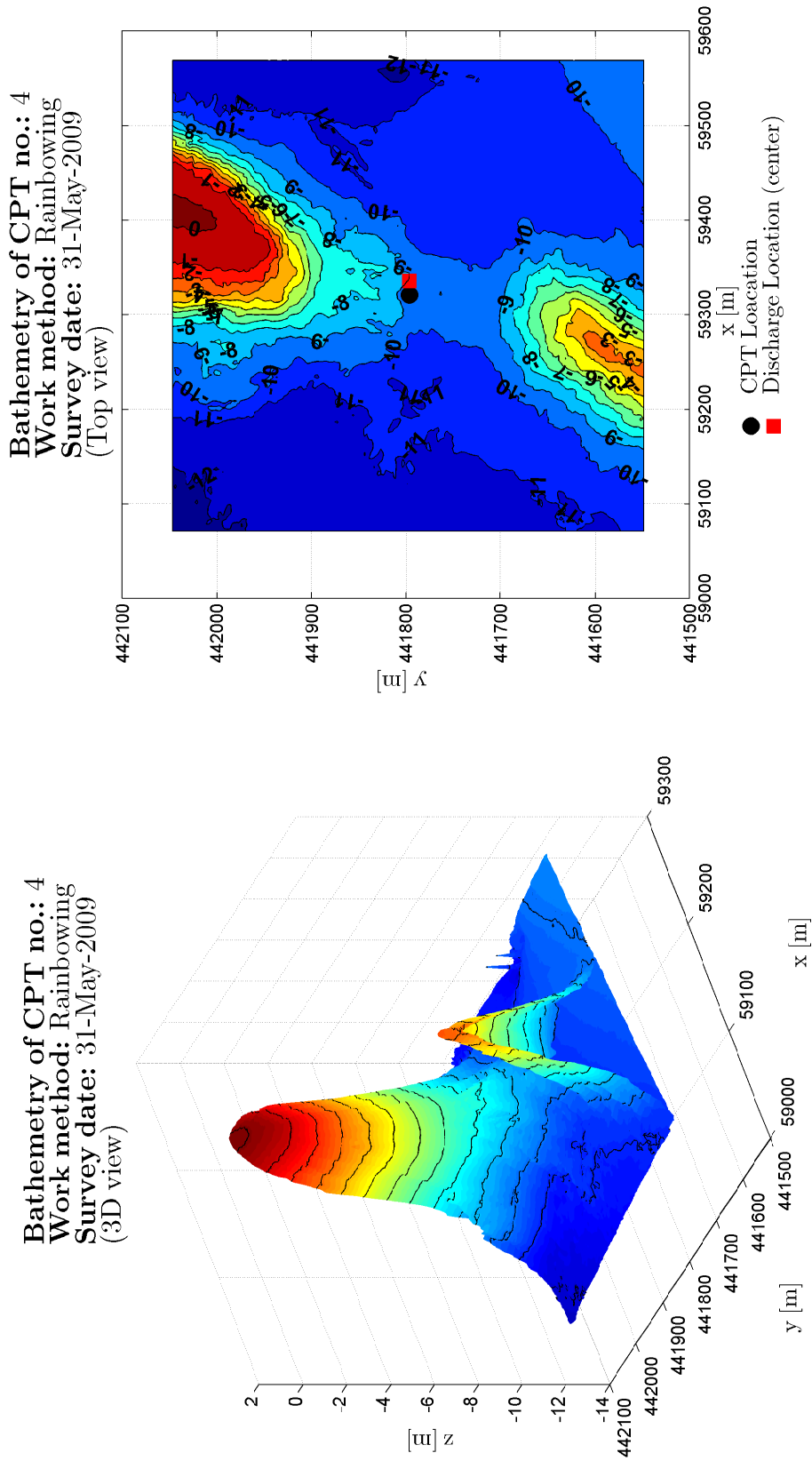


Figure I.3: Bathymetry of CPT no. 4 for work method: Rainbowing.

Appendix I: Bathymetry and Profiles

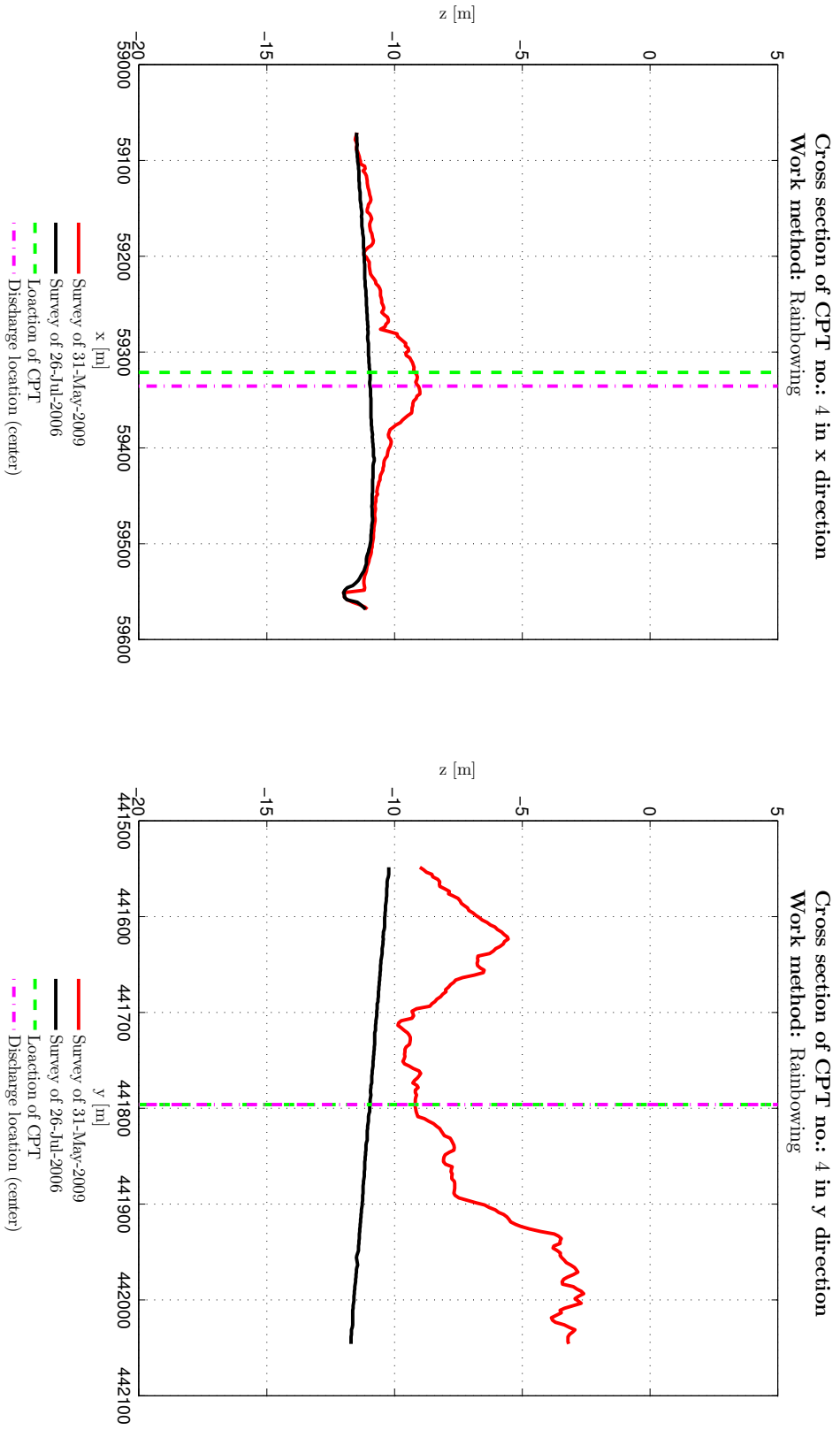


Figure I.4: Profiles of CPT no. 4 for work method: Rainbowing.

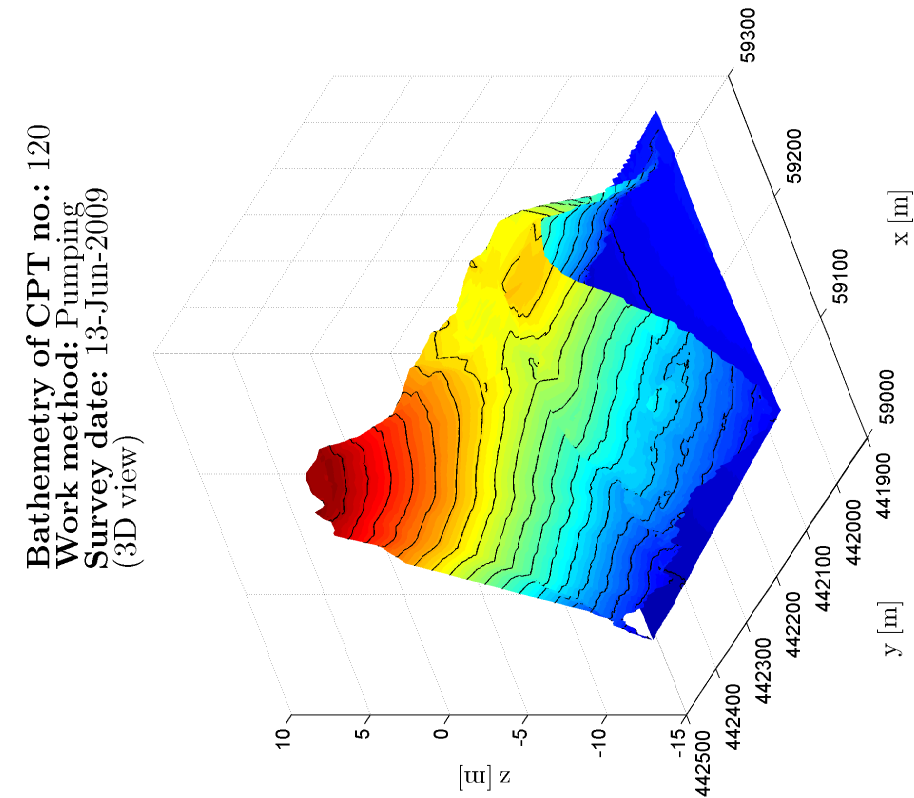
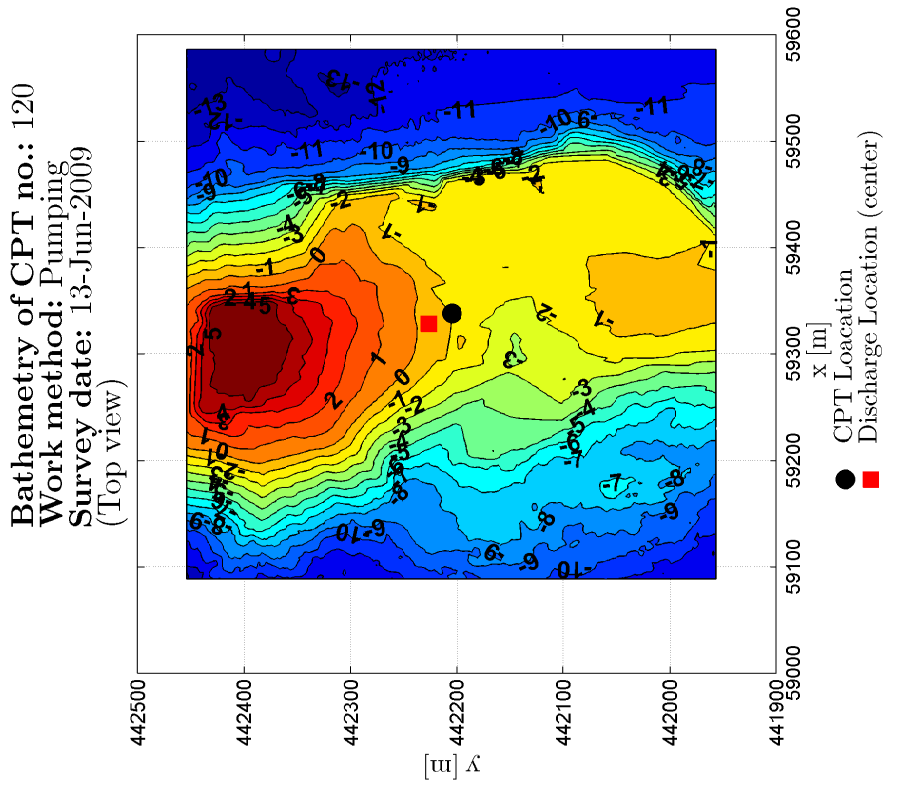


Figure I.5: Bathymetry of CPT no. 120 for work method: Pumping.

Appendix I: Bathymetry and Profiles

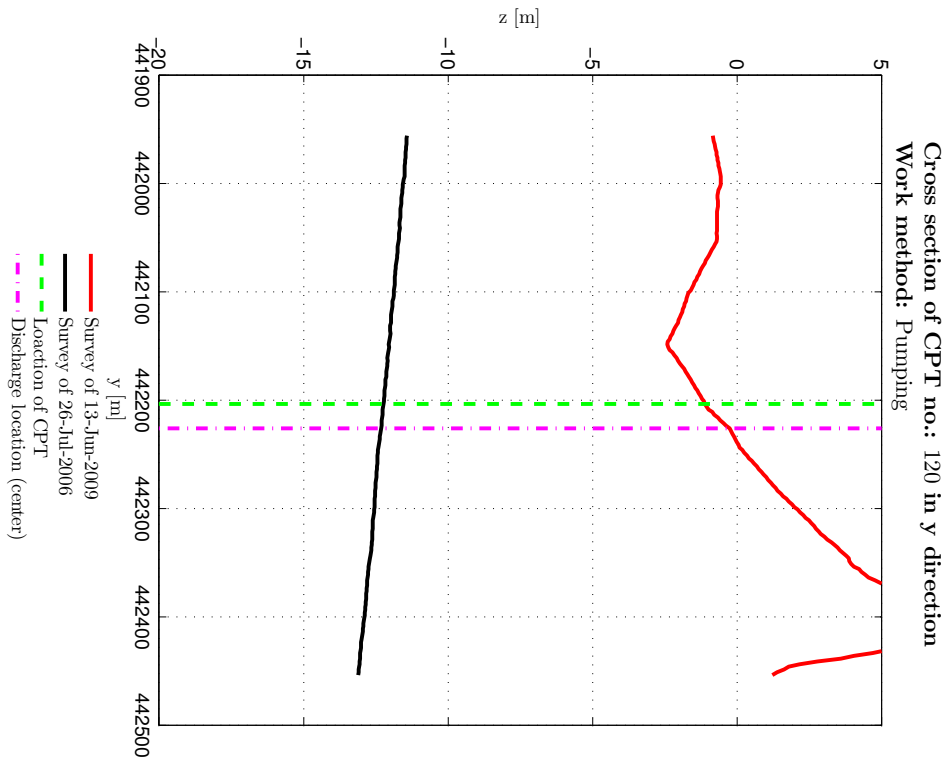
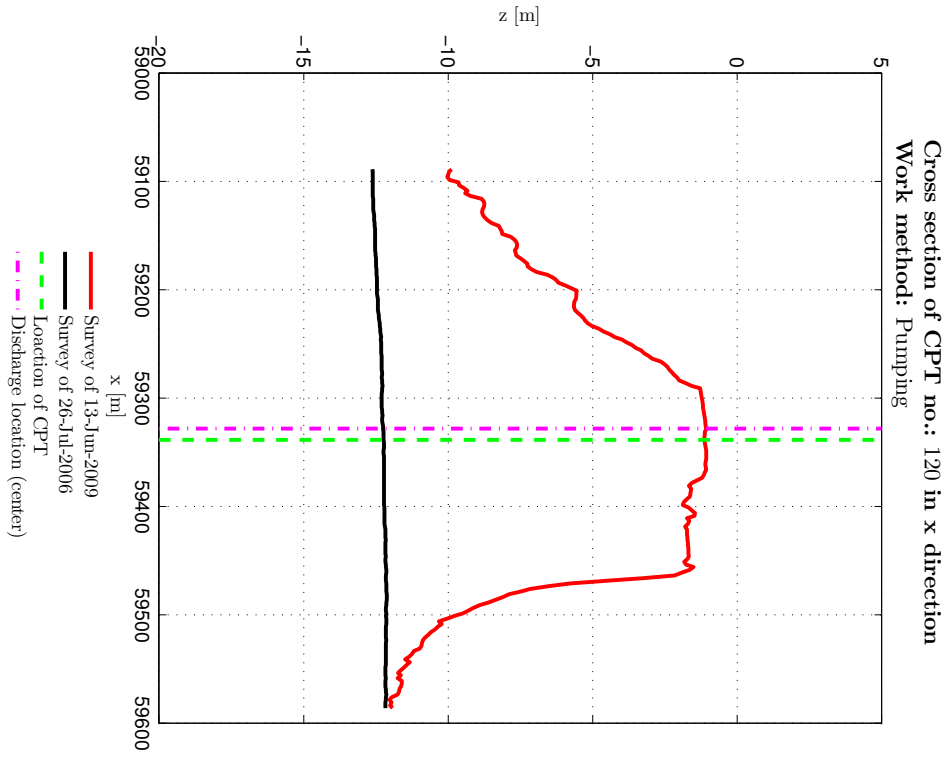
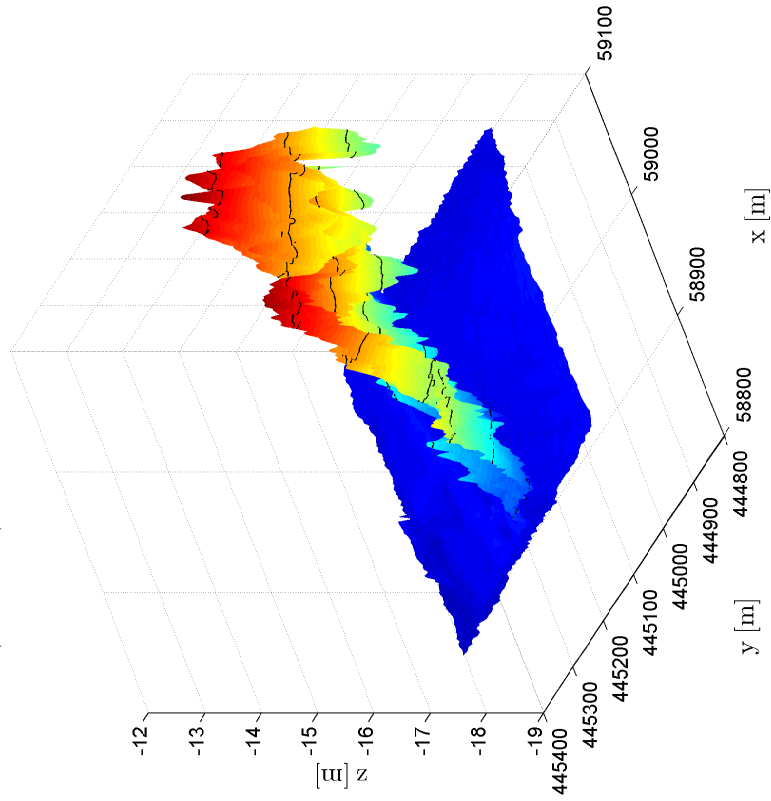


Figure I.6: Profiles of CPT no. 120 for work method: Pumping.

Bathymetry of CPT no.: 214
Work method: Back filling through suction pipe
Survey date: 14-Oct-2009
 (3D view)



Bathymetry of CPT no.: 214
Work method: Back filling through suction pipe
Survey date: 14-Oct-2009
 (Top view)

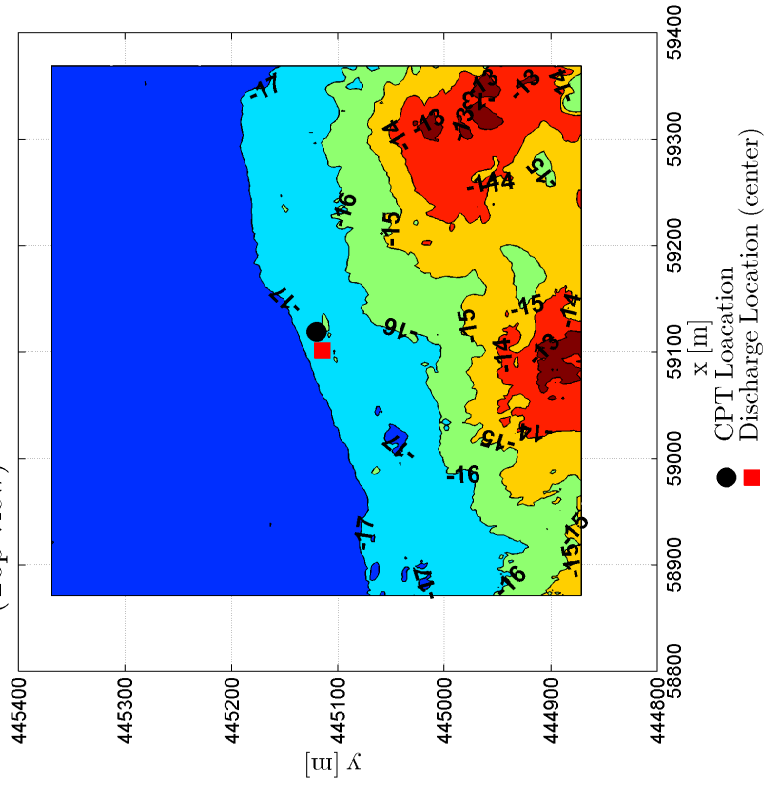


Figure I.7: Bathymetry of CPT no. 214 for work method: Back filling through suction pipe.

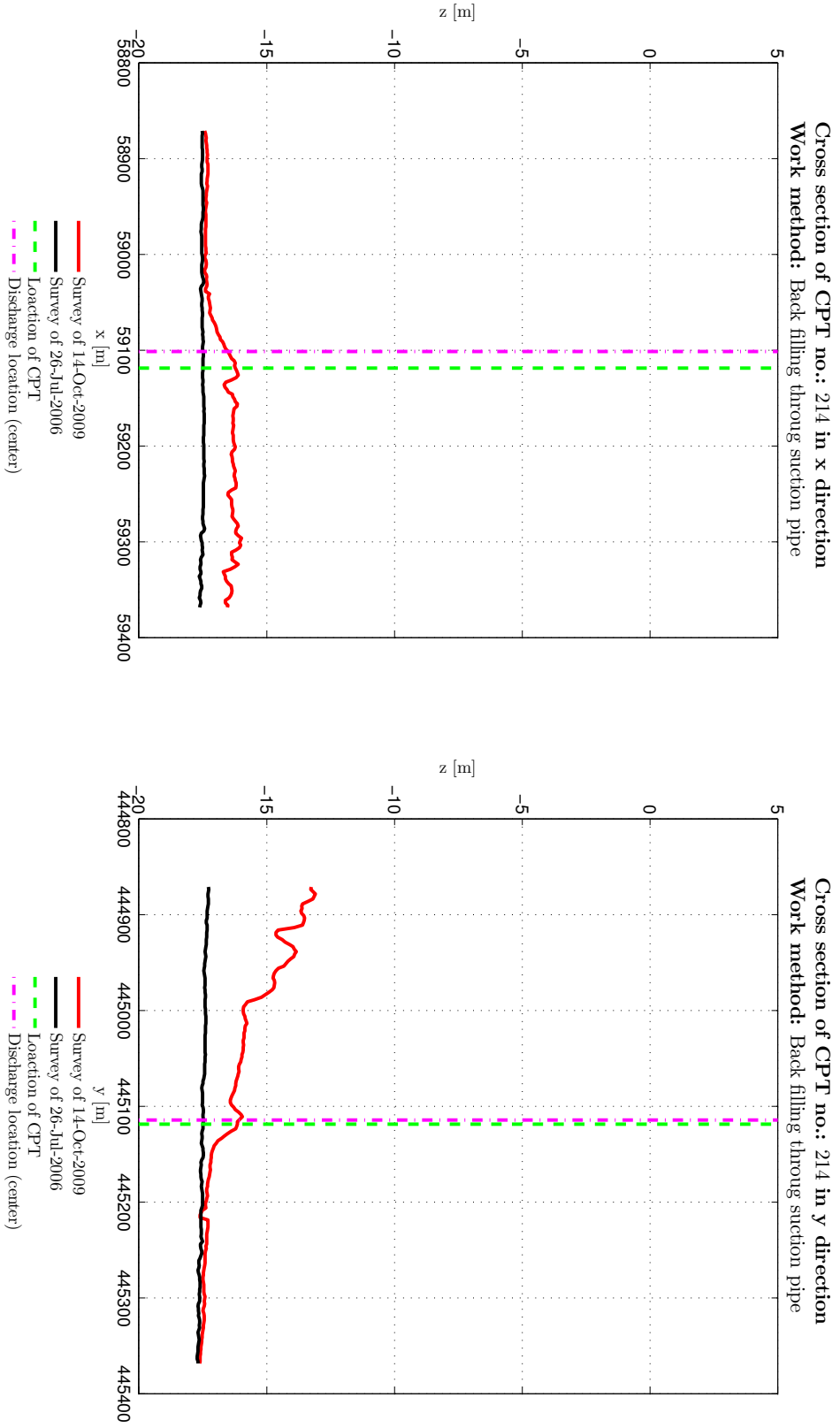
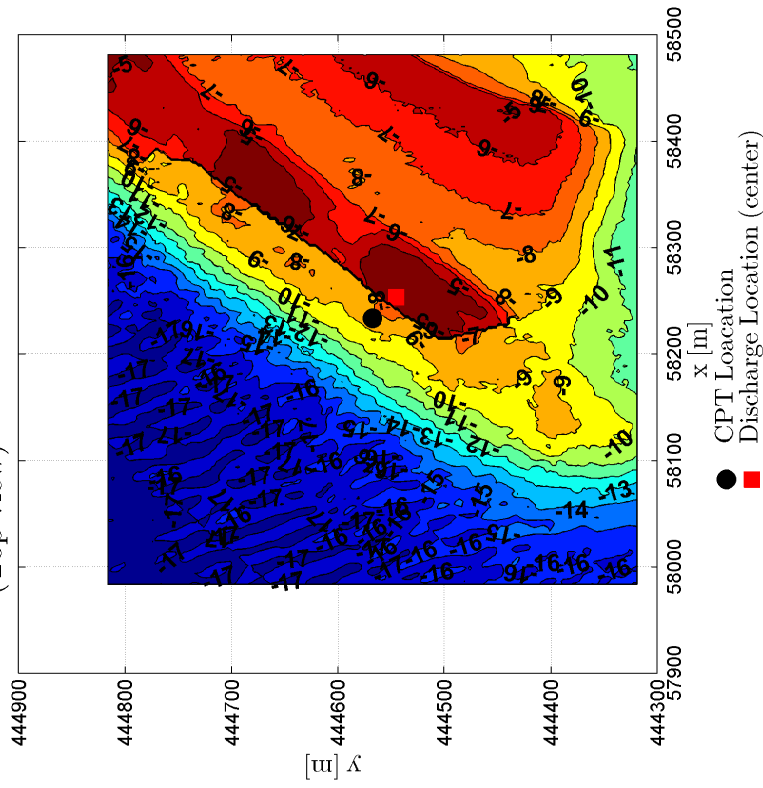


Figure I.8: Profiles of CPT no. 214 for work method: Back filling through suction pipe.

Bathymetry of CPT no.: 238
 Work method: Spraying with Sliedrecht 2;
 Survey date: 26-Mar-2010
 (Top view)



Bathymetry of CPT no.: 238
 Work method: Spraying with Sliedrecht 27
 Survey date: 26-Mar-2010
 (3D view)

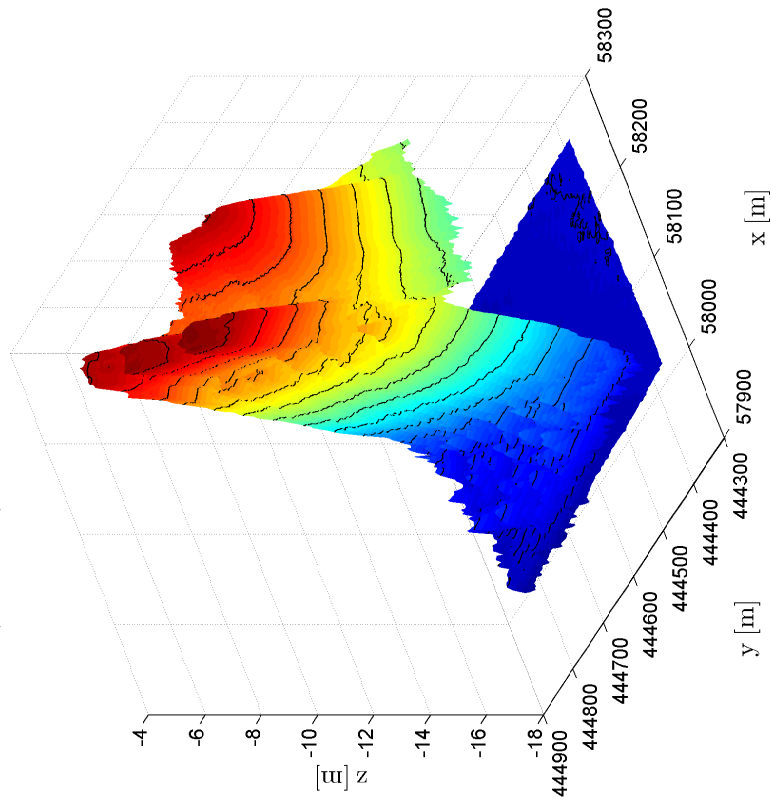


Figure I.9: Bathymetry of CPT no. 238 for work method: Spraying with “Sliedrecht 27”.

Appendix I: Bathymetry and Profiles

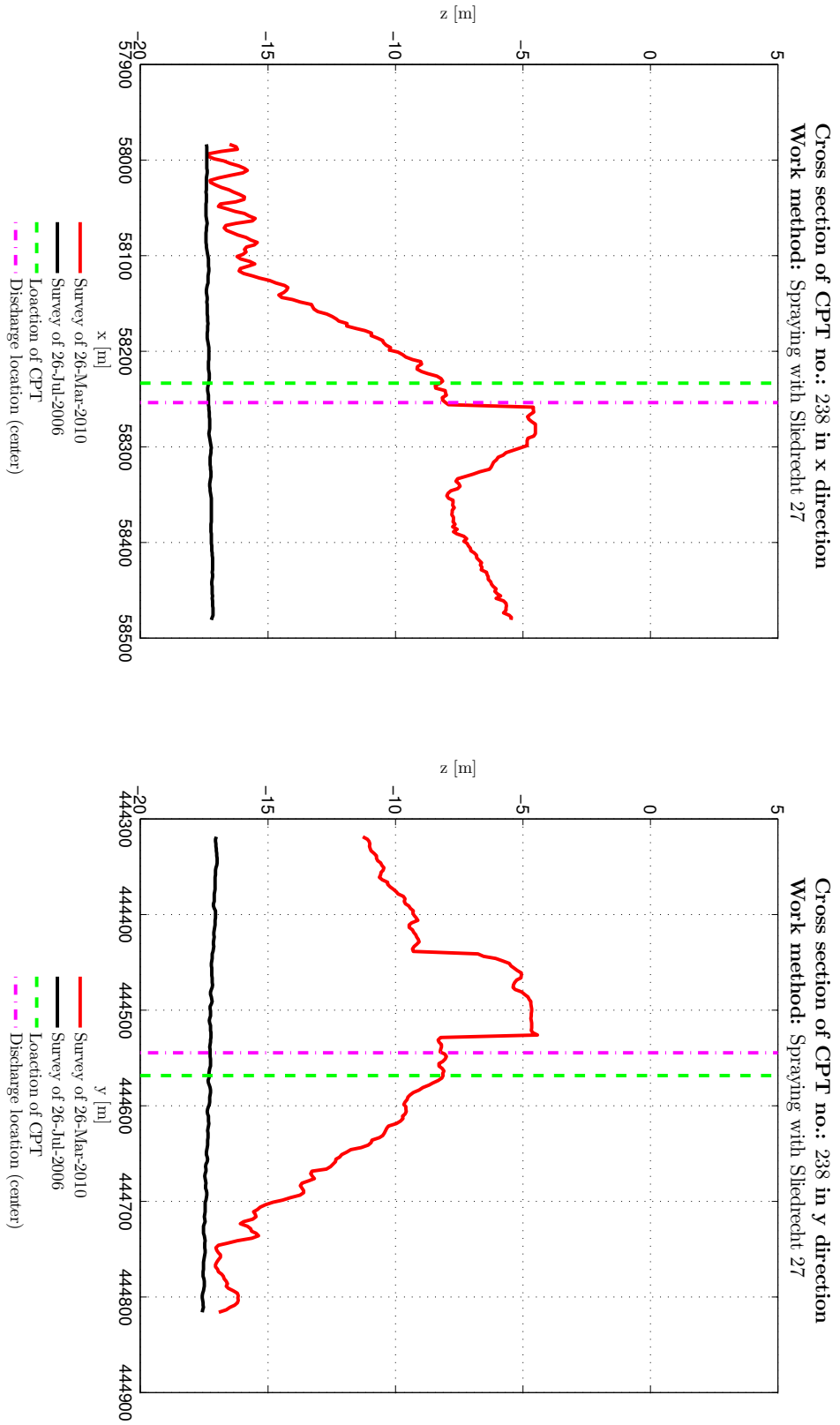


Figure I.10: Profiles of CPT no. 238 for work method: Spraying with “Shiedrecht 27”.

Appendix J: Initiation of Motion and Suspension as an Indicator of the Shear Stress Level

Appendix J: Initiation of Motion and Suspension as an Indicator of the Shear Stress Level

J.1 Critical Shields Parameter

van Rijn [1984b,c, 1993]; Shields [1936]; Shields *et al.* [1936] and Zanke [2001, 2003] are used to compute the critical shear stress. If the shear stress exceeds the critical shear stress, then particle movement will occur. The initiation of motion and initiation of suspension of sediment is considered, for the description of the movement of particles. Shields, van Rijn and Zanke uses the critical Shields parameter (θ_{cr}), for initiation of motion. The critical Shields parameter gives the initiation of motion by a certain threshold value. Values above the critical Shields parameter (θ_{cr}) results in a particle movement and below this value an incidentally particle movement exist. The initiation of motion is defined as movement, such as rolling, saltation and sliding, of the particles over the bed also called bed load transport (see figure (J.1)). The initiation of motion and sus-

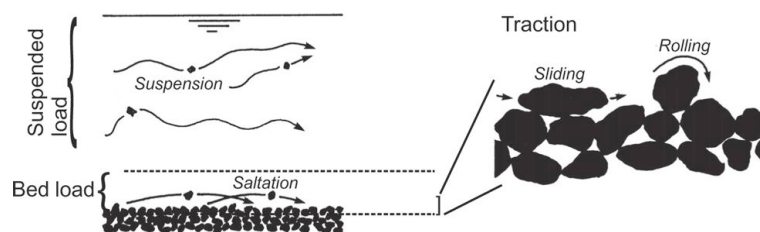


Figure J.1: Schematic representation of sediment transport modes showing particle paths. Note that bed load includes both saltation and traction. (From Masselink *et al.* [2011], modified from Allen [1994].)

pension determines the type of sediment transport that occurs by exceeding the critical shear stress. Bed load transport takes place, for initiation of motion and suspended load transport takes place, for the initiation of suspension. Both sediment transport processes can occur at the same time.

J.2 Initiation of Motion by Shields

Shields [1936] gives a relation between a dimensionless shear stress (θ)(also called Shields parameter) and the so called particle Reynolds number (Re_*).

$$\theta = \frac{\tau}{(\rho_s - \rho_w) \cdot g \cdot d_{50}} = \frac{u_*^2}{\Delta \cdot g \cdot d_{50}} = f(Re_*) = f\left(\frac{u_* \cdot d_{50}}{\nu}\right) \quad [\text{J.1}]$$

Where:

u_* = shear velocity [m/s].

In this case the particle Reynolds number (Re_*) is defined by:

$$Re_* = \frac{u_* \cdot d_{50}}{\nu} \quad [\text{J.2}]$$

Appendix J: Initiation of Motion and Suspension as an Indicator of the Shear Stress Level

This looks similar to equation (6.8) but is not the same because $u_* \neq w_0$. Both are velocities by dimension but are not the same, u_* is defined by:

$$u_* = \sqrt{\frac{\tau}{\rho_w}} \quad [\text{J.3}]$$

From equation (J.3) it is now obvious that u_* is not a real velocity. In figure (J.2) the original Shields graph is illustrated.

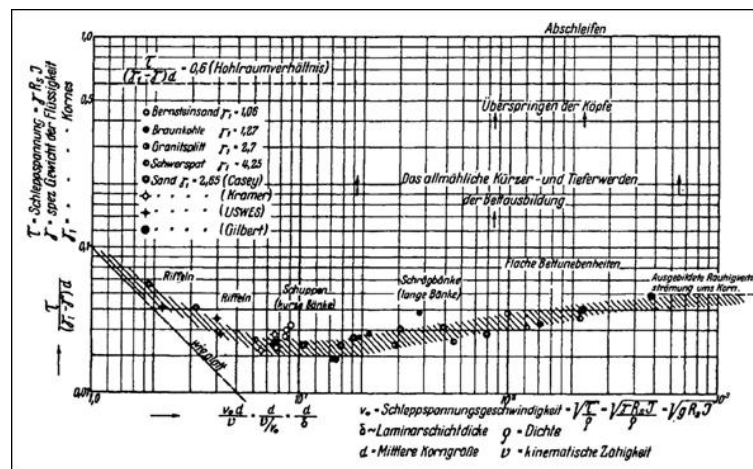


Figure J.2: Original Shields diagram [Shields, 1936].

By using the shear velocity, the Shields parameter is called a stability parameter. By using the flow velocity, the Shields parameter is called a mobility parameter [Schiereck, 2004].

WL|Delft Hydraulics [1969] has also done research about the incipient motion of particles. They derived 7 stages of particle movement, namely:

1. Occasional movement at some locations;
2. Frequent movement at some locations;
3. Frequent movement at several locations;
4. Frequent movement at many locations;
5. Frequent movement at all locations;
6. Continuous movement at all locations;
7. General transport of the grains.

The Shields curve (figure (J.2) and (J.3)) fits rather well between stage 5 and 6. So, the Shields parameter could be seen as the start of sediment transport or erosion [van Rijn, 1993; Schiereck, 2004].

J.3 Initiation of Motion by van Rijn

In van Rijn [1984b] the approach of Bagnold [1966] is followed, which means that the motion of the bed load particles is assumed to be dominated by gravity forces, while the effect of turbulence of the overall trajectory is supposed to be of minor importance.

van Rijn [1984b] has replaced the particle Reynolds number with the particle parameter (D^*). Yalin [1977] describes how to rewrite the particle Reynolds number (Re_*) into the particle diameter (D^*). The particle parameter is defined as followed:

$$D^* = \sqrt[3]{\frac{Re_*^2}{\theta}} = d_{50} \cdot \sqrt[3]{\frac{\Delta \cdot g}{\nu^2}} \quad [J.4]$$

This has the advantage that iteration on u_* is not necessary any more. So, the Shields curve becomes now the Shields - van Rijn curve and is illustrated in figure (J.3). In Miedema [2008, 2010] also other researchers are mentioned who have elaborated a fit, based on the particle diameter, through the original Shields data.

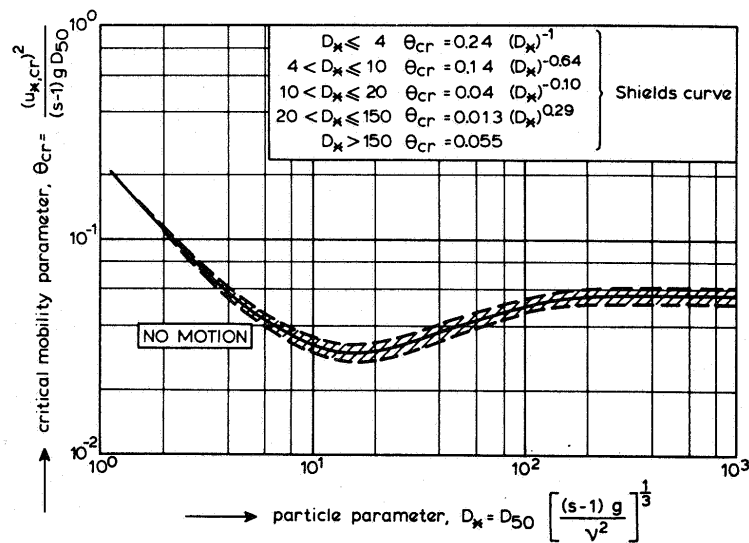


Figure J.3: Initiation of motion according to Shields by van Rijn [1984b].

J.4 Initiation of Motion by Zanke

Zanke [2001, 2003] has taken into account the influence of turbulence on the initiation of sediment motion. Only Zanke uses not the particle Reynolds number but the non-

Appendix J: Initiation of Motion and Suspension as an Indicator of the Shear Stress Level

dimensional roughness height (k_s^+). This is commonly adopted in recent literature as:

$$k_s^+ = \frac{u_* \cdot k_s}{\nu} \quad [\text{J.5}]$$

The definition of the particle Reynolds number is equivalent, in fact identical for $k_s = d_{50}$ [Zanke, 2003]. Zanke derived the following equation for the Shields parameter:

$$\theta = \frac{0.7 \cdot \tan \phi}{\left(1 + \alpha \cdot \frac{u'_{rms,b}}{u_b}\right)^2 \cdot \left(1 + \frac{1}{2.5} \cdot \left(\alpha \cdot \frac{u'_{rms,b}}{u_*}\right)^2 \cdot \tan \phi\right)} \quad [\text{J.6}]$$

Where:

- u_b = time averaged velocity at a particle [m/s];
- $u'_b(t)$ = instantaneous deviation from u_b , where $u'_b(t) = u_b(t) - u_b$ [m/s];
- $u_{rms,b}$ = $\sqrt{u'^2}$ = standard deviation of $u'_b(t)$ [m/s];
- α = factor, multiple of u'_{rms} [-].

Of prime importance is the fact that the internal angle of friction (ϕ) and the angle of grain contact (ϕ') are equivalent and may be equally applied with regard to the initiation of motion [Zanke, 2003]. Zanke substitutes $\alpha \approx 1.8$ and $\phi' \approx 20^\circ$ as representative values into equation (J.6) and the equation becomes:

$$\theta_{b,cr} = \frac{0.24 \cdot K}{\left(1 + 1.8 \cdot \frac{u'_{rms,b}}{u_b}\right)^2 \cdot \left(1 + 0.14 \cdot \left(1.8 \cdot \frac{u'_{rms,b}}{u_*}\right)^2 \cdot K\right)} \quad [\text{J.7}]$$

With, K based on experiments of Unsöld [1984],

$$K = 1 + \frac{3 \cdot 10^{-8}}{(\rho_s - \rho_w) \cdot d_{50}^2} \quad [\text{J.8}]$$

and

$$\frac{u'_{rms,b}}{u_*} = 0.31 \cdot k_s^+ \cdot e^{-0.1 \cdot k_s^+} + 1.8 \cdot e^{-0.0088} \cdot \left(1 - e^{-0.1 \cdot k_s^+}\right) \quad [\text{J.9}]$$

As a representative value for $\frac{u'_{rms,b}}{u_b}$ is taken 0.225. Zanke [2003] has made comparative computations for θ and shows that even for a constant value of $\frac{u'_{rms,b}}{u_b}$, reasonable results are obtained for θ . In figure (J.4) the equation (J.7) of Zanke is illustrated.

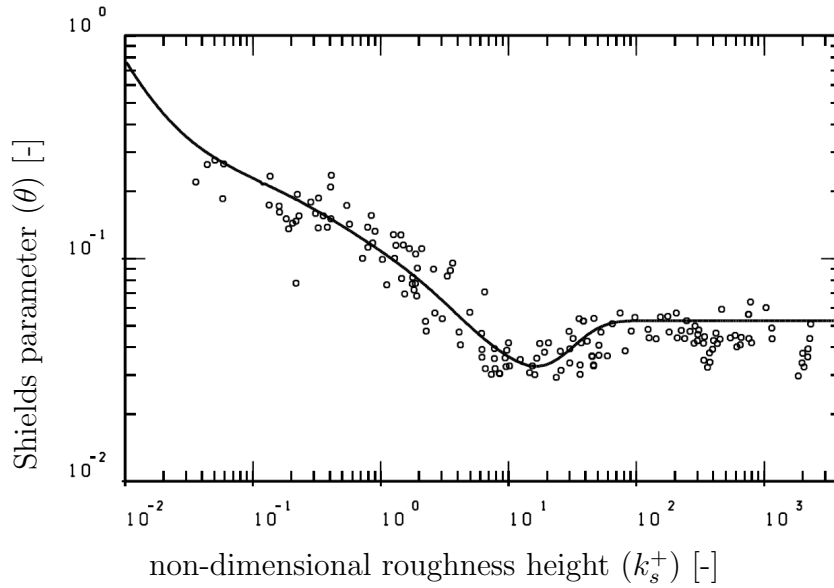


Figure J.4: Initiation of motion by Zanke [2003].

J.5 Initiation of Suspension

In this paragraph the flow conditions are described at which Shields parameter initiation of suspension will occur. In other words suspended load transport will occur. Bagnold [1966] states that a particle only remains in suspension when turbulent eddies have dominant vertical velocity components which exceed the particle fall velocity (w_s). Bagnolds criterion for initiation of suspension (suspended load transport) becomes:

$$\theta_{s,cr} = \frac{w_s^2}{\Delta \cdot g \cdot d_{50}} \quad [\text{J.10}]$$

Equation (J.10) can be seen as the upper boundary of where suspended load transport will occur. By exceeding this critical value, suspended load transport takes places. Engelund [1965] has also done research about a criterion for initiation of suspension. Engelunds criterion is as follows:

$$\theta_{s,cr} = \frac{0.0625 \cdot w_s^2}{\Delta \cdot g \cdot d_{50}} \quad [\text{J.11}]$$

The criterion of Engelund can be considered as the lower boundary from which suspended load transport will occur. van Rijn [1984c] has derived the following equations for initiation of suspension from experimental research by WL|Delft Hydraulics. The criterion of

Appendix J: Initiation of Motion and Suspension as an Indicator of the Shear Stress Level

van Rijn lies between that of Bagnold and Engelund.

$$\theta_{s,cr} = \frac{16 \cdot w_s^2}{D^{*2} \cdot \Delta \cdot g \cdot d_{50}} \quad \text{for } 1 < D^* \leq 10 \quad [\text{J.12}]$$

$$\theta_{s,cr} = \frac{0.16 \cdot w_s^2}{\Delta \cdot g \cdot d_{50}} \quad \text{for } D^* > 10$$

All three relations for initiation of suspension are illustrated in figure (J.5). The following equations have been used to compute the fall velocity (w_s). Equation (J.13) describes, for particles $< 100 \mu\text{m}$ (Stokes-range), the fall velocity.

$$w_s = \frac{\Delta \cdot d_{50}^2}{18 \cdot \nu} \quad [\text{J.13}]$$

Zanke [1977] proposed for particles between the $100 \mu\text{m}$ and $1000 \mu\text{m}$ the following equation:

$$w_s = 10 \cdot \frac{\nu}{d_{50}} \cdot \left(\sqrt{1 + \frac{0.01 \cdot \Delta \cdot g \cdot d_{50}^3}{\nu^2}} - 1 \right) \quad [\text{J.14}]$$

Figure (J.5) uses the above described relations for the fall velocity. But, in this case, it is better to use an expression for the fall velocity based on Richardson & Zaki [1954], because of the high concentrations and the effect on hindered settling. van Rijn [1984c] suggests for flows with a high concentration and particles in the range of $50 - 500 \mu\text{m}$, to use equation (6.15).

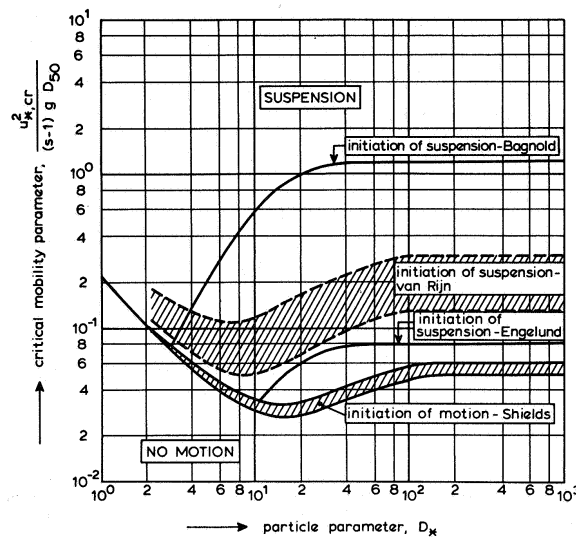


Figure J.5: Initiation of motion and suspension by van Rijn [1984c].

J.6 Computation Results for the Critical Shear Stress

For the input table (7.1) and (7.2) is used. The critical Shields values are compute with the relations of van Rijn [1984b]. In table (J.1) the results of the computation are mentioned and in figure (J.6) the results are illustrated in the Shields graph.

Table J.1: Computation results for the critical shear stress and Shields parameter.

	Work methods				
	DU	RB	PU	BF	SP
D^*	5.139 -	6.151 -	6.770 -	7.368 -	9.143 -
Re_*	2.582 -	3.191 -	3.574 -	3.950 -	5.095 -
$\theta_{b,cr}$	0.049 -	0.044 -	0.041 -	0.039 -	0.034 -
$\tau_{b,cr}$	0.195 N/m ²	0.174 N/m ²	0.163 N/m ²	0.155 N/m ²	0.135 N/m ²

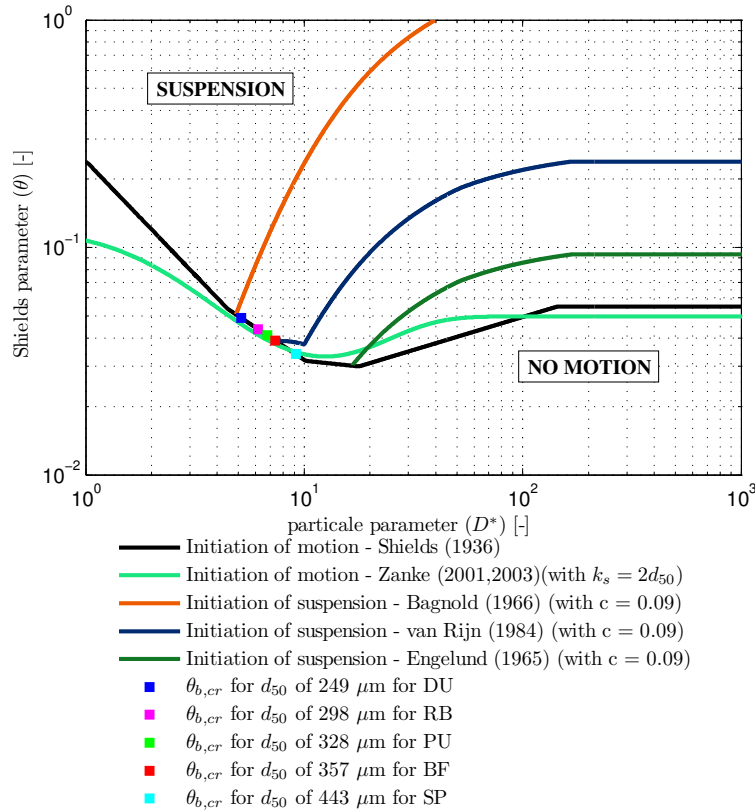


Figure J.6: Computation results for the critical Shields parameter.

Appendix J: Initiation of Motion and Suspension as an Indicator of the Shear Stress Level

Appendix K: Computation Results for the Density Current

Appendix K: Computation Results for the Density Current

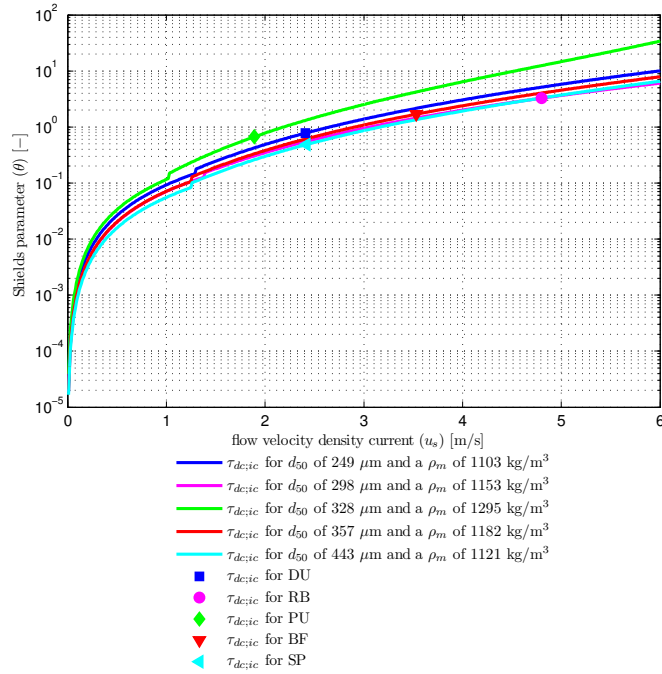


Figure K.1: Relation between the Shields parameter and flow velocity of a density current (initial conditions).

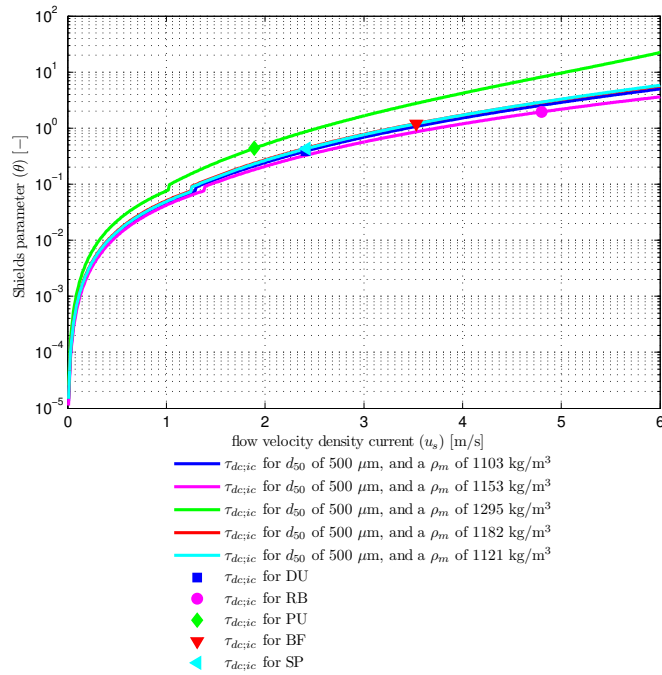


Figure K.2: Relation between the Shields parameter and flow velocity, with equal particle diameter (initial conditions).

Appendix K: Computation Results for the Density Current

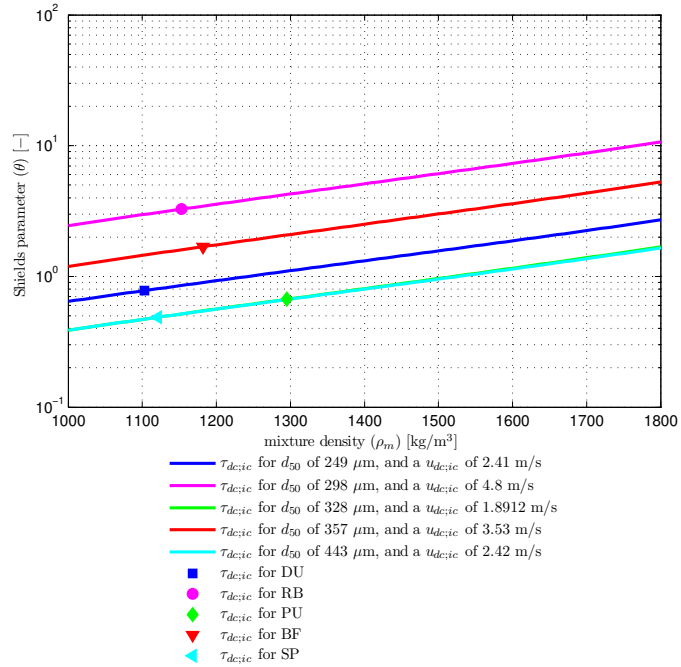


Figure K.3: Relation between the Shields parameter and mixture density of a density current (initial conditions).

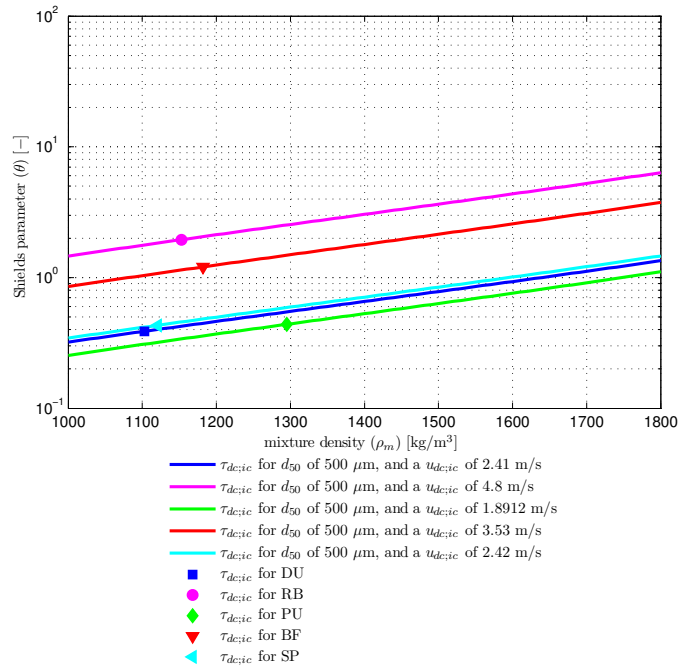


Figure K.4: Relation between the Shields parameter and mixture density, with equal particle diameter (initial conditions).

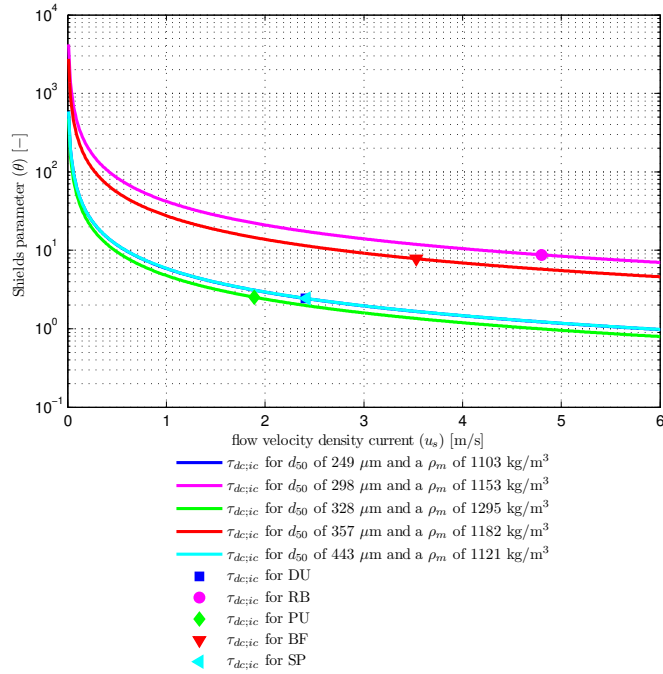


Figure K.5: Relation between the Shields parameter and flow velocity of a density current (stationary conditions).

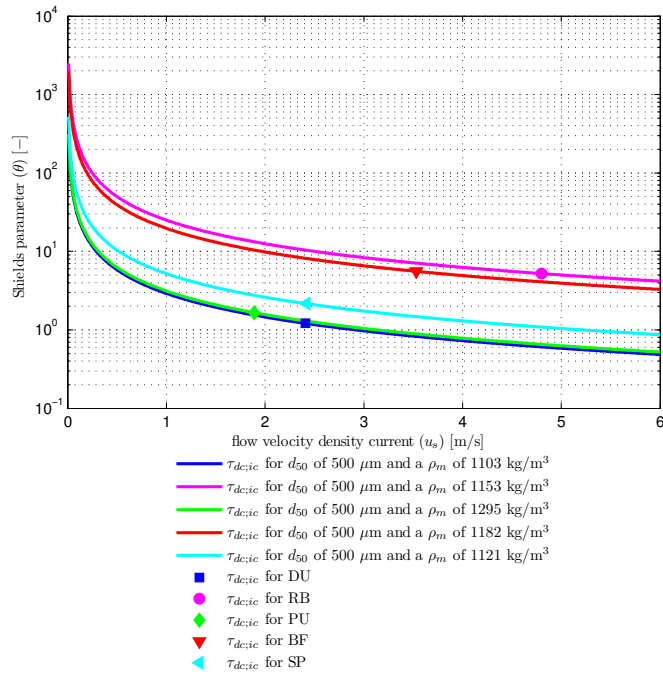


Figure K.6: Relation between the Shields parameter and flow velocity, with equal particle diameter (stationary conditions).

Appendix K: Computation Results for the Density Current

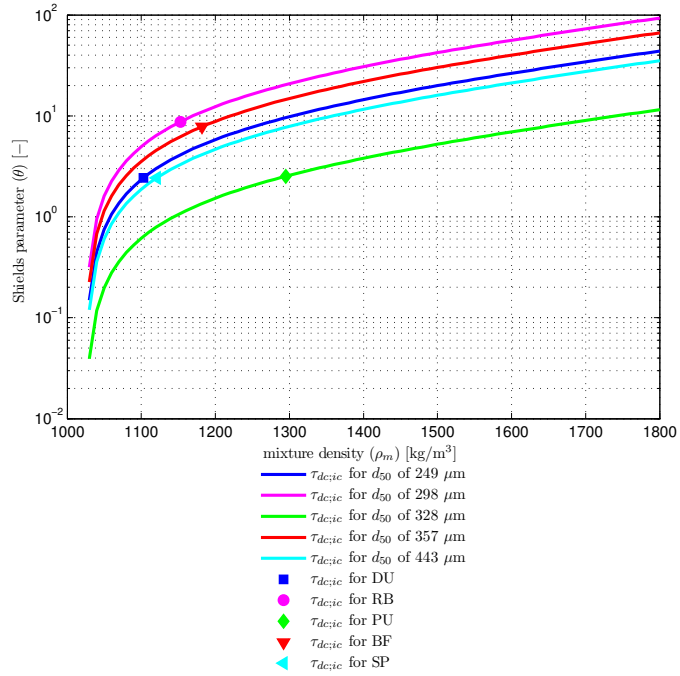


Figure K.7: Relation between the Shields parameter and mixture density of a density current (stationary conditions).

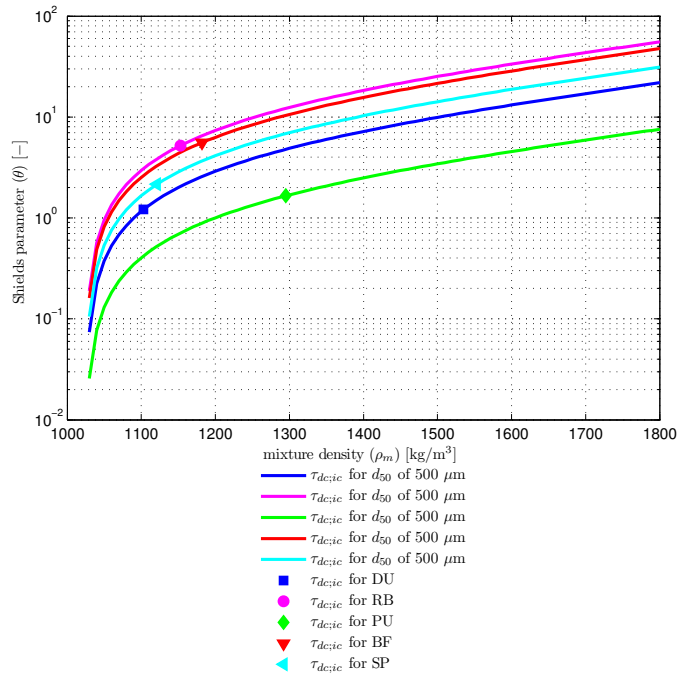


Figure K.8: Relation between the Shields parameter and mixture density, with equal particle diameter (stationary conditions).

Appendix L: Computations Results for Hydrodynamics

Appendix L: Computations Results for Hydrodynamics

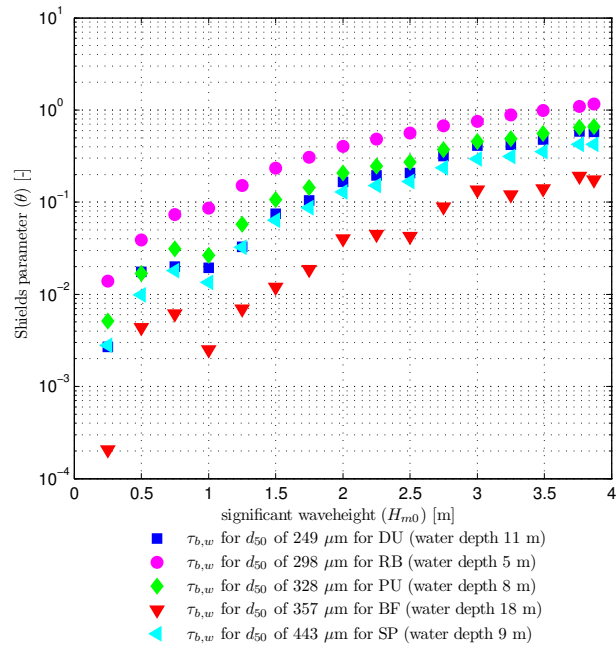


Figure L.1: Relation between Shields parameter and significant wave height.

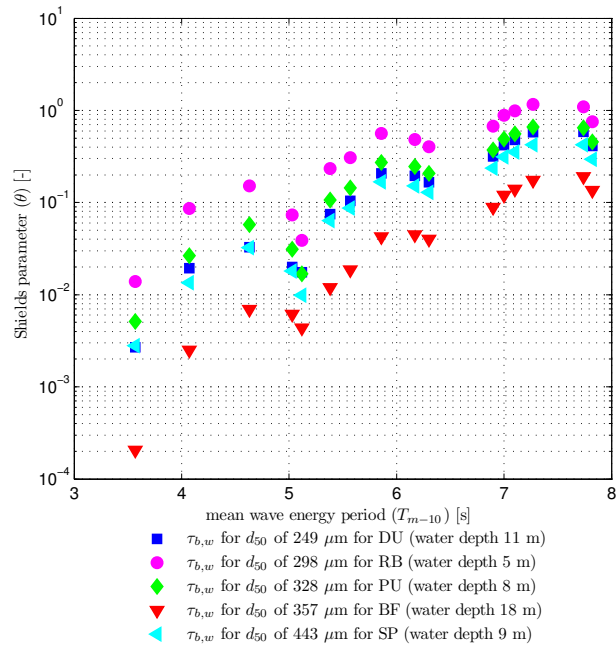


Figure L.2: Relation between Shields parameter and mean wave energy period.

Appendix L: Computations Results for Hydrodynamics

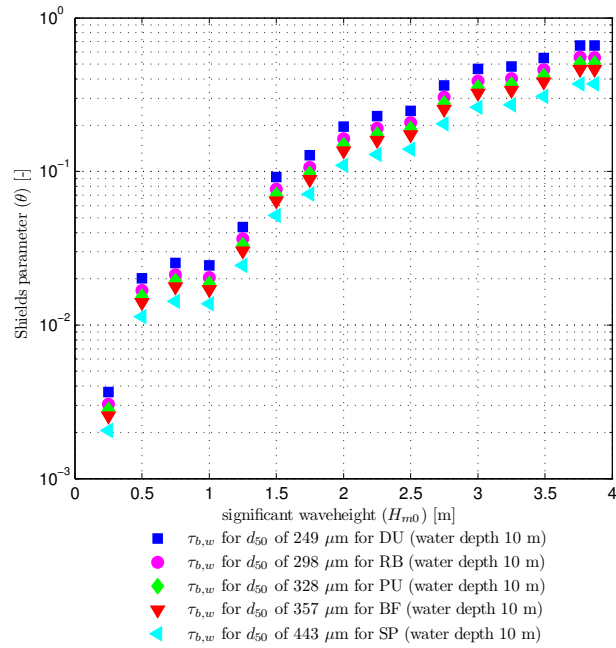


Figure L.3: Relation between Shields parameter and significant wave height, with equal water depth per work method.

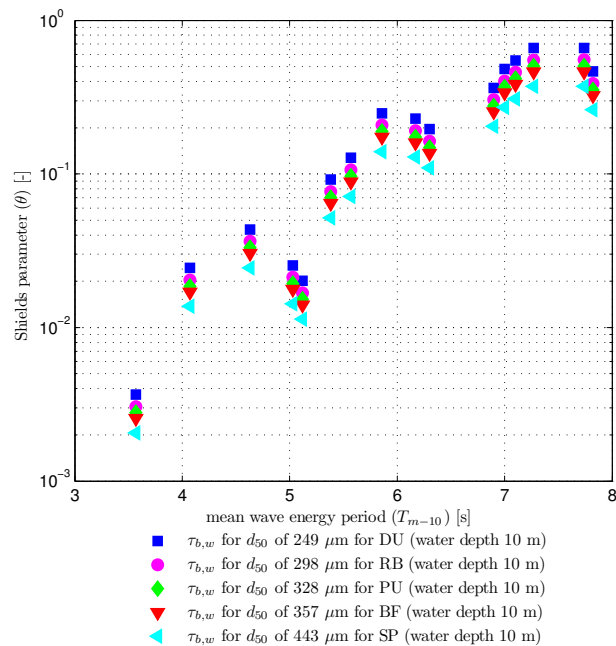


Figure L.4: Relation between Shields parameter and mean wave energy period, with equal water depth per work method.

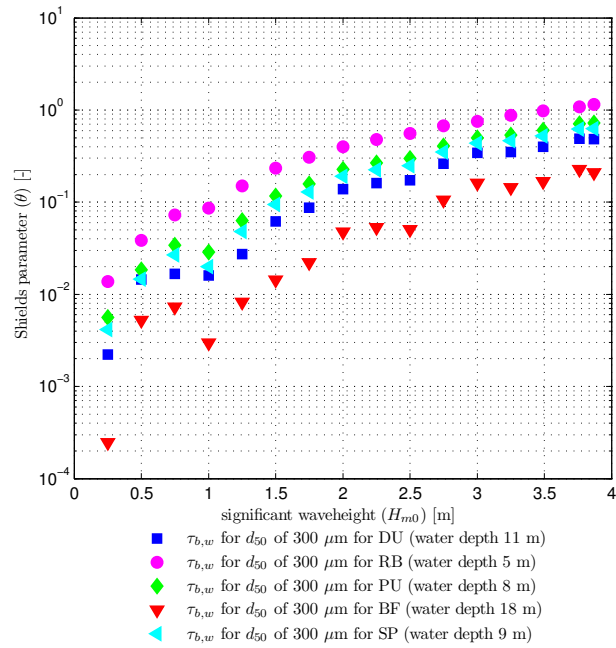


Figure L.5: Relation between Shields parameter and significant wave height, equal particle diameter depth per work method.

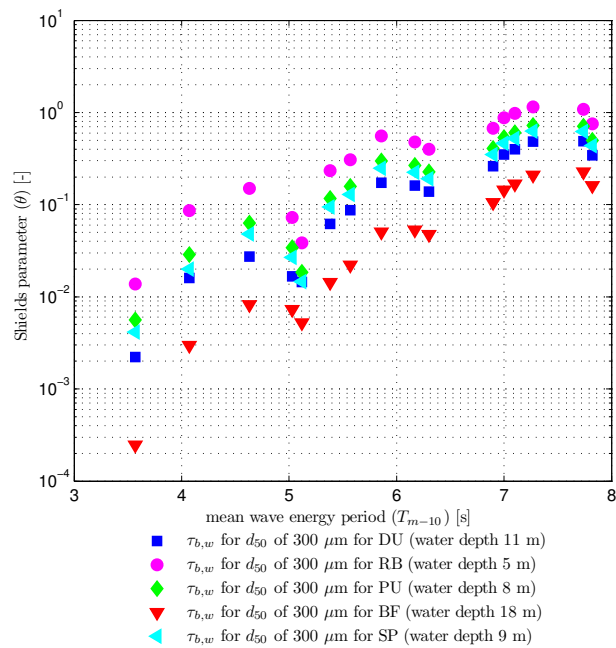


Figure L.6: Relation between Shields parameter and mean wave energy period, with equal particle diameter per work method.

Appendix L: Computations Results for Hydrodynamics

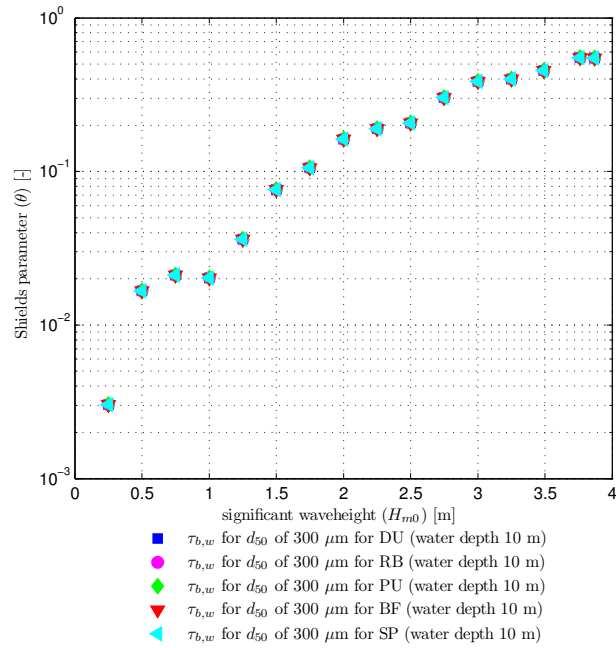


Figure L.7: Relation between Shields parameter and significant wave height, with equal water depth and particle diameter per work method.

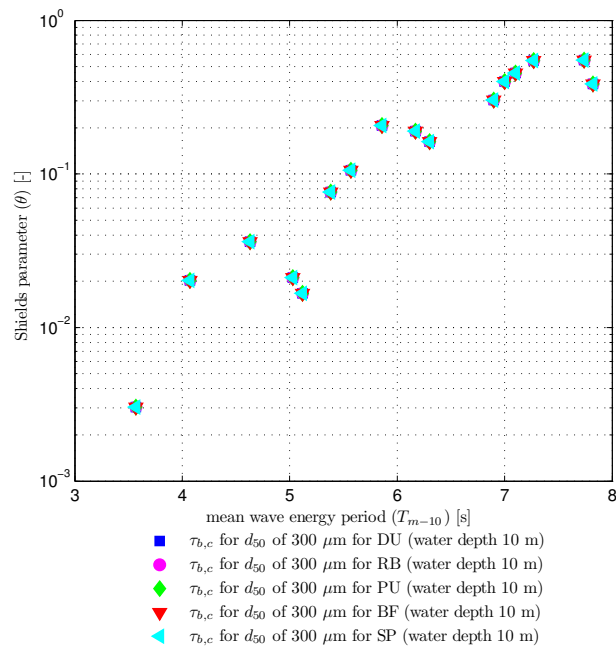


Figure L.8: Relation between Shields parameter and mean wave energy period, with equal water depth and particle diameter per work method.

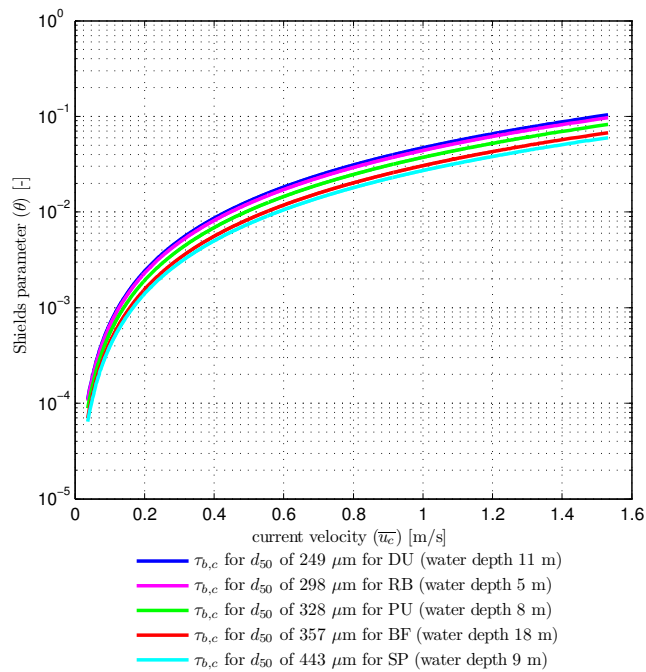


Figure L.9: Relation between Shields parameter and current velocity.

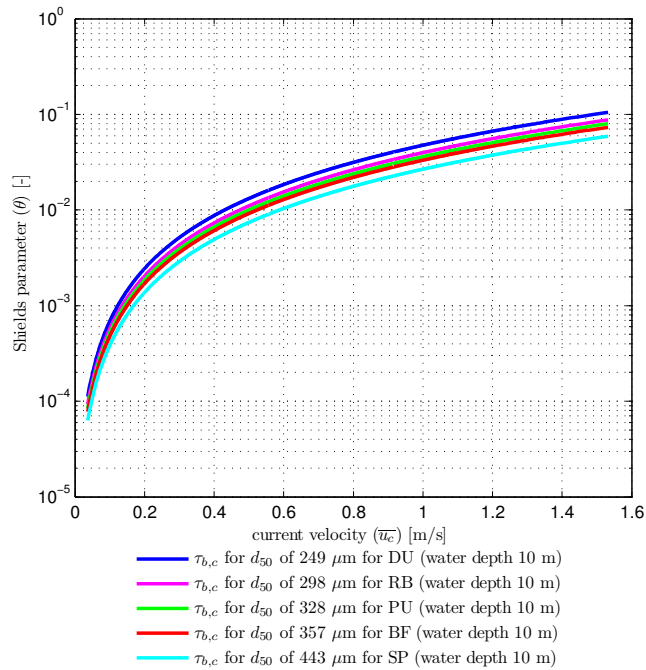


Figure L.10: Relation between Shields parameter and current velocity, with equal water depth per work method.

Appendix L: Computations Results for Hydrodynamics

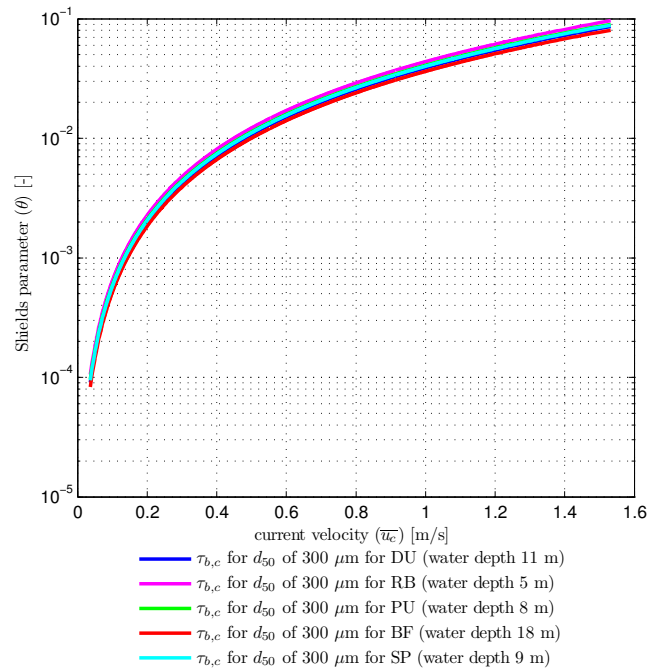


Figure L.11: Relation between Shields parameter and current velocity, with equal particle diameter per work method.

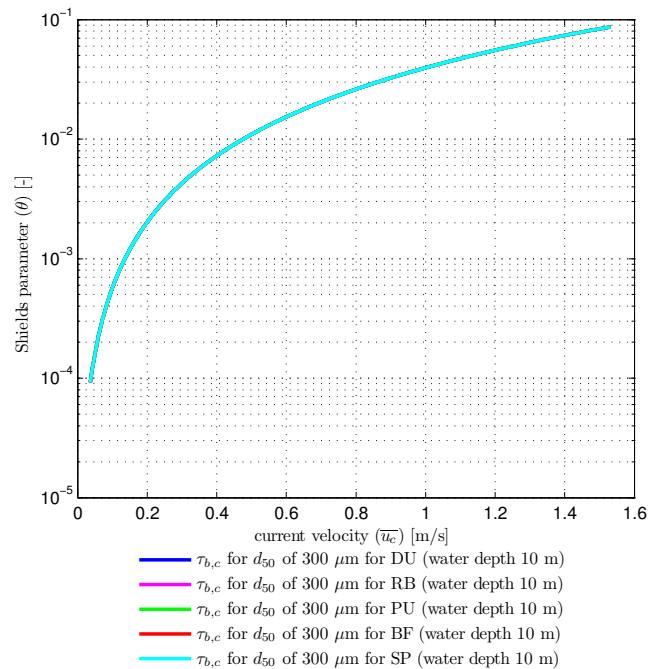


Figure L.12: Relation between Shields parameter and current velocity, with equal water depth and particle diameter per work method.